Development of Preliminary Load and Resistance Factor Design of Drilled Shafts in Iowa

BRIDGE ENGINEERING CENTER

Final Report
October 2014

IOWA STATE UNIVERSITY
Institute for Transportation

Sponsored by
Iowa Department of Transportation
Federal Highway Administration
(InTrans Project 11-410)

About the Bridge Engineering Center

The mission of the Bridge Engineering Center (BEC) is to conduct research on bridge technologies to help bridge designers/owners design, build, and maintain long-lasting bridges.

About the Institute for Transportation

The mission of the Institute for Transportation (InTrans) at Iowa State University is to develop and implement innovative methods, materials, and technologies for improving transportation efficiency, safety, reliability, and sustainability while improving the learning environment of students, faculty, and staff in transportation-related fields.

Disclaimer Notice

The contents of this report reflect the views of the authors, who are responsible for the facts and the accuracy of the information presented herein. The opinions, findings and conclusions expressed in this publication are those of the authors and not necessarily those of the sponsors.

The sponsors assume no liability for the contents or use of the information contained in this document. This report does not constitute a standard, specification, or regulation.

The sponsors do not endorse products or manufacturers. Trademarks or manufacturers' names appear in this report only because they are considered essential to the objective of the document.

Non-Discrimination Statement

Iowa State University does not discriminate on the basis of race, color, age, religion, national origin, pregnancy, sexual orientation, gender identity, genetic information, sex, marital status, disability, or status as a U.S. veteran. Inquiries regarding non-discrimination policies may be directed to Office of Equal Opportunity, Title IX/ADA Coordinator and Affirmative Action Officer, 3350 Beardshear Hall, Ames, Iowa 50011, 515-294-7612, eooffice@iastate.edu.

Iowa Department of Transportation Statements

Federal and state laws prohibit employment and/or public accommodation discrimination on the basis of age, color, creed, disability, gender identity, national origin, pregnancy, race, religion, sex, sexual orientation or veteran's status. If you believe you have been discriminated against, please contact the Iowa Civil Rights Commission at 800-457-4416 or Iowa Department of Transportation's affirmative action officer. If you need accommodations because of a disability to access the Iowa Department of Transportation's services, contact the agency's affirmative action officer at 800-262-0003.

The preparation of this report was financed in part through funds provided by the Iowa Department of Transportation through its "Second Revised Agreement for the Management of Research Conducted by Iowa State University for the Iowa Department of Transportation" and its amendments.
The opinions, findings, and conclusions expressed in this publication are those of the authors and not necessarily those of the Iowa Department of Transportation or the U.S. Department of Transportation Federal Highway Administration.

Technical Report Documentation Page

1. Report No. InTrans Project 11-410	**2. Government Accession No.**	**3. Recipient's Catalog No.**	
4. Title and Subtitle Development of Preliminary Load and Resistance Factor Design of Drilled Shafts in Iowa		**5. Report Date** October 2014 **6. Performing Organization Code**	
7. Author(s) Kam W. Ng, Sri Sritharan, and Jeramy C. Ashlock		**8. Performing Organization Report No.** InTrans Project 11-410	
9. Performing Organization Name and Address Bridge Engineering Center Iowa State University 2711 South Loop Drive, Suite 4700 Ames, IA 50010-8664		**10. Work Unit No. (TRAIS)** **11. Contract or Grant No.**	
12. Sponsoring Organization Name and Address Iowa Department of Transportation 800 Lincoln Way Ames, IA 50010	Federal Highway Administration U.S. Department of Transportation 1200 New Jersey Avenue SE Washington, DC 20590	**13. Type of Report and Period Covered** Final Report **14. Sponsoring Agency Code** SPR RB03-012	
15. Supplementary Notes Visit www.intrans.iastate.edu for color PDFs of this and other research reports.			

16. Abstract

The Federal Highway Administration (FHWA) mandated utilizing the Load and Resistance Factor Design (LRFD) approach for all new bridges initiated in the United States after October 1, 2007. To achieve part of this goal, a database for Drilled SHAft Foundation Testing (DSHAFT) was developed and reported on by Garder, Ng, Sritharan, and Roling in 2012. DSHAFT is aimed at assimilating high-quality drilled shaft test data from Iowa and the surrounding regions. DSHAFT is currently housed on a project website (http://srg.cce.iastate.edu/dshaft) and contains data for 41 drilled shaft tests.

The objective of this research was to utilize the DSHAFT database and develop a regional LRFD procedure for drilled shafts in Iowa with preliminary resistance factors using a probability-based reliability theory. This was done by examining current design and construction practices used by the Iowa Department of Transportation (DOT) as well as recommendations given in the American Association of State Highway and Transportation Officials (AASHTO) LRFD Bridge Design Specifications and the FHWA drilled shaft guidelines.

Various analytical methods were used to estimate side resistance and end bearing of drilled shafts in clay, sand, intermediate geomaterial (IGM), and rock. Since most of the load test results obtained from O-cell do not pass the 1-in. top displacement criterion used by the Iowa DOT and the 5% of shaft diameter for top displacement criterion recommended by AASHTO, three improved procedures are proposed to generate and extend equivalent top load-displacement curves that enable the quantification of measured resistances corresponding to the displacement criteria.

Using the estimated and measured resistances, regional resistance factors were calibrated following the AASHTO LRFD framework and adjusted to resolve any anomalies observed among the factors. To illustrate the potential and successful use of drilled shafts in Iowa, the design procedures of drilled shaft foundations were demonstrated and the advantages of drilled shafts over driven piles were addressed in two case studies.

17. Key Words bridge design—drilled shafts—end bearing—load factors—resistance factors—side resistance		**18. Distribution Statement** No restrictions.	
19. Security Classification (of this report) Unclassified.	**20. Security Classification (of this page)** Unclassified.	**21. No. of Pages** 230	**22. Price** NA

Form DOT F 1700.7 (8-72) **Reproduction of completed page authorized**

DEVELOPMENT OF PRELIMINARY LOAD AND RESISTANCE FACTOR DESIGN OF DRILLED SHAFTS IN IOWA

Final Report
October 2014

Principal Investigator
Sri Sritharan
Wilson Engineering Professor
Department of Civil, Construction, and Environmental Engineering, Iowa State University

Co-Principal Investigator
Kam W. Ng
Post-doctoral Research Associate
Department of Civil, Construction, and Environmental Engineering, Iowa State University

Jeramy C. Ashlock
Assistant Professor
Department of Civil, Construction, and Environmental Engineering, Iowa State University

Authors
Kam W. Ng, Sri Sritharan, and Jeramy C. Ashlock

Sponsored by
the Iowa Department of Transportation and
the Federal Highway Administration
(SPR RB03-012)

Preparation of this report was financed in part
through funds provided by the Iowa Department of Transportation
through its Research Management Agreement with the
Institute for Transportation
(InTrans Project 11-410)

A report from
Institute for Transportation
Iowa State University
2711 South Loop Drive, Suite 4700
Ames, IA 50010-8664
Phone: 515-294-8103 Fax: 515-294-0467
www.intrans.iastate.edu

TABLE OF CONTENTS

LIST OF FIGURES

LIST OF TABLES

ACKNOWLEDGMENTS

The authors would like to thank the Iowa Department of Transportation (DOT) for sponsoring this research, the Federal Highway Administration for state planning and research (SPR) funds used for this project, and the technical advisory committee (TAC) for their guidance.

The following individuals served on the TAC: Ahmad Abu-Hawash, Ken Dunker, Mark Dunn, Kyle Frame, Steve Megivern, Michael Nop, and Bob Stanley. The members of this committee represent Bridges and Structures, Soils Design, Construction, and the Research and Technology Bureau of the Iowa DOT.

EXECUTIVE SUMMARY

The Federal Highway Administration (FHWA) mandated utilizing the Load and Resistance Factor Design (LRFD) approach for all new bridges initiated in the United States after October 1, 2007. To achieve part of this goal, a database for Drilled SHAft Foundation Testing (DSHAFT) was developed and reported on by Garder, Ng, Sritharan, and Roling in 2012. DSHAFT is aimed at assimilating high-quality drilled shaft test data from Iowa and the surrounding regions. DSHAFT is currently housed on a project website (http://srg.cce.iastate.edu/dshaft) and contains data for 41 drilled shaft tests.

The objective of this research was to utilize the DSHAFT database and develop a regional LRFD procedure for drilled shafts in Iowa with preliminary resistance factors using a probability-based reliability theory. This was done by examining current design and construction practices used by the Iowa Department of Transportation (DOT) as well as recommendations given in the American Association of State Highway and Transportation Officials (AASHTO) LRFD Bridge Design Specifications and the FHWA drilled shaft guidelines.

Various analytical methods were used to estimate side resistance and end bearing of drilled shafts in clay, sand, intermediate geomaterial (IGM), and rock. Since most of the load test results obtained from O-cell do not pass the 1-in. top displacement criterion used by the Iowa DOT and the 5% of shaft diameter for top displacement criterion recommended by AASHTO, three improved procedures are proposed to generate and extend equivalent top load-displacement curves that enable the quantification of measured resistances corresponding to the displacement criteria.

Using the estimated and measured resistances, regional resistance factors were calibrated following the AASHTO LRFD framework and adjusted to resolve any anomalies observed among the factors. To illustrate the potential and successful use of drilled shafts in Iowa, the design procedures of drilled shaft foundations were demonstrated and the advantages of drilled shafts over driven piles were addressed in two case studies.

CHAPTER 1. OVERVIEW

1.1. Background

Deep foundations are typically used to support bridges in Iowa with driven steel H-piles being the preferred choice for pile foundations. However, steel H-piles may not be the most cost effective foundation solution under all soil and construction conditions. For instance, driven steel H-piles are difficult to install at deep scour conditions and require expensive cofferdams during construction while drilled shafts can be efficiently constructed with steel casings and socketed into bedrock, thereby increasing their load resistance. Steel piles are vulnerable to corrosion and can be damaged by major obstructions during installation. Alternatively, cast-in-place drilled shafts provide a cost-competitive deep foundation solution, because they are relatively easy to construct in firm cohesive soils, areas requiring minimal foundation footprint, and/or locations with low overhead clearance, and may not require design and construction of pile cap or pile-to-cap connections. In the latter case, the drilled shaft can be continued above ground as a structural column. Drilled shafts can provide large axial resistance when the base is socketed into rock or other strong bearing strata. They can also be designed to provide large lateral load resistance with adequate displacement capacity. Unlike driven piles, drilled shaft constructions produce low noise and vibration, which reduce the impact on the traveling public as well as the adjacent environment.

Despite the aforementioned advantages, drilled shafts are used infrequently in the State of Iowa although the soil conditions in several regions of Iowa are ideal for using this foundation option. According to the geotechnical program review conducted recently by the Federal Highway Administration (FHWA) and Iowa Department of Transportation (DOT) professionals (FHWA 2009), the reasons for the limited use of drilled shafts are primarily attributed to: 1) lack of a formal process for selection of appropriate foundation types, especially in evaluating the advantages of drilled shafts over driven piles; 2) limited design guidelines and details for drilled shafts in the Iowa Bridge Design Manual; and 3) the absence of standard construction inspection checklists for drilled shafts. However, some of these limitations have been alleviated with the latest Iowa DOT Load and Resistance Factor Design (LRFD) Bridge Design Manual (2011) that incorporates the latest FHWA's drilled shaft construction procedures and LRFD design methods presented by Brown et al. (2010).

Compared to the drilled shaft foundations, driven pile foundations have been extensively investigated following the completion of three research projects (TR-573, -583, and -584) sponsored by the Iowa DOT and Iowa Highway Research Board (IHRB). The outcomes of these projects 1) led to the successful development of the regional LRFD method for driven pile foundations in Iowa; 2) satisfy the mandate issued by the FHWA to use the LRFD approach on all new bridges initiated after October 1, 2007; 3) improve the relaibility of bridge foundations when designed with driven piles; and 4) elevate the cost competitiveness of driven pile foundations. The complete research outcomes are presented on the project website at http://srg.cce.iastate.edu/lrfd/. Although the American Association of State Highway and Transportation Officials (AASHTO) LRFD Bridge Design Specifications (2010) provide LRFD recommendations for drilled shafts, resistance factors developed for drilled shafts were determined primarily by fitting to the Allowable Strength Design (ASD) factor of safety (Brown

et al. 2010) and were evaluated against the resistance factors calculated by Allen (2005) using the probability-based reliability methods based on a general national database. Since AASHTO LRFD Bridge Design Specifications (2010) have not been written for direct application in Iowa, these specifications cannot reflect the local design and construction practices and the regional soil conditions. The limitations associated with current AASHTO Specifications become significant, because the accuracy of estimating drilled shaft performance is extremely sensitive to the local ground conditions and construction techniques used (Brown et al. 2010). In adherence to the FHWA's mandate, the Iowa DOT Office of Bridges and Structures has, in recent years, designed drilled shafts based on the AASHTO LRFD Bridge Design Specifications, which is not believed to be cost effective due to not using regionally calibrated resistant factors.

1.2. Scope of Research Project

Because of the aforementioned advantages of drilled shaft foundations and in order to make the drilled shaft foundation option equally competitive to driven pile foundations, the Iowa DOT sponsored a research project (RT-328: Integration of drilled shaft load test data into PILOT) in 2010 to develop an electronic database for Drilled SHAft Foundation Testing (DSHAFT) following the concept of PIle LOad Test (PILOT) Database developed for driven piles (Roling et al. 2010). DSHAFT was created using Microsoft Office Access™ to conveniently assemble, review and integrate static load tests on drilled shafts in the Midwest region as well as neighboring states into a quality assured, electronic database (Garder et al. 2012). DSHAFT, available in electronic form at project website: http://srg.cce.iastate.edu/dshaft/, is currently comprised of forty-one drilled shaft load tests conducted in eleven states (Colorado, Iowa, Illinois, Kansas, Kentucky, Minnesota, Missouri, Nebraska, Nevada, South Dakota, and Tennessee). DSHAFT embodies a model for efficient, regional LRFD analysis on the amassed dataset and lays an important groundwork for improving the current LRFD procedure for drilled shafts in Iowa.

The overall objective of this research project is to utilize DSHAFT for preliminary development of a regional LRFD procedure for drilled shafts in Iowa, thereby ensuring reliability while increasing the cost effectiveness of drilled shaft foundations. This overall objective was accomplished by: 1) conducting a literature review on current design and construction practices used by the Iowa DOT and neighboring DOTs as well as recommendations given in AASHTO LRFD Bridge Design Specifications (2010) and the FHWA drilled shaft guidelines reported by Brown et al (2010); 2) examining and analyzing DSHAFT data sets; 3) performing static analyses; 4) quantifying the measured capacity of each test drilled shaft; 5) determining regional LRFD resistance factors; and 6) conducting cost analyses. The outcome of this research improves the economy of drilled shaft foundations in Iowa, as similarly acknowledged by DOTs in neighboring states, such as the Missouri DOT.

1.3. Report Layout

The purpose of this report is to clearly depict the preliminary development of a regional LRFD procedure for drilled shafts in Iowa. This report consists of six chapters and three appendices. The content of each chapter is briefly described as follows:

Chapter 1: Overview – A brief description of the background of the deep foundations implemented in Iowa and the scope of the research project.

Chapter 2: Literature Review – A summary of a literature review on LRFD design and construction procedures for drilled shafts in Iowa and neighboring states and AASHTO and FHWA guidelines for drilled shafts.

Chapter 3: Examination and Analysis of DSHAFT Data – A brief summary of the DSHAFT database and drilled shaft resistance estimations and measurements.

Chapter 4: Development of Regional LRFD Resistance Factors – A brief description of the LRFD calibration framework. Resistance factor calculations for side resistance, end bearing, and total resistance. Resistance factor calculations based on various failure defining criteria. Presents a summary of recommended resistance factors.

Chapter 5: Design Comparison – Evaluation of drilled shafts and driven steel H-piles using the LRFD recommendations developed in Chapter 4 to illustrate the potential and successful use of drilled shafts in Iowa. Demonstrates design procedures of drilled shaft foundations and addresses the advantages of drilled shafts.

Chapter 6: Summary and Future Research – A summary of the research outcomes for the development of regional LRFD procedures for drilled shafts in Iowa. Proposes several topics for future research.

CHAPTER 2. LITERATURE REVIEW

2.1. General Background

Drilled shafts are considered cast-in-place or non-displacement piles in which a volume of geomaterials is removed by drilling using a rig, and the resulting cylindrical void is filled with reinforced concrete. This installation method does not push the surrounding geomaterials away from the drilled shaft or displace geomaterials from their original position (Salgado 2008). Drilled shafts can have diameters as small as 1 ft, but typical diameters range from 3 ft to 12 ft. It is common for drilled shafts that support bridge structures to have depths of up 200 ft in the United States. However, the depth can be extended to as deep as 300 ft or more (Brown et al. 2010).

Similar to other deep foundations, drilled shafts were traditionally designed using the Allowable Stress Design (ASD) philosophy. To achieve consistent and reliable foundation designs, Load and Resistance Factor Design (LRFD) philosophy is being implemented in the United States. A drilled shaft supports axial loads through a combination of its side resistance and end bearing. Depending on surrounding geomaterials, static analysis methods are available in the literature for estimating the side resistance and end bearing of a drilled shaft. The supporting resistances are also influenced by different construction methods (i.e., dry, casing and wet methods), which are selected based on the nature of the ground. A famous quote: "*Do not design on paper what you have to wish into the ground,"* by the father of soil mechanics, Karl Terzaghi, implies that it is indispensable to verify the drilled shaft response and performance in the field, so that the drilled shaft indeed satisfies the desired performance established during design. Verification can be performed using various field load tests. Top-down static load test, Osterberg (O-cell) load tests, rapid load tests and high-strain dynamic load tests are the common axial compressive load tests. Each method has its unique interpretation of load test data. The aforementioned design, construction and testing of drilled shafts are discussed in Sections 2.2 to 2.6. The current design and construction practices of Iowa DOT as well as neighboring DOTs are summarized in Section 2.7. AASHTO LRFD specifications and FHWA guidelines for drilled shafts are also included in Section 2.7.

2.2. Design Philosophy

2.2.1. Allowable Stress Design

Drilled shafts were traditionally designed based on Allowable Stress Design (ASD) philosophy, which combines uncertainties of applied load (Q) and resistance (R) through a global factor of safety (FS):

$$Q \leq \frac{R}{FS} \tag{2-1}$$

The applied load (Q) consists of the actual forces estimated to be applied to the drilled shaft, which has the resistance (R) contributed from its surrounding geomaterials. In this ASD approach, the risk of any adverse performance of a drilled shaft is addressed through a single and subjective FS. The FS is highly dependent on an individual designer's experience and judgment,

and it does not reflect the variation in soil conditions and design methods that also depend on the pile types. Hence, ASD philosophy cannot provide a consistent and reliable framework for accounting for individual sources of uncertainties into the design.

2.2.2. Load and Resistance Factor Design

To overcome the limitations of ASD, LRFD philosophy is being implemented for bridge foundation designs throughout the United States. The basic principle of the LRFD uses probabilistic approaches and accounts for uncertainties individually for the resistance as well as for different design loads. Additionally, the LRFD approach allows all components of the superstructure and foundations to be designed to a uniform level of safety. The focus of LRFD is to achieve a consistent and reliable design by separating the variability of the load and resistance components. The applied load (Q) and supporting resistance components are multiplied by load factors (γ) and a resistance factor (φ), respectively, represented by the strength limit state Eq. (2-2):

$$\sum \gamma_i Q_i \leq \varphi R \tag{2-2}$$

The strength limit state is satisfied when the summation of all factored loads does not exceed the factored resistance. With the focus on the axial resistance of a drilled shaft, the AASHTO (2010) Strength I load combination is used, in which only dead load (Q_D) and live load (Q_L) are considered in the limit state Eq. (2-2). The assumed probabilistic characteristics of dead and live loads, as documented by Nowak (1999) and adopted by Paikowsky et al. (2004), are summarized in Table 2.1.

Table 2.1. Probabilistic characteristics of dead load and live load

Load (Q)	Load Factor (γ)	Load Bias (λ)	Coefficient of Variation (COV_Q)
Dead (D)	1.25	1.05	0.1
Live (L)	1.75	1.15	0.2

The resistance factor (φ) for drilled shafts can be calibrated using: 1) fitting to ASD's FS; 2) probabilistic-based reliability analysis methods; or 3) a combination of approaches from available load test data, such as DSHAFT. However, only the second approach, probabilistic-based reliability analysis methods, conforms to the LRFD philosophy in achieving a target probability of failure (p_f) and maintaining a uniform level of safety throughout the structure (Brown et al. 2010). The commonly used probabilistic-based reliability analysis methods are First-Order Second Moment (FOSM) method, First-Order Reliability Method (FORM) and Monte Carlo simulation method. In compliance with the strength limit state Eq. (2-2) and assuming the load and resistance are mutually independent and follow lognormal distributions, the resistance factor in accordance to the FOSM method can be calculated using Eq. (2-3) as suggested by Barker et al. (1991). A regression analysis performed by Paikowsky et al. (2004) on driven piles concluded that the FORM provides resistance factors approximately 10% higher than those obtained from FOSM. A similar comparison conducted by Allen (2005) on drilled shafts concluded that the resistance factors obtained from Monte Carlo simulation method were approximately 9% higher than those obtained from FOSM.

$$\varphi = \frac{\lambda_R\left(\frac{\gamma_D Q_D}{Q_L}+\gamma_L\right)\sqrt{\left[\frac{(1+COV_D^2+COV_L^2)}{(1+COV_R^2)}\right]}}{\left(\frac{\lambda_D Q_D}{Q_L}+\lambda_L\right)\exp\left\{\beta_T\sqrt{\ln[(1+COV_R^2)(1+COV_D^2+COV_L^2)]}\right\}} \quad (2\text{-}3)$$

where,

COV_R = coefficient of variation of resistance,
COV_D = coefficient of variation of dead load (refer to Table 2.1),
COV_L = coefficient of variation of live load (refer to Table 2.1),
β_T = target or desired reliability index,
λ_R = resistance bias factor (ratio of measured to predicted value for resistance),
λ_D = dead load bias factor (ratio of measured to predicted value for dead load),
λ_L = live load bias factor (ratio of measured to predicted value for live load),
γ_D = dead load factor (refer to Table 2.1),
γ_L = live load factor (refer to Table 2.1),
Q_D = dead load, and
Q_L = live load.

To reduce the difference in resistance factors calibrated using the FOSM method and the FORM as well as the Monte Carlo simulation method, Bloomquist et al. (2007) proposed a modified FOSM method where the coefficient of variation for loads was replaced with Eq. (2-4).

$$COV_D^2+COV_L^2 = \frac{\frac{Q_D^2}{Q_L^2}\lambda_D^2 COV_D^2+\lambda_L^2 COV_L^2}{\frac{Q_D^2}{Q_L^2}\lambda_D^2+2\frac{Q_D}{Q_L}\lambda_D\lambda_L+\lambda_D^2} \quad (2\text{-}4)$$

Substituting Eq. (2-4) into the resistance factor Eq. (2-3), the modified FOSM equation yields

$$\varphi = \frac{\lambda_R\left(\frac{\gamma_D Q_D}{Q_L}+\gamma_L\right)\sqrt{\left(1+\frac{\frac{Q_D^2}{Q_L^2}\lambda_D^2 COV_D^2+\lambda_L^2 COV_L^2}{\frac{Q_D^2}{Q_L^2}\lambda_D^2+2\frac{Q_D}{Q_L}\lambda_D\lambda_L+\lambda_D^2}\right)}{(1+COV_R^2)}}{\left(\frac{\lambda_D Q_D}{Q_L}+\lambda_L\right)\exp\left\{\beta_T\sqrt{\ln\left[(1+COV_R^2)\left(1+\frac{\frac{Q_D^2}{Q_L^2}\lambda_D^2 COV_D^2+\lambda_L^2 COV_L^2}{\frac{Q_D^2}{Q_L^2}\lambda_D^2+2\frac{Q_D}{Q_L}\lambda_D\lambda_L+\lambda_D^2}\right)\right]}\right\}} \quad (2\text{-}5)$$

The dead to live load ratio (Q_D/Q_L) in Eq. (2-5) could range between 1.0 and 4.0 depending on the bridge span. Barker et al. (1991) recommended the Q_D/Q_L ratio of 3.0 while Paikowsky et al. (2004) suggested that the Q_D/Q_L ratio should be within the range of 2.0 to 2.5. Nevertheless, Paikowsky et al. (2004) and Allen (2005) reported that the Q_D/Q_L ratio has no significant

influence on the resistance factor obtained using the probabilistic-based reliability analysis methods.

The calibration of resistance factors requires a proper selection of a set of target reliability levels that are represented by a target reliability index (β_T) corresponding to a probability of failure (p_f). An approximate relationship between the probability of failure and the target reliability index for lognormal distribution can be expressed by Eq. (2-6). However, this approximation is not accurate for β_T below 2.5, which is in the mid range of suggested β_T (from 2 to 3) for foundation design (Baecher, 2001). Kulhawy and Phoon (2006) noted that a β_T between 2.0 and 3.5 is generally used in resistance factor calibration for deep foundation designs and can be adjusted to represent design needs. The general relationship between β_T and p_f is summarized in Table 2.2. Paikowsky et al. (2004) recommended a β_T of 3.0, corresponding to a p_f of 1 in 1,000, for drilled shafts, because a bridge foundation normally has four or fewer drilled shafts per cap. For a redundant foundation with five or more drilled shafts per pile, a lower β_T of 2.33, corresponding to a p_f of 1 in 100, was recommended. These recommendations have been adopted by AASHTO (2010) for the Strength I limit state.

$$p_f = 460e^{-4.3\beta_T} \tag{2-6}$$

Table 2.2. Relationship between reliability index and probability of failure

Target Reliability Index, β_T	Probability of Failure
2.00	1:10
2.33	1:100
3.00	1:1,000
3.50	1:10,000

2.3. Design Methods for Side Resistance

2.3.1. Introduction

Depending on the properties of geomaterials and construction procedure, the axial resistance of a drilled shaft could be partially or totally supplied from side shear resistance along its embedded depth. Static analysis methods have been developed by various researchers and are available in literature to estimate the side resistance of a drilled shaft. Although static methods are easily used in design, they have numerous limitations. The selection of the most appropriate method for a specific design problem will depend on the site geology, extent of available soil parameters, and local practice. Static methods estimate the ultimate nominal resistance without determining the corresponding movement. Many soil strength parameters are required for different static analysis methods, and they are either directly measured from in-situ and/or laboratory soil tests or calculated based on available correlations found in literature. Additionally, static analysis methods cannot be used to verify the estimated shaft resistance during installation as routinely performed for driven piles. The factored side resistance of drilled shafts shall be taken as:

$$\varphi_s R_s = \varphi_s q_s A_s = \varphi_s q_s \pi B \Delta z \tag{2-7}$$

where

φ_s = resistance factor for side resistance,

R_s = side resistance,
q_s = unit side resistance,
A_s = area of side surface,
B = shaft diameter, and
Δz = thickness of the soil layer over which the side resistance is calculated.

2.3.2. Cohesive Soils

Side resistance of drilled shafts in cohesive soil should be designed based on total stress concepts for undrained loading conditions. The nominal unit side resistance (q_s) for shafts in cohesive soil can be estimated using the α-method proposed by Tomlinson (1971) and adopted by O'Neill and Reese (1999). The α-method is based on a dimensionless adhesion factor (α) and undrained shear strength (S_u) given as

$$q_s = \alpha S_u \tag{2-8}$$

where

α = 0.55 for $\frac{S_u}{P_a} \leq 1.5$,
α = $0.55 - 0.1\left(\frac{S_u}{P_a} - 1.5\right)$ for $1.5 \leq \frac{S_u}{P_a} \leq 2.5$; and
P_a = atmospheric pressure (2.12 ksf).

Although the recommendation is based on back-analysis of load test results of timber, pipe and precast concrete piles in cohesive soils (Tomlinson 1971), it is recommended in AASHTO (2010) for drilled shafts in cohesive soil. When the ratio $\left(\frac{S_u}{P_a}\right)$ exceeds 2.5, the material will not be considered as a cohesive soil and Eq. (2-8) shall not be used to estimate the unit side resistance. This material could be classified as intermediate geomaterial (IGM) or rock, depending on the magnitude of the unconfined compressive strength and the geology of the material. The undrained shear strength (S_u) for low permeability cohesive soils can be approximated by total stress cohesion (c). The S_u value of cohesive soil is typically obtained from laboratory unconfined compression (UC) tests. Additionally, in-situ tests, such as the Standard Penetration Test (SPT), can be used to estimate S_u based on the correlation established by Bjerrum (1972);

$$S_u = \frac{f_1 N_{60} P_a}{100} \tag{2-9}$$

where

f_1 = empirical factor (4.5 for PI = 50 and 5.5 for PI = 15),
PI = plasticity index,
N_{60} = SPT blow count corrected for hammer efficiency, and
P_a = atmospheric pressure (2.12 ksf).

However, the side resistance between cohesive materials and a drilled shaft is not completely effective over the entire embedded length. Due to the effects of seasonal moisture changes, construction disturbance, cyclic lateral loading, and low lateral pressure from freshly placed

concrete, the side resistance at the upper 5 ft of a drilled shaft is routinely ignored in accordance with the AASHTO LRFD Bridge Design Specifications (2010). Additionally, due to the development of tensile cracks induced by the change in lateral concrete pressure on the soil before and after the hardening of concrete, the side resistance at one diameter length (B) above the shaft base is also neglected.

2.3.3. Cohesionless Soils

Side resistance of drilled shafts in cohesionless soil should be designed using the β-method suggested by Burland (1973) based on the following assumptions for driven piles and adopted by O'Neill and Reese (1999) for drilled shafts.

- The effective stress cohesion intercept (c') is reduced to zero due to the remolding of adjacent soil during pile installation
- After dissipating excess pore pressure induced during pile installation, the effective stress on the pile surface is at least equal to the horizontal effective stress prior to pile installation
- Major shear distortion during loading is confined to a relatively thin zone around pile shaft, where excess pore pressure dissipates quickly or has completely dissipated from installation to loading.

The β-method is expressed in terms of a load transfer coefficient (β) and vertical geostatic effective stress (σ'_v) as

$$q_s = \beta\, \sigma'_v \leq 4.0 \text{ ksf} \quad \text{for } 0.25 \leq \beta \leq 1.2 \tag{2-10}$$

where

β = $1.5 - 0.135\sqrt{z}$ for sandy soils and $N_{60} \geq 15$,
β = $2.0 - 0.06(z)^{0.75}$ for gravelly sands and gravels and $N_{60} \geq 15$,
β = $\frac{N_{60}}{15}\left(1.5 - 0.135\sqrt{z}\right)$ for all cohesionless soils and $N_{60} < 15$,
σ'_v = vertical geostatic effective stress at soil layer mid-depth (ksf),
z = depth below ground at soil layer mid depth (ft), and
N_{60} = average SPT blow count in the design zone under consideration and corrected for hammer efficiency.

2.3.4. Intermediate Geo Materials

Cohesive Intermediate Geo Materials

O'Neill et al. (1996) identified the following materials as cohesive Intermediate Geo Materials: 1) argillaceous geomaterials such as heavily overconsolidated clays, clay shales, saprolites, and mudstones that are prone to smearing during drilling; and 2) calcareous rocks such as limestone, limerock and argillaceous geomaterials that are not prone to smearing during drilling. Although the engineering definition of cohesive IGM is subject to discussion, cohesive IGM is defined by O'Neill and Reese (1999) as material that exhibits unconfined or uniaxial compressive strengths (q_u) in the range of 10 ksf to 100 ksf (i.e., S_u of 5 to 50 ksf as identified in AASHTO, 2010). Side resistance of drilled shafts in cohesive IGM should be designed using the modified α-method developed by Hassan et al. (1997). The design calculations of unit side resistance are similar to

the α-method described in Section 2.3.2 with the necessary modifications described below. The nominal unit side resistance for cohesive IGM is given by:

$$q_s = \alpha \, \phi \, q_u \tag{2-11}$$

where

α = empirical factor determined from Figure 2.1,
q_u = uniaxial compressive strength of intact rock (ksf), and
ϕ = a correction factor to account for the degree of jointing (see Table 2.3).

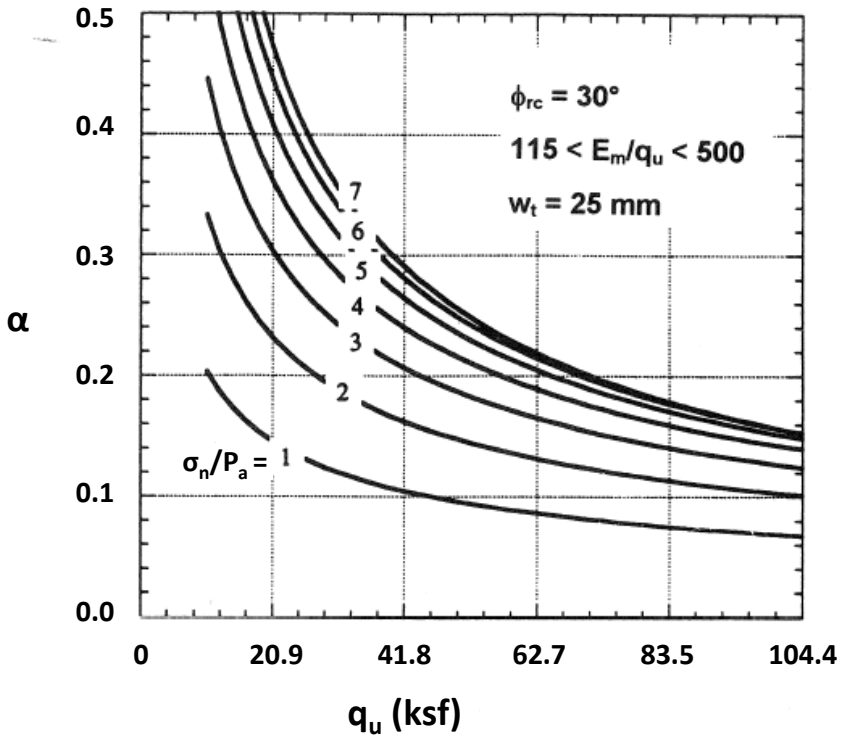

Figure 2.1. Factor α for cohesive IGM (adapted from O'Neill et al. 1996)

Note that the α value determined in Figure 2.1 is based on an assumed value of interface friction angle (ϕ_{rc}) of 30 degrees. If a different ϕ_{rc} value is known, the α value can be adjusted by

$$\alpha = \alpha_{\text{Figure 2.1}} \frac{\tan \phi_{rc}}{\tan 30^{\circ}} \tag{2-12}$$

Figure 2.1 is only applicable if the ratio of modulus of rock mass (E_m) to q_u is between 115 and 500. It is assumed that the side resistance can be mobilized if the total vertical displacement (w_t) at the tip of a drilled shaft is at least 1 in. Figure 2.1 shows that the α value is dependent on the ratio of freshly placed concrete pressure at the middle of a cohesive IGM layer (σ_n) to atmospheric pressure (P_a). The concrete pressure (σ_n) at the depth below cutoff elevation (z_i^*) can be estimated using Eq. (2-13) if the concrete has a slump of 7 in. or greater and is placed in the borehole at a rate of 40 ft per hour or greater. The concrete pressure at greater depths should

be determined using Eq. (2-13) at $z_i^* = 40$ ft.

$$\sigma_n = 0.65\gamma_c z_i^* \tag{2-13}$$

where

γ_c = concrete unit weight (kcf), and
z_i^* = depth below the slected cutoff elevation to the middle of a material layer i, which is limited to 40 ft.

The effect of joints on unit side resistance is accounted for using the joint reduction factor (ϕ) given in Table 2.3. The ϕ value is determined according to the Rock Quality Designation (RQD) of the cohesive IGM and the characteristics of the joint (i.e., either closed joints or open/gouge-filled joints). RQD is calculated as the sum of the length of recovered cores, which are 4 in or more in length, expressed as a percentage of total core length (Deere and Deere 1989). It is noted that the ϕ value cannot be recommended for cohesive IGM with RQD less than 20%, and it was suggested by Brown et al. (2010) to conduct load tests on drilled shafts to determine the side resistance.

Table 2.3. Side resistance reduction factor for cohesive IGM

Rock Quality Designation, RQD (%)	Joint Reduction Factor, ϕ	
	Closed Joints	Open or Gouge-Filled Joints
100	1.00	0.85
70	0.85	0.55
50	0.60	0.55
30	0.50	0.50
20	0.45	0.45

Cohesionless Intermediate Geo Materials

Cohesionless Intermediate Geo Materials are defined by O'Neill et al. (1996) as very dense granular tills or granular residual materials with SPT N_{60} value ranging between 50 and 100 blows per foot. This definition is currently adopted in the AASHTO (2010). The original β-method suggested by Burland (1973) should be used to estimate the unit side resistance of drilled shafts in cohesionless IGM. The unit side resistance as documented in O'Neill and Reese (1999) is expressed as

$$q_s = K \tan(\phi')\ \sigma_v' \tag{2-14}$$

where

K = coefficient of horizontal soil stress, which is assumed as the coefficient at rest K_o,
K_o = $(1 - \sin\phi')OCR^{\sin\phi'}$,
ϕ' = effective friction angle in degrees, which can be evaluated through direct field and/or laboratory testing or can be estimated using Eq. (2-15),
OCR = overconsolidation ratio = $\frac{\sigma_p'}{\sigma_v'} = \frac{0.2\ N_{60}P_a}{\sigma_v'}$,

σ'_p = effective vertical preconsolidation stress (ksf),
σ'_v = vertical geostatic effective stress at soil layer mid-depth (ksf),
N_{60} = SPT blow count corrected for hammer efficiency, and
P_a = atmospheric pressure (2.12 ksf).

$$\phi' = \tan^{-1}\left\{\left[\frac{N_{60}}{12.3 + 20.3\left(\frac{\sigma'_v}{P_a}\right)}\right]^{0.34}\right\} \quad (2\text{-}15)$$

2.3.5. Rock

Compared to IGM, rock has higher stiffness and compressive strength. In this report, geomaterials, such as shale, sandstone, limestone and mudstone, that have uniaxial compressive strength (q_u) greater than 100 ksf or SPT N_{60} value larger than 100 are identified as rock. Unit side resistance for drilled shafts in rock is evaluated based on the measured uniaxial compressive strength (q_u) of the rock typically determined from laboratory unconfined compression tests on rock specimens at field moisture levels. However, q_u values should not exceed the 28-day compressive strength of the drilled shaft concrete (f'_c). The unit side resistance given as Eq. (2-16) and adopted in the AASHTO (2010) is based on the recommendation suggested by Horvath and Kenney (1979).

$$q_s = 0.65\alpha_E P_a\left(\frac{q_u}{P_a}\right)^{0.5} < 7.8P_a\left(\frac{f'_c}{P_a}\right)^{0.5} \quad (2\text{-}16)$$

where

q_u = uniaxial compressive strength of rock (ksf),
P_a = atmospheric pressure (2.12 ksf),
α_E = reduction factor to account for jointing in rock as provided in Table 2.4,
f'_c = drilled shaft 28-day concrete compressive strength (ksf),
E_m = elastic modulus of rock mass (ksf), and
E_i = elastic modulus of intact rock from tests (ksf).

The empirical reduction factor (α_E) is included by O'Neill and Reese (1999) to account for the degree of rock fracturing, and is determined as a function of the estimated ratio of rock mass modulus to intact rock modulus (E_m/E_i) as shown in Table 2.4. The E_m/E_i can be estimated from the RQD of the rock depending on the type of rock joints as shown in Table 2.5. Brown et al. (2010) provided the following brief description for intact rock and rock mass:

> *"Intact rock refers to the consolidated and cemented assemblage of mineral particles forming the rock material, excluding the effects of macro-scale discontinuities such as joints, bedding planes, minor faults, or other recurrent planar features. The term rock mass is used to describe the system comprised of intact rock and discontinuities. Characteristics of intact rock are determined from index and laboratory tests on core specimens. Properties of rock mass may be estimated on the basis of intact rock properties plus characteristics of discontinuities."*

Table 2.4. Estimation of α_E (adapted from O'Neill and Reese 1999)

E_m/E_i	α_E
1.0	1.0
0.5	0.8
0.3	0.7
0.1	0.55
0.05	0.45

Table 2.5. Estimation of E_m based on RQD (adapted from O'Neill and Reese 1999)

Rock Quality Designation, RQD (%)	E_m/E_i Closed Joints	E_m/E_i Open Joints
100	1.00	0.60
70	0.70	0.10
50	0.15	0.10
20	0.05	0.05

Eq. (2-16) applies to drilled shafts constructed using a drilling slurry or drilled shafts with a smooth rock-socket surface. Side resistance will be significantly increased if the side of the rock socket is artificially roughened by grooving. The side resistance of a roughened, rock socketed drilled shaft can be estimated using Eq. (2-17) proposed by Horvath et al. (1983). Figure 2.2 illustrates the geometric terms in Eq. (2-17). However, Eq. (2-17) should be used with cautioun unless the geometric terms are assured during drilled shaft construction or load tests are performed to verify the effect of roughening.

$$q_s = 0.80\left[\frac{\Delta r}{r}\left(\frac{L'}{L}\right)\right]^{0.45} q_u \qquad (2\text{-}17)$$

where

q_u = uniaxial compressive strength of rock (ksf),
Δr = height of asperities or grooves in rock sidewall (ft),
r = radius of drilled shaft (ft),
L' = distance along surface of rock socket (ft), and
L = depth of rock socket (ft).

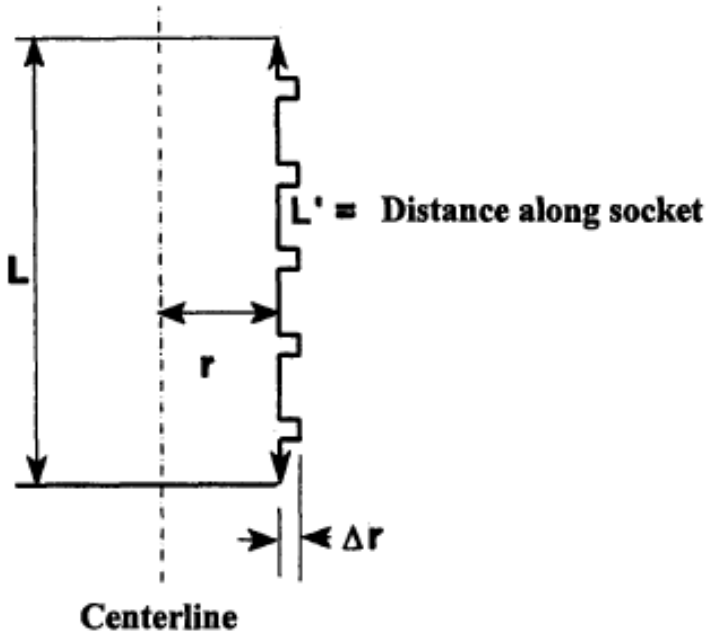

Figure 2.2. Definition of geometric terms in equation (2-17) (adapted from O'Neill and Reese 1999)

2.4. Design Methods for End Bearing

2.4.1. Introduction

Drilled shafts can support axial loads through end bearing. The magnitude of end bearing depends on construction methods and practices, properties of supporting geomaterials near and beneath the toe of drilled shafts, and the base diameter of the drilled shaft. End bearing develops as a function of downward displacement, which mobilizes the contact stresses beneath the base. Static analysis methods are available in literature to estimate the end bearing. Similar to side resistance estimation, many soil strength parameters, either directly measured from in-situ and/or laboratory soil tests or calculated based on available correlations found in literature, are required in end bearing calculations. The factored end bearing of drilled shafts shall be taken as:

$$\varphi_p R_p = \varphi_p q_p A_p = \varphi_p q_p \pi \frac{B^2}{4} \tag{2-18}$$

where

φ_p = resistance factor for end bearing,
R_p = end bearing (kip),
q_p = unit end bearing (ksf),
A_p = area of shaft base (ft^2), and
B = shaft base diameter (ft).

2.4.2. Cohesive Soils

End bearing of drilled shafts on a cohesive soil should be estimated based on total stress concepts for undrained loading conditions. The unit end bearing can be estimated using Eq. (2-19) as suggested by O'Neill and Reese (1999)

$$q_p = N_c S_u \leq 80.0 \text{ ksf} \tag{2-19}$$

where

N_c = bearing capacity factor = $6\left[1 + 0.2\left(\frac{Z}{B}\right)\right] \leq 9$,
S_u = mean undrained shear strength of the cohesive soil over a depth of 2B below base,
Z = embedded depth of shaft in cohesive soil (ft), and
B = diameter of drilled shaft (ft).

The N_c factor of 9 can be taken if the shaft embedded depth in the cohesive soil is at least three times the diameter and the mean S_u is at least 2 ksf. For drilled shafts with embedded depth in cohesive soil less than three times the diameter, the N_c factor, given in Eq. (2-19) and recommended in AASHTO (2010) is approximated from Eq. (2-20) by equating the bearing factor N_c^* to 9 corresponding to S_u of 2 ksf given in Table 2.6. Hence, it is important to design the drilled shaft with the axial resistance from end bearing in cohesive soil with S_u of at least 2 ksf.

$$N_c = \frac{2}{3}\left[1 + \frac{1}{6}\left(\frac{Z}{B}\right)\right] N_c^* \tag{2-20}$$

Table 2.6. Bearing factor N_c^* (adapted from Brown et al. 2010)

Undrained Shear Strength, S_u (ksf)	N_c^*
0.50	6.5
1.00	8.0
2.00	9.0

2.4.3. Cohesionless Soils

Bearing capacity theory proposed by Terzaghi (1943) can be used to estimate the end bearing of drilled shafts in cohesionless soil. However, due to the effect of construction on cohesionless soil properties and stresses beneath the shaft base, the end bearing estimation becomes unreliable with the high degree of variability. For drilled shafts in cohesionless soils with corrected SPT N-value (N_{60}) smaller than 50, the unit end bearing suggested by Reese and O'Neill (1989) based on correlation studies can be pragmatically used in routine design;

$$q_p = 1.2\, N_{60} \leq 60 \text{ ksf} \tag{2-21}$$

The N_{60} is the average corrected SPT N-value obtained in cohesionless soil between the base and two diameters below the base. Eq. (2-21) was established from five load tests on drilled shafts with clean bases in cohesionless soil and ultimate end bearings corresponding to settlements

equal to 5% of the base diameter (Reese and O'Neill 1988). The maximum q_p of 60 ksf specified in Eq. (2-21) is based on the largest value obtained from the load tests. For drilled shafts in cohesionless soil with N_{60} larger than 50, load testing is recommended to determine the q_p; otherwise the maximum limit of 60 ksf shall be used. If the base geomaterials with N_{60} larger than 50 are treated as cohesionless IGM instead of cohesionless soil as recommended in AASHTO (2010), Section 2.4.4 of this report should be used to estimate q_p.

2.4.4. Cohesionless Intermediate Geo Materials

According to AASHTO LRFD Bridge Design Specifications (2010), cohesionless geomaterials beneath shaft bases with N_{60} greater than 50 are treated as cohesionless IGM and the unit toe resistance is taken as

$$q_p = 0.59\left[N_{60}\left(\frac{P_a}{\sigma'_v}\right)\right]^{0.8}\sigma'_v \tag{2-22}$$

where

σ'_v = vertical geostatic effective stress at the base elevation of the shaft (ksf),
P_a = atmospheric pressure (2.12 ksf), and
N_{60} = SPT blow count corrected for hammer efficiency, limited to 100.

The N_{60} is the average corrected SPT N-value obtained in cohesionless IGM between the base and two diameters below the base. If settlement estimates for large-diameter drilled shafts of 4.17 ft or larger are not performed to verify their serviceability limit state conditions and prevent excessive settlement, the unit end bearing estimated by Eq. (2-22) should be reduced to

$$q_{p,max} = \left(\frac{4.17}{B}\right)0.59\left[N_{60}\left(\frac{P_a}{\sigma'_v}\right)\right]^{0.8}\sigma'_v \tag{2-23}$$

where B is the diameter of the base of the drilled shaft in feet.

2.4.5. Cohesive Intermediate Geo Materials and Rock

End bearing in cohesive IGM or rock is significantly influenced by a wide range of rock mass conditions beneath the drilled shaft, such as spacing, condition and orientation of rock discontinuities, and strength of the rock mass (Turner 2006). Table 2.7 shows the different failure modes in rock bearing capacity corresponding to different rock mass conditions. Rock mass conditions can be categorized as intact or massive, jointed, layered, and fractured. Rock failures generally occur in shear, compression and/or tension depending on the relative spacing of joint (S) to shaft diameter (B), joint dip angle (α) from horizontal, closed or open joint, types, rock thickness (H) over compressible layers, and rock properties. The rock unconfined compressive strength (q_u) is the most commonly used rock property in end bearing estimation. The q_u value is typically determined by conducting uniaxial compression tests of rock. Some representative q_u values from uniaxial compression tests of rock are given in Table 2.8.

Table 2.7. Bearing capacity failure modes in rock (adapted from U.S. Army Corps of Engineers 1994)

Rock Mass Condition			Failure		Bearing Capacity Equation
Type	Joint Dip Angle from Horizontal	Joint Spacing	Illustration	Mode	
INTACT/MASSIVE	N/A	S >> B	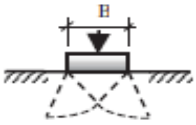	(a) Brittle Rock: Local shear failure caused by localized brittle fracture	Eq. (2-24)
			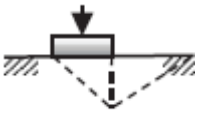	(b) Ductile Rock: General shear failure along well-defined shear surface	Eq. (2-24)
STEEPLY DIPPING JOINTS	70° < α < 90°	S < B	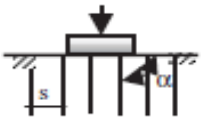	(c) Open Joints: Compression failure of individual rock columns	Eq. (2-26)
			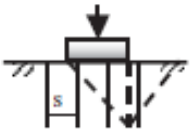	(d) Closed Joints: General shear failure along well defined failure surfaces; near vertical joints	Eq. (2-27)
		S > B	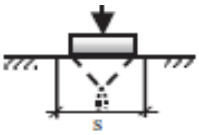	(e) Open or Closed Joints: Failure initiated by splitting leading to general shear failure; near vertical joints	Eq. (2-31)
JOINTED	20° < α < 70°	S < B or S > B if failure wedge can develop along joints	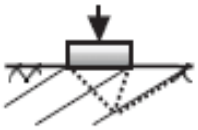	(f) General shear failure with potential for failure along joints; moderately dipping joint sets	Eq. (2-27)
LAYERED	0° < α < 20°	Limiting value of H wrt B is dependent upon material properties	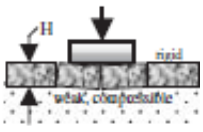	(g) Rigid layer over weak compressible layer: Failure is initiated by tensile failure caused by flexure of rigid upper layer	N/A
			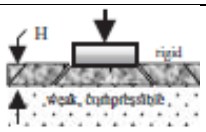	(h) Thin rigid layer over weak compressible layer: Failure is by punching shear through upper layer	N/A
FRACTURED	N/A	S << B	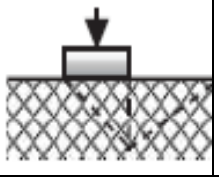	(i) General shear failure with irregular failure surface through fractured rock mass; two or more closely spaced joint sets	Eq. (2-33)

Additionally, typical rock properties required in the general bearing capacity equation are the rock mass cohesion (c′) and angle of friction (ϕ′), which can be determined from laboratory triaxial tests. Some representative ϕ′ values of rock are given in Table 2.8.

Table 2.8. Typical unconfined compressive strength and angle of friction of rock (adapted from Das 1999)

Rock Type	Unconfined Compressive Strength, q_u (ksf)	Angle of Friction, ϕ' (degree)
Sandstone	1440 – 2880	27 – 45
Limestone	2160 − 4320	30 − 40
Shale	720 − 1440	10 − 20
Granite	2880 − 4320	40 − 50
Marble	1224 − 1440	25 − 30

The end bearing of drilled shafts can be estimated using the general bearing capacity equation for soils initially proposed by Terzaghi (1943) with appropriate modifications to account for different rock mass or cohesive IGM conditions. Although the following analytical methods are presented for rock, they can be appropriately used for cohesive IGM.

The unit toe resistance for drilled shafts in intact/massive rock can be estimated using Eq. (2-24) proposed by Rowe and Armitage (1987) and recommended in AASHTO (2010) if the following criteria are met: 1) the rock from below the base of the drilled shaft to a depth of two times the shaft diameter (B) is either intact or tightly jointed with the visible joint spacing (S) much greater than the shaft diameter; and 2) the depth of the rock socket is greater than one and one-half diameters. However, O'Neill and Reese (1999) suggested limiting the unit end bearing to 2.0 q_u if the depth of the rock socket is less than one diameter. The failure mode of intact rock is indicated in Table 2.7 as (a) for brittle rock and (b) for ductile rock. The characteristics of intact rock are determined from rock specimens obtained from coring. For routine drilled shaft designs, the bearing rock is considered intact if RQD of 100% is obtained from the rock specimen (O'Neill and Reese 1999). If the RQD of rock is between 70% and 100%, all joints are closed and approximately horizontal, and the q_u value is greater than 10.4 ksf, the unit end bearing can be determined using Eq. (2-25) as suggested by O'Neill and Reese (1999).

$$q_p = 2.5\, q_u \tag{2-24}$$

$$q_p(\text{MPa}) = 4.83[q_u(\text{MPa})]^{0.51} \tag{2-25}$$

For rock mass with steeply dipping open joints (i.e., dip angle between 70° and 90°) and joint spacing smaller than the shaft diameter (failure mode c in Table 2.7), the end bearing is composed of the unconfined compressive strength of each individual rock column. Hence, the unit end bearing proposed by Sowers (1976) is taken as

$$q_p = q_u \tag{2-26}$$

For the same rock mass condition with closed joints (failure mode d in Table 2.7), the unit end bearing can be estimated using the general bearing capacity equation for circular cross sections proposed by Terzaghi (1943) as

$$q_p = c'N_c s_c + \frac{B}{2}\gamma N_\gamma s_\gamma + \gamma D N_q s_q \quad (2\text{-}27)$$

where,

c' = rock mass cohesion (ksf),
N_c = $2\sqrt{N_\phi}\left(N_\phi + 1\right)$,
N_γ = $\sqrt{N_\phi}\left(N_\phi^2 - 1\right)$,
N_q = N_ϕ^2,
N_ϕ = $\tan^2\left(45^o + \frac{\phi'}{2}\right)$,
ϕ' = rock friction angle,
s_c = $1 + \frac{N_q}{N_c}$,
s_γ = 0.6,
s_q = 1 + tan (ϕ'),
B = shaft rock-socket diameter (ft),
D = foundation depth (ft), and
γ = effective unit weight of the rock mass.

The application of Eq. (2-27) relies on the rock ϕ' and c', which are difficult to determine accurately for rock mass beneath the shaft base. These parameters can be determined from laboratory triaxial tests following the Mohr-Coulomb failure criterion or approximated using Eqs. (2-28) and (2-29) proposed by Hoek et al. (2002) for fractured rock mass, respectively.

$$\phi' = \sin^{-1}\left[\frac{6\,a\,m(s + m\sigma_3')^{a-1}}{2(1+a)(2+a) + 6\,a\,m(s + m\sigma_3')^{a-1}}\right] \quad (2\text{-}28)$$

$$c' = \frac{q_u[(1+2a)s + (1-a)m\sigma_3'](s + m\sigma_3')^{a-1}}{(1+a)(2+a)\sqrt{\frac{1 + 6\,a\,m(s + m\sigma_3')^{a-1}}{(1+a)(2+a)}}} \quad (2\text{-}29)$$

where,

q_u = rock uniaxial compressive strength,
a = empirical parameter = $\frac{1}{2} + \frac{1}{6}\left(e^{\frac{-GSI}{15}} - e^{\frac{-20}{3}}\right)$,
m = empirical parameter = $m_i \exp\left(\frac{GSI-100}{28-14D}\right)$,
m_i = empirical parameter for intact rock by rock group given in Table 2.9,
s = empirical parameter = $\exp\left(\frac{GSI-100}{9-3D}\right)$,
σ_3' = minor principal effective stresses,
GSI = geological strength index = RMR−5 for RMR greater than 23 or $(9\log_e Q' + 44)$ for RMR less than 23,

D = damage factor caused by blast damage and stress relaxation ranging from zero for undisturbed in situ rock masses to 1.0 for very disturbed rock masses (Note: no work has been published relating D to drilled shaft construction),

RMR = rock mass rating by summing all relative ratings determined in Table 2.12,

Q' = a modified tunneling quality index = $\frac{RQD}{J_n} \times \frac{J_\gamma}{J_a}$,

RQD = rock quality designation as described in Section 2.3.4,

J_n = joint parameter based on no. of sets of discontinuities (refer to Table 2.10),

J_γ = joint parameter based on roughness of discontinuities (refer to Table 2.10), and

J_a = joint parameter based on discontinuity condition & infilling (refer to Table 2.10).

Table 2.9. Values of the constant m_i by rock group (Hoek et al. 1995)

Rock Type	Class	Group	Texture			
			Coarse	**Medium**	**Fine**	**Very Fine**
Sedimentary	Clastic		Conglomerate (22)	Sandstone 19 Graywacke (18)	Siltstone 9	Claystone 4
	Non-clastic	Organic		Chalk 7 Coal (8-21)		
		Carbonate	Breccia (20)	Sparitic limestone (10)	Micritic limestone 8	-
		Chemical	-	Gypstone 16	Anhydrite 13	-
Metamorphic	Non-foliated		Marble 9	Hornfels (19)	Quartzite 24	-
	Slightly foliated		Migmatite (30)	Amphibolite 31	Mylonites (6)	-
	Foliated*		Gneiss 33	Schists (10)	Phyllites (10)	Slate 9
Igneous	Light		Granite 33	-	Rhyolite (16)	Obsidian (19)
			Granodiorite (30)	-	Dacite (17)	-
	Dark		Diorite (28)	-	Andesite (19)	-
			Gabbro 27	Dolerite (19)	Basalt (17)	-
			Norite 22	-	-	-
	Extrusive pyroclastic type		Agglomerate (20)	Breccia (18)	Tuff (15)	-

* − Value of m_i will be significantly different if failure occurs along a foliation plane; Values in parentheses are estimates.

Table 2.10. Joint parameters used to determine Q′

No. of Sets of Discontinuities	Joint Parameter J_n
Massive	0.5
One set	2
Two sets	4
Three sets	9
Four or more sets	15
Crushed rock	20

Roughness of Discontinuities	Joint Parameter J_γ
Noncontinuous joints	4
Rough, wavy	3
Smooth, wavy	2
Rough, planar	1.5
Smooth, planar	1
Slick and planar	0.5
Filled discontinuities	1

Discontinuity Condition & Filling	Joint Parameter J_a
Unfilled cases:	
Healed	0.75
Stained, no alteration	1
Silty or sandy coating	3
Clay coating	4
Filled Discontinuities:	
Sand or crushed rock infill	4
Stiff clay infilling < 0.2 in.	6
Soft clay infill < 0.2 in. thick	8
Swelling clay < 0.2 in.	12
Stiff clay infill > 0.2 in. thick	10
Soft clay infill > 0.2 in. thick	15
Swelling clay > 0.2 in.	20

Alternatively, Goodman (1980) proposed a simplified bearing capacity equation to approximate the unit end bearing of jointed rock given by

$$q_p = q_{u,design}\left(N_\phi + 1\right) \tag{2-30}$$

Unlike Eqs. (2-27) through (2-29), the unconfined compressive strength used in design ($q_{u,design}$) is taken as one-fifth of the q_u value determined from laboratory uniaxial compression tests. This reduction is attributed to the scale effect in rock caused by randomly distributed large and small fractures, and also progressive ruptures along joints, which may not be picked up by a small diameter rock specimen.

For the failure mode e in Table 2.7 (dip angle between 70° and 90° and S>B), the end bearing reaches ultimate when splitting of rock occurs and leads to general shear failure. Kulhawy and Goodman (1980) provided the following expression for the unit end bearing estimation.

$$q_p = J\, c\, N_{cr} \tag{2-31}$$

where,

- J = a correction factor that depends on the ratio of horizontal discontinuity spacing to socket diameter (H/B) as shown in Figure 2.3,
- c = rock mass cohesion can be approximated as $0.1q_u$ suggested by Kulhawy and Cater (1992) or using Eq.(2-29) for fractured rock masses (ksf),
- N_{cr} = a bearing capacity factor $= \frac{2N_\phi^2}{1+N_\phi}(\cot\phi)\frac{S}{B}\left(1-\frac{1}{N_\phi}\right) - N_\phi(\cot\phi) + 2\sqrt{N_\phi}$,
- B = shaft rock socket diameter (ft),
- S = joint spacing (ft),
- N_ϕ = $\tan^2\left(45^o + \frac{\phi}{2}\right)$, and
- ϕ = rock friction angle estimated using Eq. (2-28) for fractured rock masses.

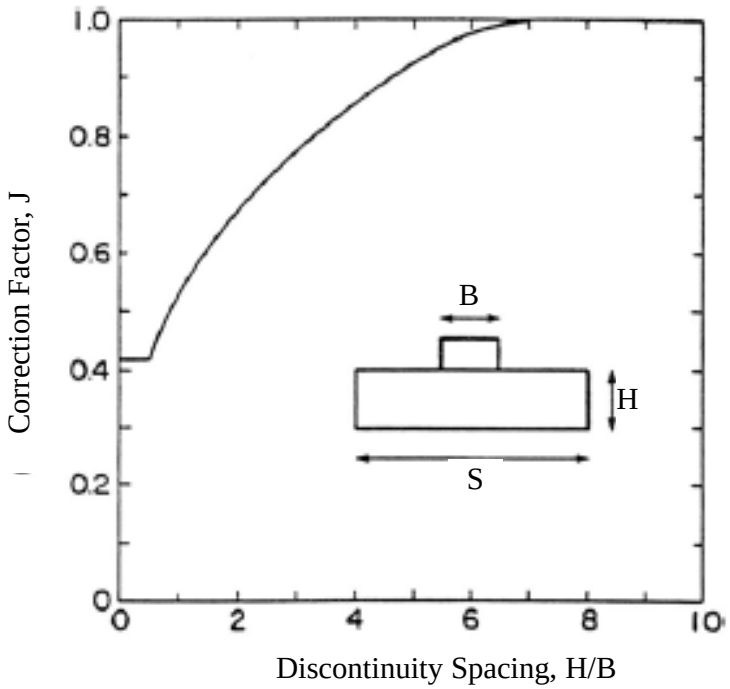

Figure 2.3. Correction factor for discontinuity spacing (adapted from Kulhawy and Carter 1992)

For base rock with moderate dipping angles between 20° and 70°, where the shear failure wedge is likely to develop along the joint planes, and the general bearing capacity Eq. (2-27) can be used to estimate unit end bearing. The accuracy of estimation will improve if the measured Rock Mass Strength (RMS) parameters (c' and ϕ') represent the jointing condition.

End bearing of drilled shafts bearing on rigid over very compressible rock layers, as shown in Table 2.7 under the failure modes g and h, has not been adequately studied due to limited test data on layered rock. Hence, no analytical method is currently available in the literature to estimate the unit end bearing. Turner (2006) related the failure modes to the relative thickness of the rigid layer. Failure mode g induced by flexure of the rigid upper layer occurs if the rigid layer is relatively thick while failure mode h occurs by punching shear of the rigid upper layer if the rigid layer is thin.

If the rock at the base of the drilled shaft is fractured (i.e., jointed with random joint orientation) as shown in Table 2.7 under failure mode i, the unit end bearing can be estimated using the general bearing capacity Eq. (2-27) in terms of the RMS parameters (c' and ϕ'). However, these parameters cannot be directly quantified from nonlinear Mohr-Coulomb failure envelopes generated using laboratory triaxial tests on fractured rock masses. Alternatively, these parameters can be approximated using Eqs. (2-28) and (2-29) and substituted into Eq. (2-27) to estimate the unit end bearing. To improve the lengthy computational process, Carter and Kulhawy (1988) adopted the Hoek-Brown (1988) strength criterion given by Eq.(2-32) in terms of empirical parameters (a, m, and s) and assumed the minor principal stress (σ_3') be zero in the adjacent passive failure Zone 2, as illustrated in Figure 2.4. Substituting $\sigma_3' = 0$ in Eq. (2-32), the minor principal stress (σ_3') in Zone 1, which is also the major principal stress (σ_1') in Zone 2, in order to satisfy equilibrium, equals s^a. When substituting $\sigma_3' = s^a$ into Eq. (2-32), the unit end bearing is obtained from Eq. (2-33), which will be a conservative, lower bound estimate due to the assumption $\sigma_3'=0$.

$$q_p = \sigma_1' = \sigma_3' + q_u \left(m \frac{\sigma_3'}{q_u} + s \right)^a \tag{2-32}$$

$$q_p = [s^a + (m\, s^a + s)^a]\, q_u \tag{2-33}$$

where,

q_u = rock uniaxial compressive strength,

a = empirical parameter = $\frac{1}{2} + \frac{1}{6}\left(e^{\frac{-GSI}{15}} - e^{\frac{-20}{3}}\right)$,

m = empirical parameter = $m_i \exp\left(\frac{GSI-100}{28-14D}\right)$,

m_i = empirical parameter for intact rock by rock group given in Table 2.9, and

s = empirical parameter = $\exp\left(\frac{GSI-100}{9-3D}\right)$,

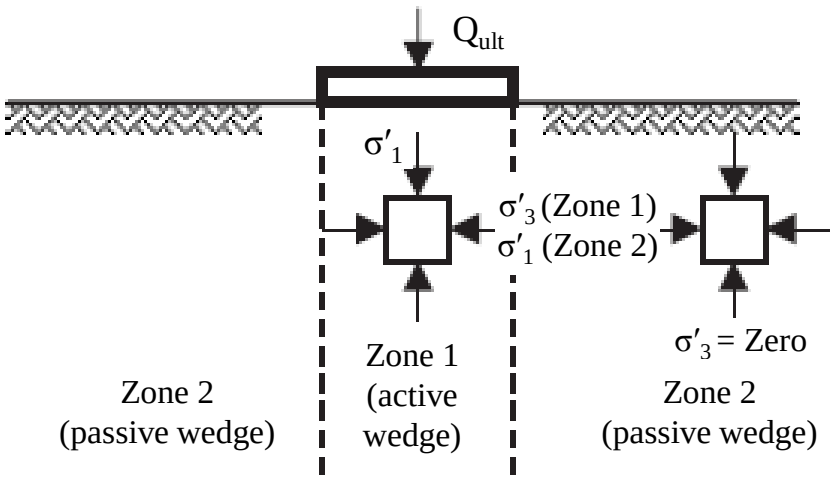

Figure 2.4. Bearing capacity analysis (after Turner 2006)

Figure 2.5 shows that the empirical parameter "a" can be approximated as 0.50 for all GSI values. Hence, Eq. (2-33) can be simplified to Eq. (2-34) as recommended in AASHTO (2010) for the fractured rock mass. To facilitate the application of this end bearing Eq. (2-34), the empirical parameters m and s can be determined from Table 2.11 based on rock type and Rock Mass Rating (RMR) calculated by adding all the corresponding relative ratings given in Table 2.12.

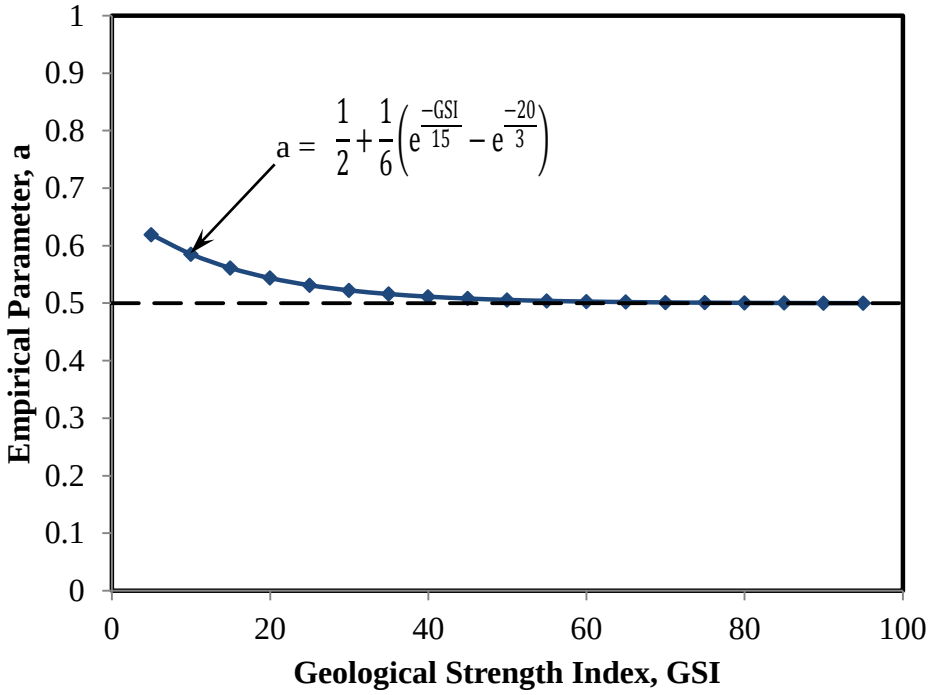

Figure 2.5. Relationship between empirical parameter a and GSI

$$q_p = \left[\sqrt{s} + \sqrt{\left(m\sqrt{s} + s\right)}\right] q_u \qquad (2\text{-}34)$$

where

q_u = uniaxial compressive strength of rock (ksf),
s, m = fractured rock mass parameters (refer to Table 2.11), and
RMR = rock-mass rating determined by summing all the relative ratings obtained in Table 2.12.

Table 2.11. Approximate relationship between rock-mass quality and fractured rock-mass parameters used in defining nonlinear strength (adapted from Hoek and Brown 1988)

Rock Quality	Parameters	Rock Type A = Carbonate rocks with well developed crystal cleavage: dolomite, limestone and marble B = Lithified argrillaceous rocks: mudstone, siltstone, shale and slate (normal to cleavage) C = Arenaceous rocks with strong crystals and poorly developed crystal cleavage: sandstone and quartzite D = Fine grained polymineralic igneous crystalline rocks: andesite, dolerite, diabase and rhyolite E = Coarse grained polymineralic igneous & metamorphic crystalline rocks: amphibolite, gabbro gneiss, granite, norite, quartz-diorite				
		A	B	C	D	E
INTACT ROCK SAMPLES Laboratory size specimens free from discontinuities. RMR = 100	m s	7.00 1.00	10.00 1.00	15.00 1.00	17.00 1.00	25.00 1.00
VERY GOOD QUALITY ROCK MASS Tightly interlocking undisturbed rock with unweathered joint at 3 to 10 ft. RMR = 85	m s	2.40 0.082	3.43 0.082	5.14 0.082	5.82 0.082	8.567 0.082
GOOD QUALITY ROCK MASS Fresh to slightly weathered rock, slightly disturbed with joints at 3 to 10 ft. RMR = 65	m s	0.575 0.00293	0.821 0.00293	1.231 0.00293	1.395 0.00293	2.052 0.00293
FAIR QUALITY ROCK MASS Several sets of moderately weathered joints spaced at 1 to 3 ft. RMR = 44	m s	0.128 0.00009	0.183 0.00009	0.275 0.00009	0.311 0.00009	0.458 0.00009
POOR QUALITY ROCK MASS Numerous weathered joints at 2 to 12 in.; some gouge. Clean compacted waste rock. RMR = 23	m s	0.029 3×10^{-6}	0.041 3×10^{-6}	0.061 3×10^{-6}	0.069 3×10^{-6}	0.102 3×10^{-6}
VERY POOR QUALITY ROCK MASS Numerous heavily weathered joints spaced < 2 in. with gouge. Waste rock with fines. RMR = 3	m s	0.007 1×10^{-7}	0.010 1×10^{-7}	0.015 1×10^{-7}	0.017 1×10^{-7}	0.025 1×10^{-7}

Table 2.12. Geomechanics classification of rock-masses (Adapted from AASHTO, 2010)

	Parameter		Ranges of Values						
1	Strength of intact rock material	Point load strength index	> 175 ksf	85 – 175 ksf	45 – 85 ksf	20 – 45 ksf	For this low range, uniaxial compressive test is preferred		
		Uniaxial compressive strength, q_u	> 4320 ksf	2160 – 4320 ksf	1080 – 2160 ksf	520 – 1080 ksf	215 – 520 ksf	70 – 215 ksf	20 – 70 ksf
	Relative Rating		15	12	7	4	2	1	0
2	Drill core quality RQD		90% to 100%	75% to 90%		50% to 75%		25% to 50%	< 25%
	Relative Rating		20	17		13		8	3
3	Spacing of joints		> 10 ft	3 – 10 ft		1 – 3 ft		2 in – 1 ft	< 2 in
	Relative Rating		30	25		20		10	5
4	Condition of joints		• Very rough surface • Not continuous • No separation • Hard joint wall rock	• Slightly rough surfaces • Separation < 0.05 in • Hard joint wall rock		• Slightly rough surface • Separation < 0.05 in • Soft joint wall rock		• Slicken-sided surface or • Gouge < 0.2 in thick or • Joints open 0.05 – 0.2 in • Continuous joints	• Soft gouge > 0.2 in thick or • Joints open > 0.2 in • Continuous joints
	Relative Rating		25	20		12		6	0
5	Ground water conditions (use one of the three) evaluation criteria as appropriate to the method of exploration	Inflow per 30 ft tunnel length	None	< 400 gal./hr		400 – 2000 gal./hr		> 2000 gal./hr	
		Ratio = joint water pressure/ major principal stress	0	0.0 – 0.2		0.2 – 0.5		> 0.5	
		General conditions	Completely Dry	Moist only (interstitial water)		Water under moderate pressure		Severe water problems	
	Relative Rating		10	7		4		0	

Table 2.7 shows that different analytical methods can be used to estimate unit end bearing if the rock mass conditions beneath the drilled shaft, such as spacing, condition and orientation of rock discontinuities, and strength of the rock mass, can be identified from subsurface investigations and made known to designers. Unfortunately, due to limited budgetary allocation to subsurface investigations, especially rock and IGM testing, it is always a challenge to accurately and confidently estimate the end bearing of drilled shafts in these geomaterials. Despite the fact that many different analytical methods are available in literature, only Eq. (2-24) for intact rock and Eq. (2-33) for fractured rock are recommended in AASHTO (2010). The estimated end bearing (R_p) shall not exceed the structural resistance (R_{sp}) of a short, reinforced concrete drilled shaft subjected to only compressive axial load given by

$$R_p \leq R_{sp} = \beta\left[0.85f'_c\left(A_g - A_s\right) + A_s f_y\right] \quad (2\text{-}35)$$

where

β = reduction factor, 0.85 for spiral reinforcement and 0.80 for tie reinforcement,
f'_c = specified minimum 28-day compressive strength of concrete,
A_g = gross area of drilled shaft section,
A_s = total area of longitudinal steel reinforcement, and
f_y = specified yield strength of steel reinforcement.

Refer to the FHWA guidelines by Brown et al. (2010) for a complete description of the structural design of drilled shafts.

2.4.6. Base Grouting

Base grouting is a mechanical process of injecting water-cement grout under pressure at the base of the shaft to improve the end bearing capacity of drilled shafts in cohesionless soils or to densify loose sediments left at the base after borehole excavation and base cleaning operations (Brown et al. 2010). There is no reliable design method at present to estimate grouted end bearing, and no LRFD resistance factors have been established for this application. Nevertheless, the total unit end bearing including the effect of base grouting in cohesionless soils recommended by Mullins et al. (2006) can be estimated by

$$q_{p,total} = (TCM) \times q_{p,un-grouted}[\text{Eq. } (2.21)] \quad (2\text{-}36)$$

where,

TCM = tip capacity multiplier = $0.713 \times GPI\left(\frac{\delta_t}{B}\%\right)^{0.364} + \left[\frac{\frac{\delta}{B}\%}{0.4\left(\frac{\delta}{B}\%\right)+3}\right]$,
δ_t = tolerable settlement of the shaft (ft),
B = shaft diameter (ft),
GPI = grout pressure index = $\frac{GP_{max}}{q_{p,\ un\text{-}grouted}}$,
GP_{max} = anticipated maximum grout pressure (ksf) = $\frac{R_s}{A_{shaft}}$,
R_s = nominal side resistance for the total length of embedded shaft (kip), and
A_{shaft} = cross-sectional area of the shaft (ft^2).

For both grouted and un-grouted unit end bearing that correspond to 5% of the base diameter (i.e., $\frac{\delta_t}{B}\% = 5\%$), the total unit end bearing can be simplified to

$$q_{p,total} = (1 + 1.28\ GPI) \times q_{p,un-grouted}[\text{Eq. } (2.21)] \quad (2\text{-}37)$$

2.5. Construction Methods

2.5.1 Introduction

Drilled shafts are referred to as non-displacement deep foundations that are constructed by excavating a borehole using mechanical auger drill equipment, and the resulting cylindrical void is filled with reinforced concrete. The anticipated performance of drilled shafts is related to the selection of an appropriate construction method and the proper execution of the construction method. The selection of a construction method is governed by subsurface conditions, local construction practices and experience, and economic factors. An effective execution of a construction method following appropriate construction specifications and inspection techniques will minimize any adverse effects on the supporting geomaterials and ensure the integrity of the drilled shaft. It is common in practice to design drilled shafts based on a specified construction method. Construction procedures of drilled shafts can be generally categorized as one of three methods as summarized in Table 2.13.

Table 2.13. Construction methods for drilled shafts

Construction Method	Subsurface Conditions	General Remarks
Dry method	Strong cohesive soil with low permeability, IGM, or rock with no presence of groundwater or above water table; minimal water seepage	Least expensive and allow visual inspection
Casing method	Caving geomaterials; below or above water table	Three construction sequences; permanent or temporary casing; expensive
Wet method	Soil with high permeability and seepage; boreholes with water; high water table	Moderately expensive

2.5.2 Dry Method

The dry method is suitable for firm clay with low permeability and for IGM and rock that will not cave into the open hole during the drilled shaft construction. The dry method is normally used for geomaterials above water the table or with minimal seepage that will not adversely affect the stability of the excavation. Dry construction allows visual inspection of the borehole and is the least expensive of the three methods. The dry construction sequence is illustrated in Figure 2.6.

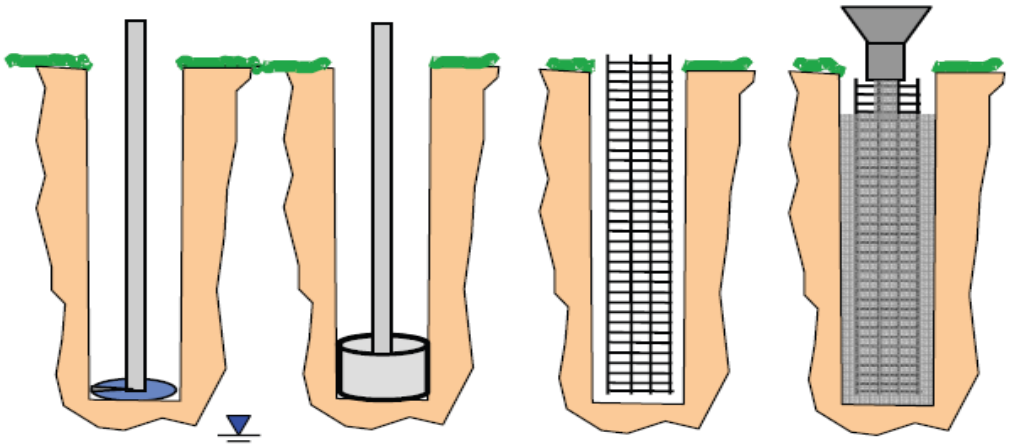

(a) (b) (c) (d)

Figure 2.6. Dry method of construction: (a) drill the hole; (b) clean the base; (c) place reinforcement; and (d) place concrete (Brown et al. 2010)

2.5.3 Casing Method

If caving of geomaterials in a borehole or excessive lateral deformation toward the shaft cavity is anticipated, construction of drilled shafts using casing should be implemented. If the casing can be socketed in an impermeable layer at the bottom of casing, this construction method can be used to seal the borehole against groundwater entry. Casing can be used in karstic soils where caves are present below grade and in excavations through water. Casing is mostly made of steel and is either placed permanently into the ground as a structural element or retrieved after placing the concrete. Casing can be installed or retrieved with a vibratory hammer or oscillator. There are three construction procedures using the casing method: (1) begin excavation using the dry method and then install the casing into the hole to prevent any caving during construction; (2) begin excavation using a starter hole filled with slurry and install the casing to the bearing stratum as shown in Figure 2.7; and (3) install casing in advance before excavation as illustrated in Figure 2.8. If the casing is left permanently in the soil as a structural element, the unit side resistance estimated using the analytical methods described in Section 2.3 should be reduced. However, there are no specific data reported in literature regarding the reduction in side resistance. A comparative study conducted by Potyondy (1961) concluded that the side resistance reduction factors for driven steel piles relative to concrete piles can vary from 50% to 75%, depending on whether the steel is clean or rusty, respectively.

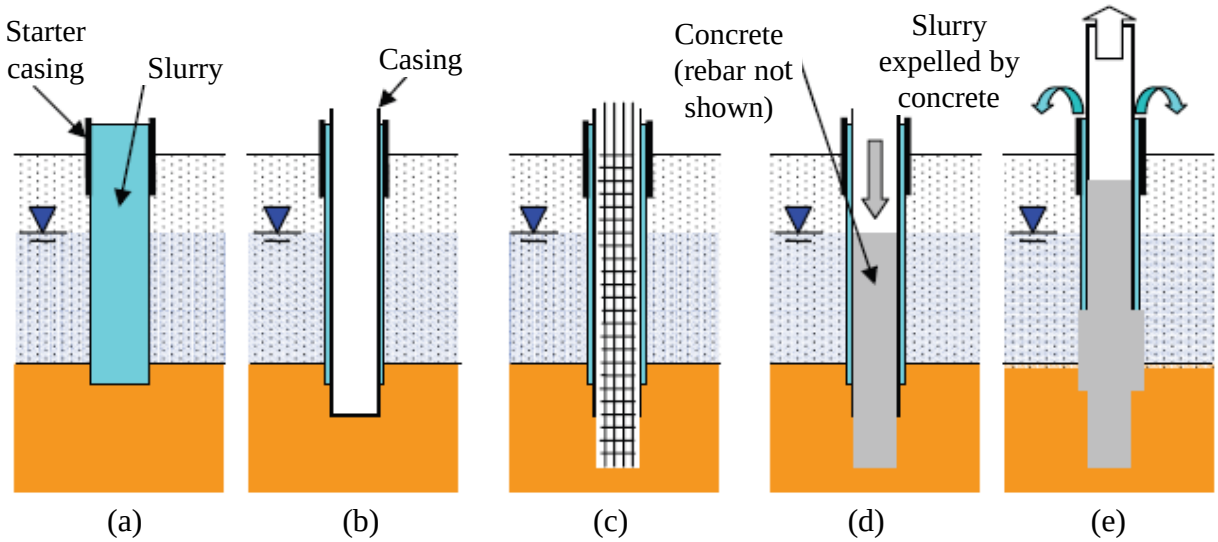

Figure 2.7. Construction using casing through slurry-filled starter hole: (a) drill with slurry; (b) set casing and bail slurry; (c) complete and clean excavation, set reinforcing; (d) place concrete to head greater than external water pressure; (e) pull casing while adding concrete (adapted from Brown et al. 2010)

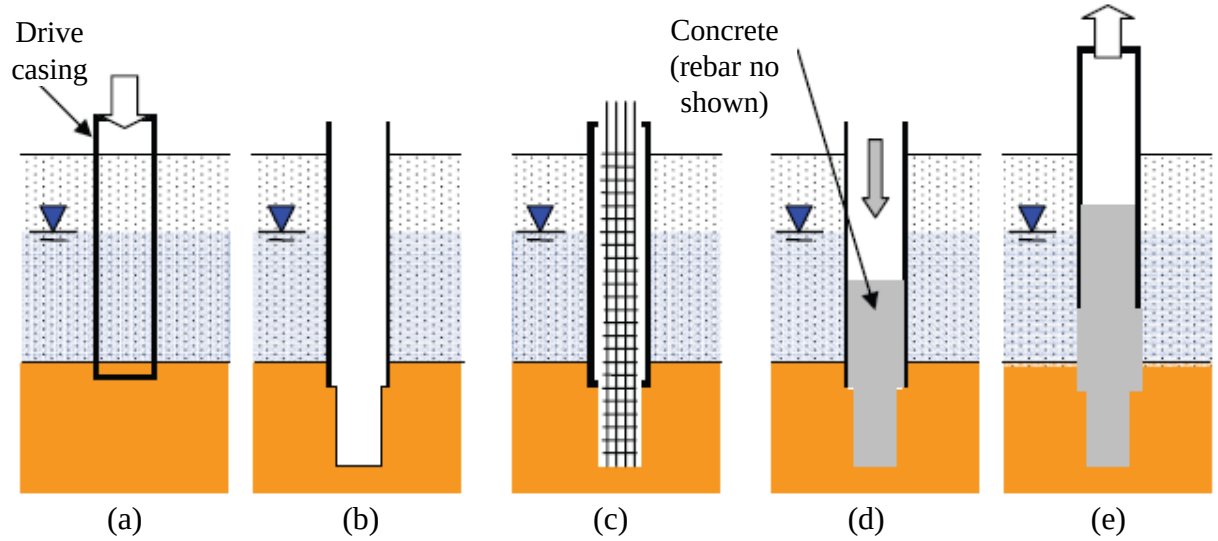

Figure 2.8. Construction using casing advanced ahead of excavation: (a) drive casing into bearing stratum; (b) drill through casing; (c) complete and clean hole, set reinforcing; (d) place concrete to head greater than external water pressure; (e) pull casing while adding concrete (Brown et al. 2010)

2.5.4 Wet Method

The wet method is applicable to situations where the casing cannot adequately keep the groundwater out of the shaft borehole, or casing cannot be installed to stabilize the shaft borehole. Wet construction utilizes drilling slurry, such as a mixture of bentonite, water and/or admixture, to maintain the stability of the shaft hole and exert a seepage pressure against the groundwater pressure. To prevent caving due to the inflow of groundwater, the slurry pressure

head should be kept at least 5 ft higher than the hydraulic head of the groundwater. The following construction practices suggested by Bowles (1996) should be considered when using wet method:

- Do not leave slurry in the shaft for a long time so that an excessively thick filter cake forms on the shaft walls and is difficult to be replaced with concrete. This will reduce the effectiveness of the side resistance.
- Screen out the larger particles in slurry suspension before concreting.
- Excavation of clay through slurry should be performed carefully to prevent the development of sufficient negative pore pressure or suction that will induce shaft collapse.

The wet method is normally preferred over permanent casing due to the lower cost. The construction sequence using the wet method is illustrated in Figure 2.9.

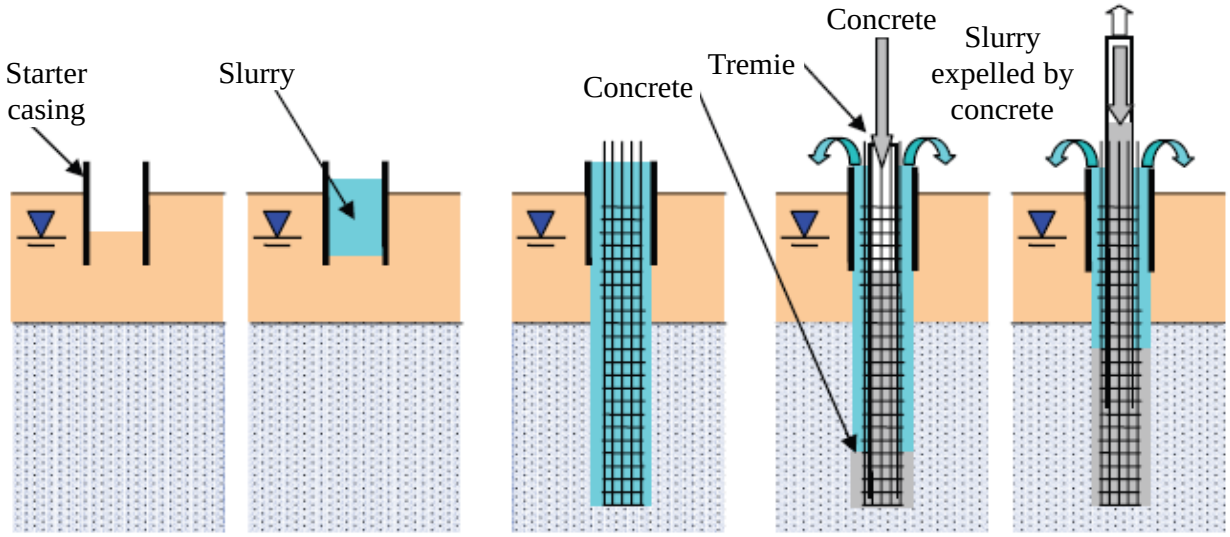

Figure 2.9. Slurry drilling process: (a) set starter casing; (b) fill with slurry; (c) complete and clean excavation, set reinforcing; (d) place concrete through tremie; and (e) pull tremie while adding concrete, optionally remove casing (adapted from Brown et al. 2010)

2.6. Field Axial Load Tests

2.6.1. Introduction

Despite the available analytical methods described in Sections 2.3 and 2.4 to estimate the resistances of drilled shafts based on correlated and/or measured geomaterial properties, the most reliable method to determine the resistance of a drilled shaft is to perform a load test. Field axial load tests are performed to serve two general purposes:

1) Load transfer test: To measure the distribution of side resistance and end bearing to further improve the design
2) Proof test: To verify if the constructed drilled shaft has the design capacity and meets the specified serviceability requirement

Field load tests can be performed at various stages of a drilled shaft project, and there are benefits and limitations associated with each stage. Additional information on various stages of

load tests can be found in the FHWA guidelines on drilled shafts by Brown et al. (2010). Performing load tests is a challenge, since drilled shafts carry a substantial axial load, and a higher capacity test frame or loading mechanism is needed. The location and number of test shafts are decided based on 1) the variability of the subsurface geology; 2) the objectives of test programs; 3) characteristics of the supporting structures; 4) the variability of the geomaterial properties; and 5) type of construction procedures. Four test methods: 1) top-down static load test; 2) Osterberg load test; 3) rapid load test; and 4) high-strain dynamic load test are currently available and chosen for load testing drilled shafts depending on the most important objectives of the test program. Each test method has advantages and limitations, and a brief delineation is provided in the following subsections.

2.6.2. Top-Down Static Load Test

Top-down static load tests directly measure the axial capacity of a constructed drilled shaft by applying a vertical axial compressive load on top of the drilled shaft using a hydraulic jack acting against a supported weight platform or a reaction girder restrained by anchor piles. Top displacement is measured concurrently with the applied load to generate a top-load displacement curve from which the ultimate capacity is determined. Depending on test objectives, strain gauges can be instrumented along the steel cage to measure the load distribution at every load increment while "telltale" displacement rods can be installed to measure the base movement. Vertical static load tests are generally performed in accordance with the American Society for Testing and Materials (ASTM) standard D1143 (2007). Top-down static load tests require multiple days for setting up and performing the tests. As the drilled shaft capacity gets larger, a larger capacity and more expensive testing system is required. The distributed load decreases from the top to the base, where most drilled shafts are socketed in IGM or rock, and the reduced load near the base may not be sufficiently large to fully mobilize the end bearing and side friction against IGM or rock.

2.6.3. Osterberg Load Test

The Osterberg load cell (O-cell) test is a bi-directional loading test developed by Jorj Osterberg (1992, 1994) and exclusively provided by Loadtest, Inc. Before concreting the shaft, one or more hydraulic jacks are attached to and between upper and lower steel bearing plate, which together comprise the O-cell. The O-cell is tack-welded to the steel cage and placed inside a shaft hole as illustrated in Figure 2.10.

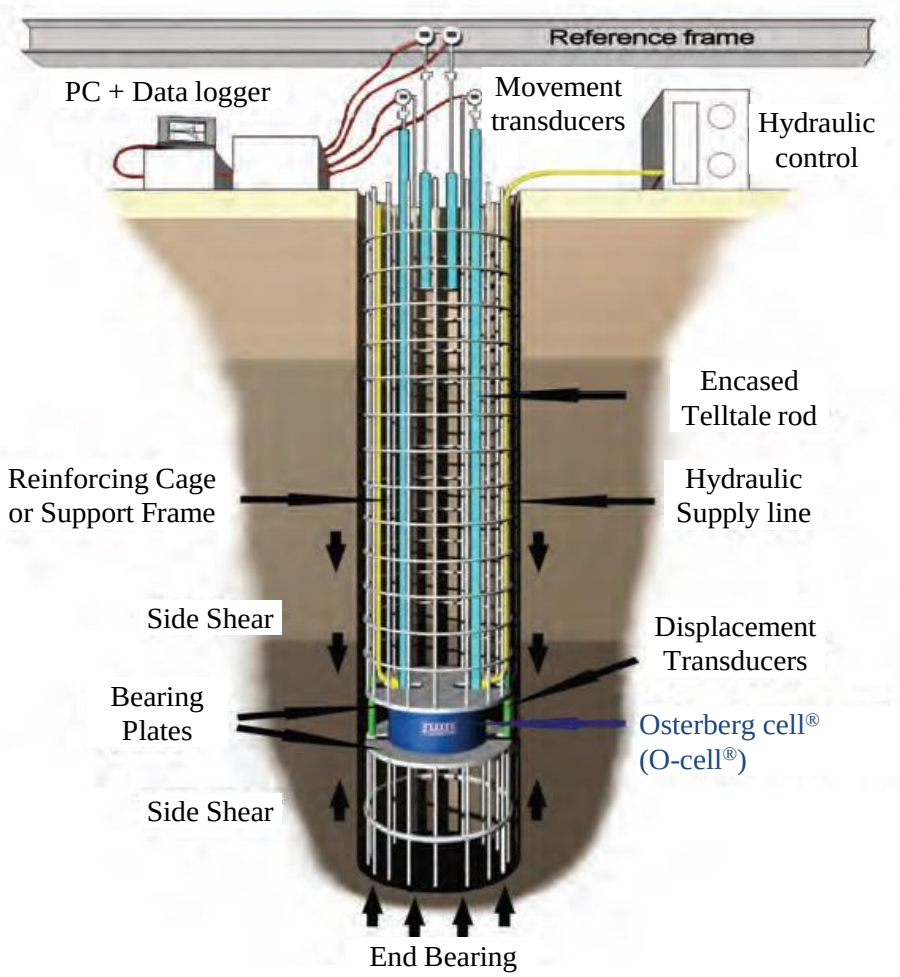

Figure 2.10. O-cell testing schematic (adapted from Loadtest, Inc.)

After placing the concrete with sufficient curing, the O-cell is pressurized to incrementally apply bi-directional load to the upper and lower shaft sections. Both the downward movement of the O-cell bottom plate and the upward movement of the O-cell upper plate are measured using telltale rods located within the shaft and extending to the ground surface where data is recorded. Additionally, the top-of-shaft displacement is measured using survey levels, and shaft strains are measured along the shaft.

A single O-cell determines the ultimate end bearing and/or the ultimate side resistance, since both resistances are used as reactions to test each other. Hence, it is important to locate the O-cell at an optimum location where the upper and lower resistances are approximately equal. If the O-cell is situated at a location where the upper resistance is higher than the lower resistance, the lower resistance will reach its ultimate value before the upper resistance is fully mobilized as illustrated in Figure 2.11, or vice-versa as illustrated in Figure 2.12.

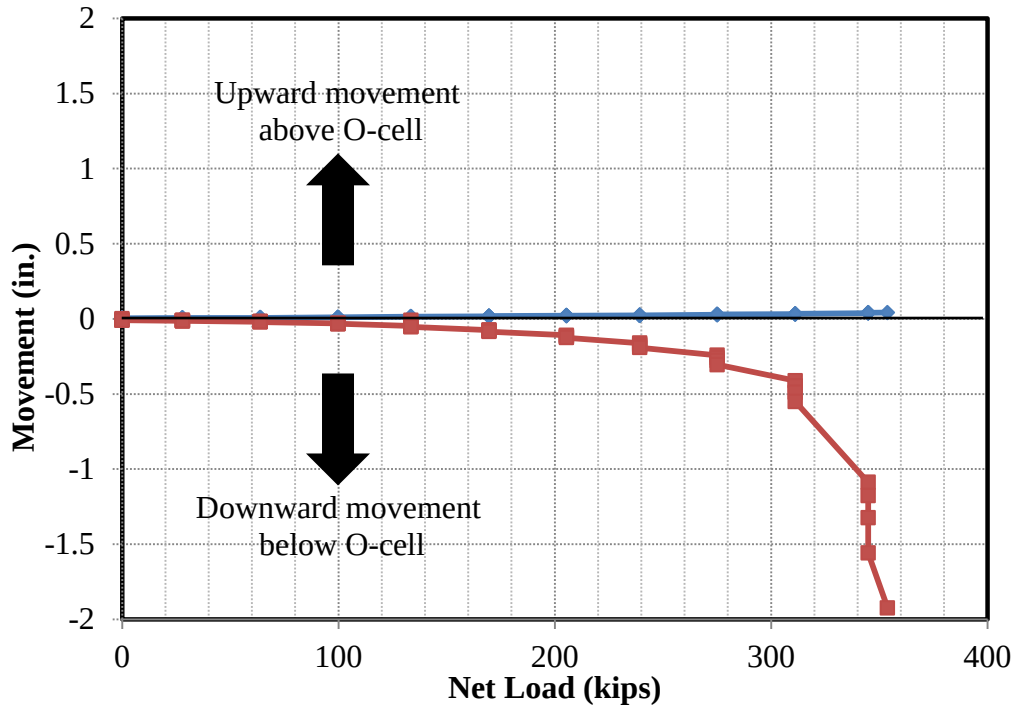

Figure 2.11. Example of O-cell test in which resistance reaches ultimate capacity

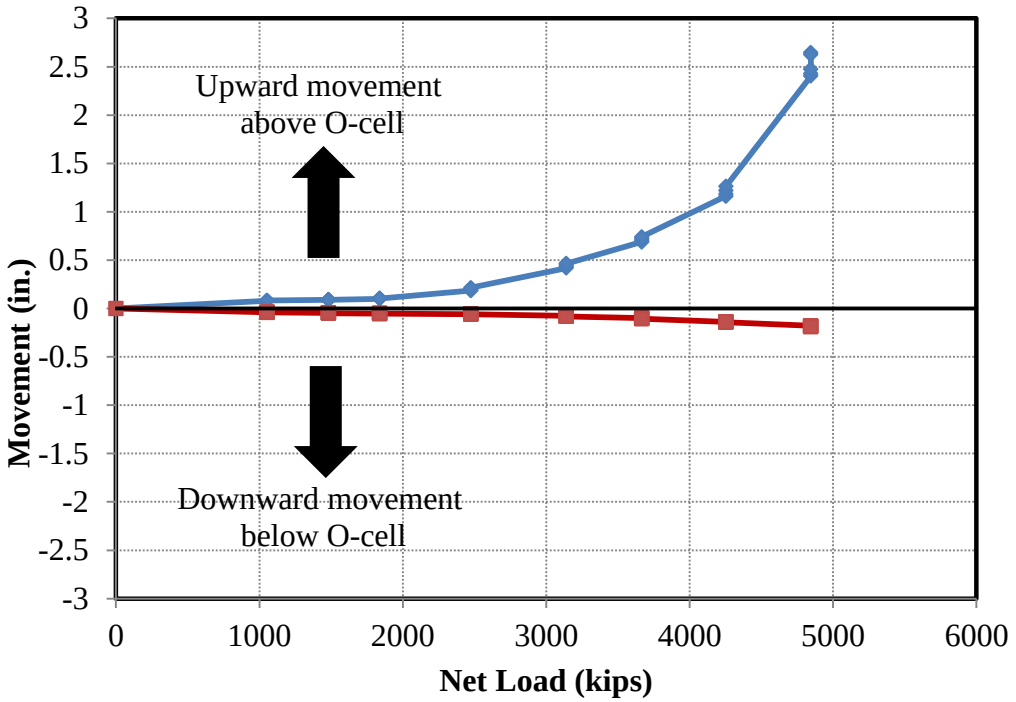

Figure 2.12. Example of O-cell test in which upper resistance reaches ultimate capacity

In some cases with rock-socketed drilled shafts, the O-cell reaches its maximum available capacity before either the upper or lower resistance reaches its ultimate value as illustrated in Figure 2.13.

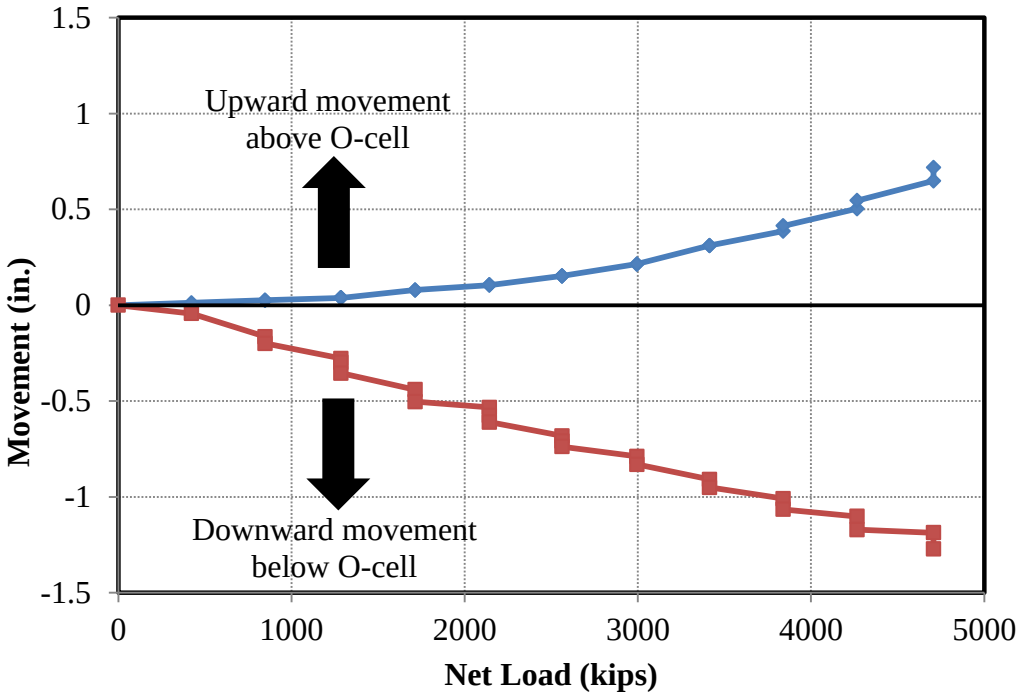

Figure 2.13. Example of O-cell test in which neither upper nor lower resistance reaches ultimate capacity

The design of the O-cell system is highly dependent on the objective of the test program. For instance, if the end bearing is the interest of investigation, test results shown in Figure 2.11 are sufficient even without fully mobilizing the side resistance. If measurements are needed at various segments of a drilled shaft to obtain a smooth and more precise load distribution, O-cell testing can be performed at multiple locations along the shaft, as illustrated in Figure 2.14 for a drilled shaft in Florida limestone.

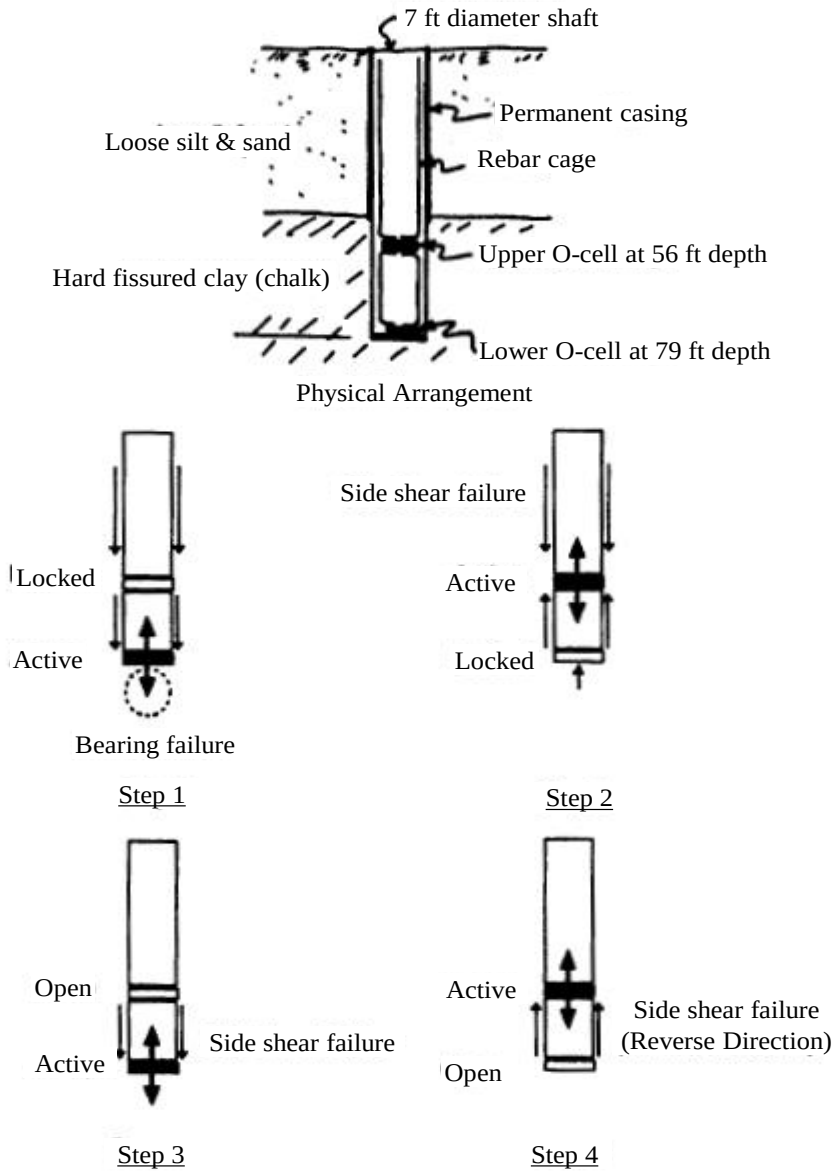

Figure 2.14. Testing arrangement of multiple O-cells (adapted from O'Neill et al. 1996)

O-cell test results given in Figure 2.15 as an example can be used to estimate an equivalent top-loaded displacement curve as shown in Figure 2.16, from which the ultimate total axial resistance of the drilled shaft can be determined.

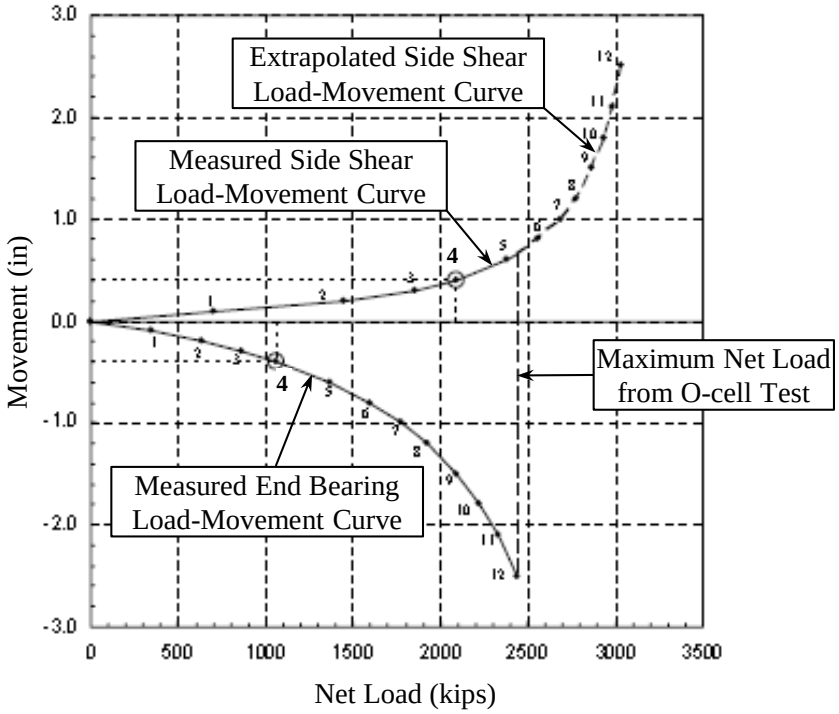

Figure 2.15. Example of measured and extrapolated O-cell load-displacement curves (Loadtest, Inc. 2006)

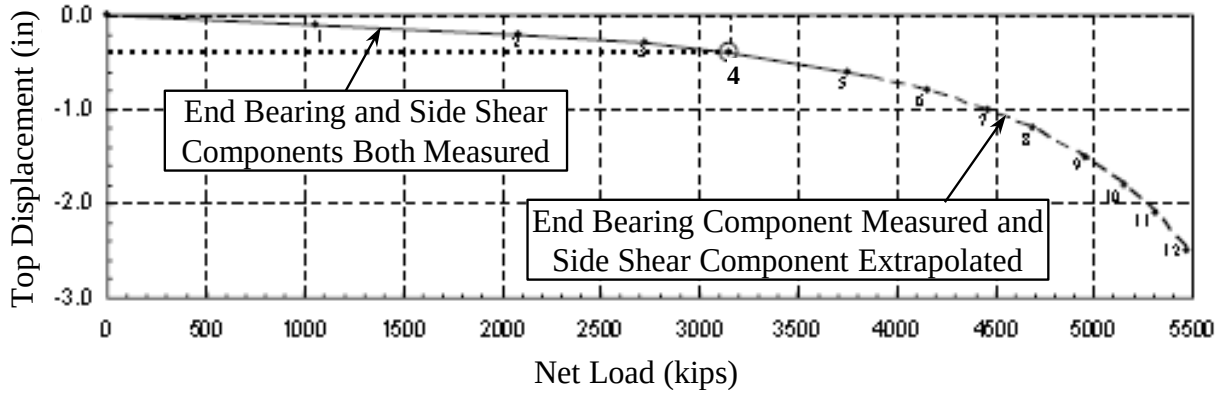

Figure 2.16. Equivalent top-loaded displacement curve based on O-cell data given in Figure 2.15 (Loadtest, Inc. 2006)

The assumptions considered in constructing the equivalent top-loaded displacement curve are as follows:

1) Initially assume the drilled shaft as a rigid element, then include the elastic compression in the equivalent top displacement calculation
2) The end bearing-displacement curve obtained from a top-loaded static test is identical to that obtained from the O-cell test
3) The shaft below the O-cell has the same side-resistance load-displacement behavior as when top-loading the entire shaft
4) The side resistance-displacement curve obtained from a top-loaded static test has the same net side resistance, multiplied by an adjustment factor (F) for a given downward

movement as occurred in the O-cell test for the same upward displacement of the upper O-cell plate. The recommended adjustment factors are 1) 1.00 for all rock socketed drilled shafts and primarily cohesive soils in compression; 2) 0.95 for all drilled shafts in primarily cohesionless soils; and 3) 0.80 for all drilled shafts in top load tension tests.

The initial procedure determines the equivalent top-loaded displacement curve for a rigid shaft by summing the upward and downward net loads that correspond to the same movement as illustrated by point 4 in Figure 2.15 and 2.16. The later procedure includes the elastic compression of the drilled shaft in the initially determined equivalent top displacement. A detailed description of the procedure is included in Appendix A. The advantages and limitations of O-cell tests are summarized in Table 2.14.

Table 2.14. Advantages and limitations of O-cell load tests

Advantages	Limitations
• Ability to test high capacity production or test drilled shafts • Ability to test at select segments of a drilled shaft • Allows investigation of creep effects	• Pre-arrangement of test setup is required • Does not allow testing on existing drilled shafts • The accuracy of the equivalent top-load displacement response may depend how the data ineterpretaion • Discrepancy in skin resistance associated with upward loading vs. downward loading is not completely known, but treated with adjustment factors • High cost

2.6.4. Rapid Load Test

A rapid load test using Statnamic device is performed by generating a gas pressure from pelletized fuel combustion that accelerates a reaction mass of about 5% to 10 % of the test load upward and imposes an equal and opposite impulsive load at a sufficient duration ranging between 80 ms and 300 ms on a test shaft. Figure 2.17 shows the schematic of the Statnamic equipment and test setup.

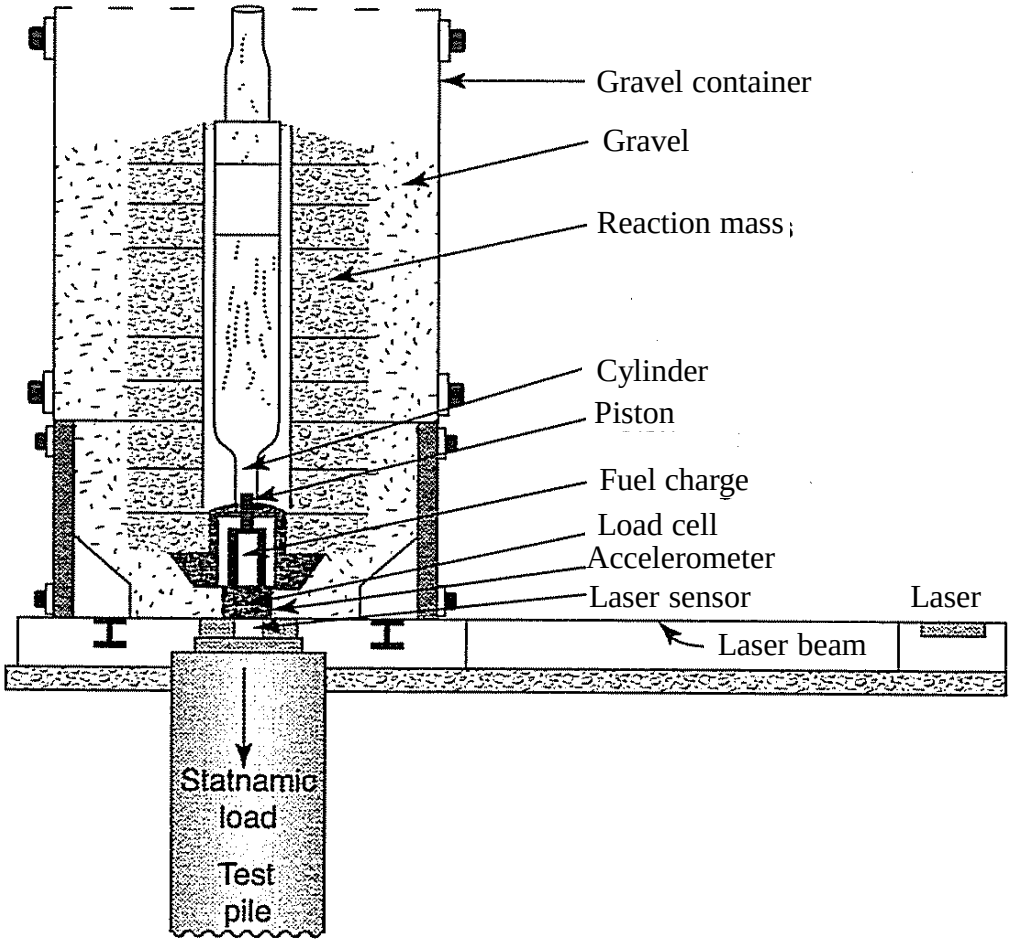

Figure 2.17. Schematic of Statnamic equipment and test setup (adapted from McCarthy 2007)

During testing, the magnitude of the impulsive load transmitted to the shaft is measured and recorded using a load cell, the shaft head downward acceleration is measured using servo-accelerometers mounted on the shaft, and the shaft vertical displacement is measured using a photovoltaic sensor mounted with the load cell. These measurements are measured and recorded as a function of time as shown in Figure 2.18.

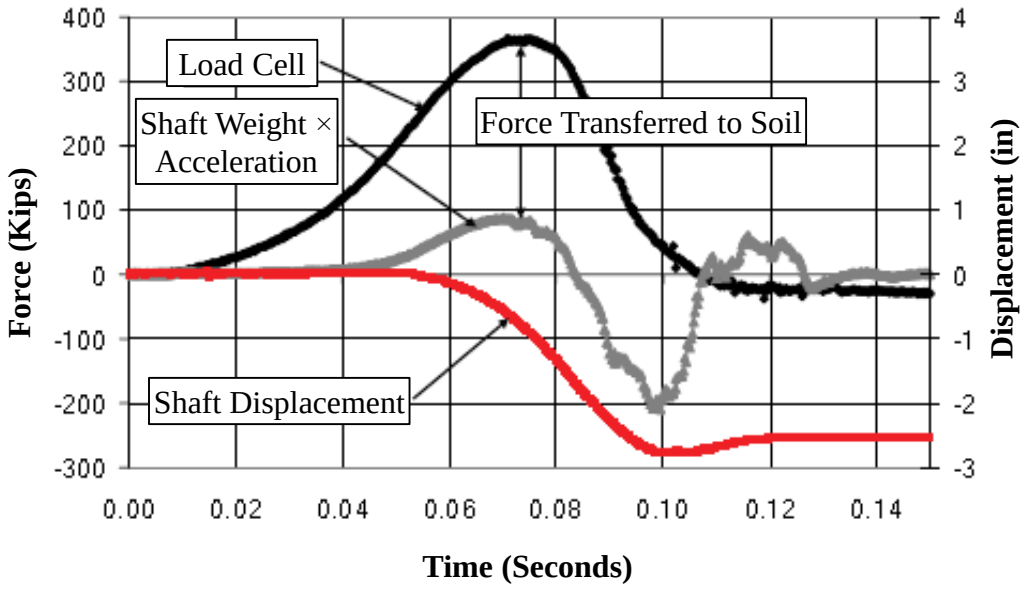

Figure 2.18. Example of force, acceleration and displacement measurements during a rapid load test (Brown et al. 2010)

The force transferred to the soil is the difference between the measured force (F_{stn}) and an inertial force (F_a), which is the product of the measured acceleration (a) and the mass of the shaft (m). The force transferred to the soil is resisted by both the static (F_s) and the dynamic (F_d) resistances due to the fact that the shaft is in a downward motion during testing. The equation of motion can be written as

$$F_{stn} = F_a + F_d + F_s = m\,a(t) + c\,v(t) + k\,u(t) \tag{2-38}$$

where,

c = damping coefficient (kip-s/in.),
v(t) = shaft velocity (in./s),
k = soil-pile stiffness (kip/in.), and
u(t) = shaft displacement (in).

The static resistance (F_s) can be determined from a rearranged form of Eq. (2-38):

$$F_s = F_{stn} - (F_a - F_d) = F_{stn} - m\,a(t) - c\,v(t) \tag{2-39}$$

This rapid load test using the Statnamic device shall be performed in accordance with ASTM standard D-7383 (2008). The advantages and limitations associated with using the rapid load test for drilled shafts are summarized in Table 2.15.

Table 2.15. Advantages and limitations of rapid load testing

Advantages	Limitations
• Ability to test do both production and test drilled shafts with relatively high capacity • Apply testing load on top of drilled shafts • Economies of scale for multiple tests • Does not require reaction system	• Duration and cost of mobilization • Test load limit 5000 tons • The rate of loading must be considered in the resistance estimation

2.6.5. High-Strain Dynamic Load Test

The high strain dynamic load test method was originally developed to determine the performance of driven piles and has been incorporated into a standard test specification for deep foundations by the ASTM D4945 (2008). A data acquisition system known as the Pile Driving Analyzer (PDA) was developed by Goble et al. (1975) using the Case method to measure strains and accelerations when a hammer or drop weight impact load is applied on the shaft. The PDA converts the strain and acceleration signals to force and velocity records as a function of time. For an ideal, uniform, elastic shaft with no resistance effects on the shaft, the relationship between the force and the velocity can be expressed by

$$F(t) = \left(\frac{EA}{C}\right) v(t) = Z\, v(t) \tag{2-40}$$

where,

$F(t)$ = force in a uniform shaft (kip),
E = elastic modulus of a uniform shaft (ksi),
A = cross-sectional area of a uniform shaft (in^2),
$v(t)$ = particle velocity in a uniform shaft (ft/s),
C = wave speed of a uniform shaft = $\sqrt{\frac{E}{\rho}}$, (ft/s),
ρ = mass density of a uniform shaft (kip-s^2/ft^4), and
Z = shaft impedance (kip-s/ft).

Using the theory of wave propagation and assuming the dynamic soil resistance is a linear function of viscous damping and pile toe velocity (Rausche 1985), the Case method was developed to determine the static soil resistance of the drilled shaft given by

$$R_s = \frac{1}{2}\left\{(1 - J_c)\left[F_T(t_m) + \frac{EA}{C} v_T(t_m)\right] + (1 + J_c)\left[F_T\left(t_m + \frac{2L}{C}\right) - \frac{EA}{C} v_T\left(t_m + \frac{2L}{C}\right)\right]\right\} \tag{2-41}$$

where,

R_s = maximum static soil resistance (kip),
t_m = time when maximum total resistance occurs (s),
$F_T(t_m)$ = measured force near pile top at time t_m (kip),
$v_T(t_m)$ = measured velocity near pile top at time t_m (ft/s),
J_c = dimensionless Case damping factor,

C = pile wave speed (ft/s),
E = modulus of elasticity of a pile material (ksi),
A = cross-sectional area of a pile (in^2), and
L = pile length below gauges (ft).

Due to the imperfect assumption of defining the dynamic soil resistance in terms of pile toe velocity, Eq. (2-41) may not provide comparable resistances measured from load tests. The prediction can be improved by performing a signal matching process using a rigorous numerical modeling technique known as the Case Pile Wave Analysis Program (CAPWAP) developed by Goble et al. (1975). The CAPWAP model adapts Smith's (1962) mathematical model (Figure 2.19), by replacing the hammer and driving accessories in the Smith model with the measured force from the PDA records.

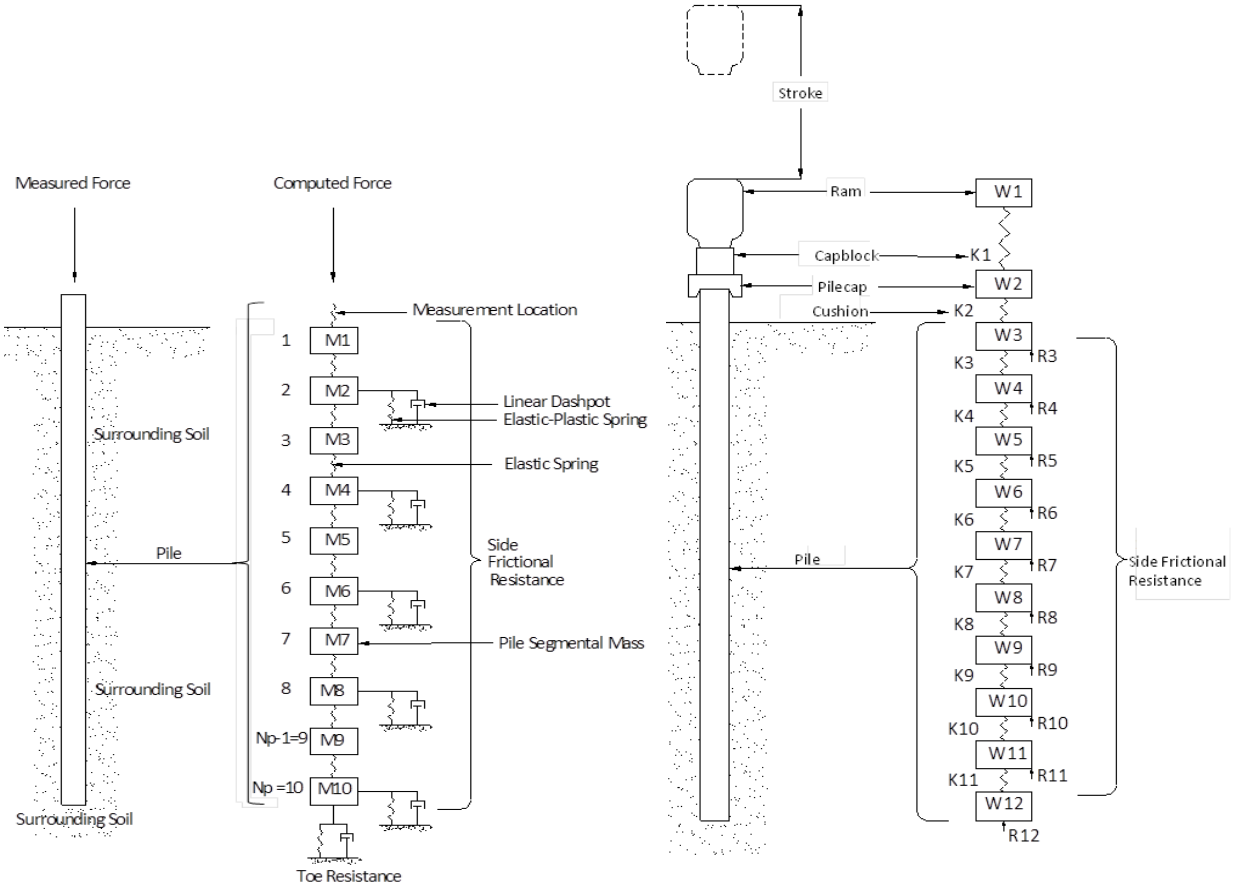

CAPWAP Model **Smith's Model**

Figure 2.19. CAPWAP model and Smith's model (adapted from Hannigan et al. 1998)

The pile or drilled shaft is divided into a series of lumped masses (M) connected with linear elastic springs and linear viscous dampers. The pile lumped masses are linked to a series of soil models described with elastic-plastic springs and linear viscous dampers. At each segment, the static side resistance can be determined using Eq. (2-42), and the end bearing can be determined using Eq. (2-43).

$$R_m = (D_m - D'_m)K'_m(1 + J'v_m) = q_s K'_m(1 + J'v_m) \quad (2\text{-}42)$$

$$R_p = (D_p - D'_p)K'_p(1 + Jv_p) = q_T K'_p(1 + Jv_p) \quad (2\text{-}43)$$

where,

R_m = side resistance along pile segment m at time interval n (kip),
D_m = displacement along pile segment m at time interval n (ft),
D'_m = ground plastic side displacement at time interval n (ft),
K'_m = ground spring constant along pile segment m (kip/ft),
J' = damping constant applicable to resistance along a pile (s/ft),
v_m = instantaneous velocity along pile segment m at time interval n-1 (ft/s),
R_p = toe resistance at the pile point (kip),
D_p = pile toe displacement at time interval n (ft),
D'_p = ground displacement at pile toe at time interval n (ft),
K'_p = ground spring constant at pile toe (kip/ft),
J = damping constant applicable to pile toe (s/ft),
v_p = instantaneous velocity at pile toe in time interval n-1 (ft/s),
q_s = soil quake along a pile shaft (ft),
q_T = soil quake at a pile toe (ft),
n = time interval for which calculations are being made, and
m = subscript denoting the general pile segment m.

The final side resistance at each segment, and end bearing as well as dynamic soil parameters are adjusted and determined until a best match of the computed and measured shaft response is achieved. The advantages and limitations of the high-strain dynamic load test are summarized in Table 2.16.

Table 2.16. Advantages and limitations of high-strain dynamic load test

Advantages	Limitations
• Ability to apply relatively large load on production or test drilled shafts • Relatively cheap • Test can be performed with minimal setup • Does not require reaction system	• Limited testing capacity • CAPWAP analysis produces non-unique resistances • Damage of shaft top • Estimation is highly dependent on soil damping and elastic characteristics • Requires shaft structural properties and surrounding soil parameters in the analysis

2.7. Current Design and Construction Procedures for Drilled Shafts

2.7.1. Iowa DOT

The Iowa DOT LRFD Design Manual (2012) Section 6.3 describes the design and construction procedures for drilled shafts in Iowa. Drilled shafts are only used for highway bridge foundations and are mainly used to support bridge piers but not integral abutments due to the lack of lateral

flexibility of the drilled shaft to accommodate the thermal movements. Drilled shafts are usually socketed at least one and one-half shaft diameters into rock and should not be battered due to construction difficulties. Grade 60 steel reinforcement with minimum yield strength of 60 ksi should be provided over the full depth of a drilled shaft. The resistance of the drilled shaft is typically based on the side resistance in the socket. However, end bearing can be considered if 1) the estimated settlement does not exceed 0.25 inches at the service limit state, and 2) the estimated settlement does not exceed 1 inch at the strength limit state, which is defined as a load of 2.5 times the service load. The construction methods described in Section 2.5 can be employed depending on the subsurface conditions, while grooving of the sidewalls of rock sockets is typically desired in softer rocks. Drilled shaft should be spaced no closer than three diameters center to center. Drilled shaft diameter shall be a minimum of 36 inches for bridge foundations. Drilled shaft concrete shall have 28-day compressive strength of 3.5 ksi or higher upon approval. All drilled shafts shall allow for crosshole sonic logging (CSL) tests. The structural design of drilled shafts is governed by the AASHTO LRFD Bridge Design Specifications (2010), and the FHWA report on drilled shafts by Brown et al. (2010) should be used as a design guide.

2.7.2. Other State DOTs

Colorado DOT

An LRFD design manual for drilled shafts is currently not available on the Colorado DOT website. The design and construction practices for drilled shafts implemented in the State of Colorado are summarized below based on the reports written by Abu-Hejleh et al. (2003), Abu-Hejleh et al. (2005) and Chang (2006). Drilled shafts in the State of Colorado are designed based on empirical methods that solely rely on measured SPT blow counts. However, these empirical methods were developed several decades ago and geared toward the ASD procedures, in which the margin of safety and expected shaft settlement are unknown. For instance, the allowable unit end bearing of a drilled shaft in kips per square foot using the Denver Magic Formula (DMF) is assumed to be equal to 0.5N, with an inherent factor of safety of 2.0 to 2.5 while the allowable unit side resistance is recommended as 10% of the allowable unit end bearing (i.e., 0.05N). Despite several deficiencies that have been highlighted on the use of this design method, it has gained popularity among Colorado design communities due to its simplicity and conservatism. In order to continue using this simple design method and satisfy the LRFD framework and possibly identify alternative efficient design methods, O-cell load tests have been conducted on drilled shafts installed in Colorado to correlate and enhance the SPT-based design method and to provide the necessary data for future development of LRFD resistance factors that reflect Colorado's soil and rock conditions. Seven of the load test results have been compiled in the DSHAFT database and are designated as IDs 33 to 39. After assessing the load test results, the ultimate axial capacity of the drilled shafts were determined based on specific site conditions, and a common failure criterion, such as 5% of shaft diameter for displacement as recommended in AASHTO (2010), was not implemented in defining the ultimate capacities. Having no locally calibrated LRFD resistance factors, CDOT adopts the AASHTO (2010) recommended resistance factors in design and increases the design efficiency by performing field load tests. CDOT has been encouraged by Abu-Hejleh et al. (2003) to perform comprehensive subsurface investigations and field load tests on test shafts that are identical to the production shafts. For drilled shafts in very hard rock, the 28-day concrete compressive strength of 4 ksi or higher upon approval should be used. Alternatively, the AASHTO (2010) and the FHWA design guides are

recommended for CDOT design practices until local LRFD recommendations are established (Chang 2006). To avoid any delay in project delivery and provide design information for comparison and calibration, a parallel design effort using both ASD and LRFD procedures are suggested.

Illinois DOT

The Illinois DOT Bridge Manual (2012) provides a brief description of drilled shafts. Both side resistance and end bearing are considered for shafts in soils. However, either side resistance or end bearing in rock, whichever is larger, is considered. Bells or enlarged bases for drilled shafts are only allowed in cohesive soil, and the angle of inclination of the bell from vertical shall not be greater than 30 degrees. Serviceability checks are not required for shafts in rock. Drilled shafts are typically designed as structural columns with spiral reinforcement set at six inch centers except those designed in seismic areas. The reinforcement cage shall have the same diameter throughout the shaft. However, the shaft diameter in rock shall be six inches smaller than the portion in soil with no less than two inches of cover in rock and five inches in soil. The design of drilled shafts shall follow the AASHTO LRFD Bridge Design Specifications. The FHWA-IF-99-025 report written by O'Neill and Reese (1999) should be referred to for additional technical guidance on drilled shafts.

Kansas DOT

Design manuals were not available from Kansas DOT's website. Kansas DOT representative, Jeffry Ruby, provides the following statement about drilled shafts:

> *"We are very similar to Iowa with one inch criterion at the Strength I load combination. We also investigate the geologic materials to assess if the settlement is realistic. Settlement in a solid limestone usually is not going to happen but does occur in other settings. The strength and service loads are given to us by the bridge designer for these calculations."*

Kentucky DOT

The Kentucky DOT Geotechnical Guidance Manual (2005) provides a very short description on drilled shafts as follows:

> *"Analysis methods for estimating the bearing capacities of individual drilled shafts, as well as allowing for group effects, are presented in FHWA IF-99-025, Drilled Shafts: Construction Procedures and Design Methods. Typically, only the axial capacity of unweathered bedrock is considered; the overburden and weathered bedrock are usually neglected."*

When rock is used as a supporting material for drilled shafts, rock descriptions from the geology logs shall be presented on the subsurface data sheets along with Kentucky method-RQD and percentage of rock recovery (REC). Battered drilled shafts are seldom used due the difficulty of constructing them. Settlement of drilled shafts in soils is equal to the settlement of the soil below the neutral plane as discussed in the National Cooperative Highway Research Program (NCHRP) Report 343 by Barker et al. (1991). Projects incorporating large numbers of drilled shafts may

provide an economic justification for conducting a load test in accordance with ASTM D1143 to verify the ultimate resistance as estimated by other methods.

Minnesota DOT

The Minnesota DOT LRFD Bridge Design manual (2007) provides design and construction procedures for drilled shafts in the State of Minnesota. To ensure drilled shafts have the anticipated design resistances, field load tests and Crosshole Sonic Logging tests (CSL) are used as construction control methods. Drilled shafts are expensive and are normally used only when driven piles 1) cannot provide the resistance at ten feet or less below footings due to the presence of bedrock or dense layers, 2) cannot be embedded below the computed scour elevation of a streambed, or 3) cannot be economically installed due to site-specific reasons. Drilled shafts are designed as structural columns subjected to axial and lateral loads. Drilled shafts should be placed with a minimum center-to-center spacing of three times the shaft diameter and appropriate group reduction factors must be applied unless the spacing is greater than eight times the shaft diameter. Shaft diameters normally range between three to five feet. For shafts in soil and rock layers, the shaft diameter in soil layers should be six inches larger than that in rock layers. Temporary casing is allowed while permanent casing should not be used in the sidewall friction area of soil or rock. The concrete cover should be three inches on the side and six inches from the bottom of the shaft. The 28-day concrete compressive strengths of 4 ksi and 5 ksi with maximum aggregate size of ¾ inch are normally used for dry and wet shaft holes, respectively. MnDOT representative, Derrick Dasenbrock, provided the following statement regarding allowable settlement of a drilled shaft:

> *"We usually develop it site-specifically, based on shaft dimensions, span lengths, and other considerations, such as tolerable deformations prior to the superstructure construction."*

Missouri DOT

The design and construction guides for drilled shafts employed by Missouri DOT are summarized based on the MoDOT Standard Construction Specification Section 701 (2003) and the latest MoDOT LRFD Bridge Design Guidelines established from a combination of the MoDOT Engineering Policy Guide (EPG) 751.37 (2011) and the AASHTO LRFD Bridge Design Specifications (2009).

Drilled shafts are designed following the LRFD concepts at different target reliabilities established for two main classes of roadways: 1) minor roads, major roads, major bridges costing less than $100 million, and 2) major bridges costing more than $100 million. Drilled shafts shall have a minimum 18 inch diameter and the rock socket shall be at least one diameter in depth. End bearing shall be established for the soil or rock located between the base of the shaft and two diameters below the base. End bearing shall be neglected if drilled shafts are located within karstic rock or other unreliable geomaterials. The design methods for determining side resistance and end bearing in different geometarials are summarized in Table 2.17. The design methods are explicitly described in the MoDOT Engineering Policy Guide (EPG) 751.37 (2011). The tolerable settlement shall be taken as S/476, where S is the span between adjacent bridge bents, and settlement shall be evaluated for the Service I load combination. The total settlement of a drilled shaft can be estimated using an approximate method or t-z method.

Contractors shall submit a drilled shaft installation plan to the engineer at least 30 days prior to drilled shaft construction. Drilled shafts shall have a 28-day minimum concrete compressive strength of 4 ksi. If casings are employed during construction, casings shall be smooth, clean and watertight, and splicing of casings is not desired. Permanent casings shall be extended into rock to provide a positive seal and to stabilize the shaft excavation. Wet construction using drilling slurry shall be approved by the engineer prior to use. No two adjacent shafts shall be excavated at the same time, and shafts shall not be constructed within 24 hours of the completion of an adjacent shaft if the center-to-center spacing is less than three shaft diameters. The construction tolerances applied to drilled shafts are 1) the final shaft diameter constructed using temporary casing shall be provided as shown on construction plans, 2) the center of the top of the shaft shall be within three inches of plan position, 3) the vertical alignment shall not vary from the plan alignment by more than ¼ inch per foot, 4) the reinforcing steel cage shall be no more than six inches above or three inches below plan position, 5) the finished elevation of the shaft shall be no more than one inch above or three inches below the plan top of shaft elevation, and 6) the bottom of the shaft excavation shall be normal to the axis of the shaft within a tolerance of ⅜ inch per foot of shaft diameter. Completed shafts shall be subjected to the specified testing methods, such as concrete coring or CSL testing. Any load tests shall be completed and submitted to the engineer for review and approval before construction of any production drilled shafts.

Table 2.17. Summary of design methods for different geomaterials used by MoDOT

Geomaterials	Design Method	
	Side Resistance	**End Bearing**
Rock ($q_u \geq 100$ ksf)	Horvath and Kenney (1979)	Wyllie (1999)
Weak Rock (5 ksf $\leq q_u \leq$ 100 ksf)	Loehr et al. (2011a) and Loehr et al. (2011b)	Loehr et al. (2011a) and Loehr et al. (2011b)
Weak Rock (SPT N $\leq$ 400)	Pierce et al. (2011)	Pierce et al. (2011)
Weak Rock (1 in/100 blows < TCP < 10 in/100 blows)	Pierce et al. (2011)	Pierce et al. (2011)
Weak Rock ($I_{s(50)} < 40$ ksf)	Loehr et al. (2011a) and Loehr et al. (2011b)	Loehr et al. (2011a) and Loehr et al. (2011b)
Cohesive Soil ($q_u < 5$ ksf)	α-method by O'Neill and Reese (1999)	α-method by O'Neill and Reese (1999)
Cohesionless Soil	β-method by O'Neill and Reese (1999)	β-method by O'Neill and Reese (1999)

TCP = penetration from Texas Cone Penetration Test measurement
$I_{s(50)}$ = point load index value

Nebraska DOR

Nebraska Department of Roads (NDOR) Bridge Office Policies and Procedure (BOPP) (2012) provides limited information on the design and construction procedures for drilled shafts. Drilled shafts shall be constructed using permanent casing and a construction joint shall be placed at the

top of the permanent casing. Drilled shafts shall have a 28-day minimum concrete compressive strength of 3 ksi. CSL tests shall be performed on the first drilled shaft, and test results shall be provided to the geotechnical engineer prior to constructing additional drilled shafts. No design procedures are described in the BOPP.

Nevada DOT

The Nevada DOT Structural Manual (2008) generally adopts the AASHTO LRFD Bridge Design Specifications for the design and construction of drilled shafts. Diaphragm-with-footing abutment is the most widely used and preferred abutment. For footings with drilled shafts, two rows of small-diameter drilled shafts spaced a minimum of six inches center-to center of the bearing lines or a large drilled shaft with a diameter of at least 36 inches is required. However, rigid drilled shafts are not suitable for use with diaphragm-with-pile abutment, especially on post-tensioned structures. Drilled shafts should be considered when significant scour is expected, construction space is limited, or driven piles are not economically feasible. Drilled shafts are typically good for seismic applications. Drilled shafts shall have a 28-day minimum concrete compressive strength of 4 ksi. Minimum concrete cover for drilled shafts with diameters less than three feet shall be four inches, or six inches for shaft diameters larger than or equal to three feet. Steel reinforcement cages shall be extended the full length of the drilled shaft. Drilled shafts shall have a minimum reinforcement of 1% of the gross concrete area and shall be extended into the footing. The diameter of a drilled shaft supporting a single column shall be at least 18 inches greater than the largest dimension of the column. The design procedures for drilled shafts are governed by the AASHTO LRFD Bridge Design Specifications.

South Dakota DOT

South Dakota DOT is gradually switching the design procedures for drilled shafts to LRFD. No LRFD design manuals were found on the South Dakota DOT's website. However, the following statement was obtained via email from SDDOT representative, Dan Vockrodt:

"In South Dakota we are slowly progressing when it comes to LRFD. Everything that is done to date is utilizing the calibration to fit method when using LRFD. We have just begun a research project that will provide us some skin friction and bearing information obtained from load tests (piling) being performed. We are very early in the process and it should help us define our LRFD process and move us to the next level. We only construct drilled shafts in shale type bedrock materials. We do not put drilled shafts in sands or glacial till materials where settlement may be a concern. Shale bedrock is for the most part at the surface west of the Missouri river where 95% of the drilled shafts are constructed. Most of our shale bedrocks are hard materials with unconfined compressive strengths in the 15 to 25 ksf range. We have never been overly concerned with settlement in our drilled shafts. We also provide a somewhat conservative skin friction value for the design of the drilled shaft and we do not allow any end bearing capacity of the drilled shaft. Our feeling is that the contractors don't clean the bottom of the shafts well enough to allow for end bearing capacity. We do however make sure the excavation is cleaned properly and we know we get additional bonus "safety factor" for our drilled shafts."

Tennessee DOT

Design manuals were not available from Tennessee DOT's website. The following design and construction practices for drilled shafts are delineated based on the O-cell test report by Brown and Associates (2008) on two test shafts conducted in Nashville, TN, which are identified as IDs 28 and 29 in the DSHAFT database. Drilled shafts in rock are traditionally designed solely based on end bearing with an allowable unit end bearing of about 80 to 100 ksf on rock that is verified by probe holes. Rock RQD and uniaxial compressive strength are typically used in design. In this test project, dry construction method with temporary casing was employed in drilled shaft constructions. After completion of the shaft excavation, an inspection probe was drilled in the base of the test shafts with an air-operated percussion tool for inspection of the rock below the base of the shafts. The concrete compressive strength was 5 ksi after only two days of curing. The analytical method proposed by Horvath and Kenney (1979) was correlated and used to estimate the unit side resistance in rock. Due to the arrangement of the O-cell tests, the end bearing was mobilized up to relative displacements of just over 1% of the diameter of the loaded area and did not fully mobilize the geotechnical limit of the predicted bearing capacity. The recommended geotechnical and inspection requirements for both "sound rock" and "fair rock" are summarized in Table 2.18.

Table 2.18. Identification, geotechnical, and inspection requirements and design parameters for drilled shafts in rocks conducted in Nashville, TN

Description	Sound Rock	Fair Rock
Identification	Rock with only one or two small seams less than a half inch thick	Rock with soil-filled seams up to 10% of the base diameter at depths greater than half of the diameter
Geotechnical and inspection Requirements	• A thorough geotechnical site investigation with rock coring and compressive strength testing • Rock q_u should be greater than 10 ksi and RQD should exceed 90% • No significant solution cavities • Dry hole with down-hole inspection • Down-hole probe to a depth of at least two shaft diameters	• A thorough geotechnical site investigation with rock coring and compressive strength testing • Rock q_u should be greater than 5 ksi and RQD should exceed 70% • No significant solution cavities • Consistent rock characteristics from excavation and boring logs
Design Parameters	• Ultimate unit end bearing = 1250 ksf corresponding to a displacement slightly over 1% of the shaft diameter • Factor of safety = 2.5	• Ultimate unit end bearing = 500 ksf corresponding to a displacement slightly over 1% of the shaft diameter • Factor of safety = 2.5

Summary

The design and construction procedures for drilled shafts in various states including the State of Iowa are briefly summarized in Table 2.19.

Table 2.19. Summary of design and construction procedures for drilled shafts in regional states

State Agencies	Design Manual	Design Procedure	Construction Procedure
Iowa DOT	Yes	• Follow AASHTO (2010) and FHWA guides by Brown et al. (2010) • Rock-socket depth at least 1½D • Side resistance and end bearing depending upon settlement criteria • Concrete $f'_c \geq 3.5$ ksi • Shaft diameter ≥ 3 ft • Shaft spacing ≥ 3D center to center • Ultimate capacity corresponding to 1 in settlement	• Depends on the subsurface conditions, while grooving of the sidewalls of rock-sockets is typically desired in softer rocks • No battered drilled shafts • Allow for CSL testing
Colorado DOT	No	• SPT-based design method • Follow AASHTO (2010) and FHWA guides • Concrete $f'_c \geq 4$ ksi • End bearing and minimal side resistance • Ultimate capacity determination varies with site conditions	• Depends on the subsurface conditions • Perform comprehensive subsurface investigations and field load tests on test shafts that are identical to the production shafts
Illinois DOT	Yes	• Follow AASHTO (2010) and FHWA guides by O'Neill and Reese (1999) • Consider both side resistance and end bearing in soil • Consider either side resistance or end bearing in rock • Serviceability check is not required in rock • Design as a structural column • Shaft diameter in rock shall be 6 in. smaller than the portion in soil	• Not available
Kansas DOT	No	• Similar to Iowa DOT's design procedures	• Not available
Kentucky DOT	Yes	• Follow FHWA guides by O'Neill and Reese (1999) • Only axial capacity of unweathered bedrock is considered • Settlement estimation follows NCHRP Report 343 by Barker et al. (1991)	• Battered drilled shafts are seldom used

Table 2.19. Summary of design and construction procedures for drilled shafts in regional states, continued

Minnesota DOT	Yes	• Design as a structural column • Shaft spacing ≥ 3D center to center • Typical shaft diameter = 3 to 5 ft • Shaft diameter in rock shall be 6 in. < the portion in soil • Concrete cover: 3 in on side and 6 in at base • Concrete f'_c: 4 ksi for dry and 5 ksi for wet holes	• Perform field load tests and CSL testing • Temporary casing is allowed but not permanent casing where side resistance is considered
Missouri DOT	Yes	• Design methods: Table 2.17 • Shaft diameter ≥ 18 in • Rock socket depth at least 1D • Tolerable settlement = S/476 • Settlement estimated using an approximate method and/or t-z method • Concrete $f'_c \geq 4$ ksi	• Depends on the subsurface conditions • Casing shall be smooth, clean, watertight, and with no splicing • Shafts shall not be constructed within 24 hours of the completion of an adjacent shaft if the spacing is less than 3D • Follow the construction tolerance requirements • Allow CSL testing and/or load testing
Nebraska DOR	Yes	• Concrete $f'_c \geq 3$ ksi • No mention of design procedures	• Use permanent casing • Test and obtain approval on test shaft before constructing additional drilled shafts
Nevada DOT	Yes	• Follow AASHTO LRFD Bridge Design Specifications • Concrete $f'_c \geq 4$ ksi • Concrete cover: 4 in. for D < 3 ft; 6 in. for D ≥ 3 ft • Full steel reinforcement	• Not available
South Dakota DOT	No	• Use only in shale bedrock, not in cohesive or cohesionless soils • Typical q_u for shale: 15 to 25 ksf • No concern for settlement • Consider only side resistance	• Not available
Tennessee DOT	No	• Mainly consider end bearing • End bearing corresponds to displacement at 1% D or more	• Rock quality identified using probe hole • Follow recommended geotechnical and inspection requirements

2.7.3. AASHTO

AASHTO LRFD Bridge Design Specifications (2010) recommend design and construction procedures for drilled shafts, which have been adopted by many state agencies. Drilled shafts shall be designed to have adequate axial and structural resistances and tolerable settlements. Adequate performance of a drilled shaft can be achieved through a combination of subsurface investigations, laboratory tests, design analyses, and field verification tests. The strength limit state Eq. (2-44) is used in the design procedure for drilled shafts.

$$\sum \gamma_i Q_i \leq \sum \varphi_{sj} R_{sj} + \varphi_p R_p \tag{2-44}$$

where,

γ_i = load factor for load type i,
Q_i = applied load type i (kips),
φ_{si} = resistance factor for shaft side resistance in soil layer j specified in Table 2.21,
R_{sj} = nominal shaft side resistance in soil layer j estimated using analytical methods given in Table 2.20 (kips),
φ_p = resistance factor for end bearing specified in Table 2.21, and
R_p = nominal end bearing estimated using analytical methods given in Table 2.20 (kip).

Table 2.20. Summary of analytical methods for drilled shafts as recommended in AASHTO (2010)

Geomaterial	Side Resistance*	End Bearing*
Cohesive Soil	α-method: Eq. (2-8) by O'Neill and Reese (1999)	Total Stress: Eq. (2-19) by O'Neill and Reese (1999)
Cohesionless Soil	β-method: Eq. (2-10) by Burland (1973) and O'Neill and Reese (1999)	Eq. (2-21) by Reese and O'Neill (1989)
Cohesive IGM	Eq. (2-11) by O'Neill and Reese (1999)	Eq. (2-24) by Rowe and Armitage (1987) for intact IGM; Eq. (2-34) by Carter and Kulhawy (1988) for fractured IGM
Coheionless IGM	Eq. (2-14) by O'Neill and Reese (1999)	Eq. (2-22) by O'Neill and Reese (1999)
Rock	Eq. (2-16) by Horvath and Kenney (1979)	Eq. (2-24) by Rowe and Armitage (1987) for intact rock; Eq. (2-34) by Carter and Kulhawy (1988) for fractured rock

* − all analytical methods are discussed in O'Neill and Reese (1999)

Table 2.21. Resistance factors for geotechnical resistance of drilled shafts (adapted from AASHTO 2010)

Method/Soil/Condition			Resistance Factor[(a)]
Nominal Axial compressive Resistance of Single-Drilled Shafts, φ_{stat}	Side resistance in clay	α-method (O'Neill and Reese 1999)	0.45
	End bearing in clay	Total Stress (O'Neill and Reese 1999)	0.40
	Side resistance in sand	β-method (O'Neill and Reese 1999)	0.55
	End bearing in sand	Reese and O'Neill (1989)	0.50[(b)]
	Side resistance in IGMs	O'Neill and Reese (1999)	0.60
	End bearing in IGMs	O'Neill and Reese (1999)	0.55
	Side resistance in rock	Horvath and Kenney (1979) O'Neill and Reese (1999)	0.55
	Side resistance in rock	Carter and Kulhawy (1988)	0.50
	End bearing in rock	Canadian Geotechnical Society (1985); Pressuremeter Method (Canadian Geotechnical Society, 1985; O'Neill and Reese 1999)	0.50
Block Failure, φ_{bl}		Clay	0.55
Uplift Resistance of Single-Drilled Shafts, φ_{up}	Clay	α-method (O'Neill and Reese 1999)	0.35
	Sand	β-method (O'Neill and Reese 1999)	0.45
	Rock	Horvath and Kenney (1979) Carter and Kulhawy (1988)	0.40
Group Uplift Resistance, φ_{ug}	Sand and clay		0.45
Horizontal Geotechnical Resistance of Single Shafts or Shaft Group	All materials		1.0
Static Load Test (compression), φ_{load}	All materials		0.70
Static Load Test (uplift), φ_{upload}	All materials		0.60

[(a)] – reduce by 20% when a single shaft is used to support a bridge pier;
[(b)] – applicable for conditions of high quality-control on the properties of drilling slurries and base cleanout procedures; otherwise a lower value should be used

It is important to note that the resistance factors were established based on various studies by Barker et al. (1991), Paikowsky et al. (2004) and Allen (2005). The recommended resistance factors are determined using a combination of fitting to ASD method, reliability theory, and/or rational engineering judgment when significantly different resistance factors are obtained from the previous two methods. When the reliability theory method was employed, the resistance factors were determined for a target reliability index of 3.0 corresponding to a probability failure of 1/1000 and non-redundant shaft groups (i.e., four or fewer shafts or less in a group). However, if a single shaft is used to support a bridge pier, the resistance factors given in Table 2.21 should be reduced by 20%.

Service limit state design should be considered for the settlement of a single shaft or group of drilled shafts. The service limit state design is satisfied when the total estimated settlement is smaller than a tolerable settlement. The total settlement of a drilled shaft could consist of short-term settlements, consolidation settlements in cohesive soils and axial elastic compression of the shaft. To facilitate the design procedure, a nominal shaft axial resistance is typically limited to a value specified for the strength limit state and the desired tolerable settlement. The normalized load-settlement curves shown in Figure 2.20 through Figure 2.23 developed by O'Neill and Reese (1999) should be used to limit the nominal side resistance and end bearing.

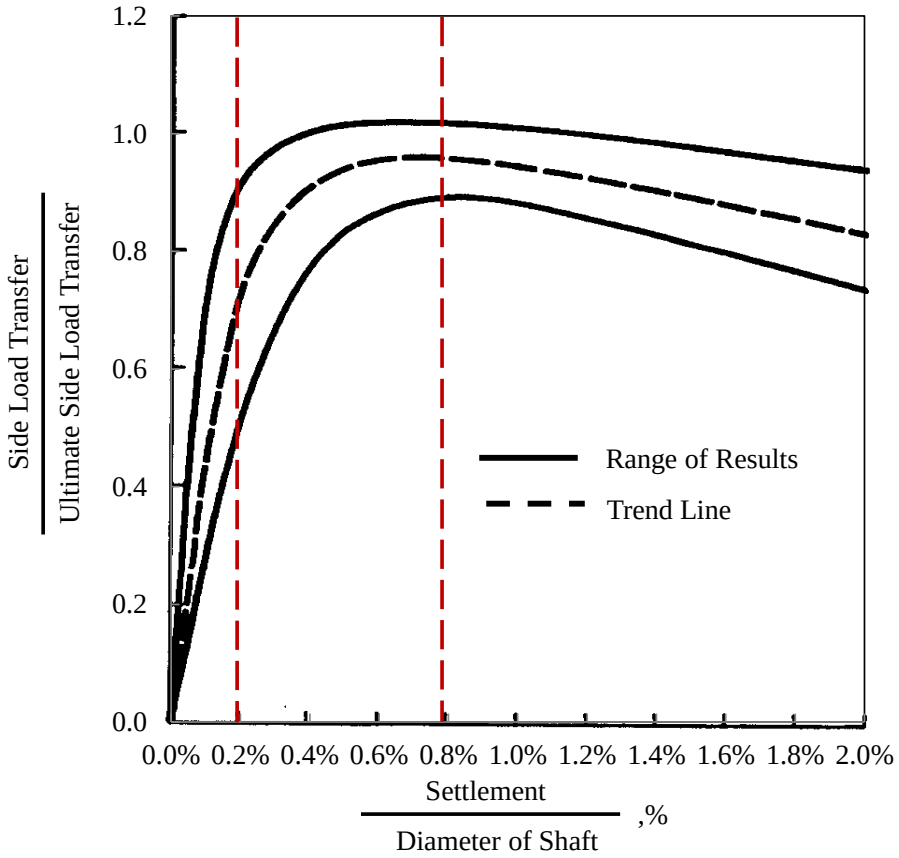

Figure 2.20. Normalized load transfer in side resistance versus settlement in cohesive soils (adapted from O'Neill and Reese 1999)

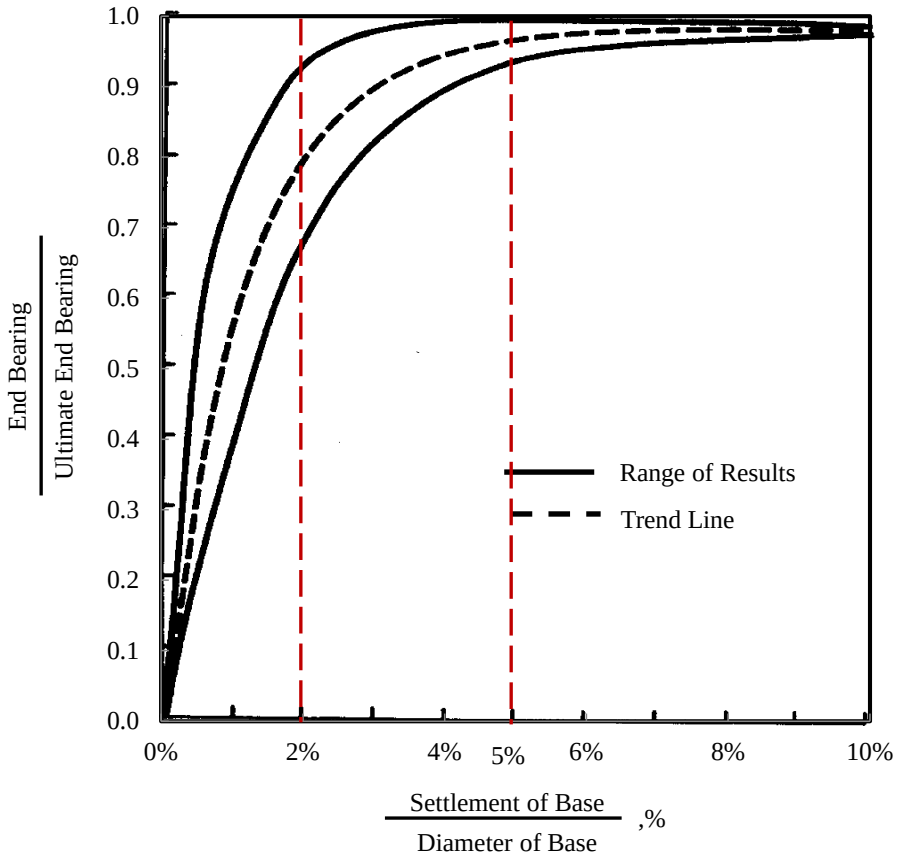

Figure 2.21. Normalized load transfer in end bearing versus settlement in cohesive soils (adapted from O'Neill and Reese 1999)

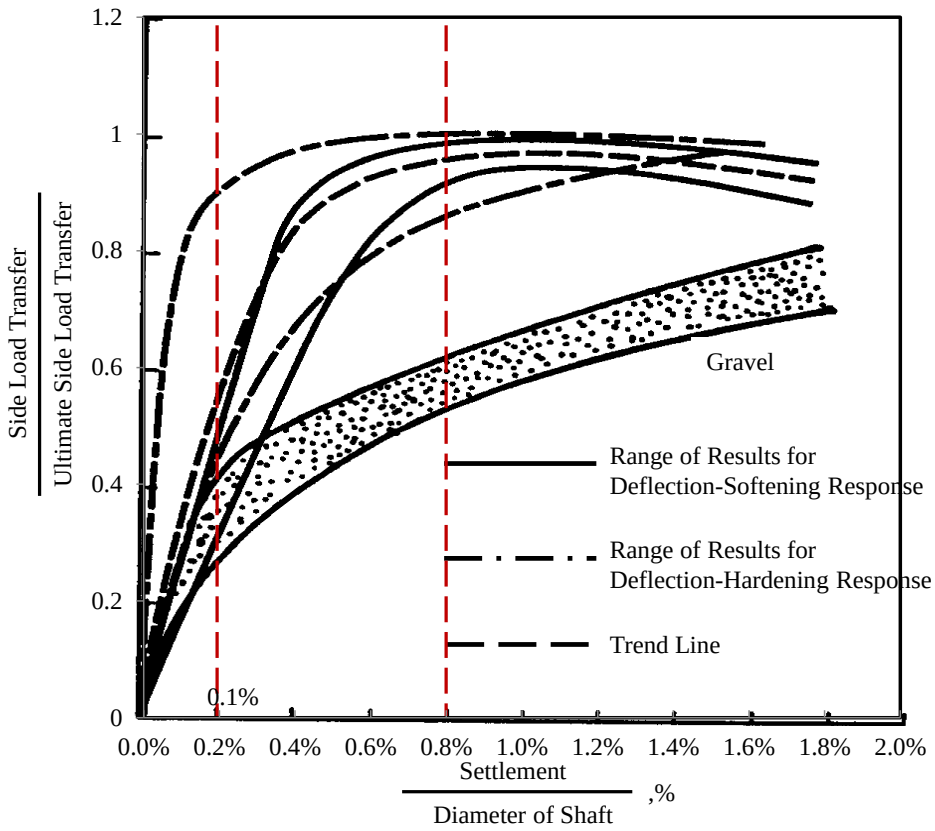

Figure 2.22. Normalized load transfer in side resistance versus settlement in cohesionless soils (adapted from O'Neill and Reese 1999)

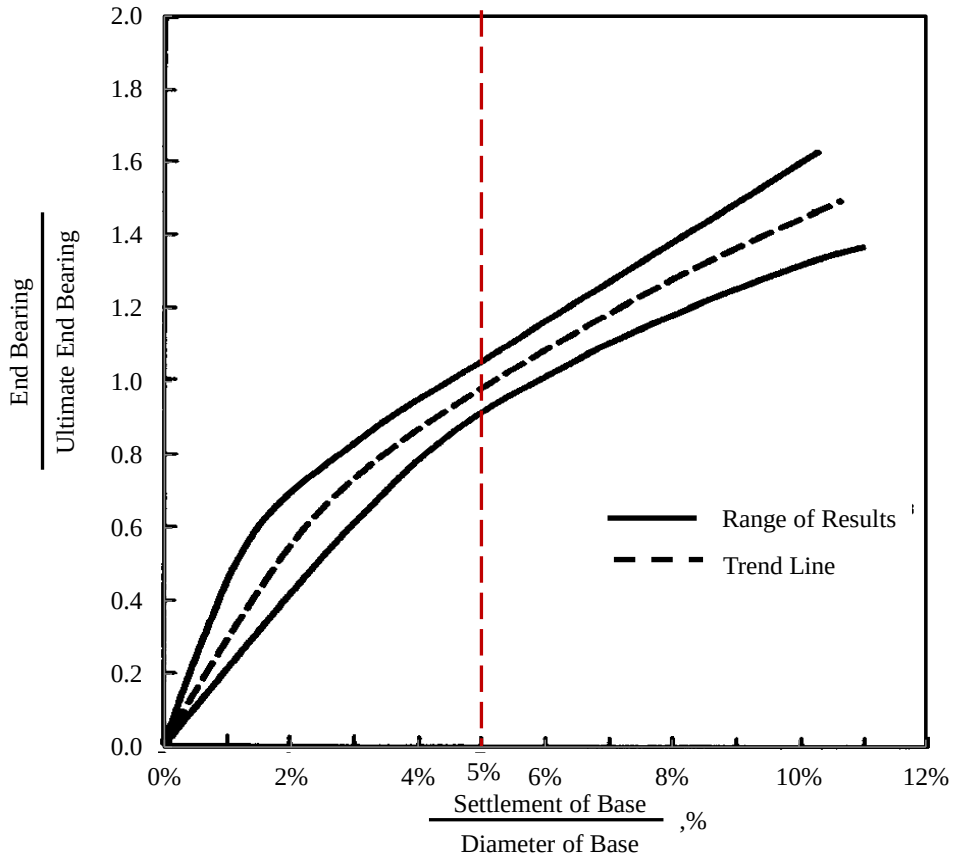

Figure 2.23. Normalized load transfer in end bearing versus settlement in cohesionless soils (adapted from O'Neill and Reese 1999)

These normalized load-settlement curves were developed based on 41 top-down load test results of full-sized drilled shafts in cohesive and cohesionless soils conducted in Arizona (8 tests), Bangkok (4 tests), Florida (2 tests), London (12 tests), South Carolina (1 test), Texas (11 tests), and unidentified locations (3 tests) as described in Reese and O'Neill (1988). The settlement indicated on the x-axis includes the short-term settlement and the elastic compression, but not the consolidation settlement. Distinctly different load-settlement curves for cohesive and cohesionless soils are observed. Figure 2.20 indicates that the side resistance in cohesive soil is fully mobilized at displacements of 0.2% to 0.8% of the shaft diameter while the side resistance in cohesionless soil shown in Figure 2.22 is fully mobilized between 0.1% and 1.0% of the shaft diameter. The end bearing in cohesive soil shown in Figure 2.21 is fully mobilized at displacements of 2% to 5% of the base shaft diameter while Figure 2.23 shows the continuous increase in end bearing of the shaft in cohesionless soil as the settlement increases beyond 5% of the base diameter. These figures provide a good reference for limiting the nominal axial resistance. Unfortunately, similar curves are currently not available for shafts in IGMs and rock. The axial resistance of drilled shafts in rock is typically dominated by side resistance until the top shaft displacement exceeds about 0.40 in. Similar to cohesive and cohesionless soils, the side resistance and end bearing in rock are not mobilized at the same displacement. Hence, the combined effect of side resistance and end bearing could over estimate the total resistance, especially when the rock is brittle. For strength limit state design, the total ultimate axial resistance of a drilled shaft is established at a settlement equal to 5% of the base diameter.

CHAPTER 3. EXAMINATION AND ANALYSIS OF DSHAFT DATA

3.1. DSHAFT Database

A quality assured, electronic database for Drilled SHAft Foundation Testing (DSHAFT) was developed by Garder et al. (2012) with the intention to establish LRFD resistance factors for the design of drilled shafts in the Midwest region. To achieve this goal, available static load test information was collected, reviewed, and integrated into DSHAFT using Microsoft Office Access. DSHAFT has an efficient, easy-to-use filtering capability and provides easy access to original field records in an electronic format. DSHAFT is currently housed on a project website (http://srg.cce.iastate.edu/dshaft) so that the information can be easily shared with foundation designers and researchers.

DSHAFT currently contains 41 drilled shaft tests performed in 11 states as illustrated in Figure 3.1(a). Out of the 41 tests, 28 have the necessary structural, subsurface, testing and construction details for the establishment of LRFD resistance factors as shown in Figure 3.1(b) distributed by state.

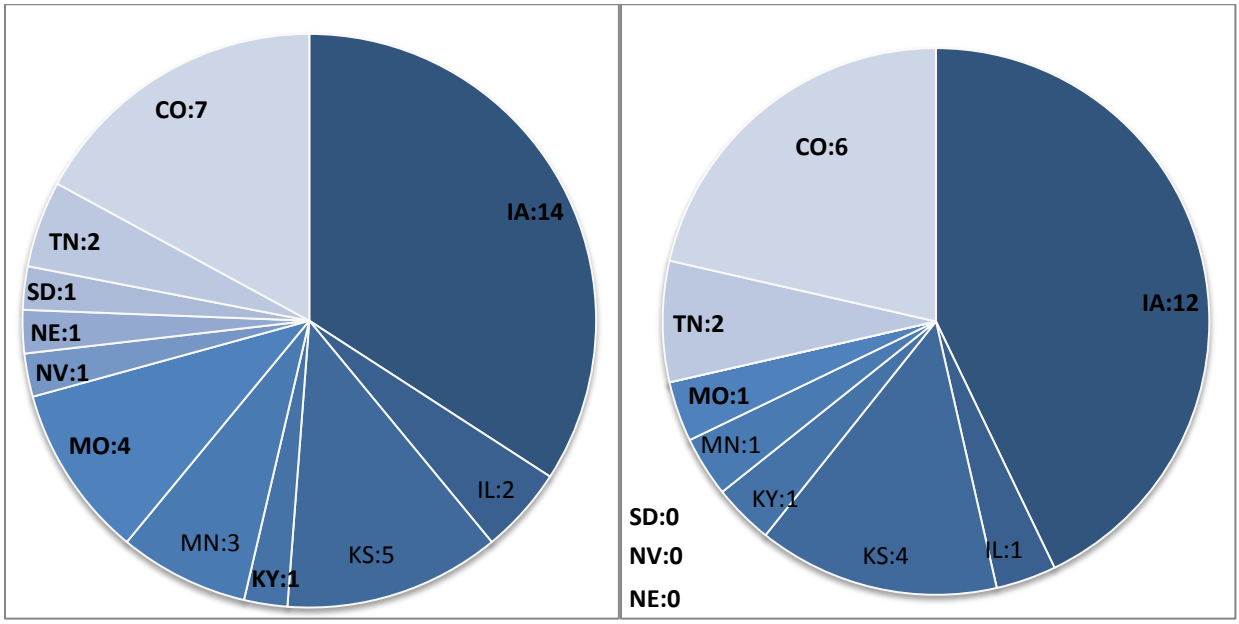

(a) (b)

Figure 3.1. Distribution of drilled shaft load tests contained in DSHAFT by states (a) available data and (b) usable data

The drilled shaft data are also distributed according to 1) three construction methods (i.e., dry, casing and wet) in Figure 3.2; 2) two testing methods (i.e., Osterberg and Statnamic) in Figure 3.3; 3) four geomaterials at the shaft bases in Figure 3.4; and 4) 13 combinations of geomaterials along the shafts in Figure 3.5.

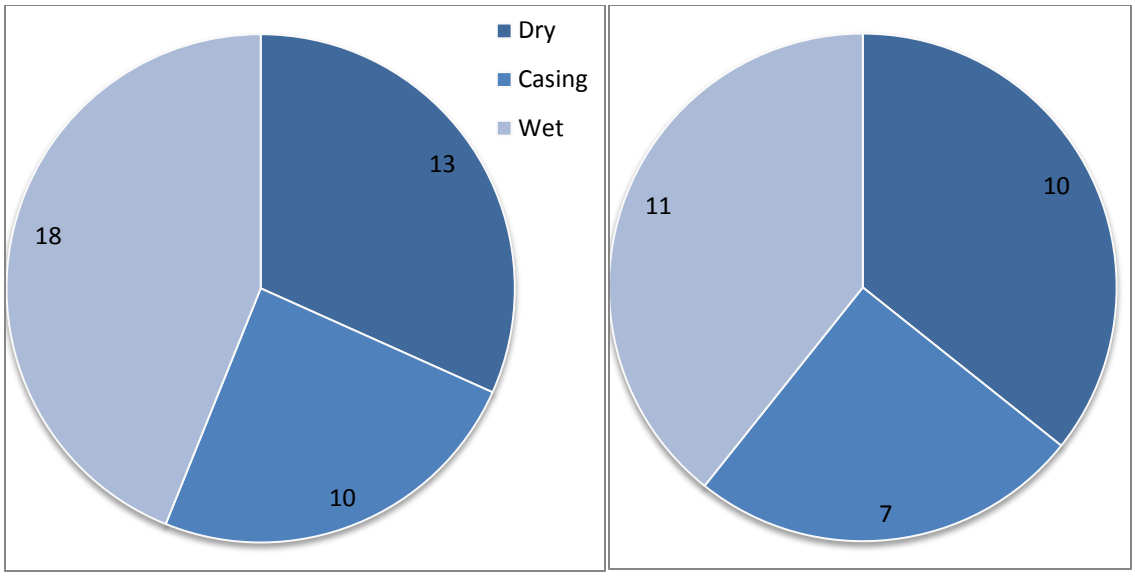

(a) (b)

Figure 3.2. Distribution of drilled shaft load tests contained in DSHAFT by construction methods (a) available data and (b) usable data

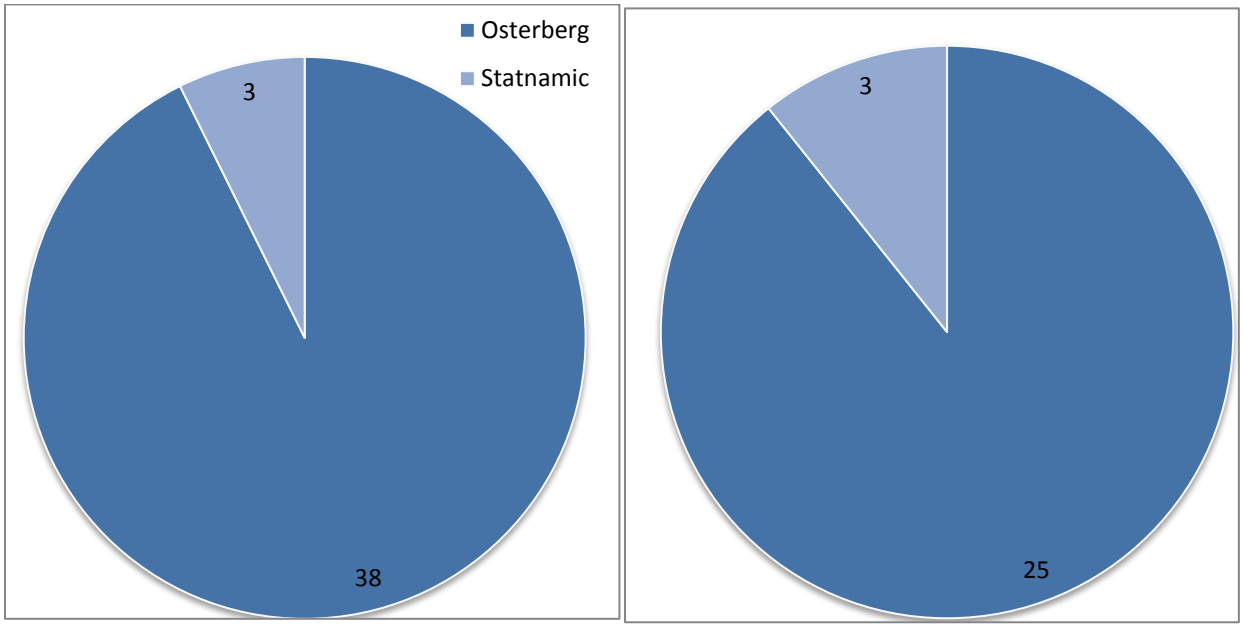

(a) (b)

Figure 3.3. Distribution of drilled shaft load tests contained in DSHAFT by testing methods (a) available data and (b) usable data

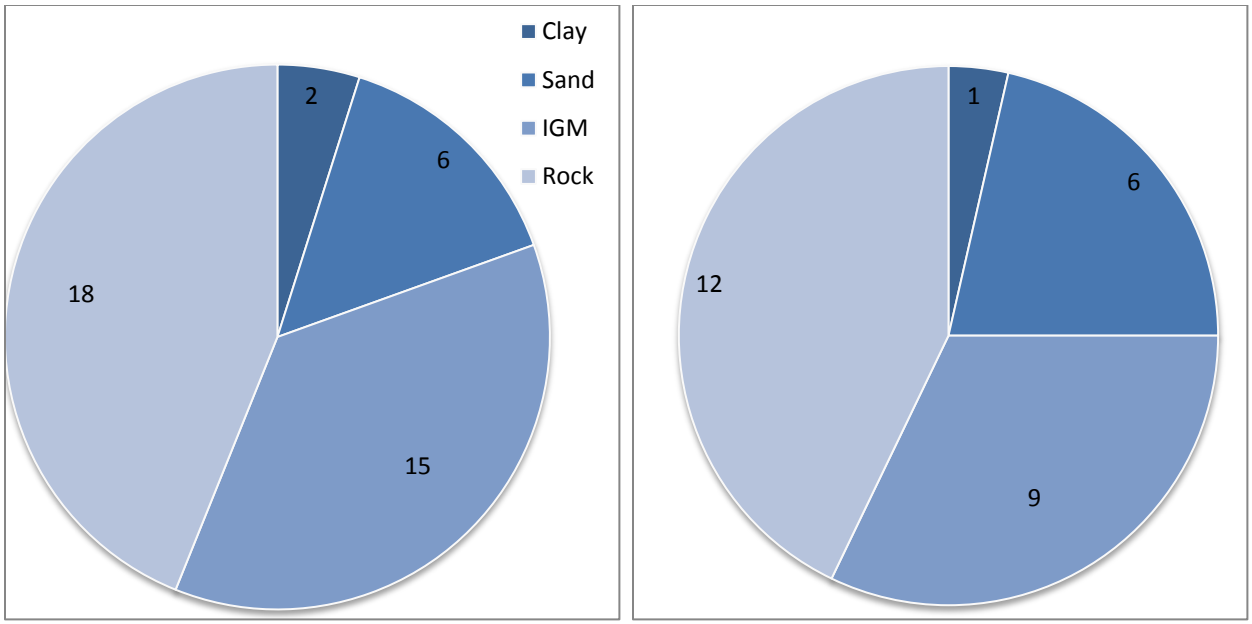

(a) (b)

Figure 3.4. Distribution of drilled shaft load tests contained in DSHAFT by geomaterials at shaft base (a) available data and (b) usable data

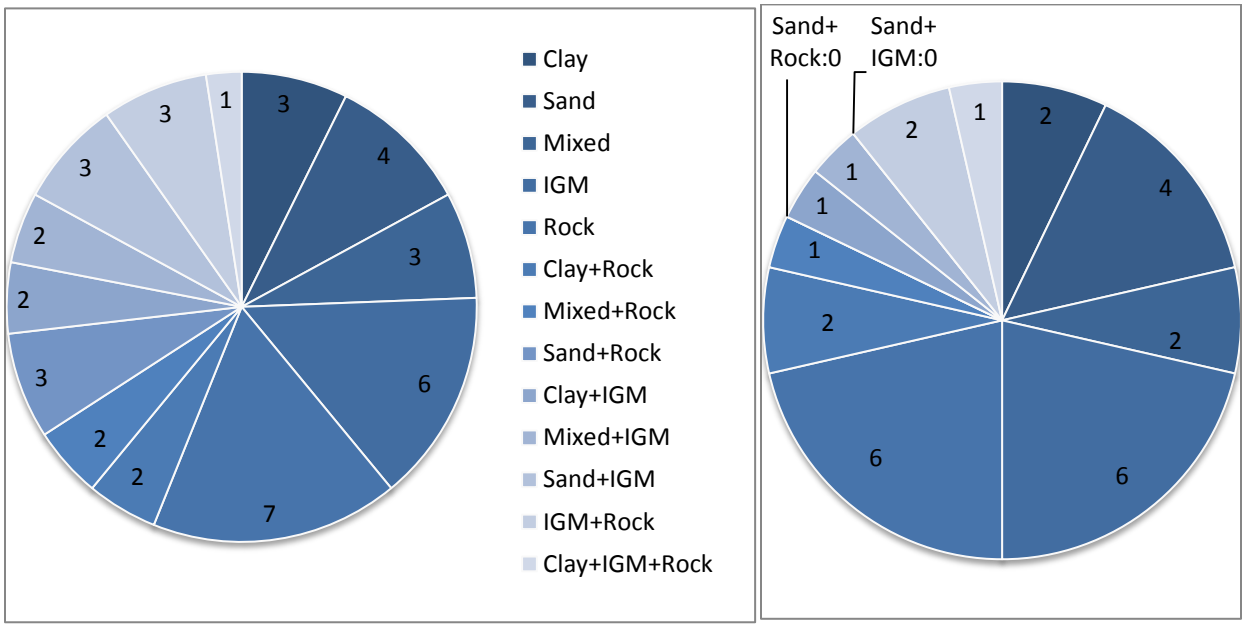

(a) (b)

Figure 3.5. Distribution of drilled shaft load tests contained in DSHAFT by geomaterials along shaft (a) available data and (b) usable data

These 41 drilled shaft tests data are summarized in Table B.1. Each data set has an identification number (ID) ranging from 1 to 41. Shaft geometry, concrete compressive strength (fc′), surrounding geomaterials, construction methods, and load test methods are reported. The data sets are identified in Table B.1 if they are usable for the development of resistance factors. The

reasons for 13 drilled shaft tests being categorized as non-usable data are described in Table 3.1 in reference to the geomaterial parameters presented in Appendix B.

Table 3.1. Reasons for 13 drilled shaft tests being categorized as non-usable

ID	Geomaterials		Reasons
	Shaft	Base	
1	Clay	IGM[(a)]	No soil boring logs were available to characterize the clay and shale layers and estimate their resistances (see Table B.2)
12	Sand+ Rock[(a)]	Rock[(a)]	No q_u values were reported to characterize the sandstone layer and estimate the shaft resistances (see Table B.13)
18	Sand+ IGM[(a)]	IGM[(a)]	No soil boring logs were available to characterize the clay shale layer and estimate the shaft resistances (see Table B.19)
21	Sand+ IGM[(a)]	IGM[(a)]	No q_u and RQD values were reported to characterize the silty shale layer and estimate the shaft resistances (see Table B.22)
22	Mixed+ Rock[(a)]	Rock[(a)]	No q_u and RQD values were reported to characterize the limestone, sandstone and shale layers and estimate the shaft resistances (see Table B.23)
23	Sand+ Rock[(a)]	Rock[(a)]	No q_u and RQD values were reported to characterize the friable sandstone layer and estimate the shaft resistances (see Table B.24)
24	IGM+ Rock	Rock[(a)]	No geomaterials were identified beneath the shaft base (see Table B.25)
30	Mixed	Clay	No material parameters were measured in the sandy clay layer beneath the shaft base (see Table B.31)Table B.25
31	Mixed+ IGM	IGM	No RQD values in the lean clay-weathered shale were reported to estimate the shaft resistances (see Table B.32)
32	Sand+ IGM[(a)]	IGM[(a)]	No q_u and RQD values were reported to characterize the shale layer and estimate the shaft resistances (see Table B.33)
37	Sand+ Rock[(a)]	Rock[(a)]	No q_u values were reported to characterize the shale bedrock layer and estimate the shaft resistances (see Table B.38)
40	Clay+ IGM[(a)]	IGM[(a)]	No q_u and RQD values were reported to characterize the hard shale layer and estimate the shaft resistances (see Table B.41)
41	Rock[(a)]	Rock[(a)]	Incomplete q_u and RQD values were reported to fully characterize the subsurface and estimate the shaft resistances (see Table B.42)

ID – identification number; IGM – intermediate geomaterial; q_u – unconfined compressive strength; RQD – rock quality designation; [(a)] – assumed geomaterials.

The estimation of nominal axial geotechnical resistances using the static analysis methods described in Sections 2.3 and 2.4 requires quantification of surrounding geomaterial parameters through in-situ subsurface investigations and/or laboratory material testing. The measured geomaterial parameters, such as SPT N-value for cohesionless materials and unconfined compressive strength of rock (q_u), were included in DSHAFT at different geomaterial layers for each drilled shaft data set. Other material parameters that were not available from the DSHAFT database were either estimated or assumed. The measured and estimated material parameters for each data set are given in Appendix B from Table B.2 for data point ID No. 1 to Table B.42 for ID No. 41. The methods used to determine or estimate the geomaterial parameters are noted with respect to the superscripted notes included in each table. The assumptions along with the estimation of parameters are described as follows:

- Closed joints were assumed in side resistance estimations in rock and IGM
- The reported SPT N-values were assumed based on a 60% hammer efficiency
- The undrained shear strength (S_u) of cohesive materials were approximated to 1) measured cohesion; 2) half of measured unconfined compressive strength; or 3) Eq. (2-9), depending on the availability of material parameters
- The unit weight of geomaterials (γ) was estimated using N_{60} based on the recommendation suggested by Bowles (1996)
- The interface friction angle (ϕ_{rc}) in cohesive IGM required for unit side resistance estimation was assumed to be 30 degrees
- The drilled shaft boreholes were not artificially roughtened

Despite tremendous subsurface information being recorded in DSHAFT, not all necessary subsurface conditions were reported or known during the subsurface investigations. For instance, the knowledge of rock mass conditions presented in Table 2.7 is required in the end bearing estimation in rock or cohesive IGM. The rock mass conditions require extensive site investigations involving multiple boreholes and expensive geophysical investigations. Hence, these conditions are rarely reported and incur many challenges in the estimation of shaft resistances for the calibration of resistance factors. The lack of adequate field data collection is due to the fact that the drilled shaft design verification relies on static load tests on either test shafts or production shafts.

Drilled shaft resistances are typically measured using the O-cell test method as illustrated in Figure 3.3. Since only a single O-cell test was performed on each test shaft, either side resistance or end bearing reaches the ultimate value with sufficient movement, but not both. In some cases, maximum O-cell capacity is reached before ultimate side resistance or end bearing is fully mobilized. When these test results are used to generate the equivalent top load-displacement curve using the procedure described in Appendix A, the curve does not go past the 1-in. or 5% diameter displacement criterion in defining the ultimate drilled shaft resistance as illustrated in Figure 3.6.

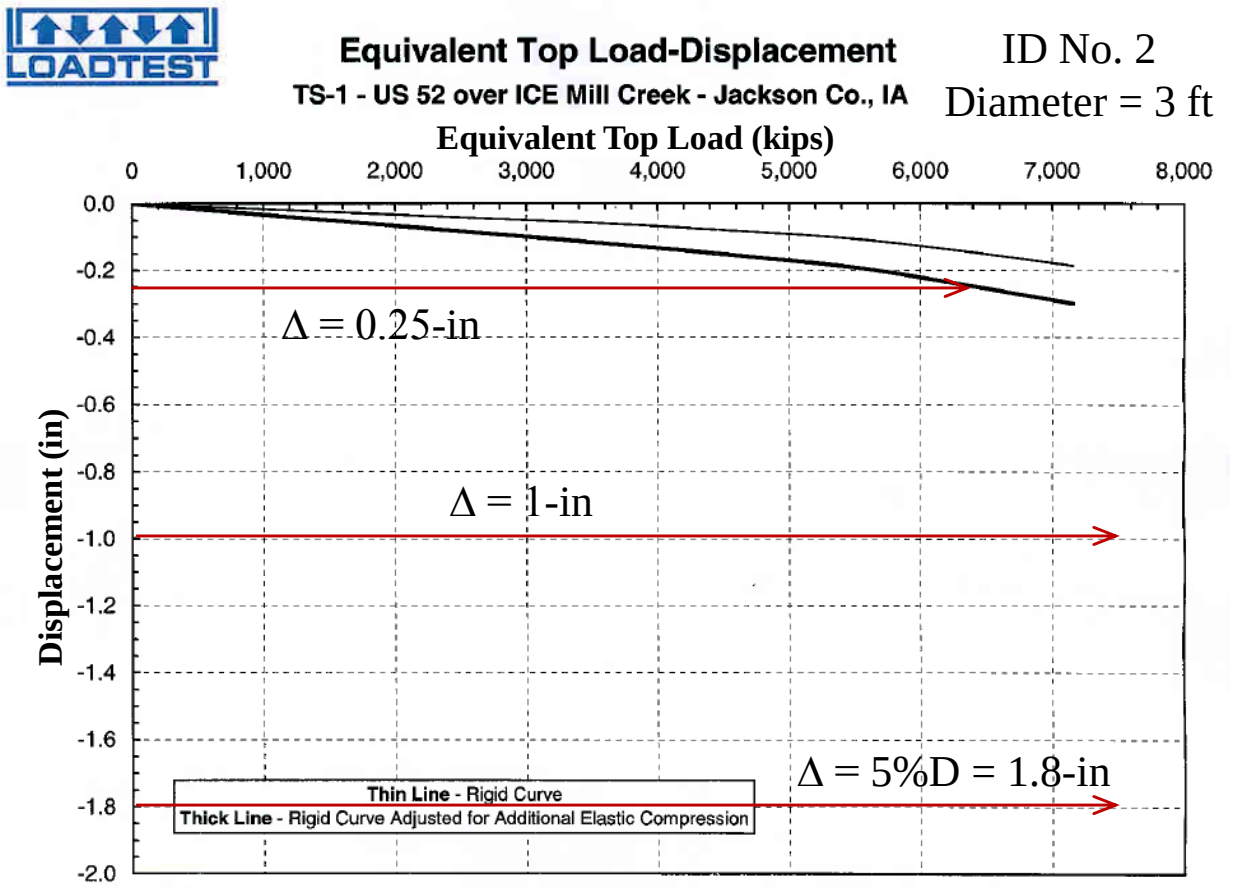

Figure 3.6. Typical equivalent top load-displacement curve from O-cell test for ID No. 2

Hence, the O-cell load test results pose some challenges in quantifying the measured ultimate resistance used in the calibration of resistance factors. Detailed description of the challenges with O-cell load test results and new procedures to overcome these limitations are discussed in Section 3.3.

3.2. Side Resistance and End Bearing Estimations

Using the shaft and subsurface information provided in DSHAFT as summarized in Appendix B, unit side resistance (q_s) in each geomaterial layer and unit end bearing (q_p) were estimated using the analytical methods summarized in Table 3.2 and described in Sections 2.3 and 2.4. Particular effort was focused on the estimation of unit end bearing in rock and cohesive IGM, in which rock mass conditions (see Table 2.7) were not clearly described or known. Nine analytical methods are currently available for unit end bearing estimation described in Section 2.4.5.

Table 3.2. Summary of static analysis methods used in the estimations of unit side resistance (q_s) and unit end bearing (q_p)

Geomaterial	Unit Side Resistance (q_s)	Unit End Bearing (q_p)
Clay	α-method by O'Neill and Reese (1999): Section 2.3.2	Total Stress method by O'Neill and Reese (1999): Section 2.4.2
Sand	β-method by Burland (1973) and O'Neill & Reese (1999): Section 2.3.3	Effective stress method by Reese and O'Neill (1989): Section 2.4.3
Cohesive IGM	Eq. (2-11) by O'Neill and Reese (1999): Section 2.3.4	See Section 2.4.5, Table 3.3 and Table 3.4
Cohesionless IGM	Eq. (2-14) by O'Neill and Reese (1999): Section 2.3.4	Eq. (2-22) by O'Neill and Reese (1999): Section 2.4.4
Rock	Eq. (2-16) by Horvath and Kenney (1979): Section 2.3.5	See Section 2.4.5, Table 3.3 and Table 3.4

Depending on the availability of geomaterial parameters, such as unconfined compressive strength and RQD, six of the nine methods were selected to estimate the end bearing in rock and cohesive IGM as enumerated in Table 3.3. Among the six methods, method No.1 for intact rock/cohesive IGM by Rowe and Armitage (1987) and method No. 4 for fractured rock/cohesive IGM by Carter and Kulhawy are recommended in AASHTO (2010).

Table 3.3. Summary of static analysis methods used in the estimation of unit end bearing (q_s) in cohesive IGM and rock

Method	Rock Mass Condition	Unit End Bearing (q_p)	Reference
1*	• Intact rock/cohesive IGM (RQD = 100%) • Joint spacing (S) >> shaft diameter (B) • Socket depth (D) ≥ 1.5 B	Eq. (2-24)	Rowe and Armitage (1987)
2	• General characteristics of rock/cohesive IGM	Eq. (2-30)	Goodman (1980)
3	• Rock/cohesive IGM with steeply dipping joints • Closed joints	Eq. (2-27)	Terzaghi (1943)
4*	• Fractured rock • Joint spacing (S) << shaft diameter (B) • Shear failure with irregular failure surface or orientation	Eq. (2-34)	Carter and Kulhawy (1988)
5	• Rock/cohesive IGM with steeply dipping joints • Joint spacing (S) ≤ shaft diameter (B) • Open joints • Compression failure of individual columns of rock/cohesive IGM	Eq. (2-26)	Sowers (1976)
6	• Rock/cohesive IGM with RQD between 70% and 100% • All joints are closed and approximately horizontal • q_u > 10.4 ksf	Eq. (2-25)	O'Neill and Reese (1999)

* – recommended in the AASHTO LRFD Bridge Design Specifications (2010)

A combination of these two methods as illustrated in Table 3.4 is proposed in this research to simplify the end bearing estimation, and its validation is presented in Chapter 4.

Table 3.4. Proposed static analysis methods used in the estimation of unit end bearing (q_s) in cohesive IGM and rock

Rock Mass Condition	Unit End Bearing (q_p)	Reference
• Intact rock/cohesive IGM (RQD = 100%) • Socket depth (D) ≥ 1.5 B	Eq. (2-24)	Rowe and Armitage (1987)
• Fractured rock • Shear failure with irregular failure surface or orientation	Eq. (2-34)	Carter and Kulhawy (1988)
• Rock/cohesive IGM (RQD < 100%)	Average of Eq. (2-24) and Eq. (2-34)	Rowe and Armitage (1987) and Carter and Kulhawy (1988)

The unit side resistance and side resistance in each geomaterial layer for each test are presented in Appendix C. The unit end bearing and end bearing in clay, sand and cohesionless IGM as well as the values in rock and cohesive IGM based on the proposed method are presented in Appendix C. Additionally, the unit end bearings in rock and cohesive IGM based on the six different methods are presented in Table 3.5.

Table 3.5. Estimated unit end bearing for drilled shafts in rock or cohesive IGM

ID	Rock/ Cohesive IGM at Shaft Base	Unit End Bearing (ksf)					
		Rowe and Armitage (1987)	Goodman (1980)	Terzaghi (1943)	Carter and Kulhawy (1988)	Sowers (1979)	O'Neill and Reese (1999)
2	Rock	1593.00	509.76	1655.40	741.34	637.20	576.57
3	Rock	276.16	59.62	56.35	5.77	110.47	235.89
4	Cohesive IGM	234.18	50.55	414.22	123.45	93.67	216.86
5	Rock	479.53	103.52	164.76	10.02	191.81	312.56
7	Rock	1900.80	713.21	1736.30	779.48	760.32	630.93
8	Rock	1383.48	519.10	337.36	132.08	553.39	536.56
13	Cohesive IGM	190.53	41.13	130.10	10.59	76.21	195.21
14	Cohesive IGM	248.75	53.70	68.90	13.29	99.50	223.65
15	Cohesive IGM	85.41	25.03	80.47	9.29	34.16	129.66
16	Cohesive IGM	126.00	27.20	67.33	n/a	n/a	158.09
17	Rock	360.00	77.71	320.88	115.68	144.00	270.04
25	Rock	972.50	284.98	379.55	105.72	389.00	448.28
28	Rock	1938.60	727.39	445.41	179.89	775.44	637.29
29	Rock	7416.00	2782.59	3897.30	1855.33	2966.40	1263.30
34	Cohesive IGM	42.12	10.24	51.77	3.77	16.85	90.41
35	Cohesive IGM	177.50	43.16	134.48	26.69	71.00	188.28
36	Rock	547.56	212.53	159.34	37.49	219.02	334.44
38	Rock	865.85	186.91	303.20	84.82	346.34	422.49
39	Rock	839.95	181.32	328.38	79.96	335.98	416.00

3.3. Equivalent Top Load-Displacement Curve

O-cell test results as shown in Figure 3.7, Figure 3.8, and Figure 3.9 for three different shaft responses are used to generate equivalent top load-displacement curves using a procedure suggested by Loadtest, Inc. as briefly described in Section 2.6.3 and Appendix A. However, in most cases, this procedure cannot generate a curve that will go past the 1-in. criterion recommended by Iowa DOT or 5% diameter displacement criterion recommended in AASHTO (2010) in defining ultimate drilled shaft resistance as illustrated in Figure 3.6. This limitation creates some challenges in this research to quantify measured ultimate resistances necessary for the calibration of resistance factors. To overcome this limitation, three different shaft responses obtained from O-cell tests are categorized as Cases A, B, and C, and three respective improved procedures are proposed to generate and extend equivalent top load-displacement curves that will intersect with the displacement criteria. Case A is identified as O-cell test results in which side resistance reaches its ultimate value with an excessive upward displacement before end bearing does, as illustrated in Figure 3.7 for data point ID No. 2.

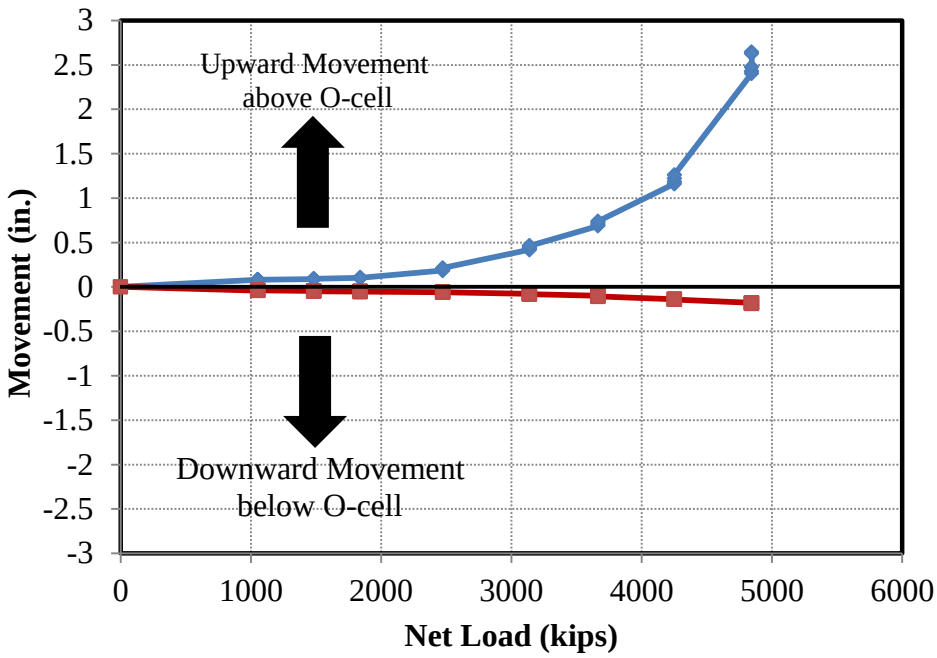

Figure 3.7. Case A: Side resistance reaches ultimate for data point ID No. 2

Case B is the opposite of Case A, in which the end bearing and/or the lower side resistance below the O-cell reaches the ultimate value with an excessive downward displacement before upper side resistance does, as illustrated in Figure 3.8 for data point ID No. 6.

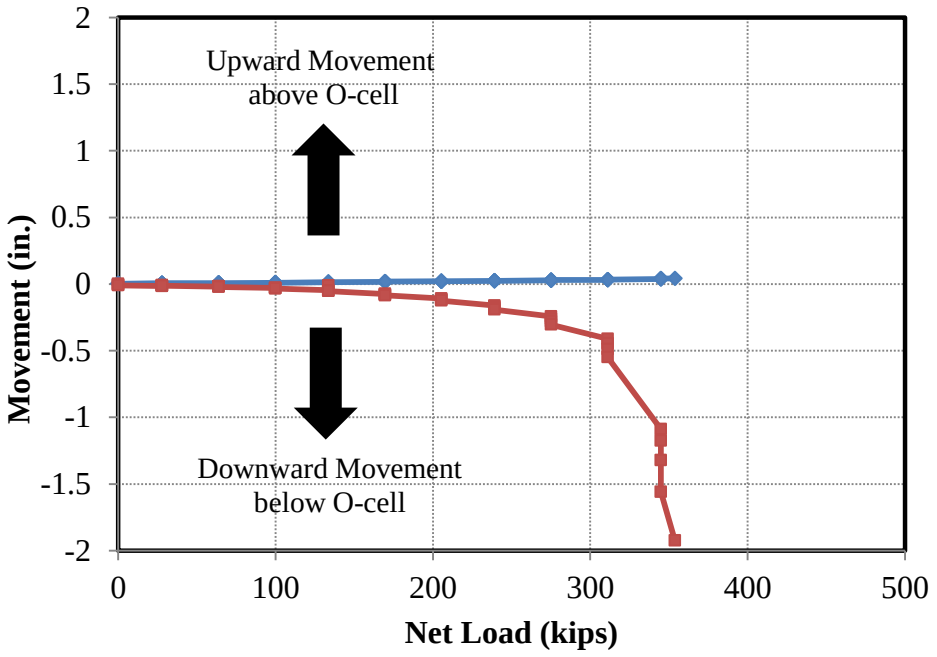

Figure 3.8. Case B: End bearing reaches ultimate for data point ID No. 6

When neither the measured side resistance nor the end bearing reaches its respective ultimate value, the shaft response is categorized as Case C as illustrated in Figure 3.9 for data point ID No. 39.

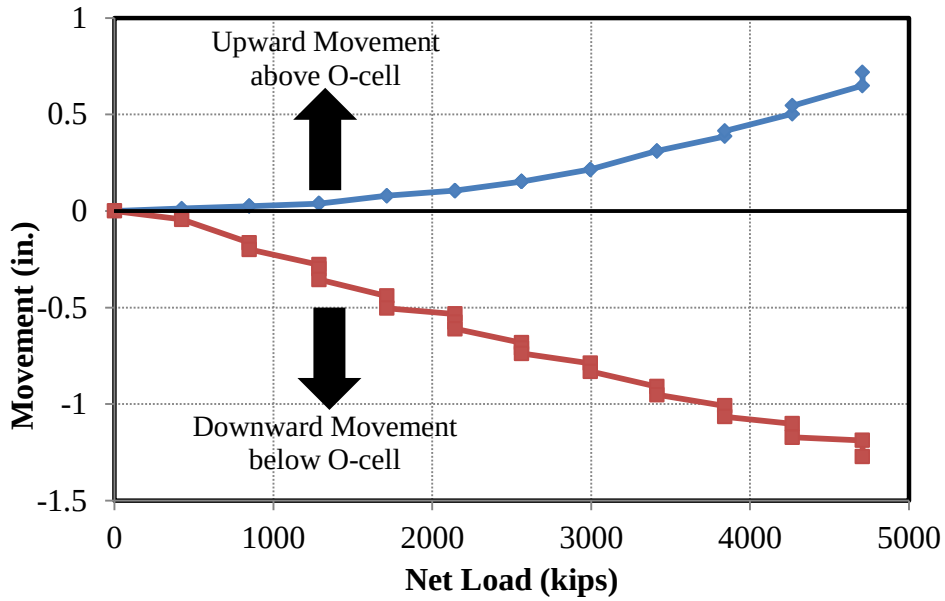

Figure 3.9. Case C: Neither end bearing nor side resistance reaches ultimate for data point ID No. 39

A summary of shaft data with respect to the three cases is shown in Table 3.6.

Table 3.6. A summary of drilled shaft data with respect to three different cases

ID	Case	ID	Case	ID	Case
1	n/a	15	B	29	C
2	A	16	C	30	B
3	A	17	A	31	n/a
4	A	18	n/a	32	n/a
5	C	19	A	33	n/a
6	B	20	A	34	B
7	C	21	n/a	35	n/a
8	C	22	n/a	36	n/a
9	Statnamic	23	n/a	37	n/a
10	Statnamic	24	C	38	A
11	Statnamic	25	C	39	C
12	n/a	26	B	40	n/a
13	A	27	B	41	n/a
14	A	28	A		

n/a – Non-usable data point or O-cell test results are not available in DSHAFT; Statnamic – load test results are obtained from Statnamic test method and are not applicable.

The three improved procedures to generate the top load-displacement curves are presented in flowcharts proposed in Figure 3.10 for Case A, Figure 3.11 for Case B, and Figure 3.12 for Case C.

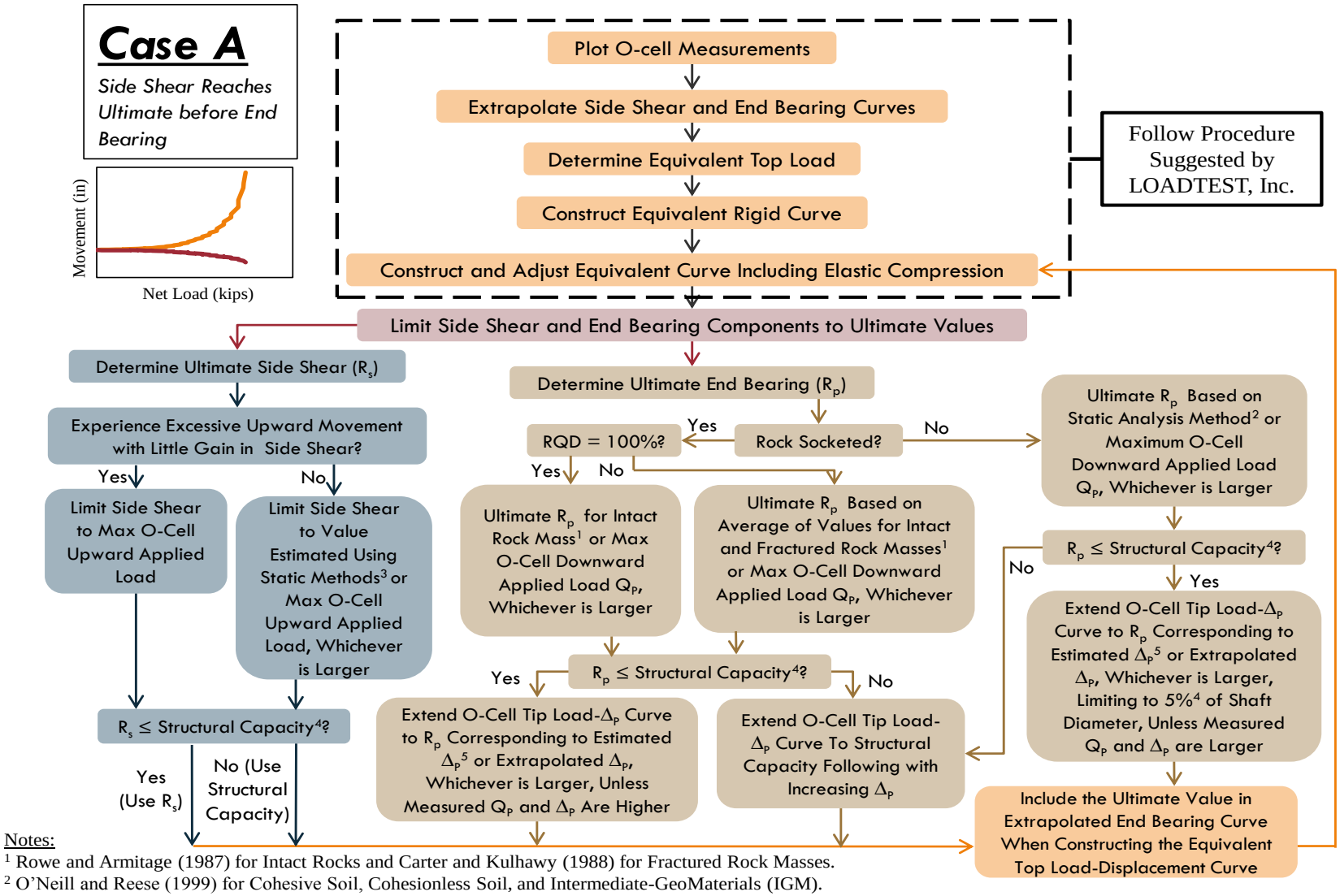

Notes:

[1] Rowe and Armitage (1987) for Intact Rocks and Carter and Kulhawy (1988) for Fractured Rock Masses.

[2] O'Neill and Reese (1999) for Cohesive Soil, Cohesionless Soil, and Intermediate-GeoMaterials (IGM).

[3] Alpha-method for Cohesive Soil, Beta-Method for Cohesionless Soil, O'Neill et al. (1996) for IGM, Horvath and Kenney (1979) for Rocks, or a Combination of All.

[4] AASHTO LRFD Bridge Design Specifications (2010).

[5] Estimated Tip Displacement: Vesic for Soils, O'Neill et al. (1996) for Cohesive IGM, Mayne and Harris (1993) for Granular IGM, and Kulhawy and Carter (1992) for Rock

Figure 3.10. Proposed procedure to generate an equivalent top load-displacement curve for Case A

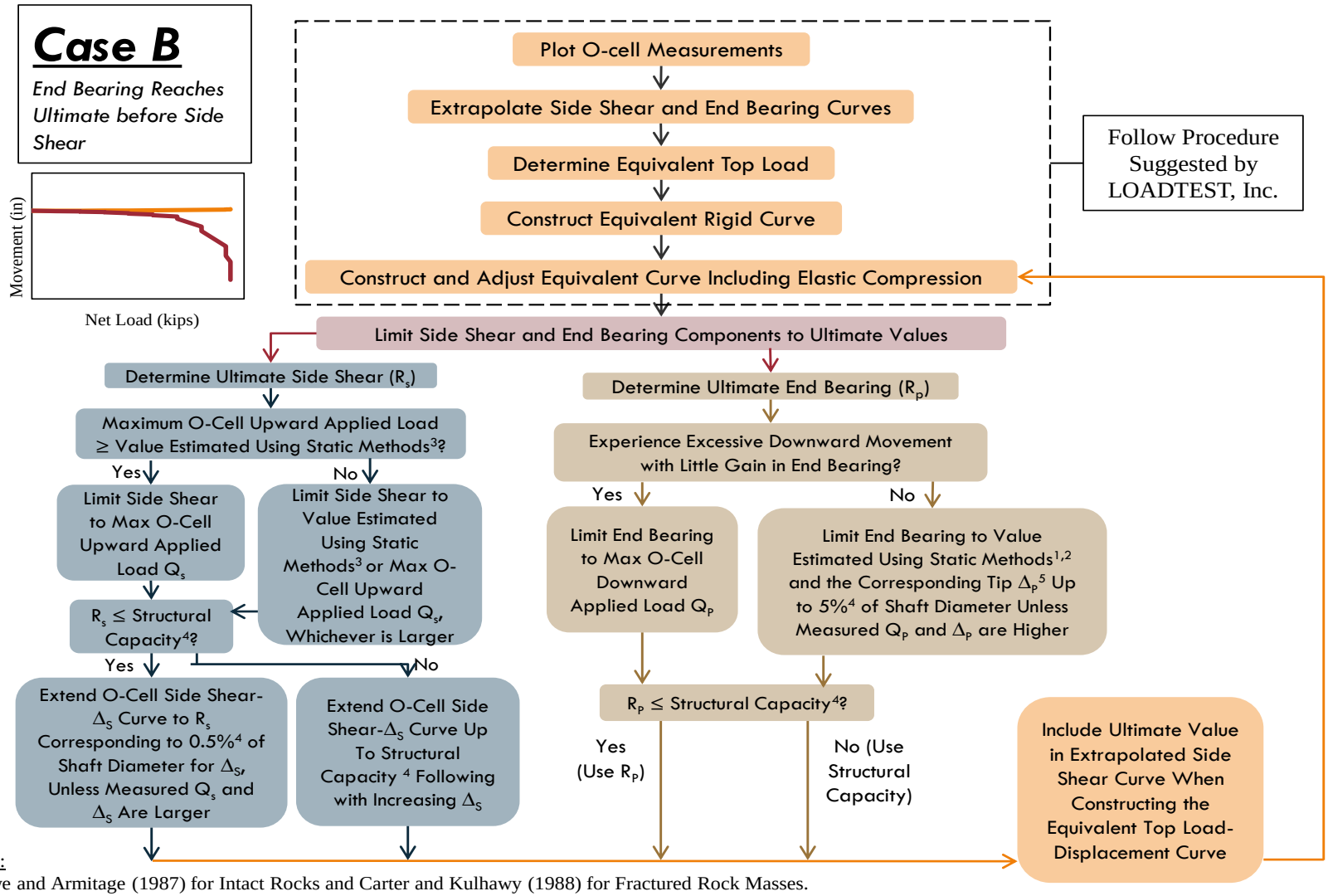

Notes:

[1] Rowe and Armitage (1987) for Intact Rocks and Carter and Kulhawy (1988) for Fractured Rock Masses.

[2] O'Neill and Reese (1999) for Cohesive Soil, Cohesionless Soil, and Intermediate-GeoMaterials (IGM).

[3] Alpha-method for Cohesive Soil, Beta-Method for Cohesionless Soil, O'Neill et al. (1996) for IGM, Horvath and Kenney (1979) for Rocks, or a Combination of All.

[4] AASHTO LRFD Bridge Design Specifications (2010).

[5] Estimated Tip Displacement: Vesic for Soils, O'Neill et al. (1996) for Cohesive IGM, Mayne and Harris (1993) for Granular IGM, and Kulhawy and Carter (1992) for Rock

Figure 3.11. Proposed procedure to generate an equivalent top load-displacement curve for Case B

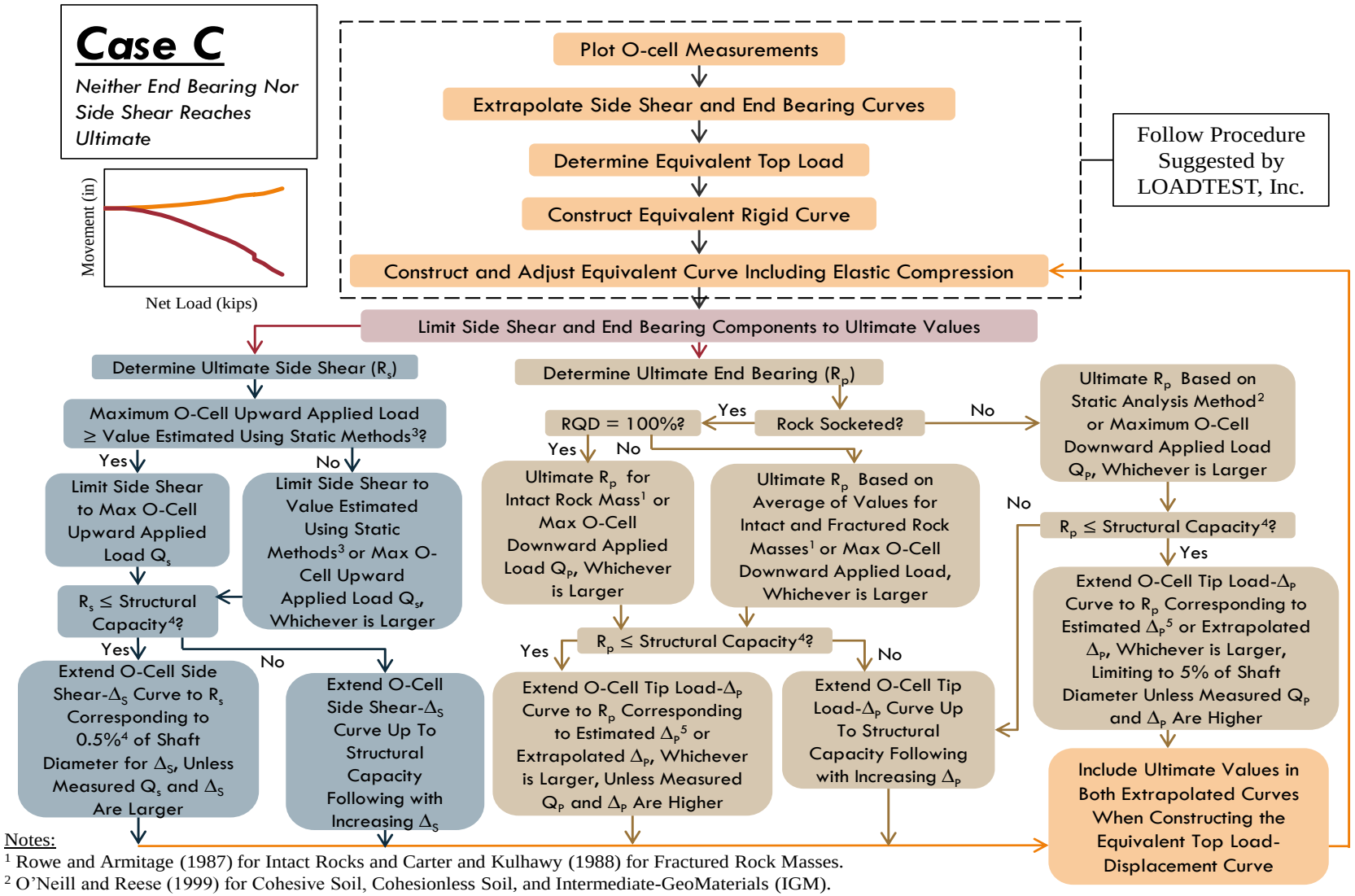

Notes:

[1] Rowe and Armitage (1987) for Intact Rocks and Carter and Kulhawy (1988) for Fractured Rock Masses.

[2] O'Neill and Reese (1999) for Cohesive Soil, Cohesionless Soil, and Intermediate-GeoMaterials (IGM).

[3] Alpha-method for Cohesive Soil, Beta-Method for Cohesionless Soil, O'Neill et al. (1996) for IGM, Horvath and Kenney (1979) for Rocks, or a Combination of All.

[4] AASHTO LRFD Bridge Design Specifications (2010).

[5] Estimated Tip Displacement: Vesic for Soils, O'Neill et al. (1996) for Cohesive IGM, Mayne and Harris (1993) for Granular IGM, and Kulhawy and Carter (1992) for Rock

Figure 3.12. Proposed procedure to generate an equivalent top load-displacement curve for Case C

Each improved procedure is described with three main flowcharts with:1) the orange flowchart at the top describing the original procedure suggested by Loadtest, Inc., 2) the blue flowchart on the left describing the proposed approach to determine the ultimate side shear and extend the measured upward load-displacement curve, and 3) the brown flow chart on the right describing the proposed approach to determine the ultimate end bearing and extend the measured downward load-displacement curve. After extending the upward and downward curves and identifying the ultimate side shear and end bearing, an equivalent top load-displacement is reconstructed and adjusted to account for shaft elastic compression. To help with understanding the application of the improved procedures, an example for each case is demonstrated.

Case A: Data Point ID No. 2

Referring to Appendix B, ID No. 2 is a 3-ft diameter drilled shaft with an embedded length of 12.7 ft in and bearing on rock with a RQD of 93%. The O-cell test response of ID No. 2 shown in Figure 3.13(a) was categorized as Case A.

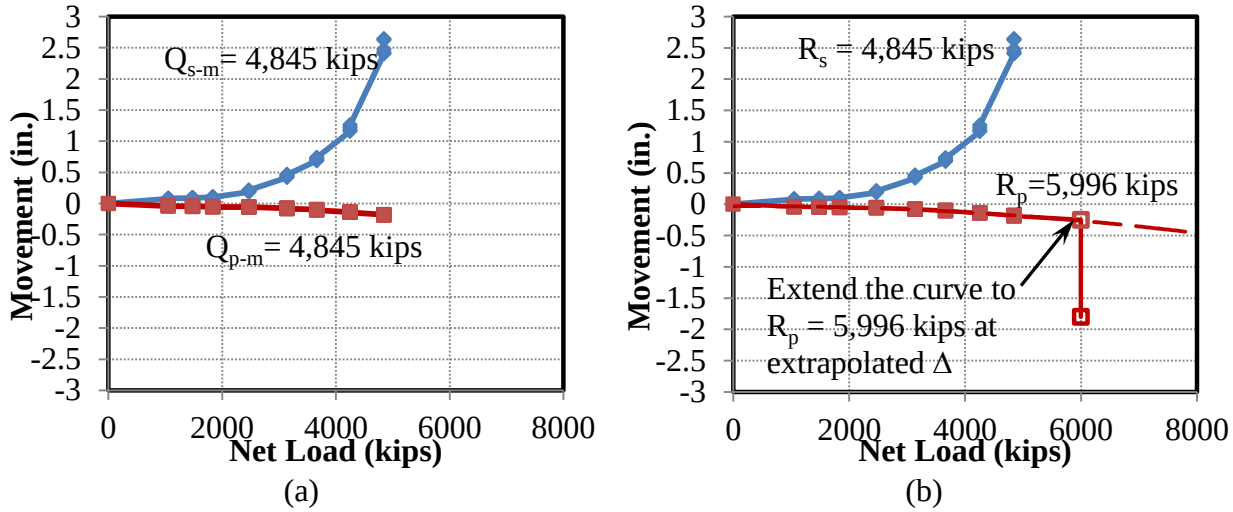

Figure 3.13. O-cell measurement for ID No. 2 (a) original curves, and (b) modified curves

A maximum load (Q_m) of 4,845 kips applied by the O-cell mobilized an excessive upward movement of 2.625 in. and a minimal downward movement of 0.189 in. Following the blue flowchart in Figure 3.10, the ultimate side resistance was limited to the maximum upward applied O-cell load of 4,845 kips. Since the ultimate side resistance was smaller than the structural side resistance of 39,488 kips calculated using the maximum limit of Eq. (2-16), the original upward load-displacement curve was used in reconstructing the top load-displacement curve. On the other hand, the end bearing indicated by the downward load-displacement curve hasn't reached its ultimate resistance since only a very small downward movement was mobilized and the curve remained almost elastic. The ultimate end bearing was determined by following the brown flowchart given in Figure 3.10. Having a rock-socketed shaft and RQD smaller than 100%, the ultimate end bearing was limited to either an end bearing of 8,250 kips estimated using the proposed analytical methods given in Table 3.4 or the maximum downward applied O-cell load of 4,845, whichever is larger. In this comparison, the ultimate end bearing of 8,250 kips was preliminarily chosen and compared with the structural capacity of 5,996 kips calculated using Eq. (2-35). Since the preliminary value of 8,250 kips was larger than the

structural capacity, the downward load-displacement curve was extended following the best-fit dashed line and the end bearing limited to the structural capacity shown in Figure 3.13(b). Using the modified downward curve and the upward curve, the equivalent top load-displacement curve was reconstructed as shown in Figure 3.14.

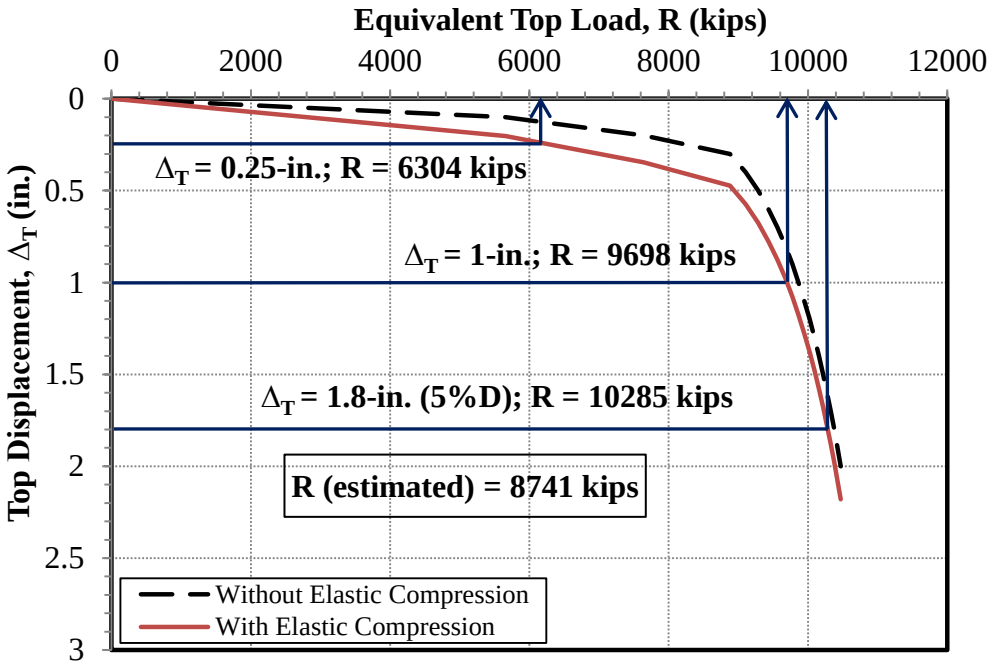

Figure 3.14. Equivalent top load-displacement curve for ID No. 2 generated using the improved procedure for Case A

To account for the shaft elastic compression described in Appendix A, the curve was adjusted from a black dashed line to a solid red line. Comparing the improved curve given in Figure 3.14 with that shown in Figure 3.6, the improved curve enables the determination of ultimate shaft resistances with respect to the 1-in. displacement criterion and the 5% diameter for displacement criterion.

Case B: Data Point ID No. 6

Test shaft ID. No.6 has a diameter of 2.5 ft and is embedded 64 ft in and clay. The O-cell test result shown in Figure 3.15(a) was categorized as Case B. A maximum load (Q_m) of 345 kips applied by the O-cell mobilized an excessive downward movement of 1.925 in. and a minimal upward movement of 0.042 in.

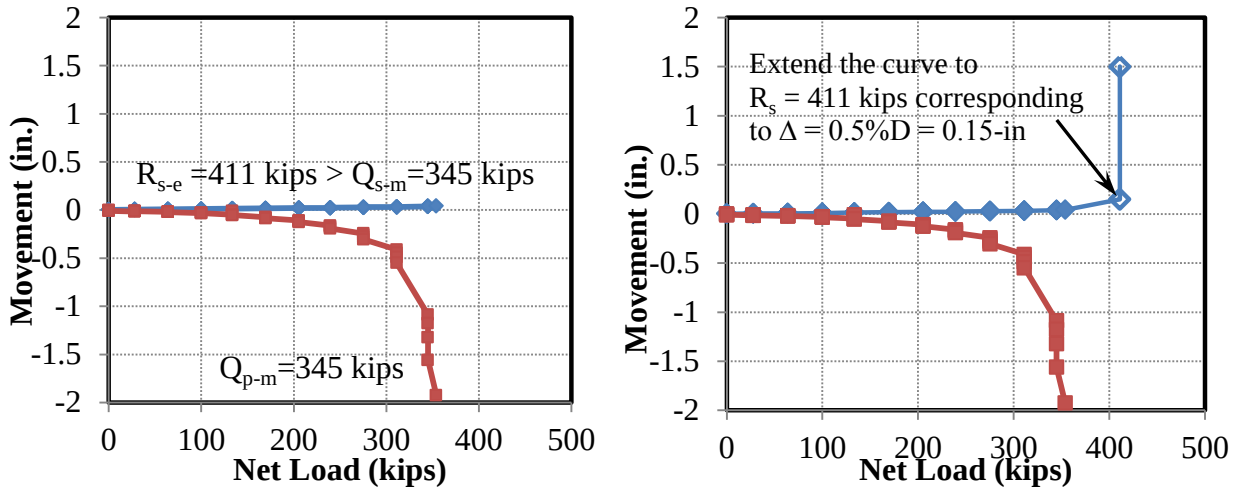

Figure 3.15. O-cell measurement for ID No. 6 (a) original curves, and (b) modified curves

The end bearing in clay was estimated to be 136 kips. Following the brown flowchart for determining ultimate end bearing in Figure 3.11, the end bearing was limited to the maximum downward applied O-cell load (Q_{p-m}) of 345 kips. Since the preliminary end bearing was smaller than the structural capacity of 2,451 kips calculated using Eq. (2-35), the original downward load-displacement curve was used in reconstructing the top load-displacement curve. On the other hand, the side resistance indicated by the upward load-displacement curve hasn't reached its ultimate resistance since only a very small upward movement was mobilized and the curve remained almost elastic. The ultimate side resistance was determined by following the blue flowchart given in Figure 3.15. Since the maximum O-cell load was smaller than the estimated value of 411 kips calculated using the α-method in Table 3.2, the ultimate side resistance was preliminarily limited to the estimated value of 411 kips. Compared with the structural side resistance of 127,792 kips calculated using the maximum limit of Eq. (2-16), the upward load-displacement curve was extended to 411 kips at a displacement corresponding to 0.5% of the shaft diameter (i.e., displacement (Δ) = 0.15 in) as shown in Figure 3.15(b). It was assumed that the shaft will not sustain additional loads larger than 411 kips since excessive upward movement will be experienced. Using the modified upward curve and the downward curve, the equivalent top load-displacement curve was reconstructed as shown in Figure 3.16.

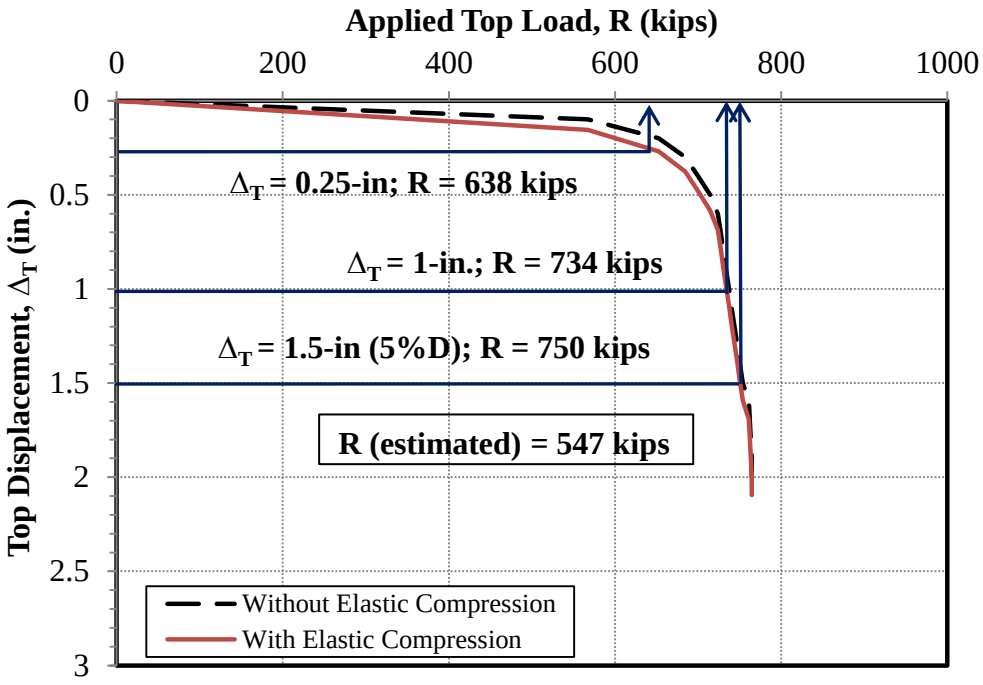

Figure 3.16. Equivalent top load-displacement curve for ID No. 6 generated using the improved procedure for Case B

To account for the shaft elastic compression described in Appendix A, the curve was adjusted from a black dashed line to a solid red line. Hence, the improved curve enables the determination of ultimate top-loaded shaft resistances with respect to the 1-in. displacement criterion and the 5% diameter for displacement criterion.

Case C: Data Point ID No. 39

Case C is demonstrated using the test shaft ID No. 39 with 4 ft diameter and 20 ft embedded in shale bedrock with a RQD of 75.5% and bearing on the same bedrock with a RQD of 88% as shown in Table B.40. The O-cell test result shown in Figure 3.17(a) indicates that the side resistance indicated by the upward curve and the end bearing indicated by the downward curve haven't reached their ultimate resistances since both curves were almost elastic and haven't experienced excessive movements with small increase in resistances.

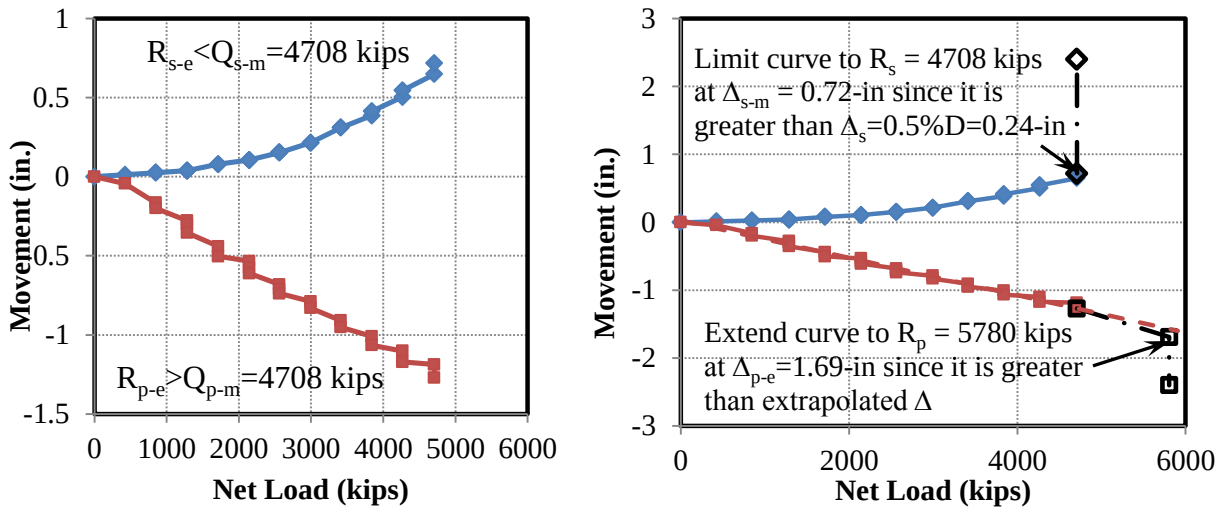

Figure 3.17. O-cell measurement for ID No. 39 (a) original curves, and (b) modified curves

Figure 3.12 shows the necessary procedures in flowcharts to modify the O-cell test results and reconstruct the equivalent top load-displacement curve. Following the blue flowchart, the maximum O-cell load of 4,708 kips was greater than the estimated side resistance of 4,325 kips using the analytical method given in Table 3.2. Thus, the side resistance was limited to the maximum O-cell load. Comparing this preliminarily chosen side resistance of 4,708 kips with the structural capacity of 89,378 kips determined using the maximum limit of Eq. (2-16), the upward curve was limited to 4,708 kips at the maximum measured upward displacement of 0.72 in, since the measured load 4,708 kips was larger than the estimated value and the measured displacement was larger than the 0.5% shaft diameter for displacement (i.e., 0.24 in). It was assumed that the shaft will not sustain additional side resistance larger than 4,708 kips since excessive upward movement will be experienced. In the case of rock-socketed end bearing and a RQD of 88%, the ultimate end bearing was taken as the estimated value of 5,780 kips, calculated using the analytical methods proposed in Table 3.4 since it was larger than the maximum O-cell load. Comparing this end bearing with the structural capacity of 5,805 kips calculated using Eq. (2-35), the downward curve was extended to 5,780 kips at a corresponding displacement of 1.69 in estimated using Kulhaway and Carter (1992) method for rock. The estimated displacement was selected because it was slightly greater than the extrapolated displacement at the same load 5,780 kips, as shown in Figure 3.17(b). Using both the modified upward and downward curves, the equivalent top load-displacement curve was reconstructed as shown in Figure 3.18.

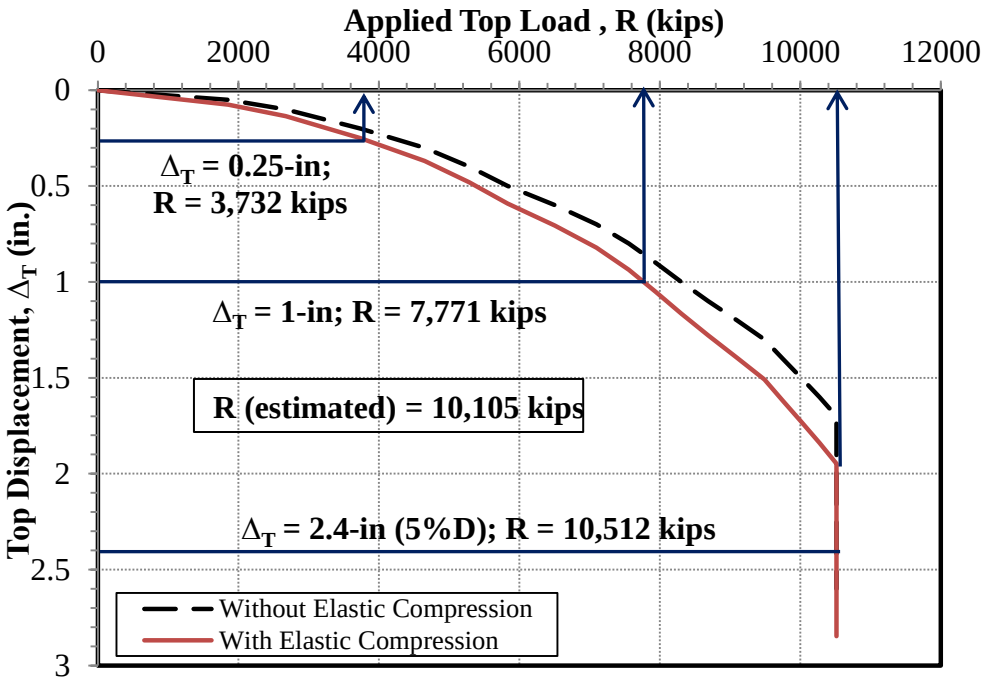

Figure 3.18. Equivalent top load-displacement curve for ID No. 39 generated using the improved procedure for Case C

To account for the shaft elastic compression described in Appendix A, the curve was adjusted from a black dashed line to a solid red line. Hence, the improved curve enables the determination of ultimate top-loaded shaft resistances with respect to the 1-in. displacement criterion and the 5% diameter for displacement criterion.

3.4. Measured Total Resistance, Side Resistance, and End Bearing

Adopting the proposed procedures for generating equivalent top load-displacement curves described in Section 3.3, estimaed shaft resistances were determined based on the following failure defining criteria:

1) Recommendation given in load test reports collected in DSHAFT
2) 0.25% of shaft diameter for top displacement
3) 1-in. top displacement
4) 0.5% of shaft diameter for top displacement

Table 3.7 summarizes the measured total resistance, side resistance and end bearing based on the aforementioned criteria. To help with the calibration of resistance factors for various geomaterials along drilled shafts in Chapter 4, the measured side resistances summarized in Table 3.7 for the third and fourth failure criteria were proportioned according to the percent of side resistance in each geomaterial layer measured from the O-cell load test. The proportioned side resistances are summarized in Table 3.8 for the clay layers, Table 3.9 for the sand layers, Table 3.10 for the IGM layers, and Table 3.11 for thr rock layers.

.

Table 3.7. Summary of measured shaft resistances with respect to various failure defining criteria

ID	Recommended in Load Test Report (kips)			0.25% Diameter for Top Displacement (kips)			1-in. Top Displacement (kips)			0.5% Diameter for Top Displacement (kips)		
	Total	Side	End	Total	Side	End	Total	Side	End	Total	Side	End
1[a]	n/a	n/a	n/a	1391	n/a	n/a	1858	n/a	n/a	n/a	n/a	n/a
2	10474	4845	5629	6265	2286	4019	9698	3702	5996	10285	4289	5996
3	4196	2425	1771	1791	787	995	3543	1620	1923	4422	2495	1927
4	6430	4177	2253	2233	1279	953	6397	3391	3006	8142	4059	4083
5	5398	2322	3076	2653	1947	705	4289	2322	1967	5160	2322	2839
6	765	411	354	638	406	232	734	411	323	751	411	340
7[b]	14767	5294	9473	6829	6491	337	10444	9241	1202	11195	9241	1954
8	26633	8629	13350	9519	3992	5526	26996	8629	13350	27102	8629	13350
9	n/a	n/a	n/a	1400	n/a	n/a	2465	1753	712	2530	1799	731
10	n/a	n/a	n/a	1400	n/a	n/a	2362	1613	749	2285	1560	725
11	n/a	n/a	n/a	1300	n/a	n/a	2033	1643	390	1950	1576	374
12[a]	2337	1169	1169	1041	786	255	1813	1169	645	2171	1169	1002
13	2377	1297	1080	1650	890	680	2165	1185	980	2327	1297	1030
14	14428	14428	n/a	5300	5300	n/a	7306	7306	n/a	7594	7594	n/a
15	4256	1412	2843	2029	1126	922	3276	1404	1873	4602	1412	3189
16	7594	7594	0	5300	5300	0	7306	7306	0	7594	7594	0
17	2998	1499	1499	2258	1499	759	2656	1499	1157	2820	1499	1321
18[a]	7072	3510	3563	5416	3503	1912	7057	3503	3553	7066	3503	3563
19	16990	8024	8966	5427	3601	1827	12837	7404	5433	17363	8024	9339
20	4390	3324	1066	1901	1127	774	3504	2258	1246	3811	2258	1553
21[a]	3098	1716	1382	1721	1288	598	3356	1716	1640	3432	1716	1716
22[a]	3819	2258	1561	1901	1127	773	3504	2258	1264	3812	2258	1553
23[a]	n/a	n/a	n/a	n/a	n/a	n/a	n/a	n/a	n/a	n/a	n/a	n/a
24[a]	n/a	n/a	n/a	n/a	n/a	n/a	n/a	n/a	n/a	n/a	n/a	n/a
25	3121	2185	936	2607	1027	1580	3160	1580	1580	3160	1580	1580
26	14325	7944	6381	12273	6611	5662	14238	7857	6381	14238	7857	6381
27	3160	1580	1580	2607	1027	1580	3160	1580	1580	3160	1580	1580
28	13899	4323	9576	6500	3716	2545	9908	4323	5585	13034	4323	8711

Table 3.7 Summary of ultimate measured shaft resistances with respect to various failure defining criteria (continued)

ID	Recommended in Load Test Report (kips)			0.25% Diameter for Top Displacement (kips)			1-in. Top Displacement (kips)			0.5% Diameter for Top Displacement (kips)		
	Total	Side	End	Total	Side	End	Total	Side	End	Total	Side	End
29	14836	5486	9350	8237	5323	2914	14724	5486	9238	14836	5486	9350
30[(a)]	6407	3207	3200	2331	1395	936	5996	3207	2789	6354	3207	3146
31[(a)]	n/a	n/a	n/a	n/a	n/a	n/a	n/a	n/a	n/a	n/a	n/a	n/a
32[(a)]	n/a	n/a	n/a	n/a	n/a	n/a	n/a	n/a	n/a	n/a	n/a	n/a
33	n/a	n/a	n/a	480	n/a	n/a	948	n/a	n/a	1067	n/a	n/a
34	1320	660	660	659	468	191	1076	660	416	1220	660	560
35	n/a	n/a	n/a	3241	n/a	n/a	5554	n/a	n/a	6504	n/a	n/a
36	n/a	n/a	n/a	4107	n/a	n/a	11582	n/a	n/a	14218	n/a	n/a
37[(a)]	n/a	n/a	n/a	n/a	n/a	n/a	n/a	n/a	n/a	n/a	n/a	n/a
38	9391	3418	5973	4421	1961	2460	9507	3357	6150	9283	3108	6175
39	10513	4708	5780	3732	2865	867	7771	4708	3063	10769	4708	5805
40[(a)]	n/a	n/a	n/a	5570	n/a	n/a	n/a	n/a	n/a	n/a	n/a	n/a
41[(a)]	n/a	n/a	n/a	3241	n/a	n/a	n/a	n/a	n/a	n/a	n/a	n/a

Total – total resistance; Side – side resistance; End – end bearing; n/a – not available; [(a)] – non-usable data; [(b)] – a gap between shaft base and bearing rock.

Table 3.8. Summary of measured ultimate side resistances in clay layers with respect to various failure criteria

ID	Side Resistance in Clay Layers (kips)		
	Recommended in Load Test Report	1-in. Top Displacement	0.5% Diameter for Top Displacement
3	300	391	603
5	417	253	253
6	613	411	411
8	275	137	137
9	424	361	371
10	424	462	447
11	401	403	386
25	16	28	28
26	40	24	24
27	60	22	24
30	3675	1814	1814
34	577	660	660

Table 3.9. Summary of measured ultimate side resistances in sand layers with respect to various failure criteria

ID	Side Resistance in Sand Layers (kips)		
	Recommended in Load Test Report	1-in. Top Displacement	0.5% Diameter for Top Displacement
5	78	47	47
7	68	49	49
8	5705	2843	2843
9	1634	1392	1428
10	1057	1151	1114
11	1233	1240	1189
20	3324	2258	2258
26	1931	1145	1145
27	3103	1163	1273
30	2823	1393	1393

Table 3.10. Summary of ultimate measured side resistances in IGM layers with respect to various failure defining criteria

ID	Side Resistance in IGM Layers (kips)		
	Recommended in Load Test Report	1-in. Top Displacement	0.5% Diameter for Top Displacement
4	5252	3391	4059
5	3007	1823	1823
13	1654	1404	1412
14	5199	2760	2869
15	1924	1499	1499
16	3641	3503	3503
17	5043	6238	6761
19	2000	1716	1716
24	572	371	371
25	892	1580	1580
33	536	n/a	n/a
35	4345	n/a	n/a

n/a – not available.

Table 3.11. Summary of ultimate measured side resistances in rock layers with respect to various failure defining criteria

ID	Side Resistance in Rock Layers (kips)		
	Recommended in Load Test Report	1-in. Top Displacement	0.5% Diameter for Top Displacement
2	5350	3702	4289
3	943	1229	1892
5	329	199	199
7	12665	9192	9192
8	11338	5649	5649
14	8563	4546	4725
17	942	1166	1263
24	11533	7486	7486
28	4021	4323	4323
29	4703	5486	5486
36	11418	n/a	n/a
38	3732	3357	3108
39	5027	4708	4708

n/a – not available.

Figure 3.19 shows a direct relationship between the measured unit end bearing in IGM and the RQD. Figure 3.20 shows a direct relationship between the measured unit end bearing in IGM and the uniaxial compressive strength (q_u) of IGM. The results confirm that the unit end bearing in IGM is influenced positively by both the RQD and q_u of the IGM. Figure 3.21 shows a poor relationship between the measured unit end bearing in rock and the RQD.

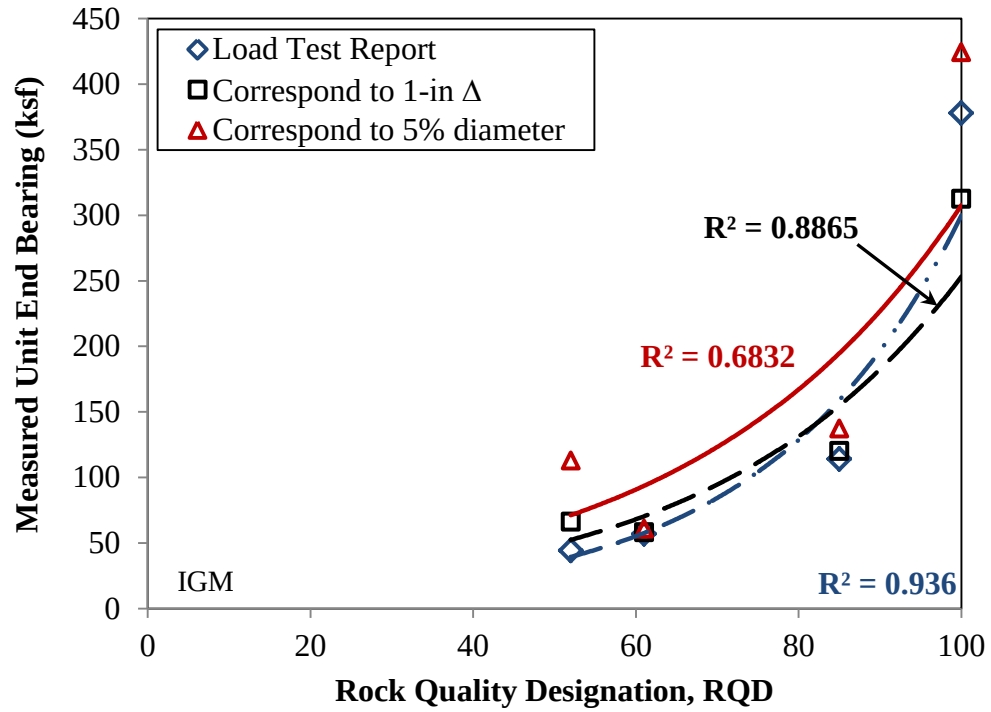

Figure 3.19. Comparison of measured unit end bearing in IGM and RQD

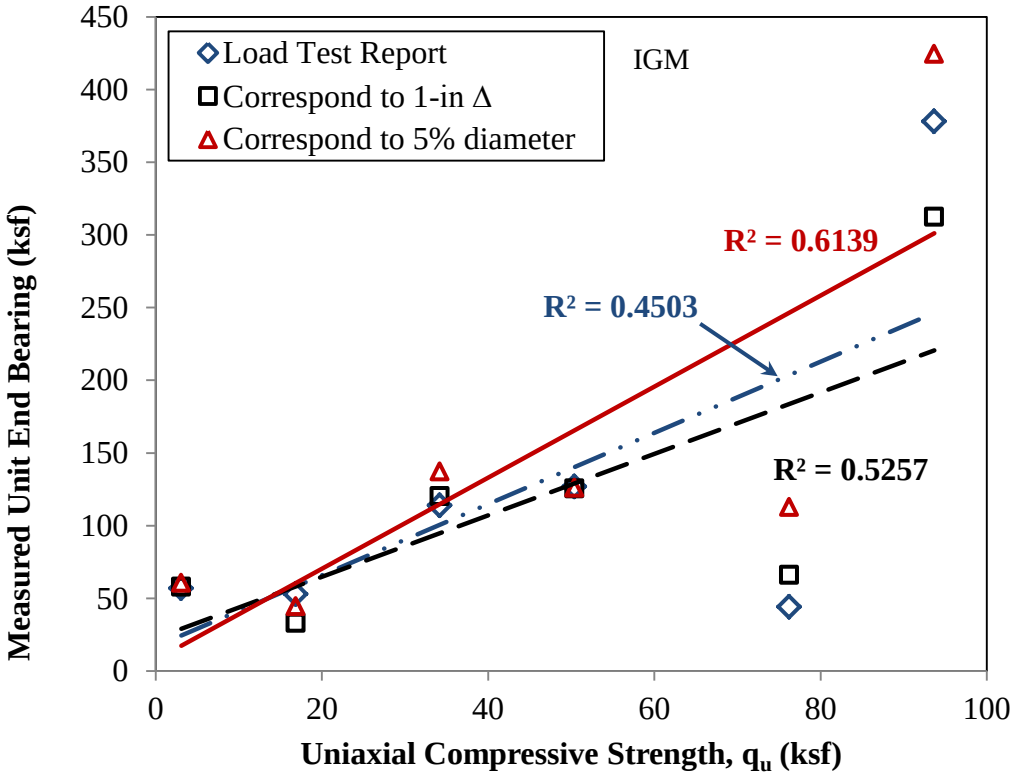

Figure 3.20. Comparison of measured unit end bearing in IGM and q_u

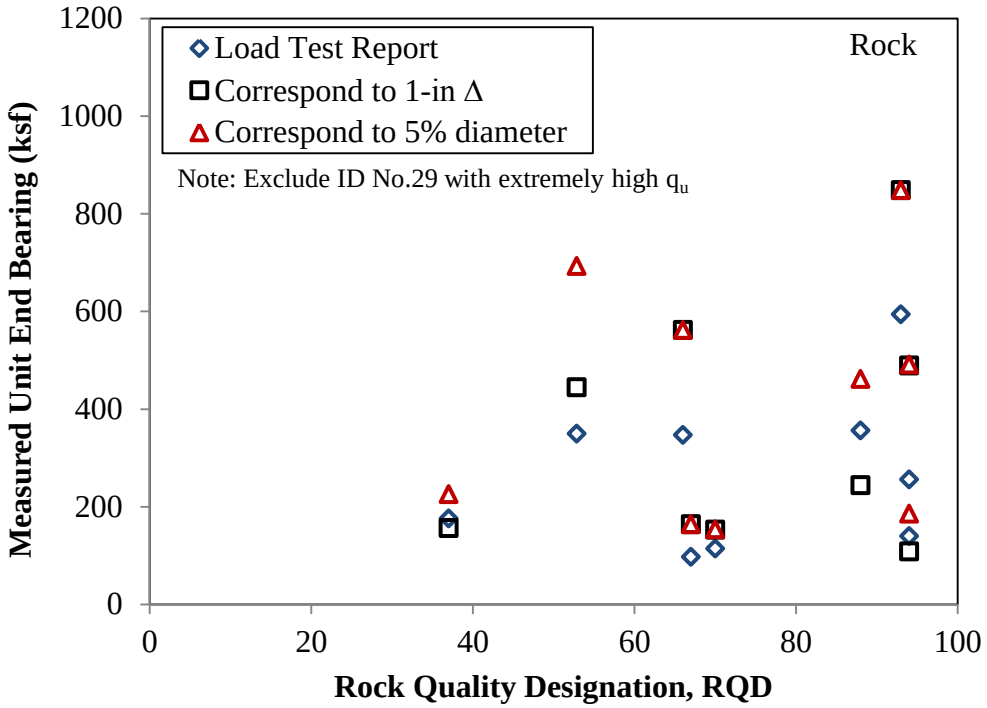

Figure 3.21. Comparison of measured unit end bearing in rock and RQD

However, Figure 3.22 shows a promising direct relationship between the measured unit end bearing in rock and the uniaxial compressive strength (q_u) of rock. The results show that the unit end bearing in rock is influenced primarily by the q_u

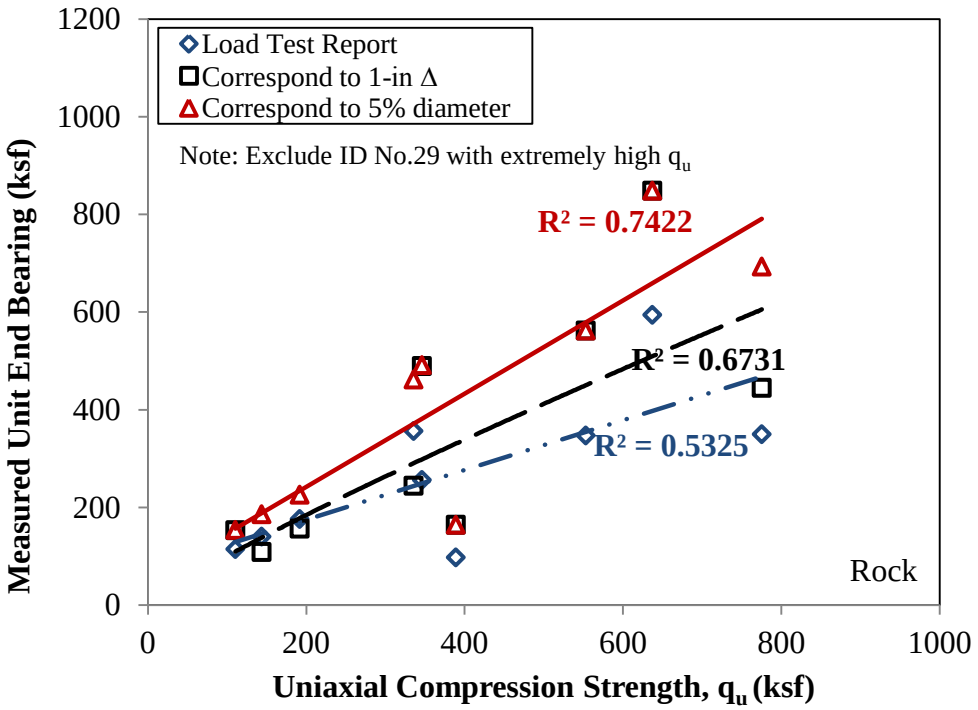

Figure 3.22. Comparison of measured unit end bearing in rock and q_u

CHAPTER 4. DEVELOPMENT OF REGIONAL LRFD RESISTANCE FACTORS

4.1. LRFD Calibration Framework

LRFD resistance factors (φ) are calibrated following the probability-based reliability theory method described in Section 2.2.2. Among the various methods, the modified FOSM method, which is simple to use and provides comparable results to other more complex methods, was selected to determine resistance factors for total resistance (R), side resistance (R_s) as well as end bearing resistance (R_p) for four different geomaterials (i.e., clay, sand, IGM and rock). Using the estimated resistances (described in Section 3.2 and summarized in Appendix C) and the measured resistances for three failure defining criteria (described in Section 3.4), statistical characteristics (i.e., mean and standard deviation) were determined for: 1) resistance ratio, and 2) ratio of measured to estimated resistances, for each resistance component and geomaterial. To verify that the drilled shaft resistances follow a lognormal distribution, a hypothesis test, based on the Anderson-Darling (AD) (1952) normality method, was used to assess the goodness-of-fit of the assumed distribution. The reason for selecting the Anderson-Darling method is because it is one of the best normality tests for a database with a relatively small sample size (Romeu, 2010). If the AD value calculated using Eq. (4-1) is smaller than the respective critical value (CV) determined using Eq. (4-2), the assumed lognormal characteristic is confirmed.

$$AD = \sum_{i=1}^{N} \frac{1-2i}{N} \{\ln(F_o[Z_i]) + \ln(1 - F_o[Z_{N+1-i}])\} - N \quad (4\text{-}1)$$

$$CV = \frac{0.752}{1 + \frac{0.75}{N} + \frac{2.25}{N^2}} \quad (4\text{-}2)$$

where,

$F_o[Z_i]$ = the cumulative probability density function of Z at i data = Pr ($Z \leq z_i$),
Pr ( ) = probability function,
Z = standardized normal distribution of expected resistance bias λ_R or $\ln(\lambda_R)$,
z_i = standardized normal distribution of estimated resistance bias λ_R or $\ln(\lambda_R)$ = $\frac{R_i - \mu_R}{\sigma_R}$ or $\frac{\ln(R_i) - \mu_{\ln(R)}}{\sigma_{\ln(R)}}$,
λ_R = resistance bias, a ratio of estimated and measured pile resistances, and
N = sample size.
$\mu_R =$ __ , $\sigma_R =$ __ , $R :=$ ___

With the focus on the axial resistance of a drilled shaft, the AASHTO (2010) Strength I load combination was selected in the calibration process, in which only dead load (Q_D) and live load (Q_L) were considered in the limit state Eq. (2-2). The assumed probabilistic characteristics of dead and live loads given in Table 2.1 were adopted in the calibration framework. Since the dead to live load ratio (Q_D/Q_L) has no significant influence on the resistance factor (Paiskowsky et al. 2004 and Allen 2005), a Q_D/Q_L ratio of 2.0, the same ratio used in the calibration of resistance factors for driven piles in Iowa (AbdelSalam et al. 2012), was selected in order to maintain design consistency. Additionally, the calibration of resistance factors requires a proper selection of a set of target reliability levels represented by a series of target reliability indices (β_T) that

correspond to a range of probability of failure (p_f) described in Section 2.2.2. Resistance factors recommended in AASHTO (2010) for drilled shafts were determined based on a β_T of 3.0, because a bridge foundation normally has four or fewer drilled shafts per cap. However, for a redundant foundation with five or more drilled shafts per cap, a lower β_T of 2.33 can be used in the resistance factor calibration. To cover a wide range of design possibilities, a range of reliability indices: 2.00, 2.33, 2.50, 3.00 and 3.50 were selected in this research. To evaluate and compare the efficiency of the three failure criteria and the different analytical methods used in estimating the end bearing in cohesive IGM or rock, efficiency factors (φ/λ), the ratio of resistance factor to resistance bias, were calculated over the range of reliability indices.

4.2. Side Resistance

4.2.1. Clay

Individual side resistance in each clay layer along a drilled shaft was estimated using the α-method described in Section 2.3.2. Depending on the number of clay layers along the shaft, the side resistance of the drilled shaft in clay is the summation of all individual side resistances in the clay layers. The measured side resistance in clay of each applicable test shaft is listed in Table 3.8 with respect to the three failure defining criteria. The comparisons of estimated and measured side resistances in clay are shown in 1) Figure 4.1 for the measured resistance obtained directly from the load test report, 2) Figure 4.2 for the measured resistance defined based on the 1-in. top displacement criterion, and 3) Figure 4.3 for the measured resistance defined based on the 5% of shaft diameter for top displacement criterion. The comparisons show that the side resistance in clay is generally underestimated with respect to the measured value since the best-fit line is above the line of equality.

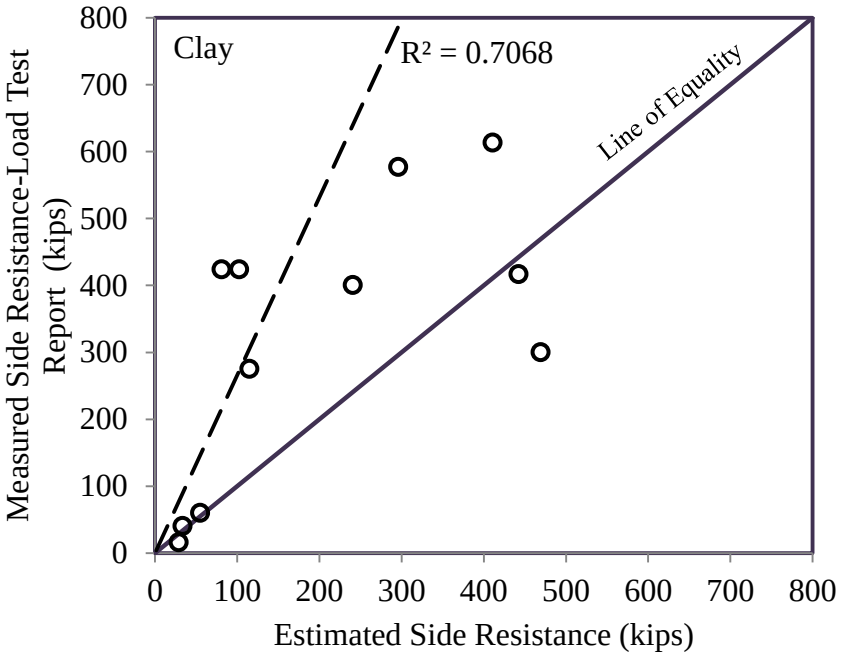

Figure 4.1. Comparison of measured side resistance obtained from load test reports and estimated side resistance in clay

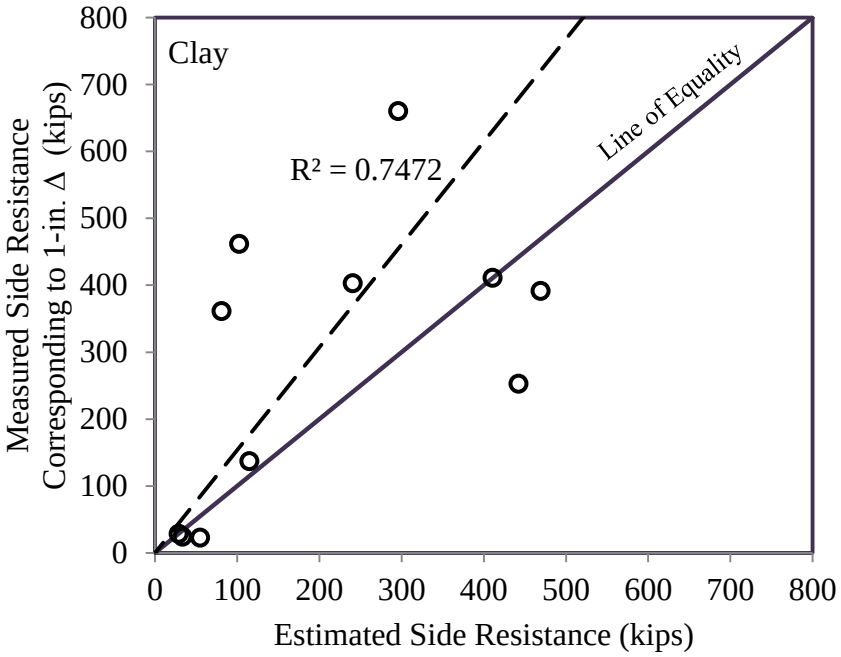

Figure 4.2. Comparison of measured side resistance corresponding to 1-in. top displacement and estimated side resistance in clay

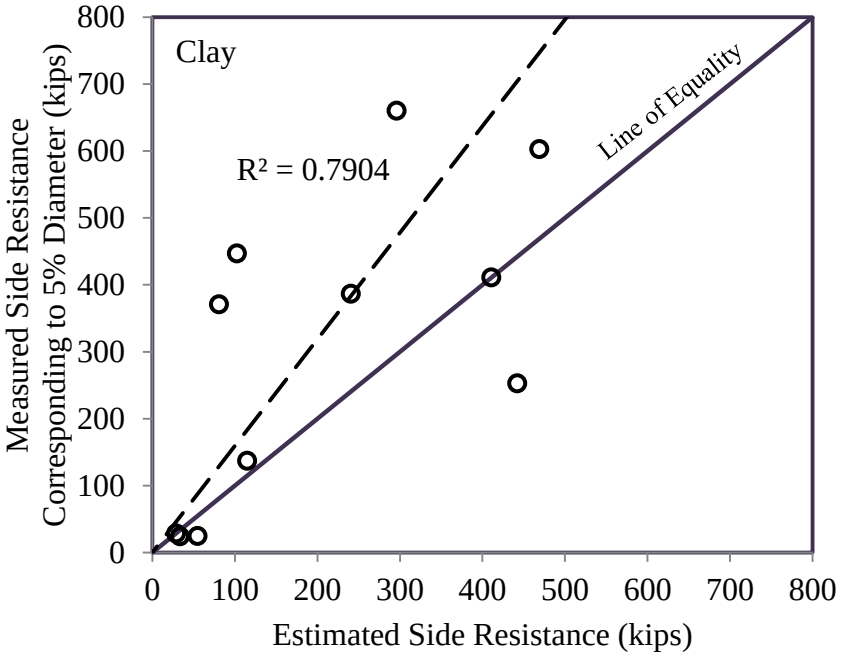

Figure 4.3. Comparison of measured side resistance corresponding to 5% of shaft diameter for top displacement and estimated side resistance in clay

Figure 4.4 shows three Anderson-Darling (AD) (1952) normality tests of the side resistance ratio for three criteria.

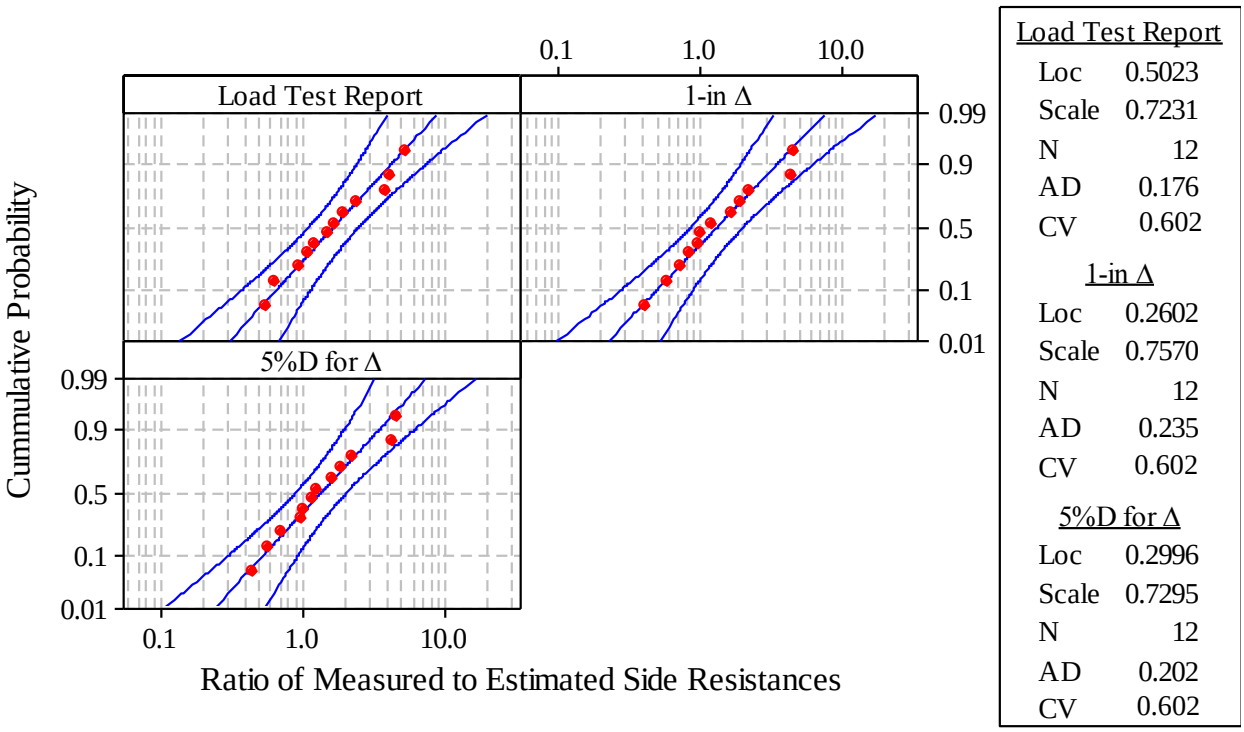

Figure 4.4. Goodness-of-fit test for side resistance in clay

The side resistance ratio is a ratio of measured to estimated side resistance. The "Loc" and "Scale" represent the mean and standard deviation of the natural logarithm of the datasets. The sample size is represented by "N", which is 12 datasets for all three criteria. Since the cumulative probability density function was plotted on a logarithmic scale, the assumed logarithmic distribution within the 95% confidence interval (CI) is confirmed when the AD value is smaller than the CV value. Figure 4.5 shows the normal distribution of the resistance ratio and the statistical characteristics (i.e., mean and standard deviation) necessary for the calibration of resistance factors.

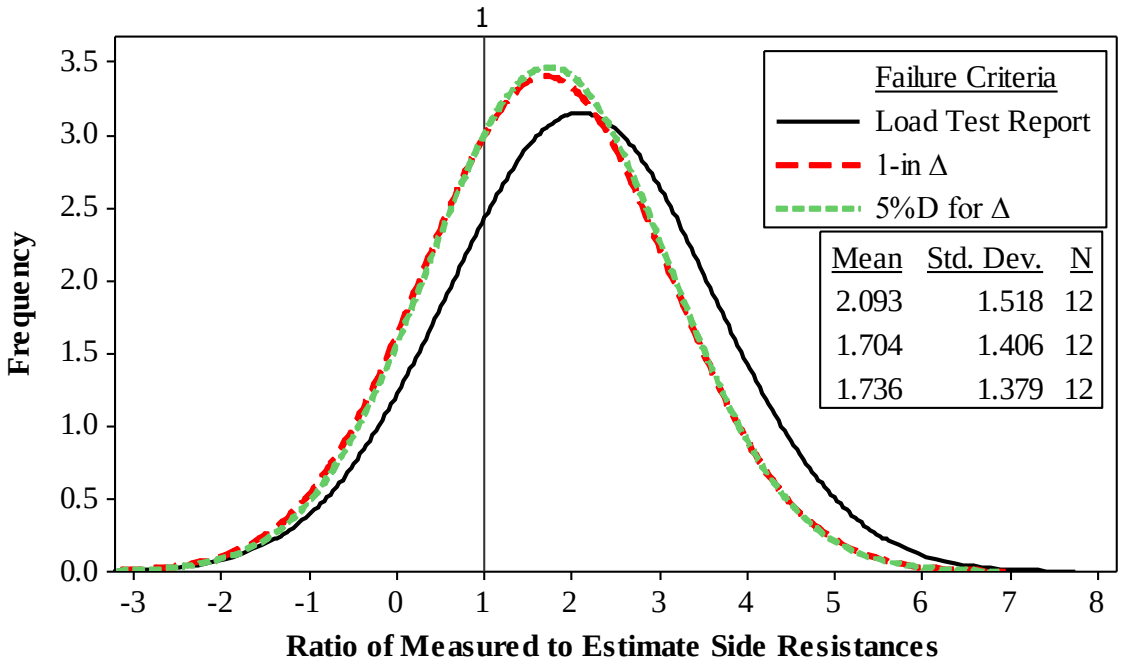

Figure 4.5. Summary of the normal distributed PDFs of the side resistance ratio in clay for various criteria

The three distributions having the mean values larger than one indicate that the side resistances are generally underestimated. Among the three, the distribution for the measured resistance obtained from the load test report has the largest mean and standard deviation. The analysis shows that the estimated side resistance has a relatively better comparison with the measured values based on the 1-in. displacement and the 5% shaft diameter for displacement criteria. Following the LRFD framework, resistance factors were determined as a function of reliability index as shown in Figure 4.6. The resistance factor decreases when a higher reliability level of the drilled shaft foundation system is desired.

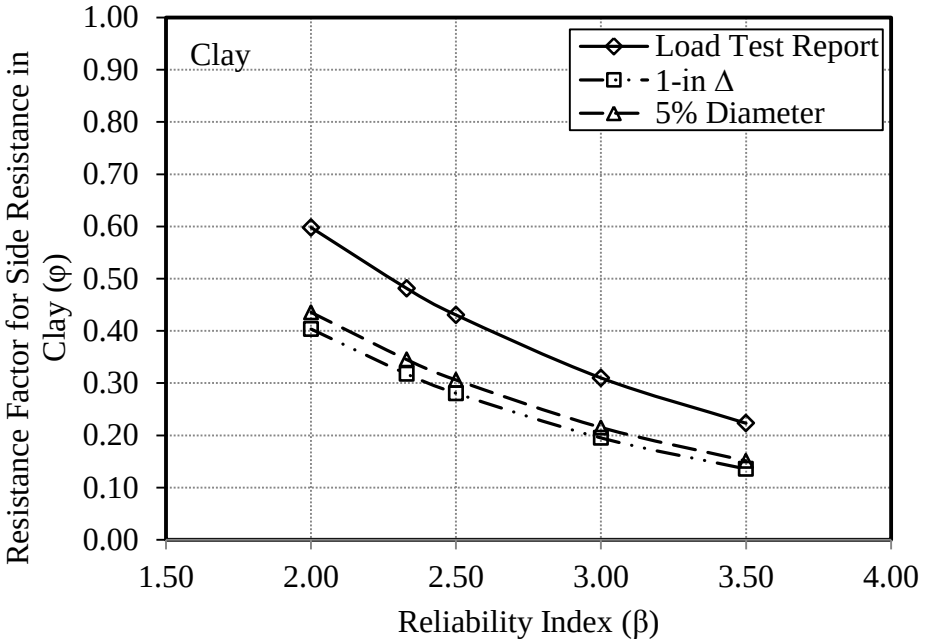

Figure 4.6. LRFD resistance factors for side resistance in clay corresponding to a range of reliability indices

Similarly, Figure 4.7 shows that the efficiency of the estimation decreases with increasing reliability index. Among the three failure-defining criteria, estimation of side resistance in clay will have the highest efficiency when compared with the measured value based on the 1-in. displacement criterion.

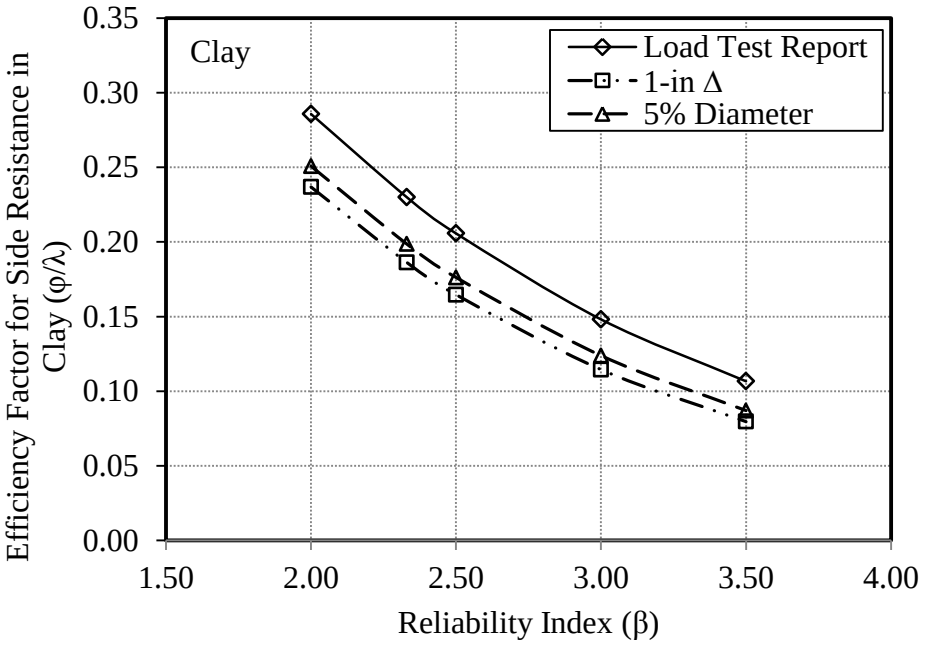

Figure 4.7. Efficiency factors for side resistance in clay corresponding to a range of reliability indices

4.2.2. Sand

Individual side resistance in each sand layer along a drilled shaft was estimated using the β-method described in Section 2.3.3. Depending on the number of sand layers along the shaft, the side resistance of the drilled shaft in sand is the summation of all individual side resistances in the sand layers. The measured side resistance in sand of each applicable test shaft is listed in Table 3.9 with respect to the three failure-defining criteria. The comparisons of estimated and measured side resistances in sand are shown in 1) Figure 4.8 for the measured resistance obtained directly from the load test report, 2) Figure 4.9 for the measured resistance defined based on the 1-in. top displacement criterion, and 3) Figure 4.10 for the measured resistance defined based on the 5% of shaft diameter for top displacement criterion. The comparison in Figure 4.8 shows that the side resistance in sand is underestimated with respect to the measured value obtained from the load test report while they are slightly overestimated based on the other two criteria as shown in Figure 4.9 and Figure 4.10.

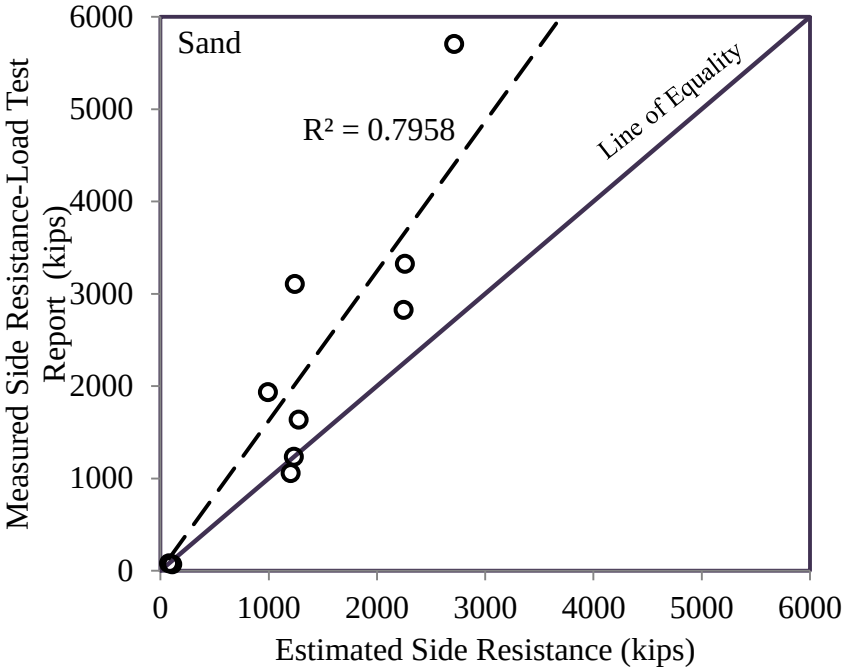

Figure 4.8. Comparison of measured side resistance obtained from load test reports and estimated side resistance in sand

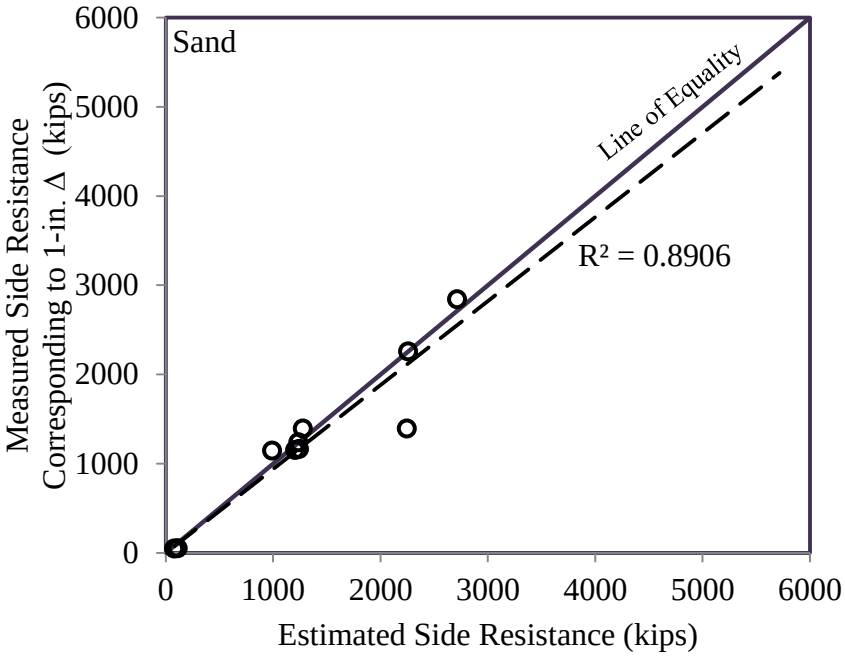

Figure 4.9. Comparison of measured side resistance corresponding to 1-in. top displacement and estimated side resistance in sand

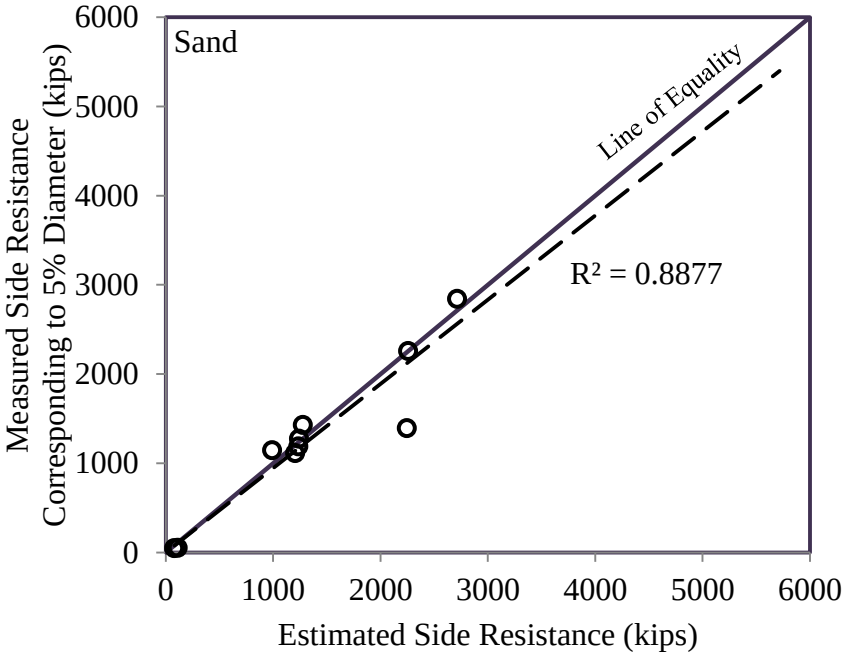

Figure 4.10. Comparison of measured side resistance corresponding to 5% of shaft diameter for top displacement and estimated side resistance in sand

Figure 4.11 shows three Anderson-Darling (AD) (1952) normality tests of the side resistance ratio for three criteria. The assumed logarithmic distribution based on the load test report criterion is confirmed when the AD value is smaller than the CV value but not for the other two distributions based on the 1-in. and 5% diameter criteria.

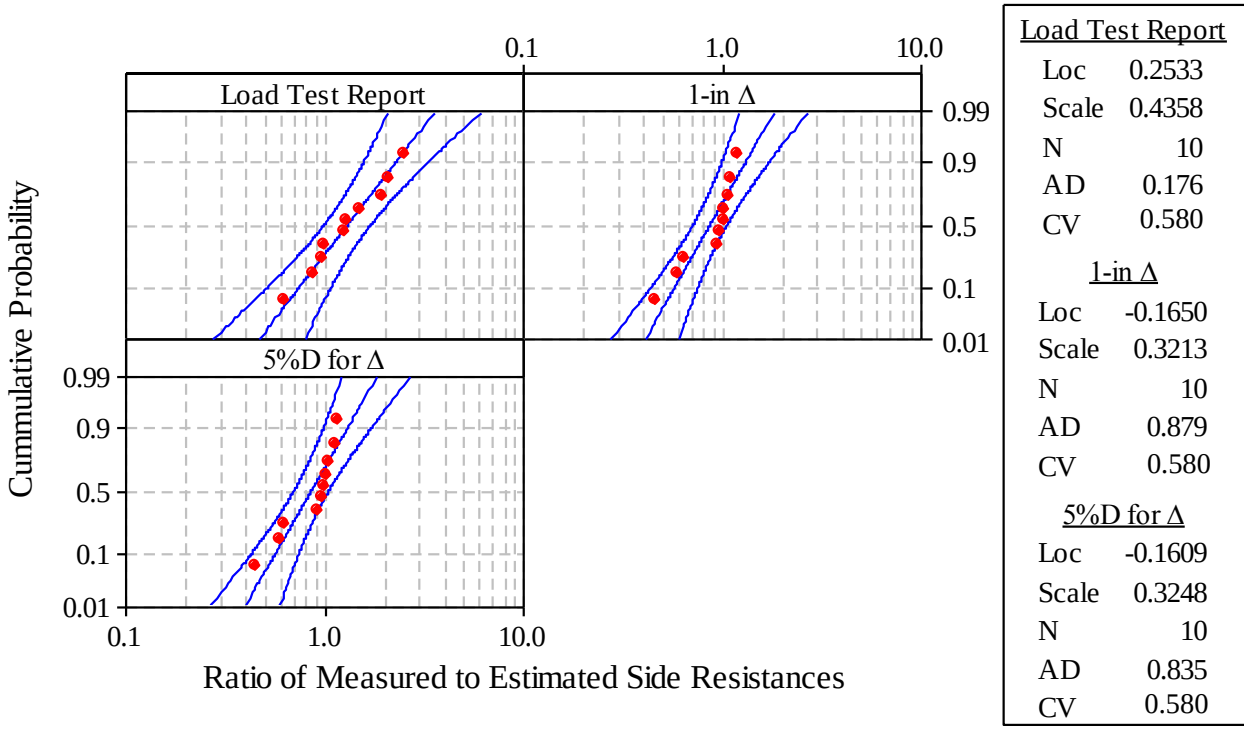

Figure 4.11. Goodness of fit test for side resistance in sand

Figure 4.12 shows that the estimated side resistance has a relatively better comparison with the measured values based on the 1-in. and the 5% diameter criteria, substantiated by mean values closer to one and smaller standard deviations.

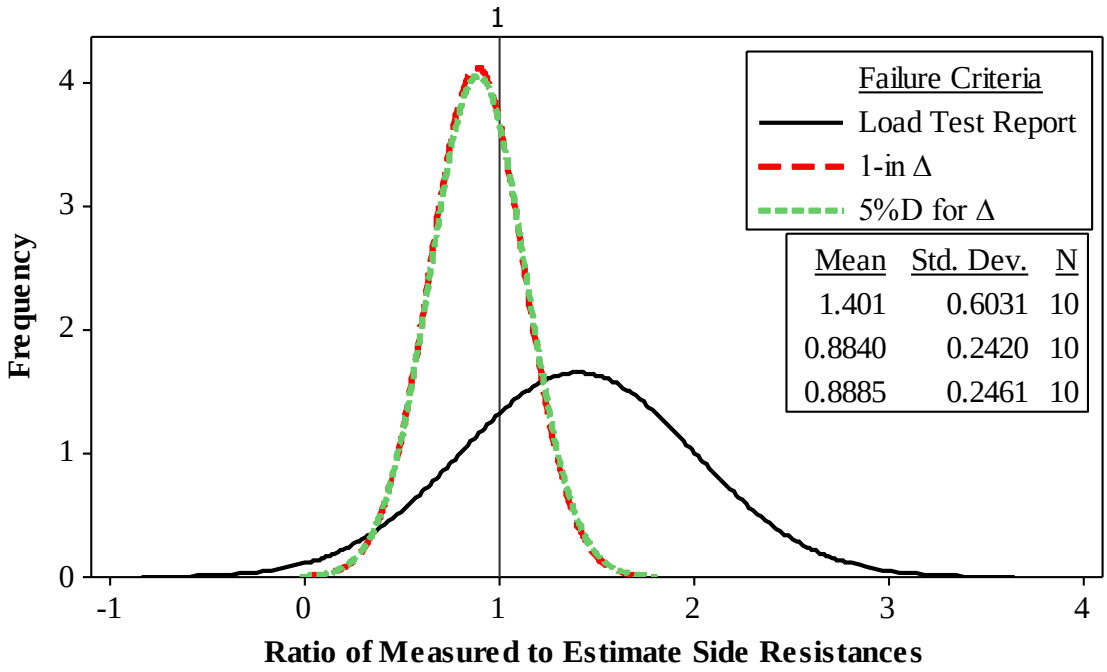

Figure 4.12. Summary of the normal distributed PDFs of the side resistance ratio in sand for various criteria

Following the LRFD framework, resistance factors were determined as a function of reliability index as shown in Figure 4.13.

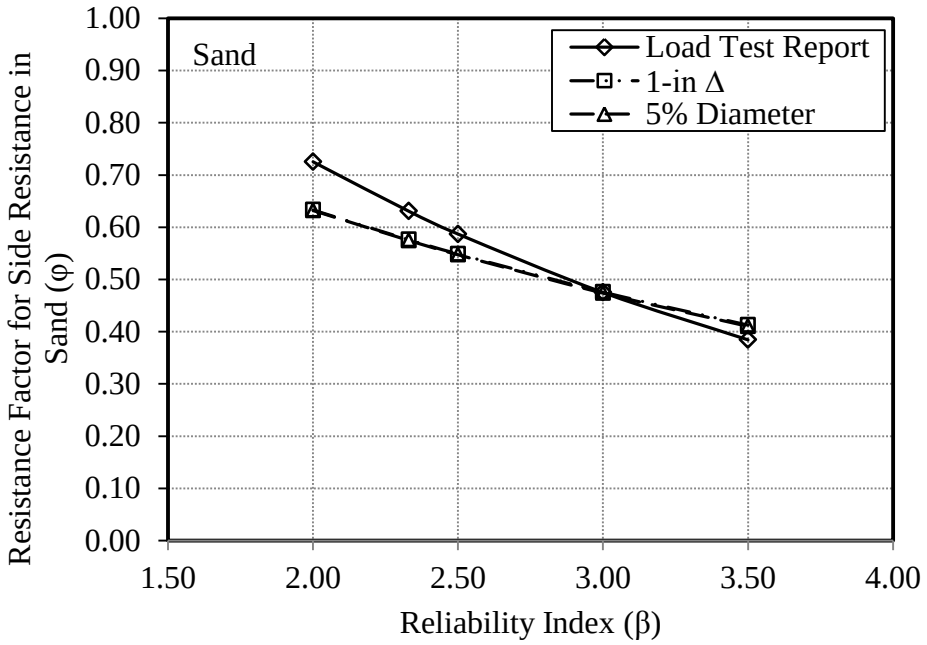

Figure 4.13. LRFD resistance factors for side resistance in sand corresponding to a range of reliability indices

Among the three criteria, estimation of side resistance in sand will have the highest efficiency when compared with the measured value evaluated based on the 1-in. or the 5% diameter displacement criteria as shown in Figure 4.14.

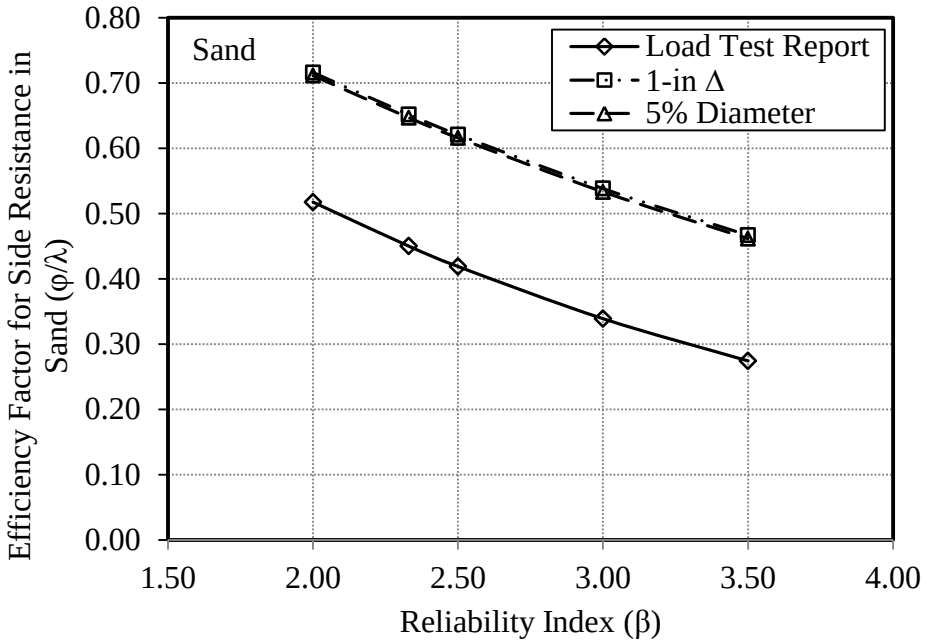

Figure 4.14. Efficiency factors for side resistance in sand corresponding to a range of reliability indices

4.2.3. Intermediate Geo Materials (IGM)

Individual side resistance in each IGM layer along a drilled shaft was estimated using the method described in Section 2.3.4. Depending on the number of IGM layers along the shaft, the side resistance of the drilled shaft in IGM is the summation of all individual side resistances in the IGM layers. The measured side resistance in IGM of each applicable test shaft is listed in Table 3.10 with respect to the three failure defining criteria. The comparisons of estimated and measured side resistances in IGM are shown in 1) Figure 4.15 for the measured resistance obtained directly from the load test report, 2) Figure 4.16 for the measured resistance defined based on the 1-in. top displacement criterion, and 3) Figure 4.17 for the measured resistance defined based on the 5% of shaft diameter for top displacement criterion. The comparisons show that the side resistance in IGM is generally underestimated with respect to the measured value since the best-fit line is above the line of equality. Figure 4.18 shows three Anderson-Darling (AD) (1952) normality tests of the side resistance ratio for three criteria. The assumed logarithmic distribution within the 95% confidence interval (CI) is confirmed when the AD value is smaller than the CV value. Figure 4.19 shows the normal distribution of the resistance ratio and the statistical characteristics (i.e., mean and standard deviation) necessary for the calibration of resistance factors. The three distributions having mean values larger than one indicate that the side resistances are generally underestimated. Among the three, the distribution for the measured resistance obtained from the load test report has the largest mean and standard deviation. The analysis shows that the estimated side resistance has a relatively better comparison with the

measured values based on the 1-in. and the 5% diameter criteria. Following the LRFD framework, resistance factors were determined as a function of reliability index as shown in Figure 4.20. Among the three criteria, estimation of side resistance in IGM will have a slightly higher efficiency when compared with the measured value based on the 5% diameter criterion.

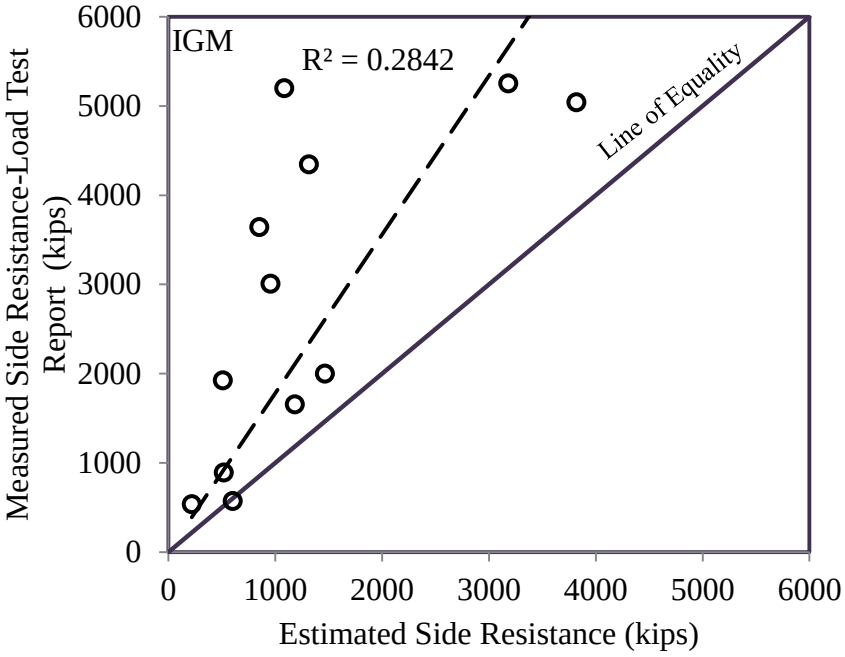

Figure 4.15. Comparison of measured side resistance obtained from load test reports and estimated side resistance in IGM

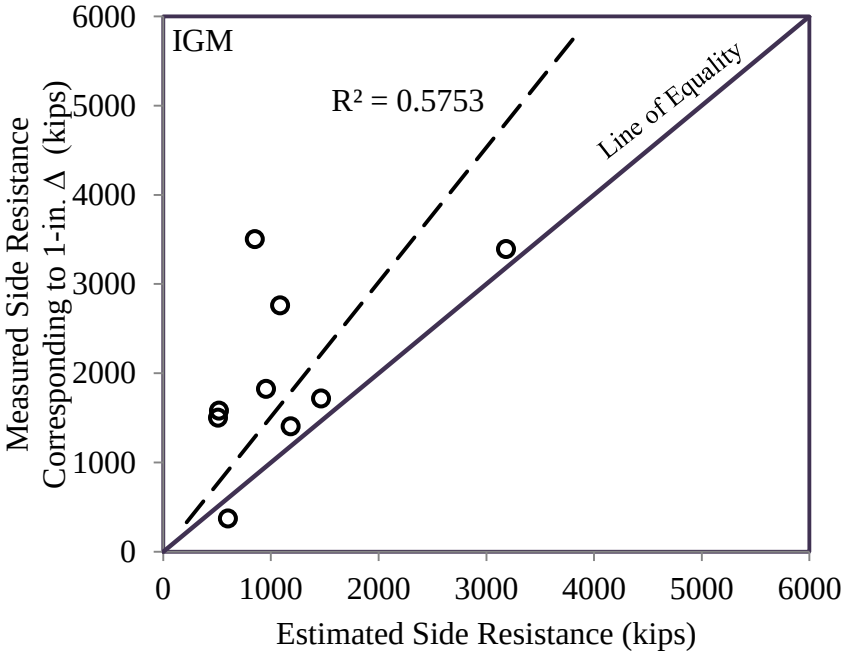

Figure 4.16. Comparison of measured side resistance corresponding to 1-in. top displacement and estimated side resistance in IGM

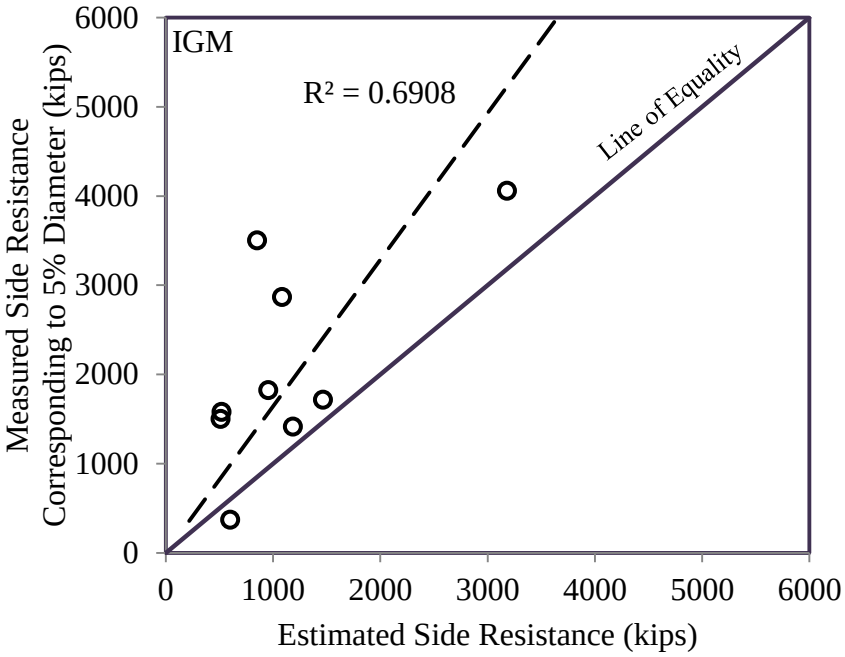

Figure 4.17. Comparison of measured side resistance corresponding to 5% of shaft diameter for top displacement and estimated side resistance in IGM

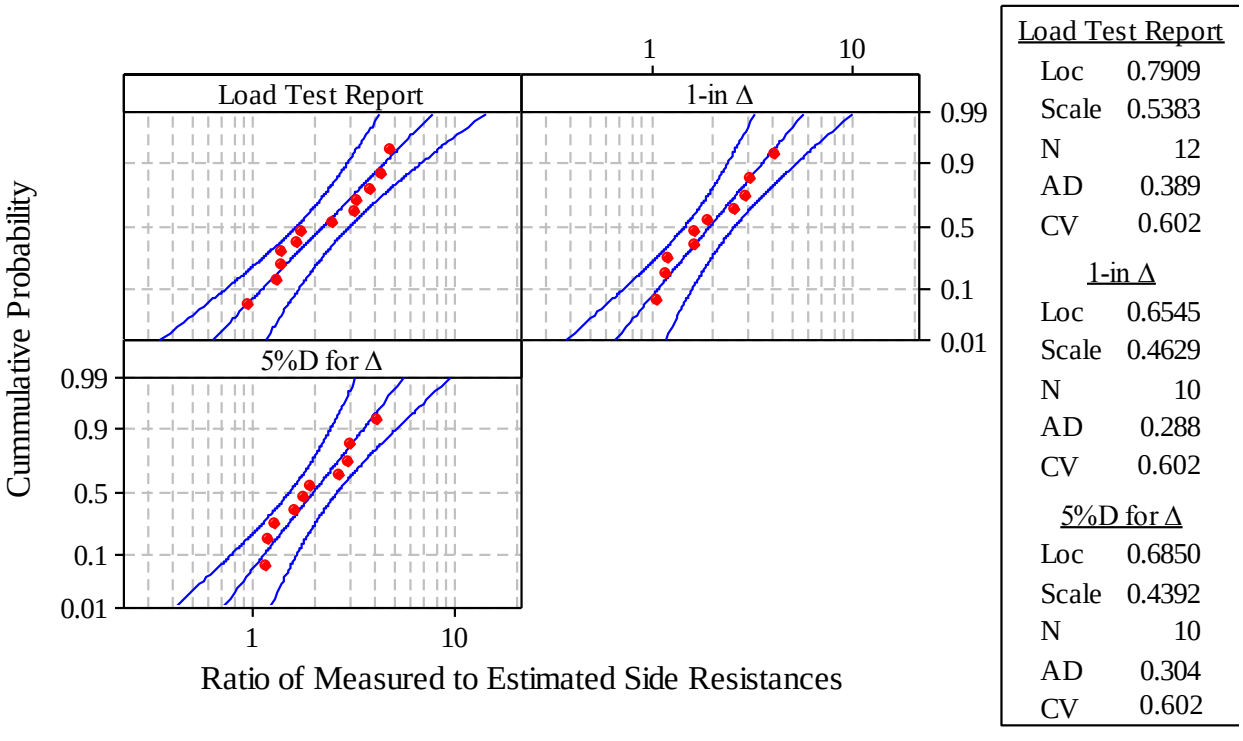

Figure 4.18. Goodness of fit test for side resistance in IGM

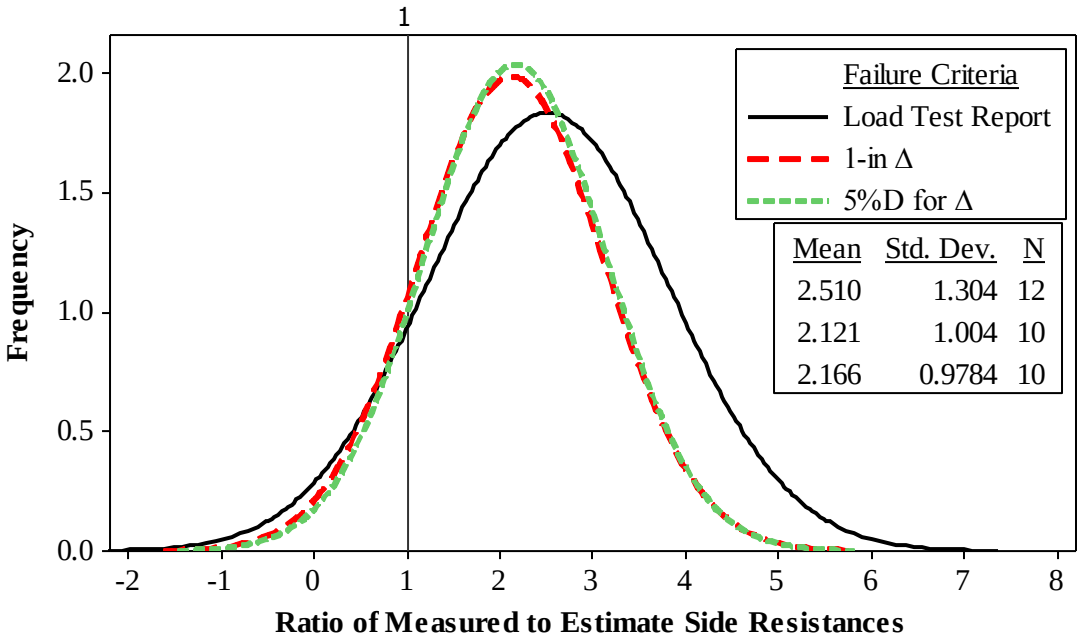

Figure 4.19. Summary of the normal distributed PDFs of the side resistance ratio in IGM for various criteria

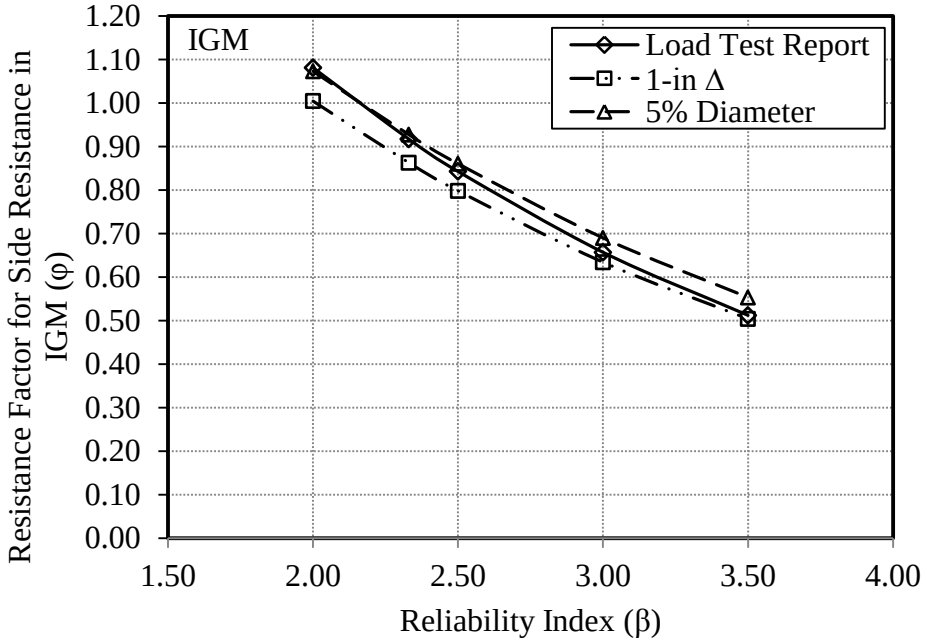

Figure 4.20. LRFD resistance factors for side resistance in IGM corresponding to a range of reliability indices

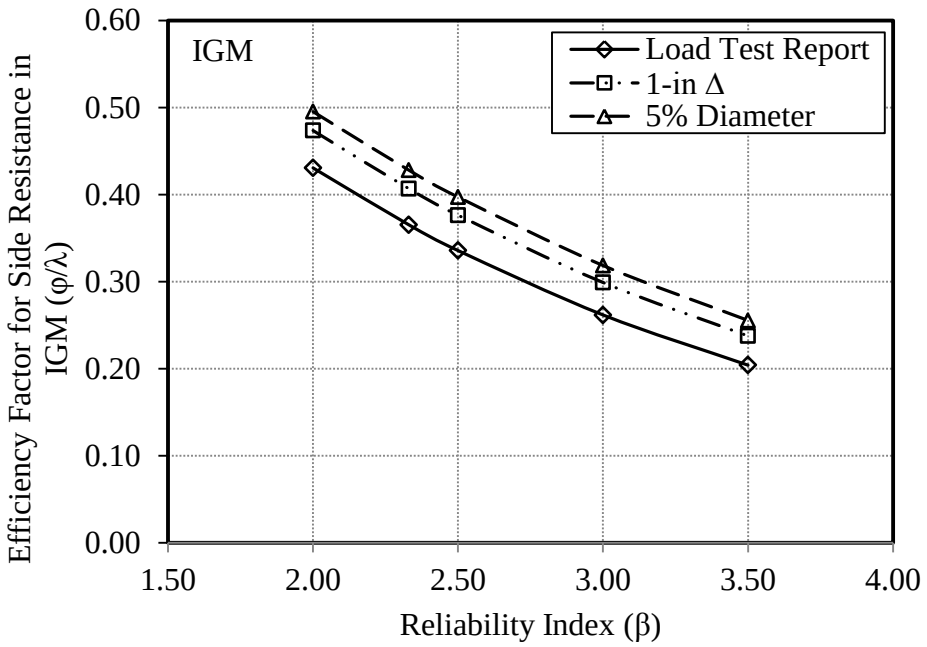

Figure 4.21. Efficiency factors for side resistance in IGM corresponding to a range of reliability indices

4.2.4. Rock

Individual side resistance in each rock layer along a drilled shaft was estimated using the method described in Section 2.3.5. Depending on the number of rock layers along the shaft, the side resistance of the drilled shaft in rock is the summation of all individual side resistances in the rock layers. The measured side resistance in rock of each applicable test shaft is listed in Table 3.11 with respect to the three failure defining criteria. The comparisons of estimated and measured side resistances in rock are shown in 1) Figure 4.22 for the measured resistance obtained directly from the load test report, 2) Figure 4.23 for the measured resistance defined based on the 1-in. top displacement criterion, and 3) Figure 4.24 for the measured resistance defined based on the 5% of shaft diameter for top displacement criterion. The comparisons show that the side resistance in rock is underestimated with respect to the measured value based on the load test report while the side resistance is only slightly underestimated when comparing with the measured value based on the 1-in. and 5% diameter criteria. Figure 4.25 shows three Anderson-Darling (AD) (1952) normality tests of the side resistance ratio for three criteria. The assumed logarithmic distribution within the 95% confidence interval (CI) is confirmed when the AD value is smaller than the CV value. Figure 4.26 shows the normal distribution of the resistance ratio and the statistical characteristics. The three distributions having the mean values larger than one indicate that the estimated side resistances are generally underestimated. Among the three, the distribution for the measured resistance obtained from the load test report has the largest mean and standard deviation. As confirmed by the mean values being closer to one together with smaller standard deviations, the estimated side resistance has a relatively better comparison with the measured values based on the 1-in. and the 5% diameter criteria. Following the LRFD framework, resistance factors were determined as a function of reliability index as shown in

Figure 4.27. Among the three criteria, estimation of side resistance in rock will have a slightly higher efficiency when comparing with the measured value based on the 5% diameter criterion.

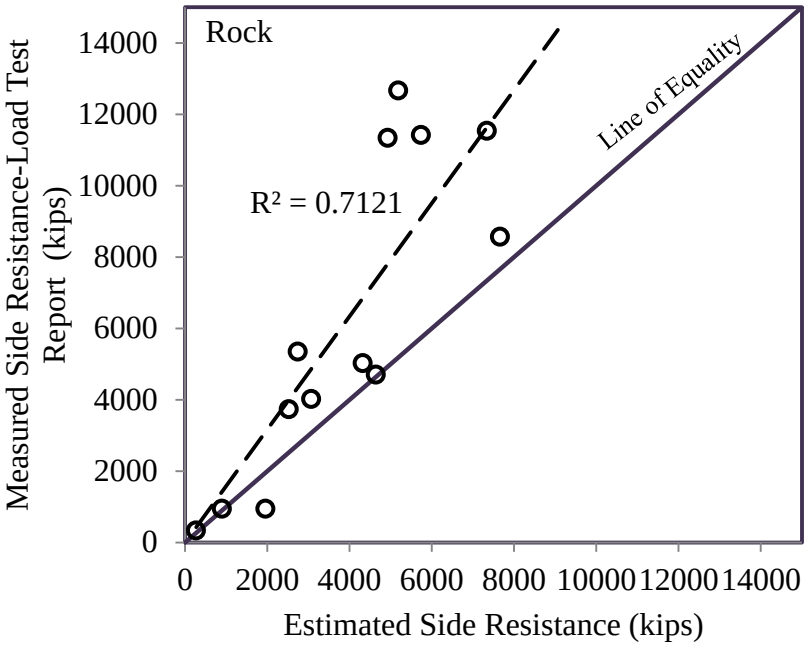

Figure 4.22. Comparison of measured side resistance obtained from load test reports and estimated side resistance in rock

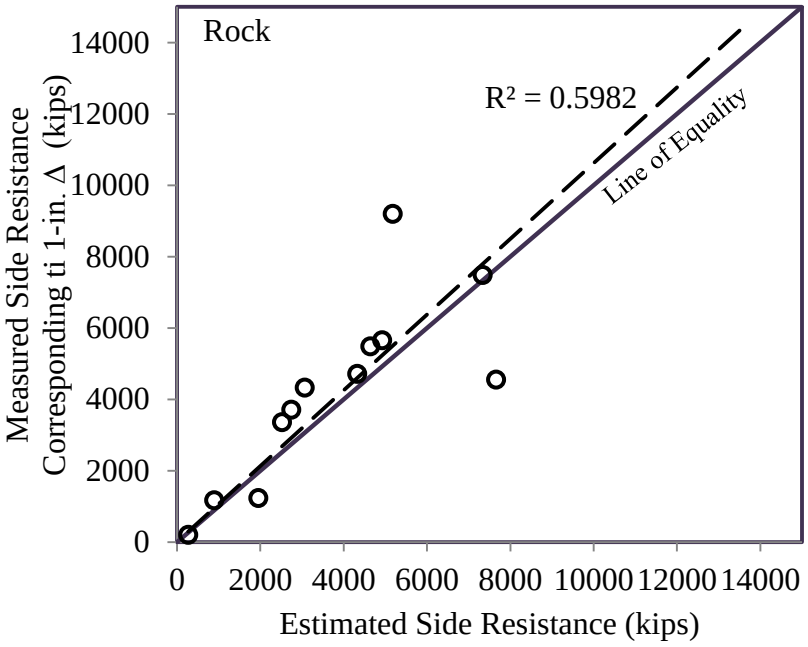

Figure 4.23. Comparison of measured side resistance corresponding to 1-in. top displacement and estimated side resistance in rock

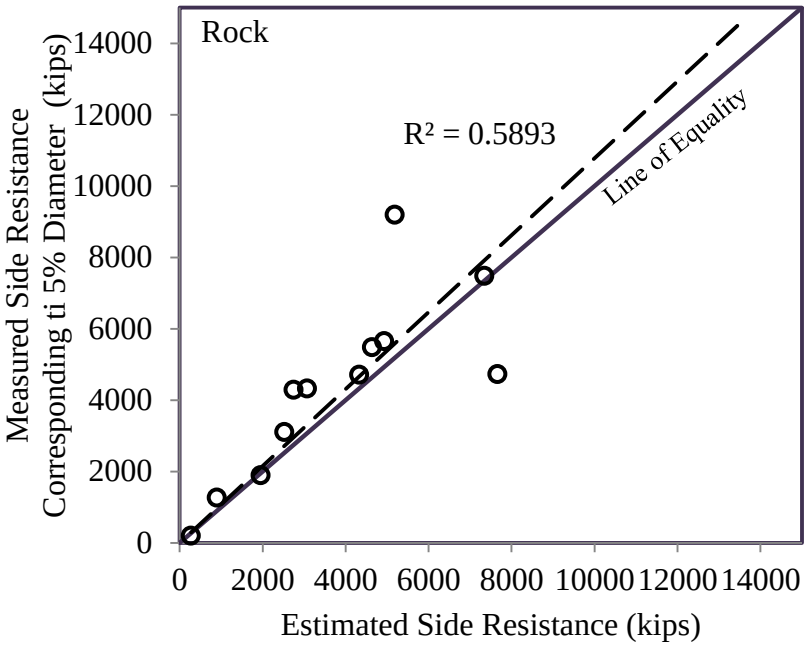

Figure 4.24. Comparison of measured side resistance corresponding to 5% of shaft diameter for top displacement and estimated side resistance in rock

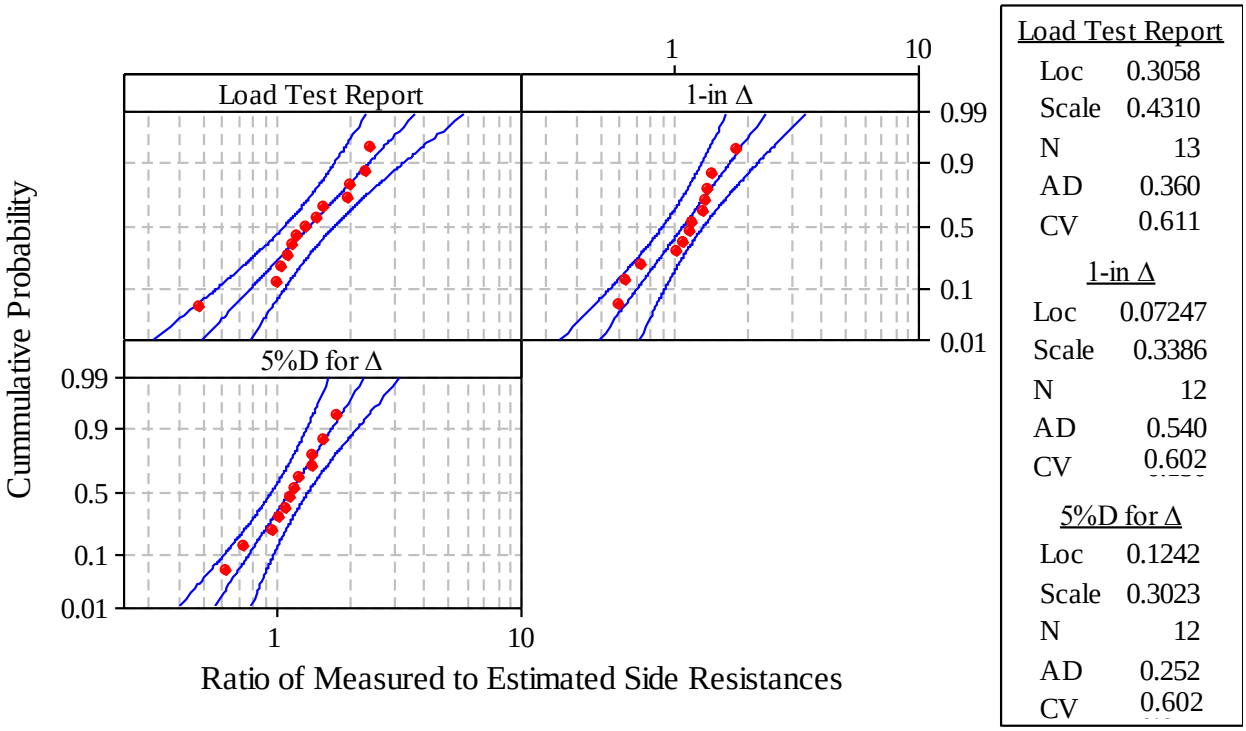

Figure 4.25. Goodness of fit test for side resistance in rock

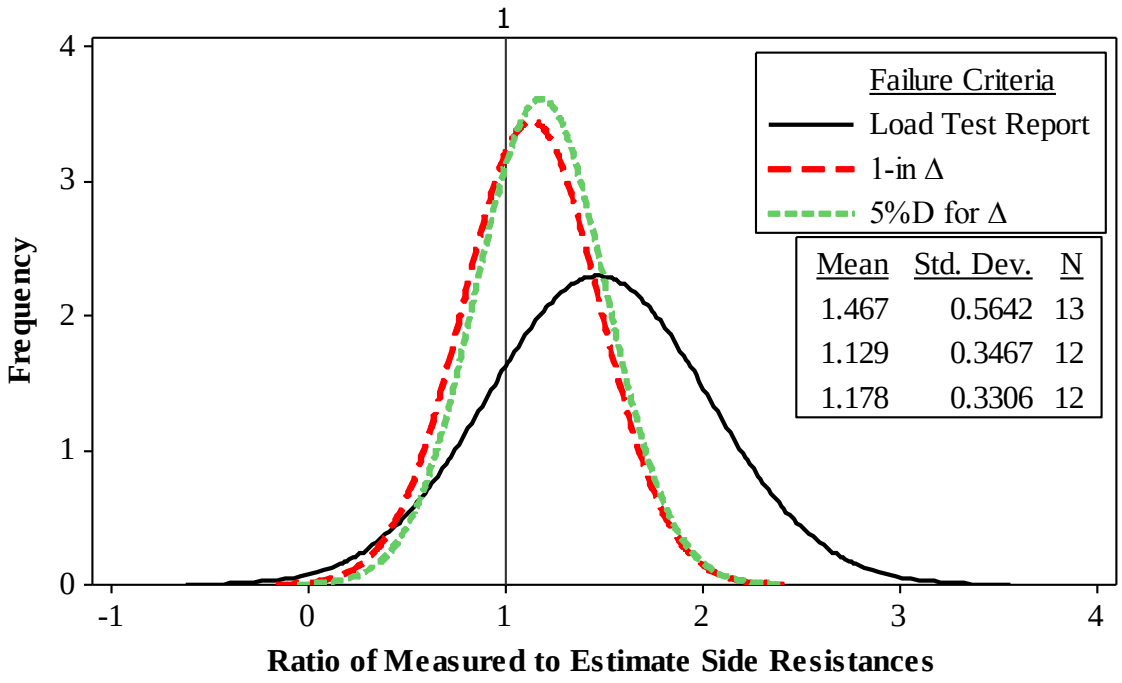

Figure 4.26. Summary of the normal distributed PDFs of the side resistance ratio in rock for various criteria

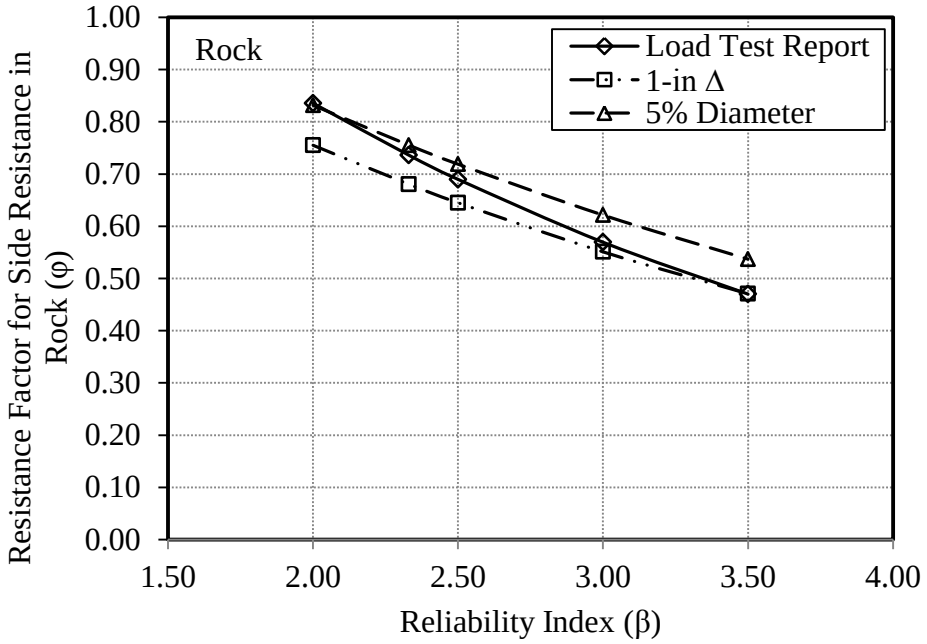

Figure 4.27. LRFD resistance factors for side resistance in rock corresponding to a range of reliability indices

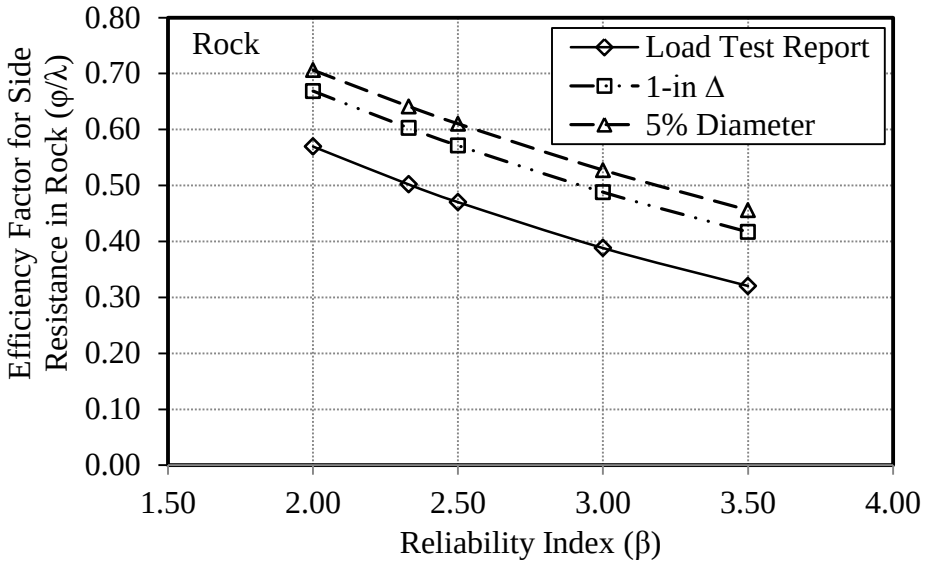

Figure 4.28. Efficiency factors for side resistance in rock corresponding to a range of reliability indices

4.3. End Bearing

4.3.1. Clay

Only one usable data point (ID No. 6) of the drilled shaft bearing in clay is available in this research. Hence, statistical analysis cannot be performed to determine its resistance factor. Nevertheless, the comparisons of estimated and measured end bearing are shown in Figure 4.29, Figure 4.30, and Figure 4.31 for the three criteria.

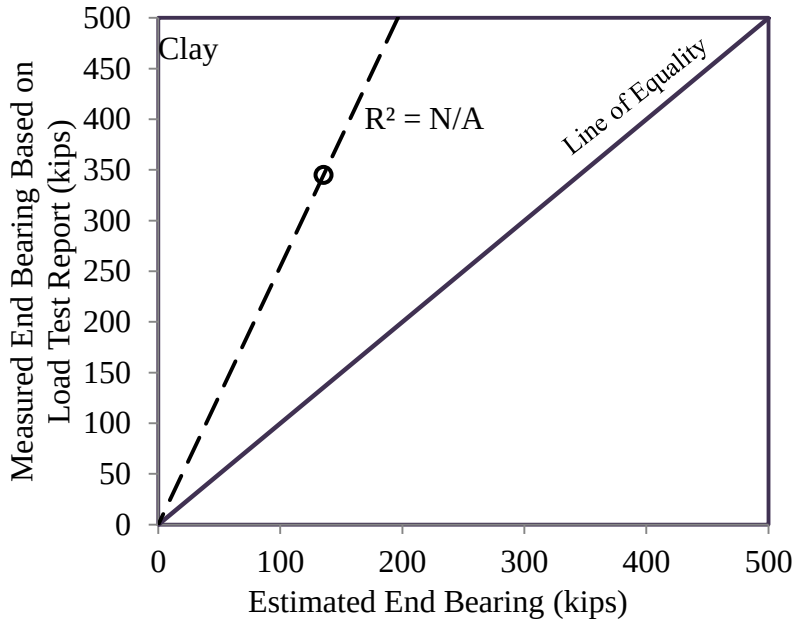

Figure 4.29. Comparison of measured end bearing obtained from load test reports and estimated end bearing in clay

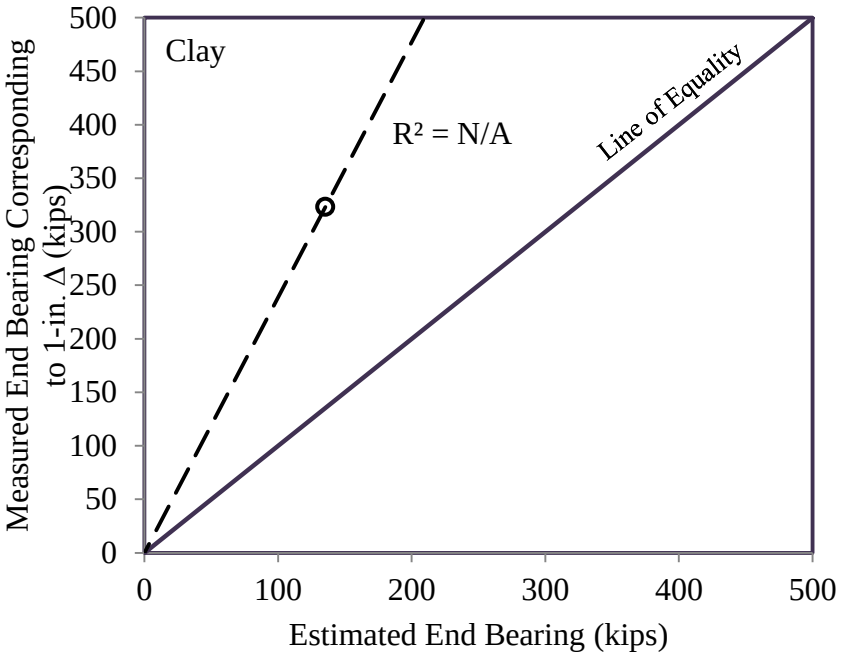

Figure 4.30. Comparison of measured end bearing corresponding to 1-in. top displacement and estimated end bearing in clay

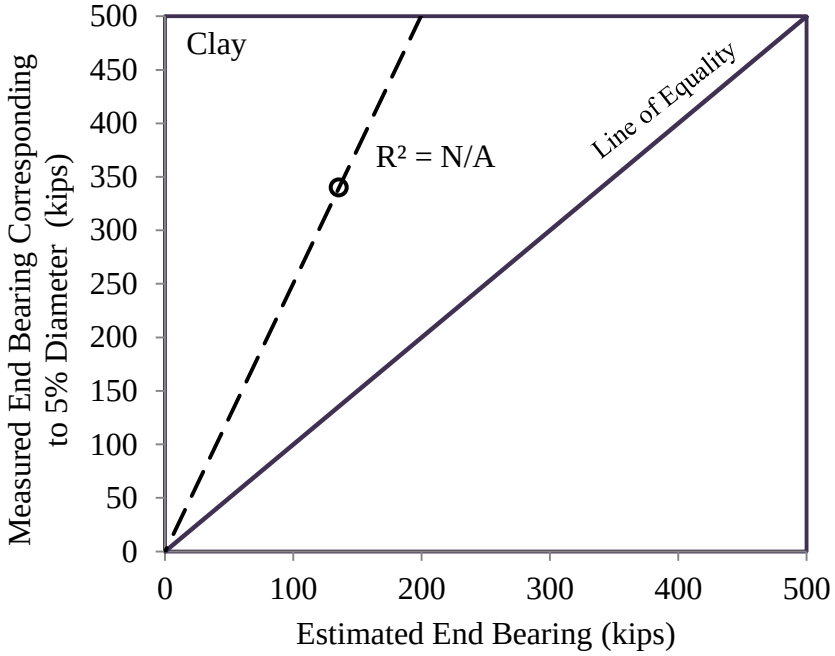

Figure 4.31. Comparison of measured end bearing corresponding to 5% of shaft diameter for top displacement and estimated end bearing in clay

4.3.2. Sand

Six drilled shafts bearing in sand are available for the calibration of resistance factors. The end bearing in sand was estimated using the method described in Section 2.4.3 and the estimated

values are summarized in Appendix C. The measured end bearings are summarized in Table 3.7 for various failure criteria. The comparisons of estimated and measured end bearings are shown in 1) Figure 4.32 for the measured end bearing obtained directly from the load test report, 2) Figure 4.33 for the measured end bearing defined based on the 1-in. top displacement criterion, and 3) Figure 4.34 for the measured resistance defined based on the 5% of shaft diameter for top displacement criterion.

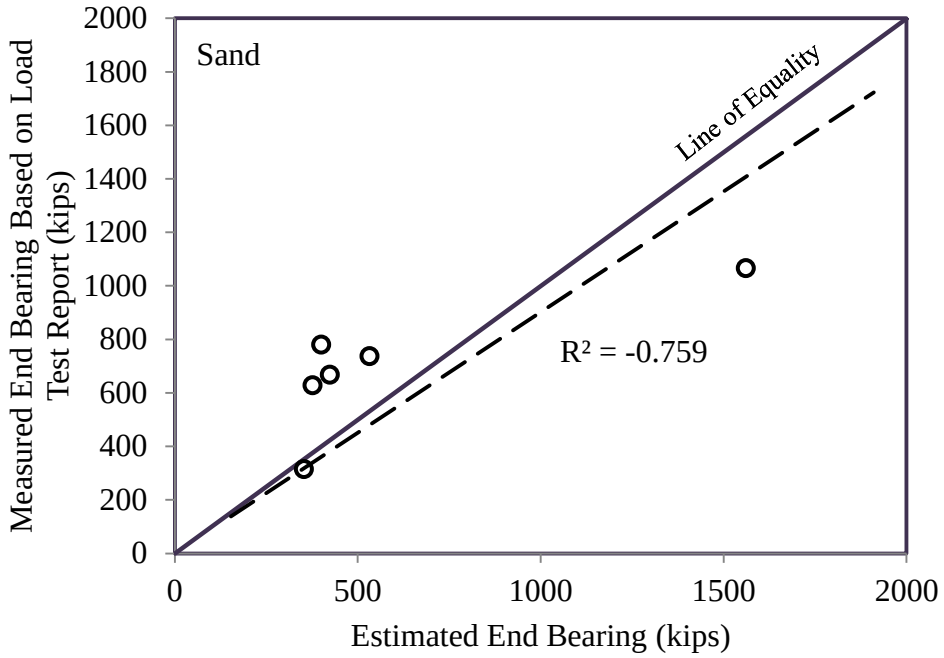

Figure 4.32. Comparison of measured end bearing obtained from load test reports and estimated end bearing in sand

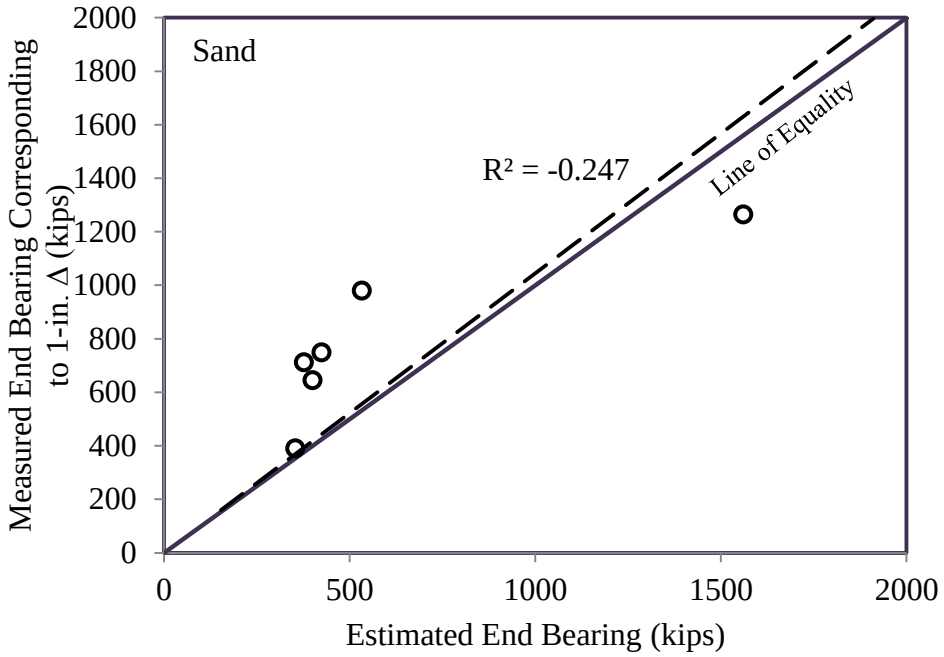

Figure 4.33. Comparison of measured end bearing corresponding to 1-in. top displacement and estimated end bearing in sand

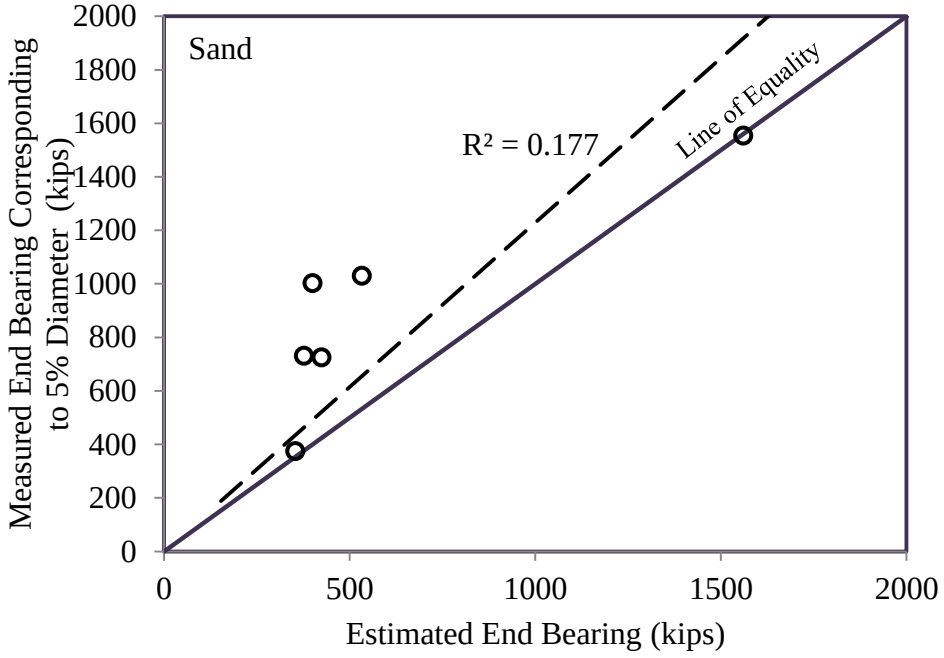

Figure 4.34. Comparison of measured end bearing corresponding to 5% of shaft diameter for top displacement and estimated end bearing in sand

The comparison shown in Figure 4.32 shows that the side resistance in sand is overestimated with respect to the measured value obtained from the load test report, while they are underestimated based on the other two criteria as shown in Figure 4.33 and Figure 4.34. Figure

4.35 shows three Anderson-Darling (AD) (1952) normality tests of the end bearing ratio for three criteria. The assumed logarithmic distribution based on the load test report criterion is confirmed when the AD value is smaller than the CV value except for the 1-in. displacement criterion.

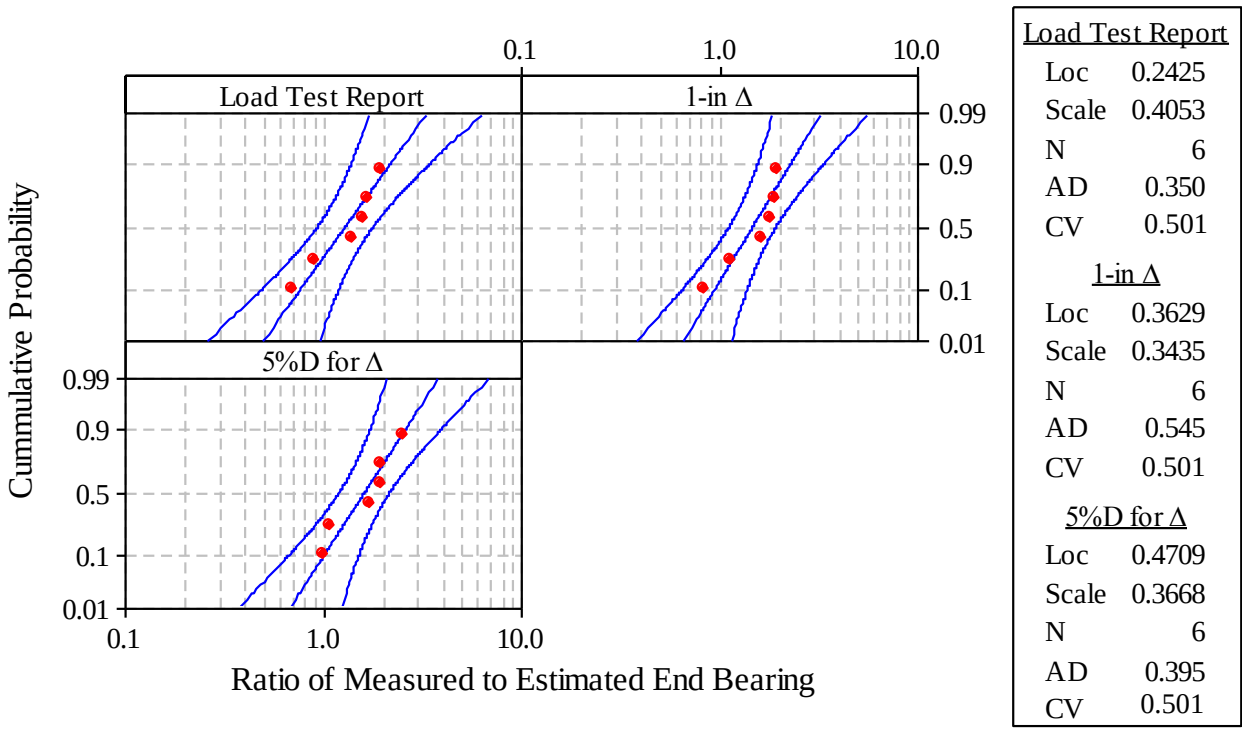

Figure 4.35. Goodness of fit test for end bearing in sand

Figure 4.36 shows that the estimated end bearing has a relatively better comparison with the measured values based on load test report criterion, as indicated by the mean value closer to one and a relatively small standard deviation.

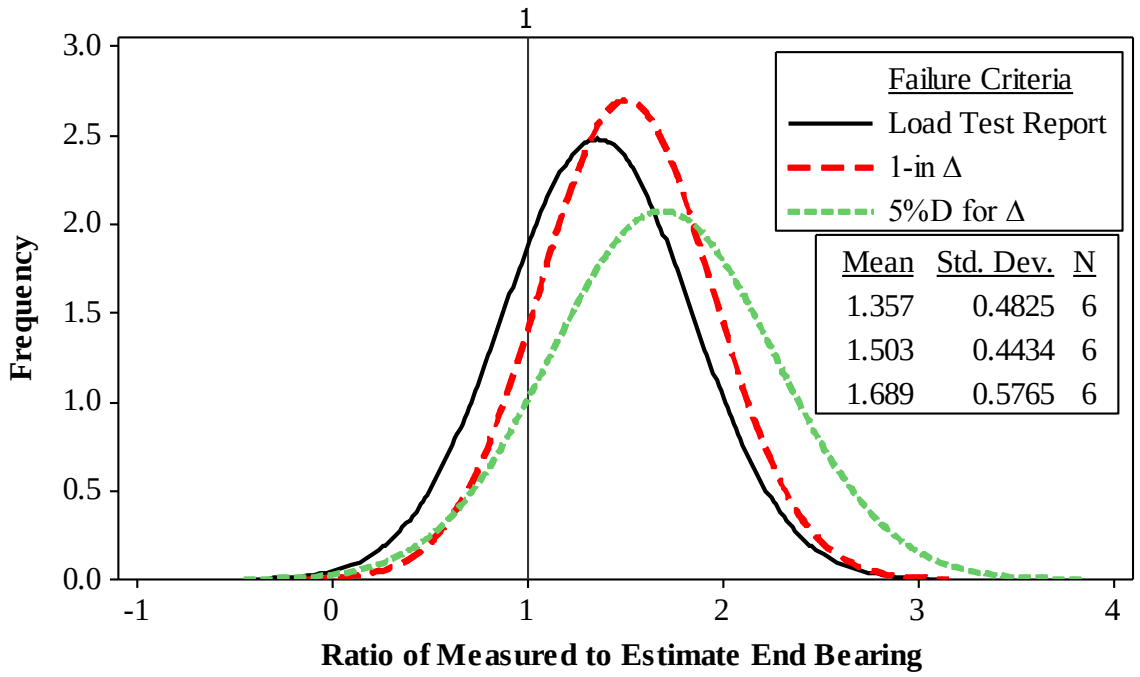

Figure 4.36. Summary of the normal distributed PDFs of the end bearing ratio in sand for various criteria

Following the LRFD framework, resistance factors were determined as a function of reliability index as shown in Figure 4.37.

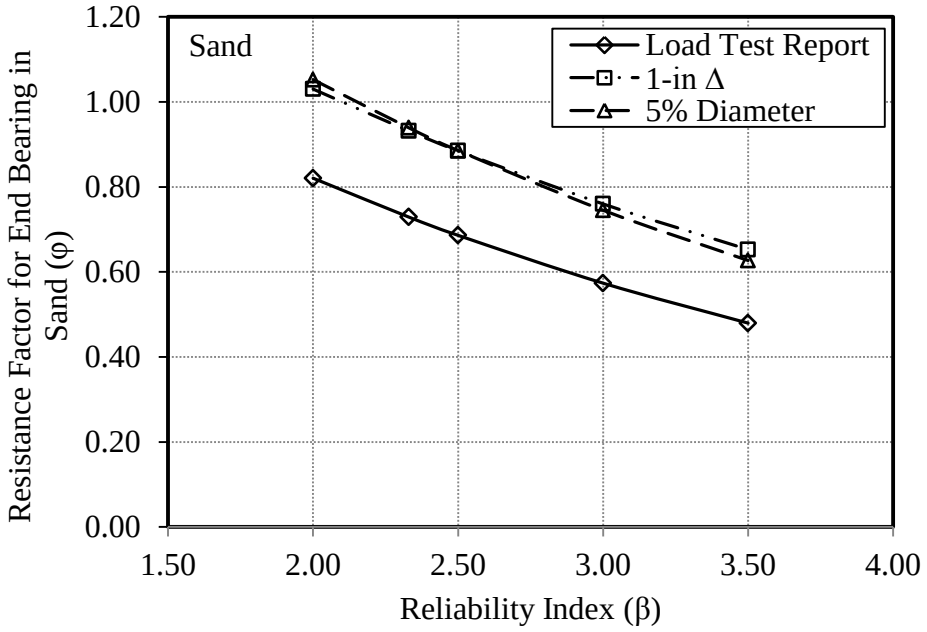

Figure 4.37. LRFD resistance factors for end bearing in sand corresponding to a range of reliability indices

Among the three criteria shown in Figure 4.38, estimation of end bearing in sand will have the highest efficiency when compared with the measured value evaluated based on the 1-in. or the 5% diameter displacement criteria.

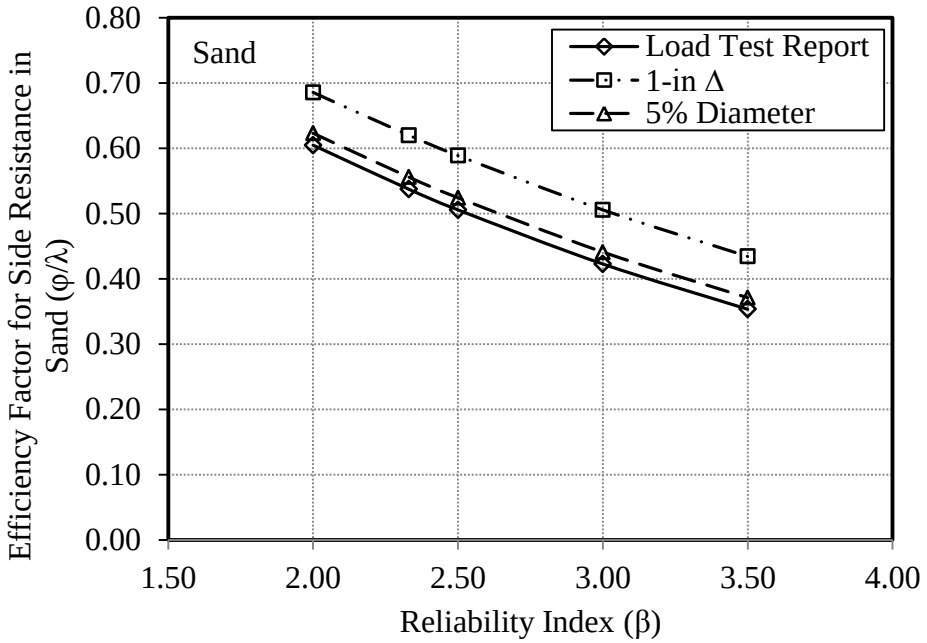

Figure 4.38. Efficiency factors for end bearing in sand corresponding to a range of reliability indices

4.3.3. Intermediate Geo Materials (IGM)

End bearings in IGM were estimated using six analytical methods given in Table 3.2 and the proposed method given in Table 3.4. The purpose of using different analytical methods was to investigate the reliability of the methods, depending on the characteristics of the bearing IGM mass that were not clearly described or not known in the load test reports collected in DSHAFT. The estimated end bearings for the six analytical methods are summarized in Table 3.5 while the estimated end bearings based on the proposed method are given in Appendix C. The measured end bearings in IGM are summarized in Table 3.7 with respect to the three failure criteria: load test report, 1-in. displacement and 5% diameter for displacement. The following analyses primarily focus on cohesive IGM while the determination of resistance and efficiency factors includes data from both cohesive and cohesionless IGM.

Figure 4.39 shows the comparisons of estimated end bearing and measured end bearing obtained directly from load test reports. The analytical method by Rowe and Armitage (1987) for an intact IGM shown in Figure 4.39(a) provides reasonable end bearing estimations except ID No. 13. In contrast, the end bearings were underestimated using the analytical methods by Goodman (1980) and Carter and Kulhawy (1980) for fractured IGM shown in Figure 4.39(b) and (d). Figure 4.39(c) and (e) show good estimations at a lower end bearing and poor estimations at a higher end bearing using the analytical methods by Terzaghi (1943) and Sowers (1979) for IGM with steeply dipping joints. The end bearing was likely to be overestimated using the analytical

method by O'Neill and Reese (1999) as shown in Figure 4.39(f). Among the methods, the proposed method, which is a combination of analytical methods by Rowe and Armitage (1987) and Carter and Kulhawy (1980), provides the best end bearing estimations.

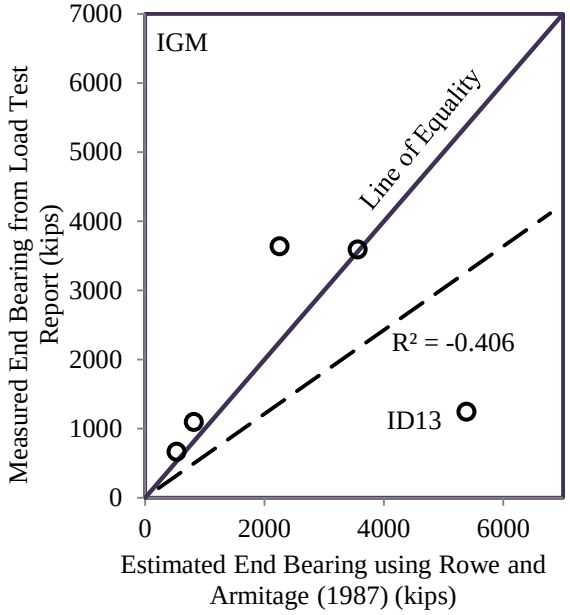

(a) Rowe and Armitage (1987)

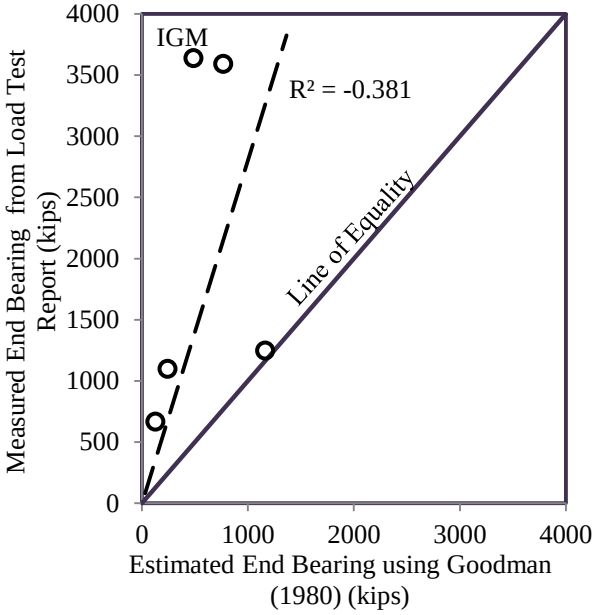

(b) Goodman (1980)

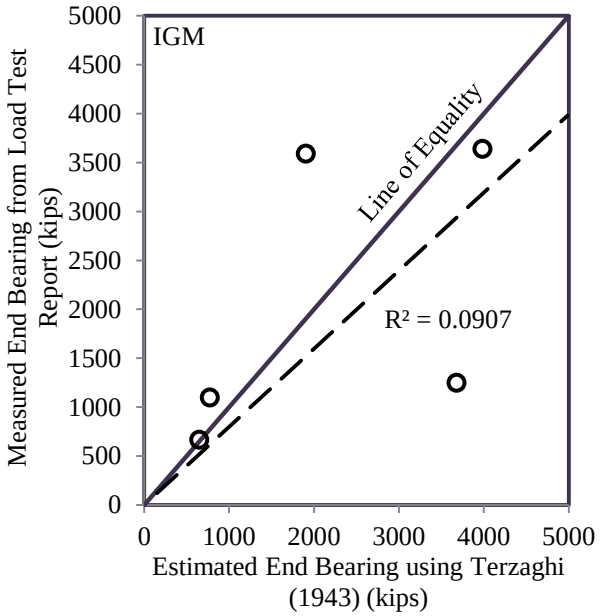

(c) Terzaghi (1943)

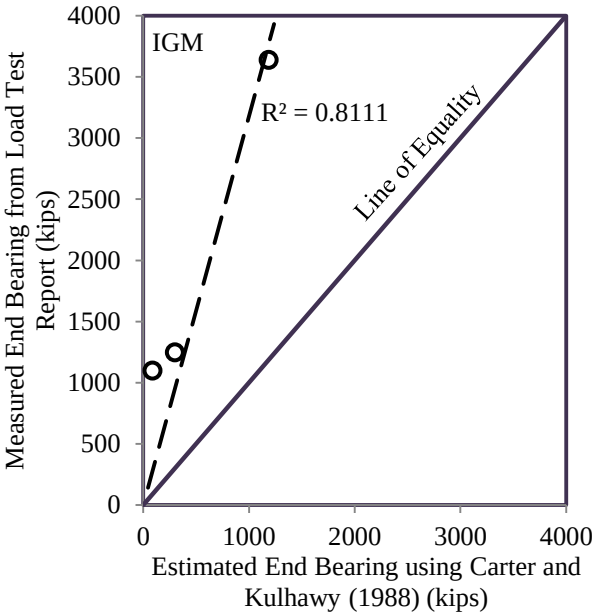

(d) Carter and Kulhawy (1988)

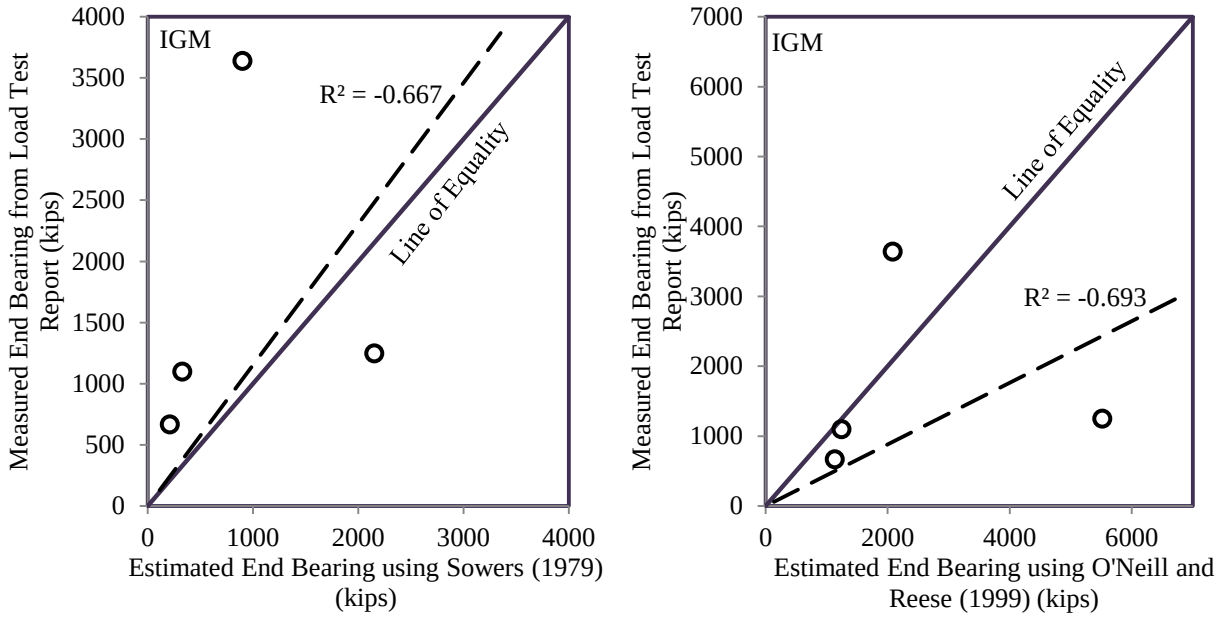

(e) Sowers (1979)

(f) O'Neill and Reese (1999)

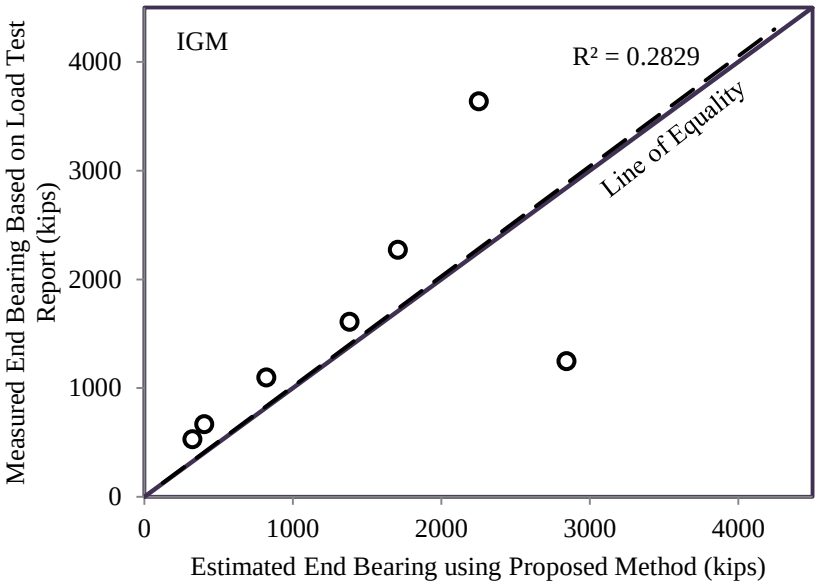

(g) Proposed Method

Figure 4.39. Comparison of measured end bearing obtained directly from load test reports and estimated end bearing in IGM for various analytical methods

Similar observations can be made from Figure 4.40 based on the 1-in. displacement criterion.

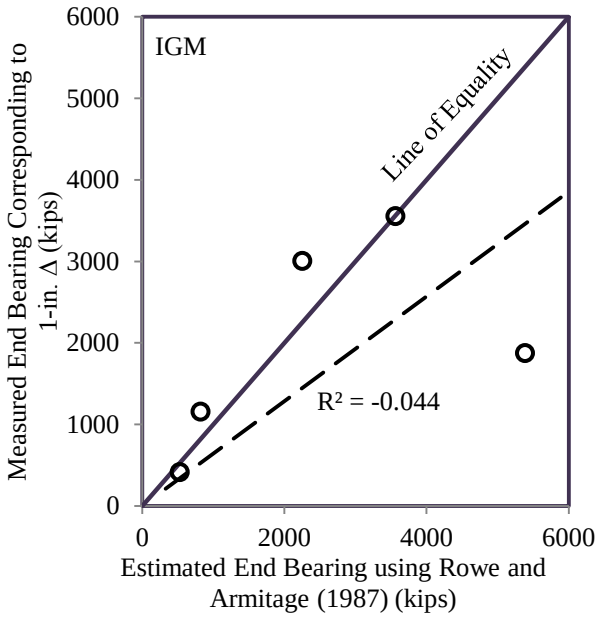

(a) Rowe and Armitage (1987)

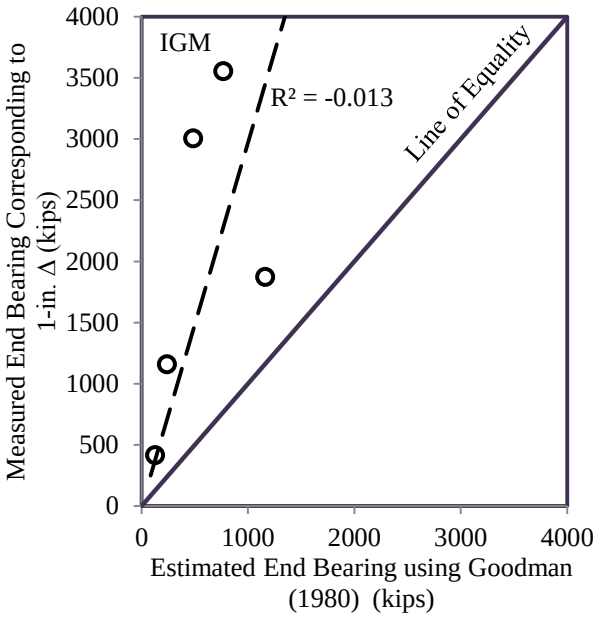

(b) Goodman (1980)

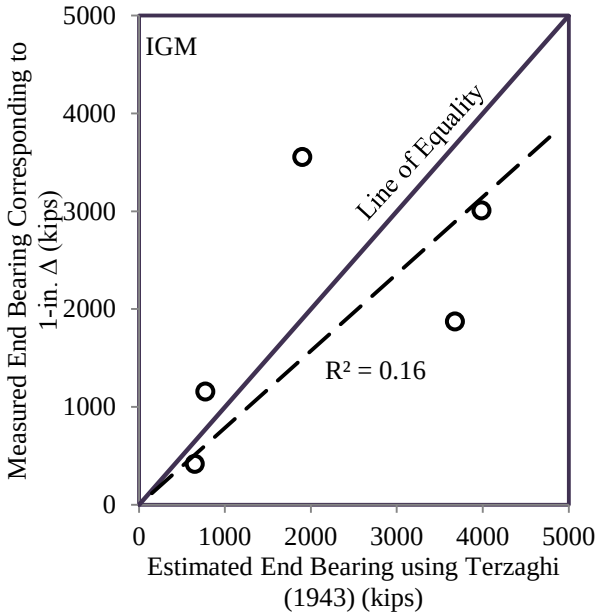

(c) Terzaghi (1943)

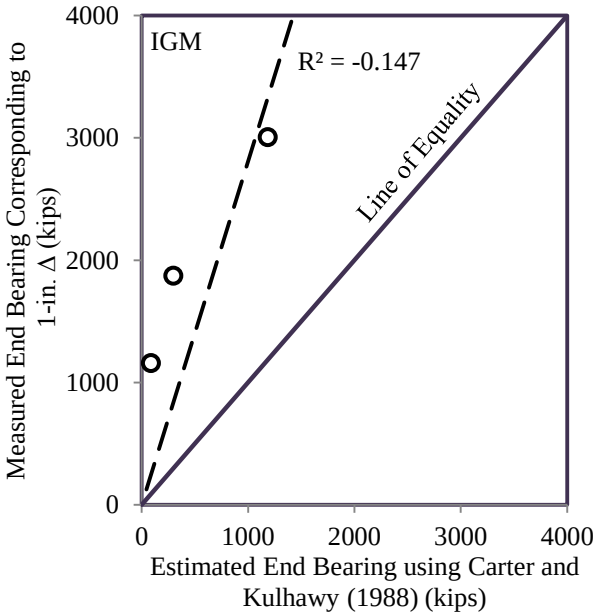

(d) Carter and Kulhawy (1988)

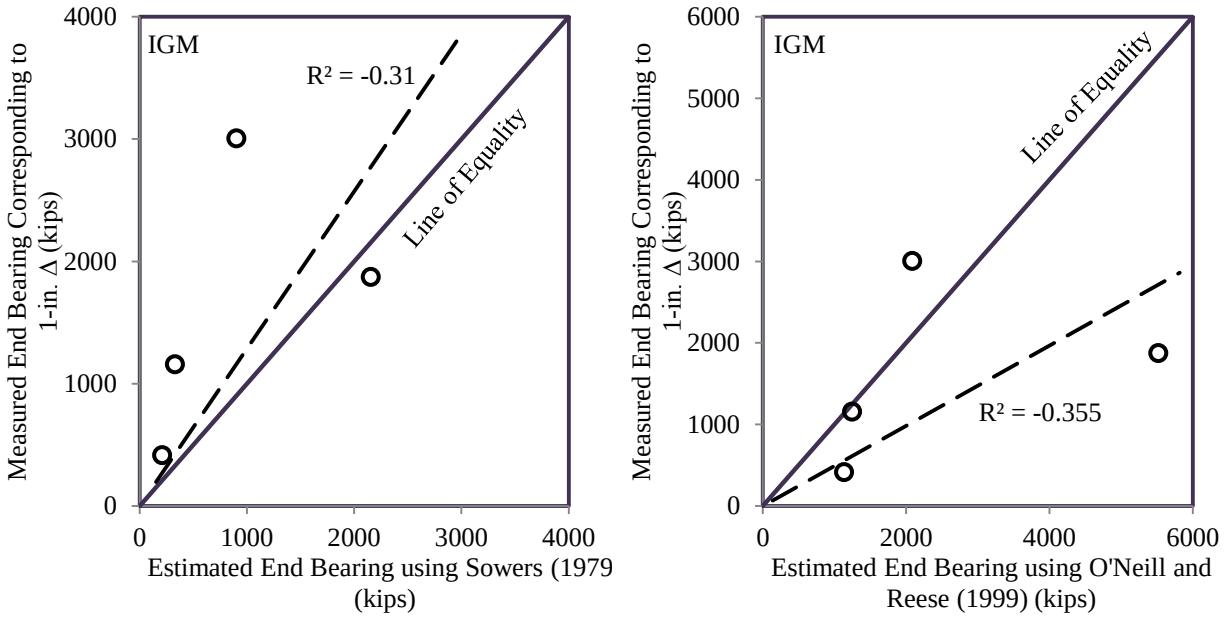

(e) Sowers (1979)

(f) O'Neill and Reese (1999)

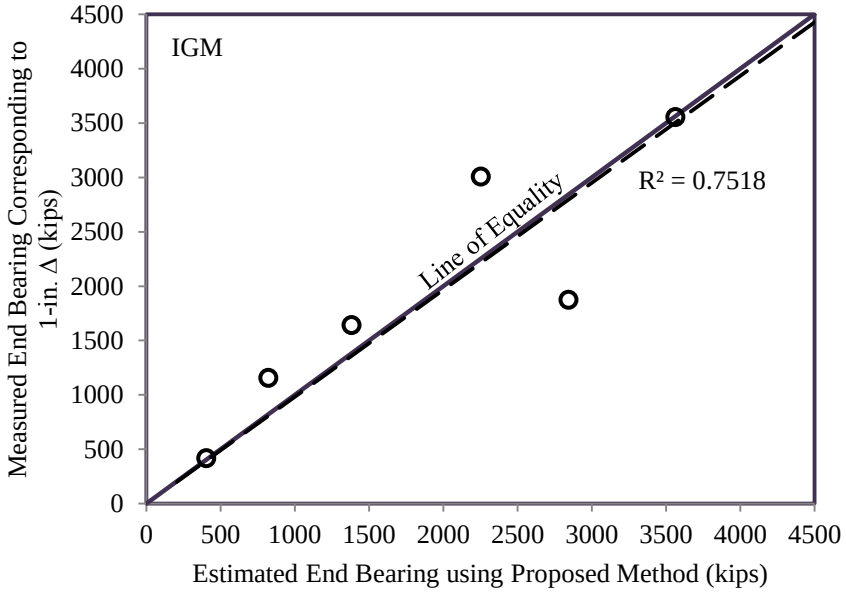

(g) Proposed Method

Figure 4.40. Comparison of measured end bearing corresponding to 1-in. top displacement and estimated end bearing in IGM for various analytical methods

Figure 4.41 considering the 5% diameter for displacement criterion shows slightly different observations. The estimations were improved using the analytical methods by Rowe and Armitage (1987), Terzaghi (1943), and O'Neill and Reese (1999).

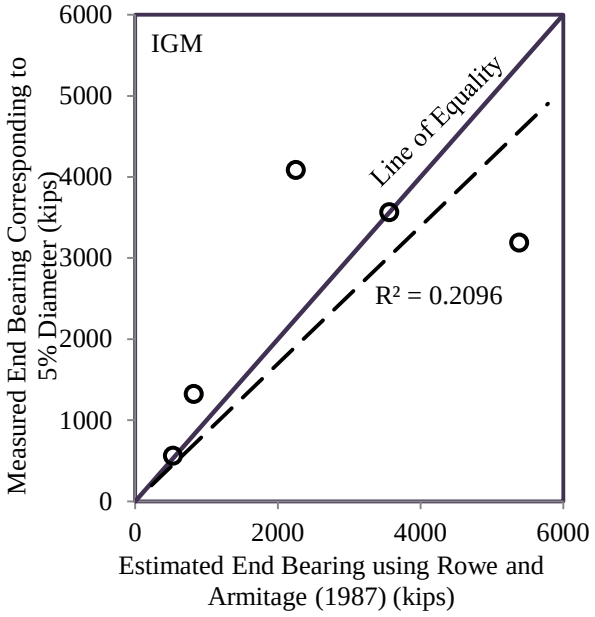

(a) Rowe and Armitage (1987)

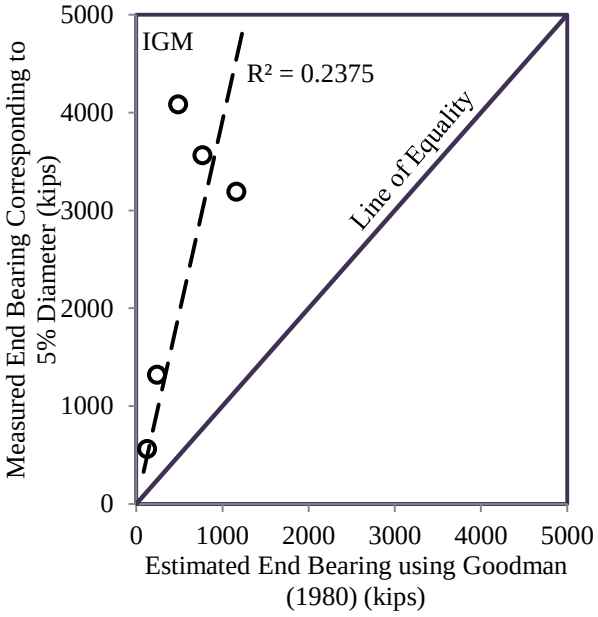

(b) Goodman (1980)

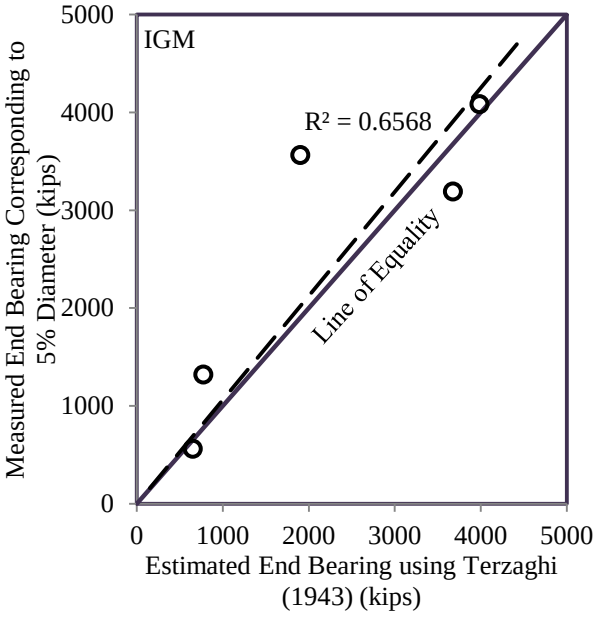

(c) Terzaghi (1943)

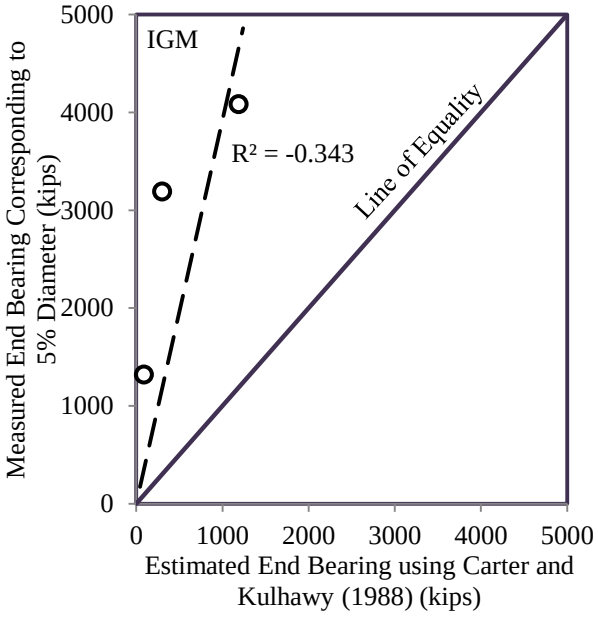

(d) Carter and Kulhawy (1988)

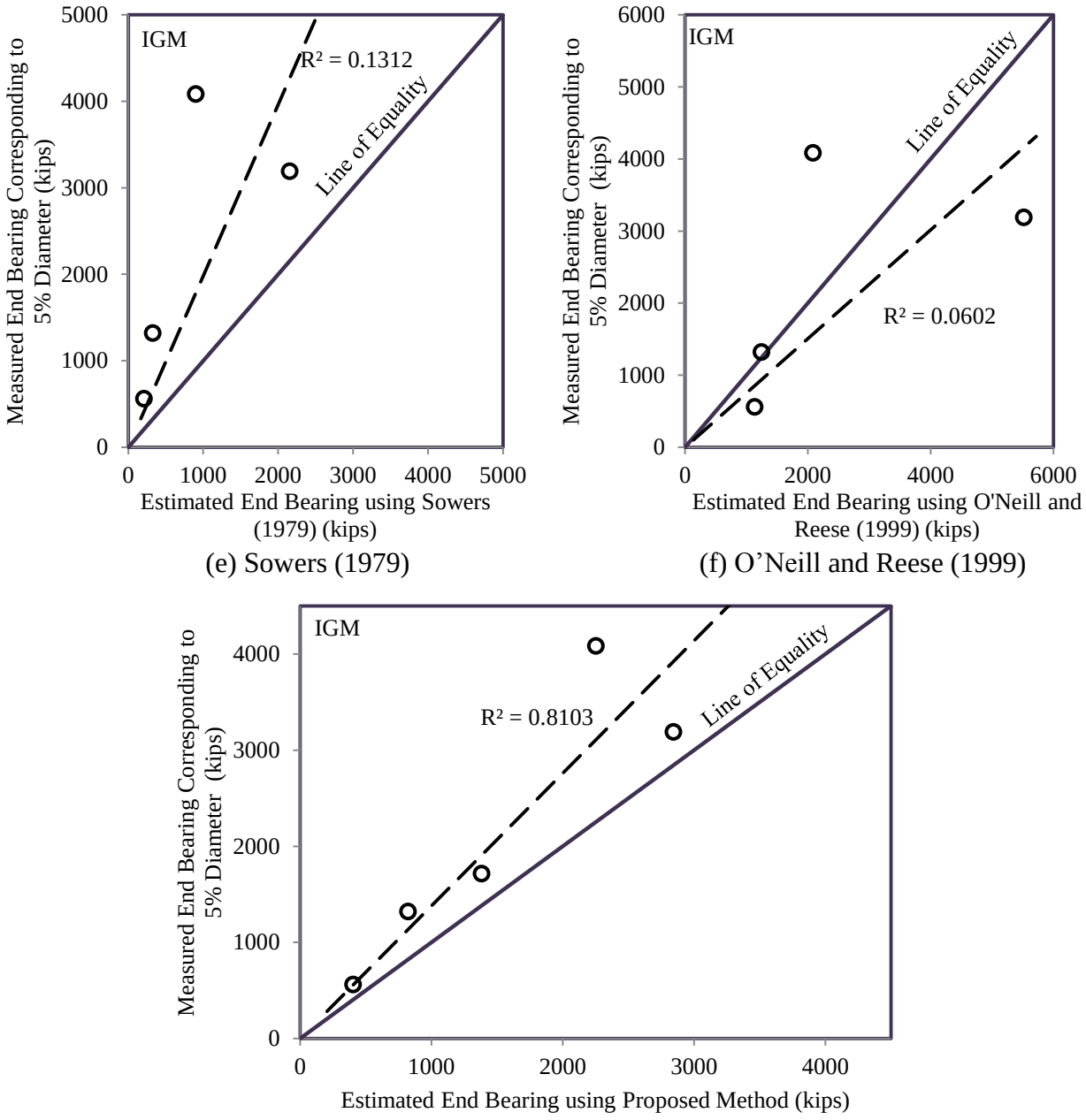

(e) Sowers (1979)

(f) O'Neill and Reese (1999)

(g) Proposed Method

Figure 4.41. Comparison of measured end bearing corresponding to 5% of shaft diameter for top displacement and estimated end bearing in IGM for various analytical methods

Figure 4.42, Figure 4.43, and Figure 4.44 show the Anderson-Darling (AD) (1952) normality tests of the end bearing ratio for three failure criteria.

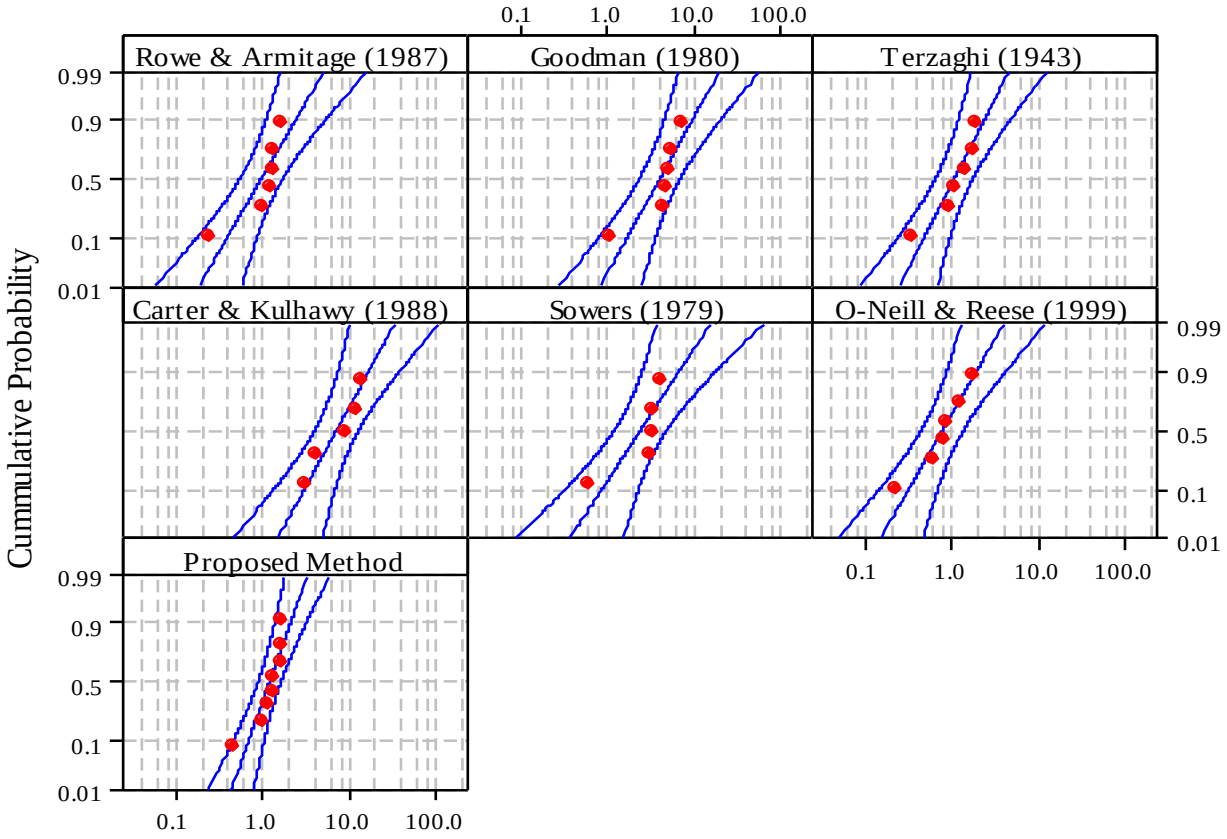

Analytical Method	Loc	Scale	N	AD	CV	Lognormal
Rowe & Armitage (1987)	-0.02887	0.7187	6	0.951	0.501	No
Goodman (1980)	1.414	0.6819	6	0.836	0.501	No
Terzaghi (1943)	0.06592	0.6314	6	0.402	0.501	Yes
Carter & Kulhawy (1988)	1.975	0.6716	5	0.308	0.470	Yes
Sowers (1979)	0.8801	0.8033	5	0.923	0.470	No
O-Neill & Reese (1999)	-0.2646	0.7074	6	0.259	0.501	Yes
Proposed Method	0.1723	0.439	8	0.811	0.547	No

Figure 4.42. Goodness of fit test for end bearing in IGM based on measured end bearing obtained directly from load test reports for various analytical methods

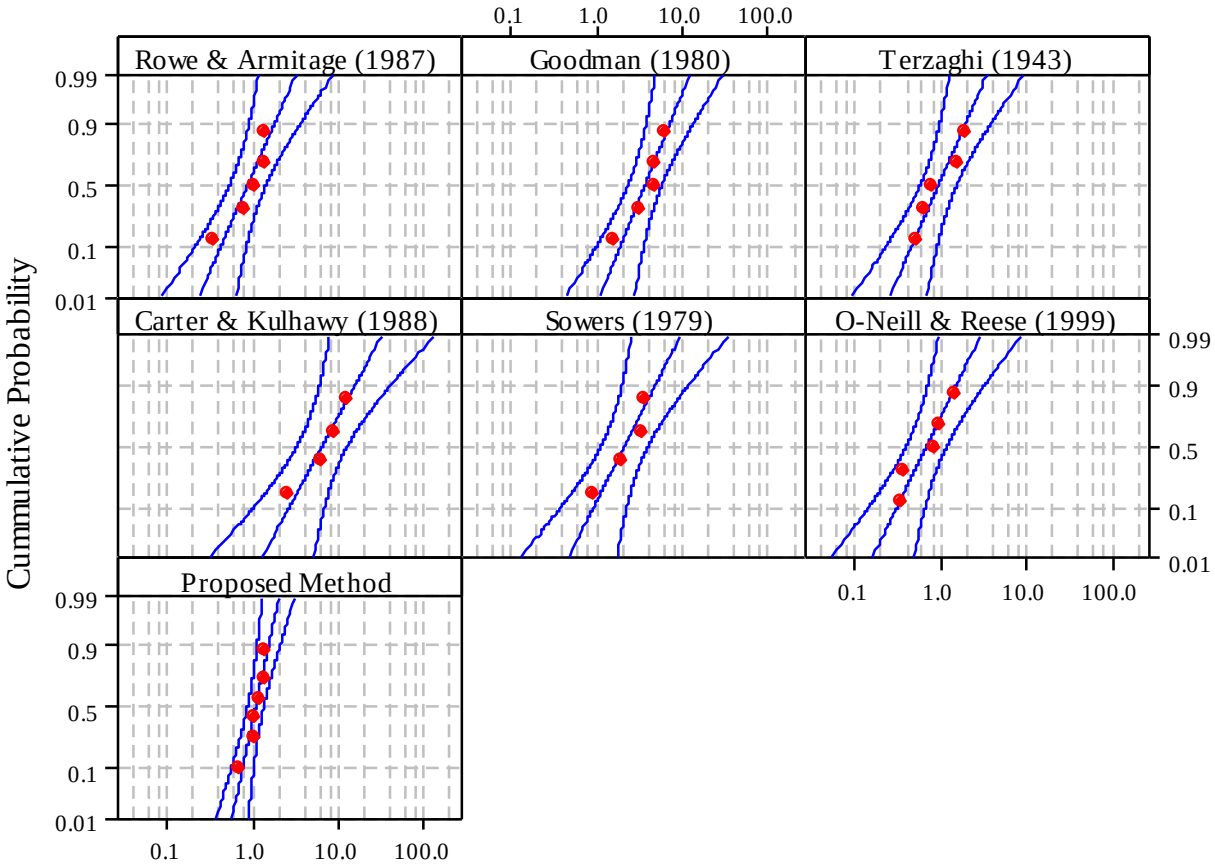

Analytical Method	Loc	Scale	N	AD	CV	Lognormal
Rowe & Armitage (1987)	-0.134	0.5668	5	0.37	0.470	Yes
Goodman (1980)	1.314	0.5223	5	0.346	0.470	Yes
Terzaghi (1943)	-0.07573	0.5607	5	0.303	0.470	Yes
Carter & Kulhawy (1988)	1.874	0.6967	4	0.229	0.430	Yes
Sowers (1979)	0.7495	0.6489	4	0.341	0.430	Yes
O-Neill & Reese (1999)	-0.4051	0.6223	5	0.302	0.470	Yes
Proposed Method	0.06826	0.2744	6	0.331	0.501	Yes

Figure 4.43. Goodness of fit test for end bearing in IGM corresponding to 1-in. top displacement for various analytical methods

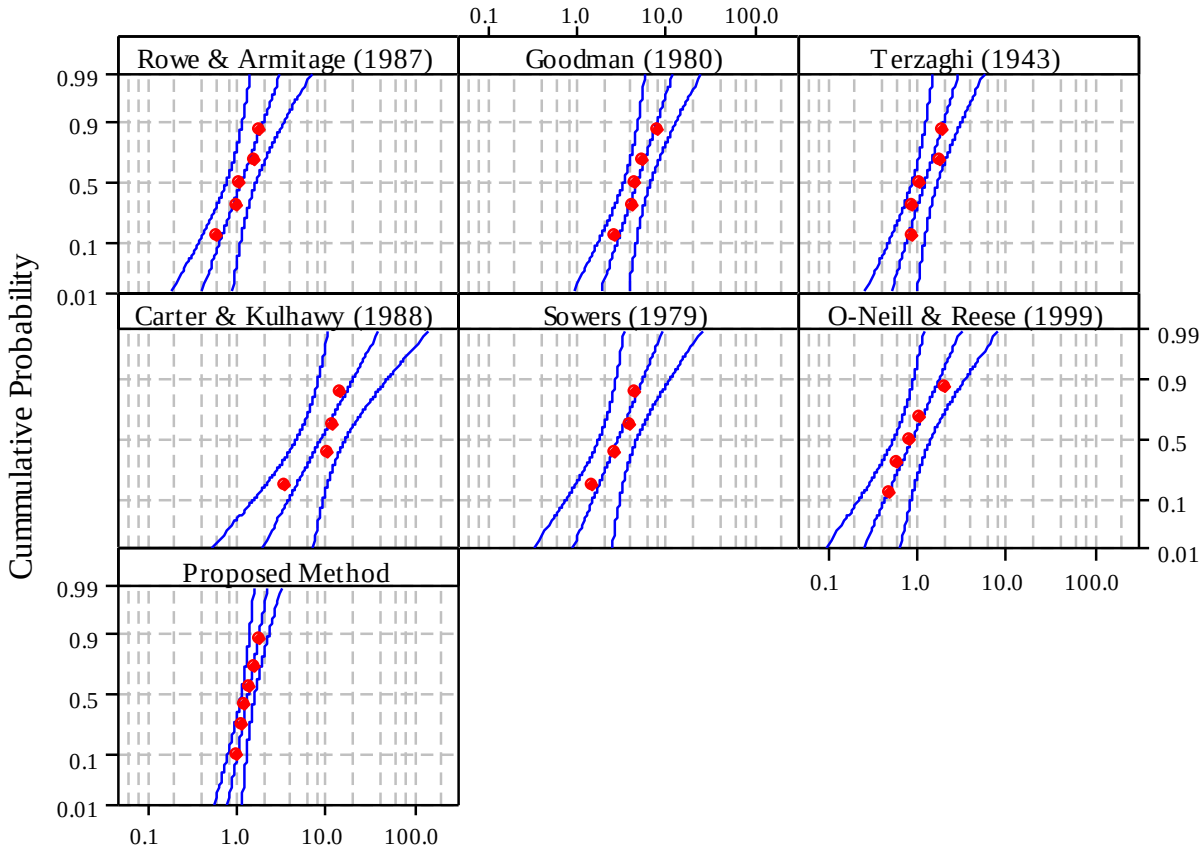

Analytical Method	Loc	Scale	N	AD	CV	Lognormal
Rowe & Armitage (1987)	0.1202	0.4429	5	0.25	0.470	Yes
Goodman (1980)	1.568	0.4046	5	0.21	0.470	Yes
Terzaghi (1943)	0.1784	0.375	5	0.463	0.470	Yes
Carter & Kulhawy (1988)	2.191	0.6519	4	0.473	0.430	No
Sowers (1979)	1.067	0.5055	4	0.27	0.430	Yes
O-Neill & Reese (1999)	-0.1509	0.5463	5	0.219	0.470	Yes
Proposed Method	0.2876	0.2228	6	0.144	0.501	Yes

Figure 4.44. Goodness of fit test for end bearing in IGM corresponding to 5% of shaft diameter for top displacement for various analytical methods

The end bearing ratio is a ratio of measured to estimated end bearing. The "Loc" and "Scale" represent the mean and standard deviation of the natural logarithm of the datasets. The sample size is represented by "N". Since the cumulative probability density function was plotted in a logarithmic scale, the assumed logarithmic distribution within the 95% confidence interval (CI) is confirmed when the AD value is smaller than the CV value. Due to the variability of the estimation of end bearing in IGM, not all assumed lognormal distributions are confirmed except for the 1-in. displacement criterion. The results of the normality tests are summarized in the figures with "Yes" or "No" indicating whether confirming the lognormal distribution was confirmed.

Figure 4.45, Figure 4.46, and Figure 4.47 show the normal distribution of the end bearing ratio and the statistical characteristics (i.e., mean and standard deviation) necessary for the calibration of resistance factors.

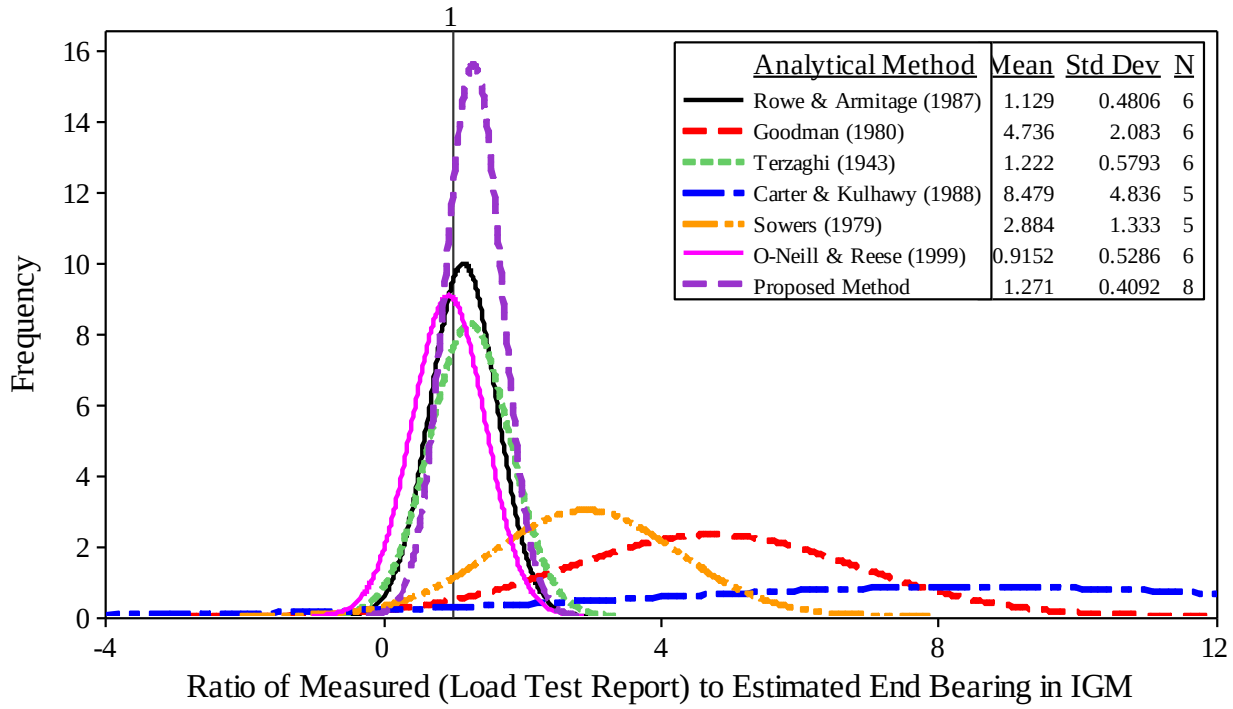

Figure 4.45. Summary of the normal distributed PDFs of the end bearing ratio in IGM based on measured end bearing obtained directly from load test reports for various analytical methods

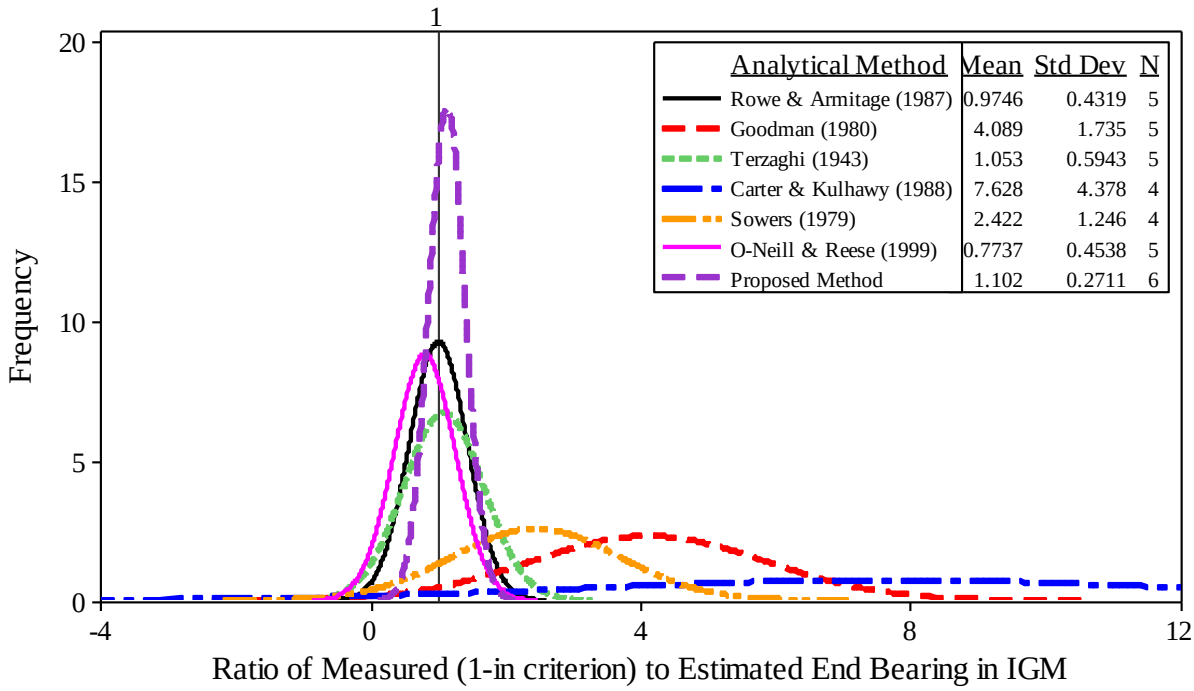

Figure 4.46. Summary of the normal distributed PDFs of the end bearing ratio in IGM corresponding to 1-in. top displacement for various analytical methods

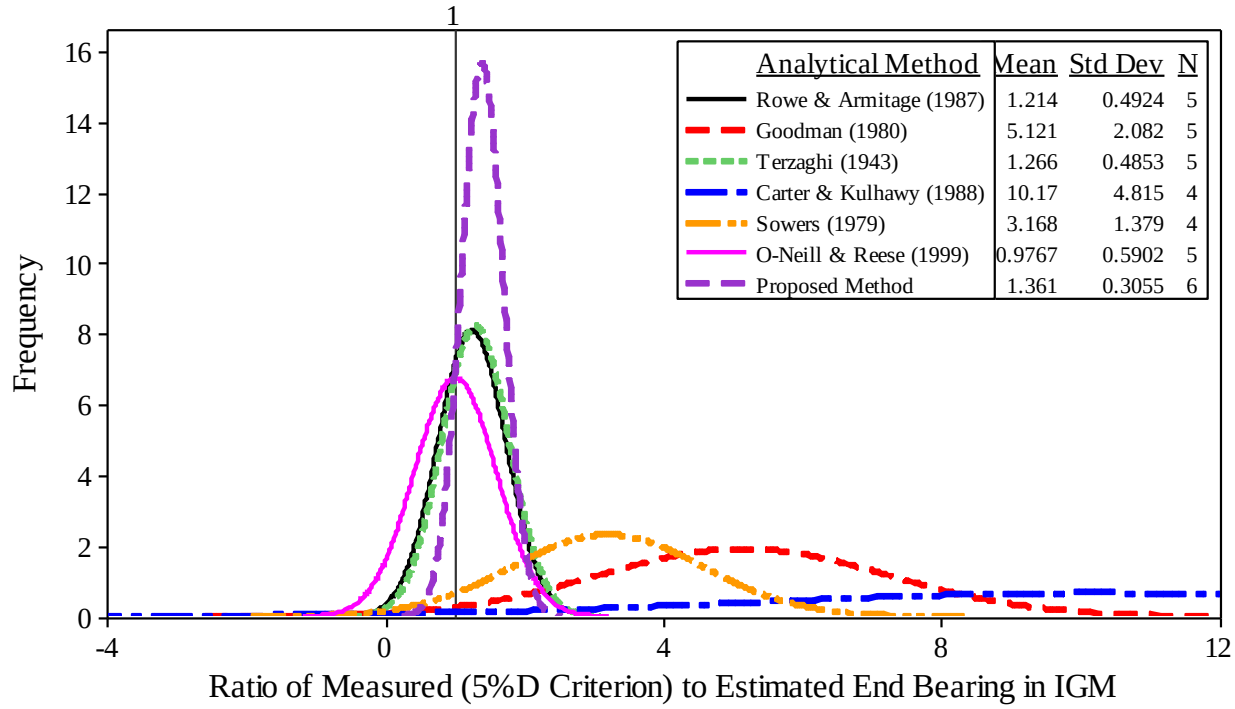

Figure 4.47. Summary of the normal distributed PDFs of the end bearing ratio in IGM corresponding to 5% of shaft diameter for top displacement for various analytical methods

The distribution with a mean value larger than one indicates that the end bearing is generally underestimated. Figure 4.45 shows that the analytical method by O'Neill and Reese (1999) has the mean of 0.915 closest to one while the proposed method has the smallest standard deviation of 0.409. Figure 4.46 shows that the analytical method by Rowe and Armitage (1987) has the mean of 0.975 closest to one while the proposed method has the smallest standard deviation of 0.271. Figure 4.47 shows that the analytical method by O'Neill and Reese (1999) has the mean of 0.977 closest to one while the proposed method has the smallest standard deviation of 0.306. The statistical characteristics indicate that the end bearing in IGM can be reasonably estimated using the analytical methods by Rowe and Armitage (1987), Terzaghi (1943), O'Neill and Reese (1999), and the proposed method. In contrast, analytical methods by Goodman (1980), Carter and Kulhawy (1988), and Sowers (1979) should not be used as they will provide inaccurate estimations of end bearing.

Following the LRFD framework, resistance factors were determined as a function of reliability index as shown in Figure 4.48, Figure 4.49, and Figure 4.50.

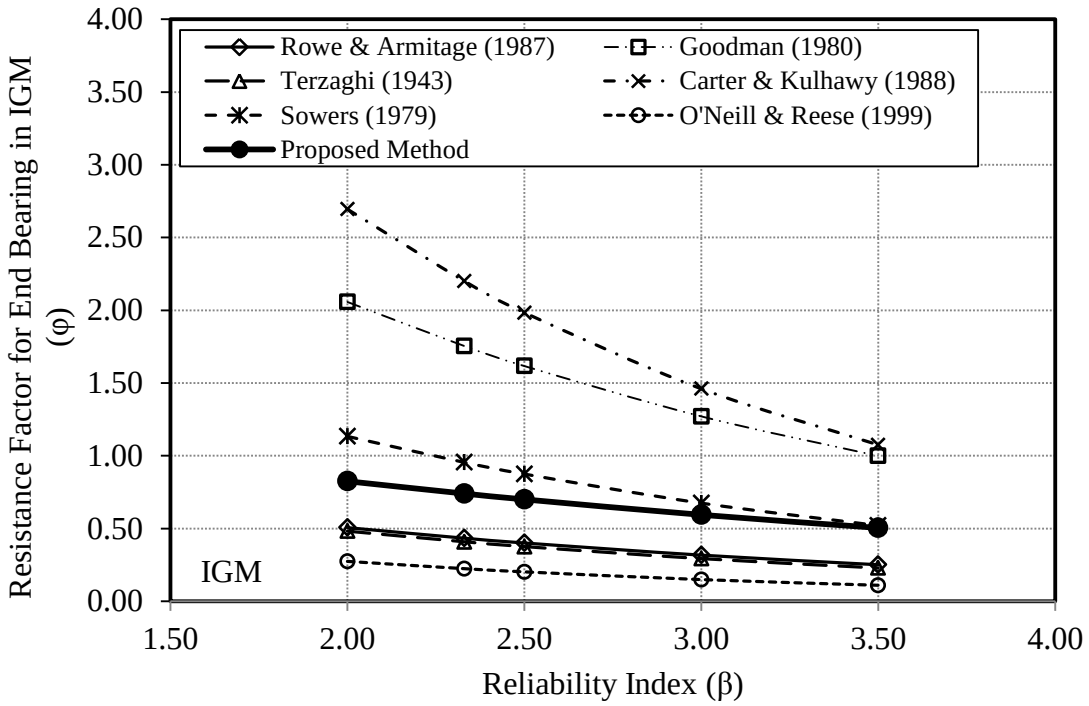

Figure 4.48. LRFD resistance factors for end bearing in IGM based on measured end bearing obtained directly from load test reports

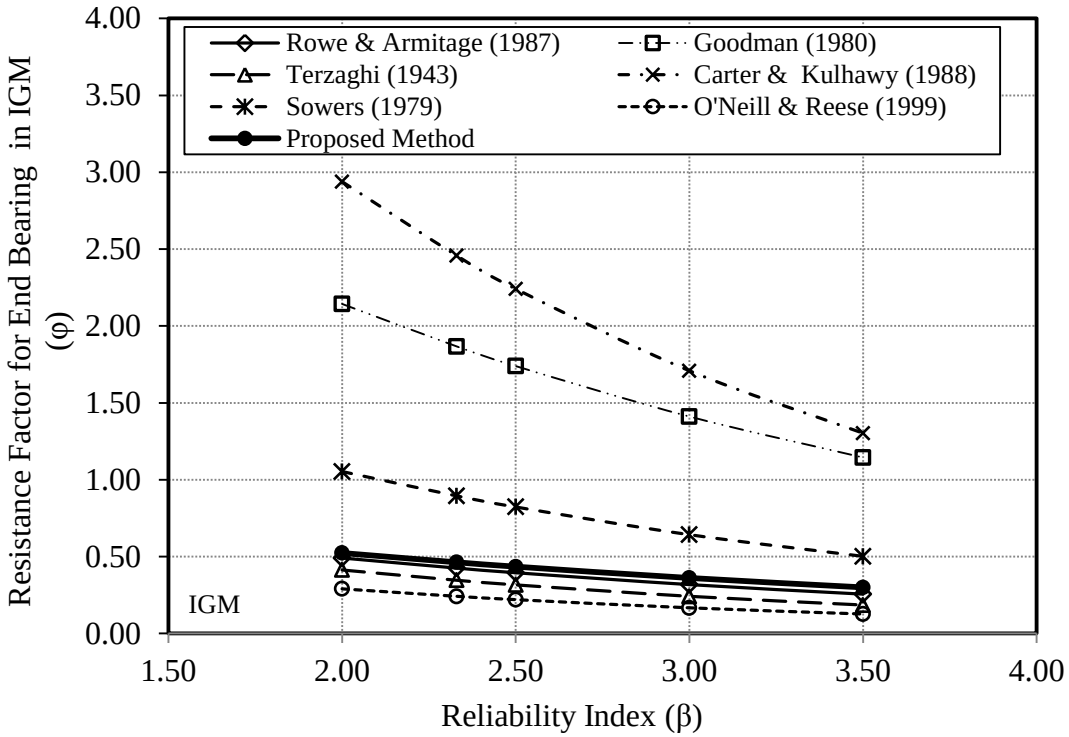

Figure 4.49. LRFD resistance factors for end bearing in IGM corresponding to 1-in. top displacement criterion

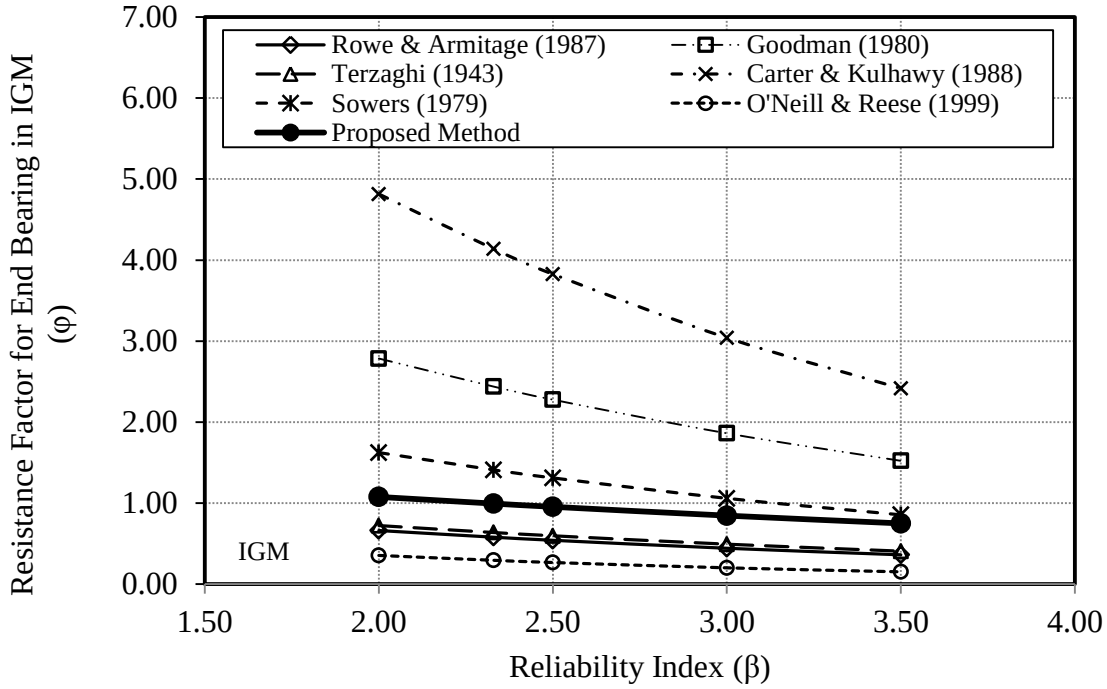

Figure 4.50. LRFD resistance factors for end bearing in IGM corresponding to 5% of shaft diameter for top displacement criterion

The resistance factor decreases when a higher reliability level of the drilled shaft foundation system is desired. It is important to note that unrealistically high resistance factors (i.e, greater than one) were determined for Goodman (1980), Carter and Kulhawy (1988), and Sowers (1979), which are not recommended for end bearing estimations. Figure 4.51, Figure 4.52, and Figure 4.53 show that the efficiency of the estimation decreases with increasing reliability index. Among the seven analytical methods, the proposed method with the highest efficiency factor provides the most efficient estimation of end bearing in IGM.

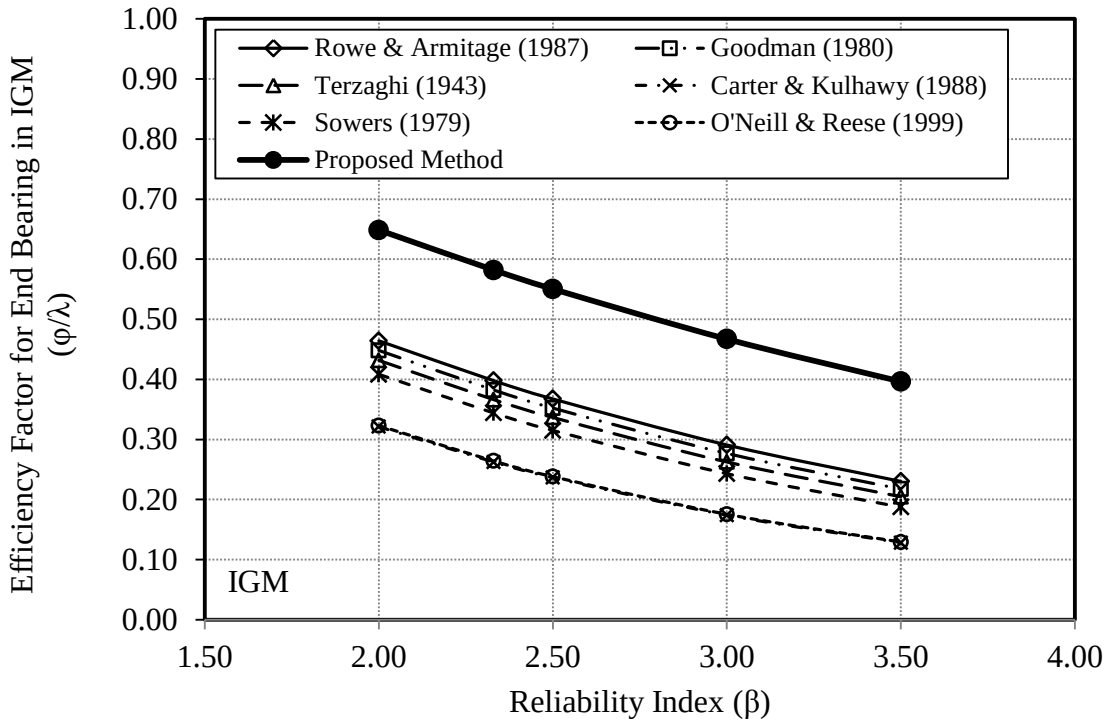

Figure 4.51. Efficiency factors for end bearing in IGM based on measured end bearing obtained directly from load test reports

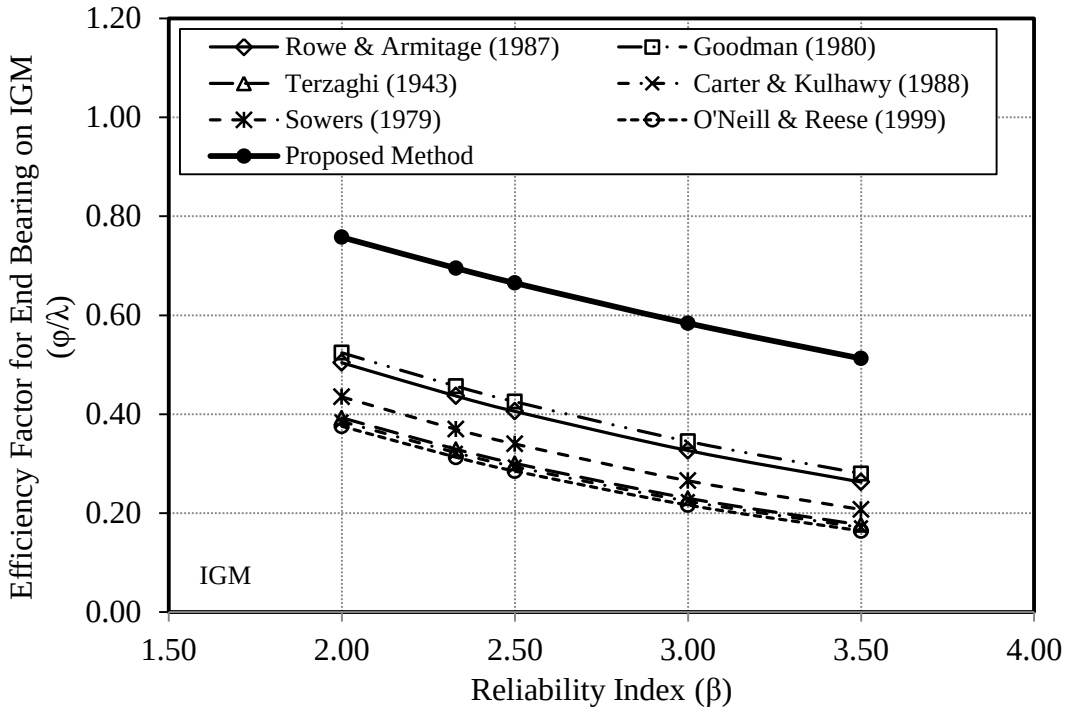

Figure 4.52. Efficiency factors for end bearing in IGM corresponding to 1-in. top displacement criterion

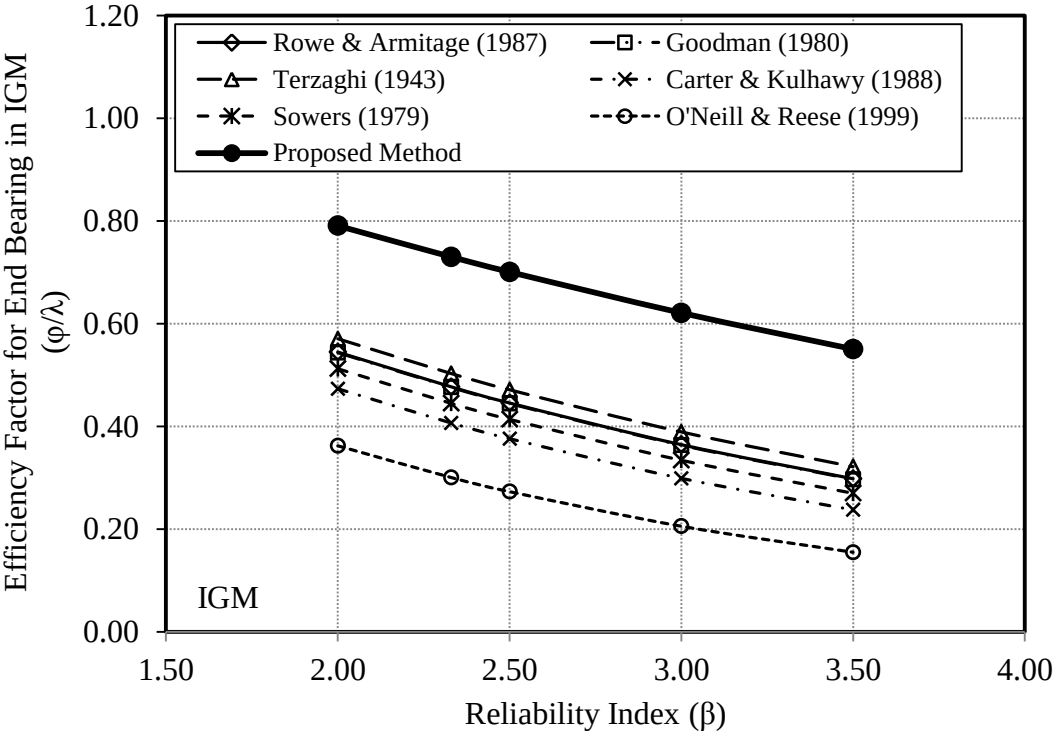

Figure 4.53. Efficiency factors for end bearing in IGM corresponding to 5% of shaft diameter for top displacement criterion

4.3.4. Rock

End bearings in rock were estimated using six analytical methods given in Table 3.2 and the proposed method given in Table 3.4. The purpose of using different analytical methods was to investigate the reliability of the methods, depending on the characteristics of the bearing rock mass that were not clearly described or not known in the load test reports collected in DSHAFT. The estimated end bearings for the six analytical methods are summarized in Table 3.5 while the estimated end bearings based on the proposed method are given in Appendix C. The measured end bearings in rock are summarized in Table 3.7 with respect to the three failure criteria: load test report, 1-in. displacement and 5% diameter for displacement. ID No. 7 was neglected because a gap between the shaft base and the bearing rock was identified from the load test results. ID No. 24 was neglected because no rock information was found near and below the shaft base. ID No. 36 was neglected because no O-cell load test measurements were available.

Figure 4.54 shows the comparisons of estimated end bearing and measured end bearing obtained directly from load test reports.

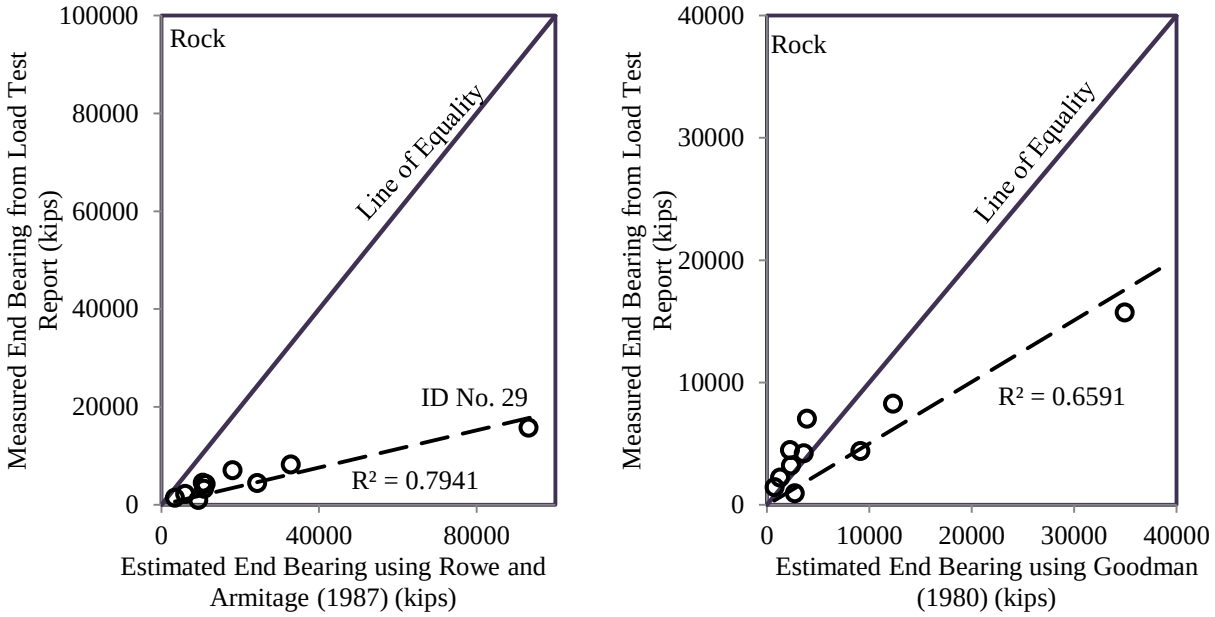

(a) Rowe and Armitage (1987)

(b) Goodman (1980)

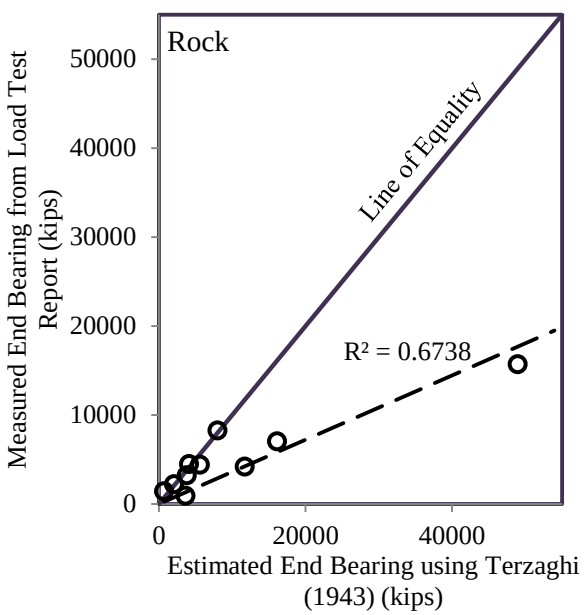

(c) Terzaghi (1943)

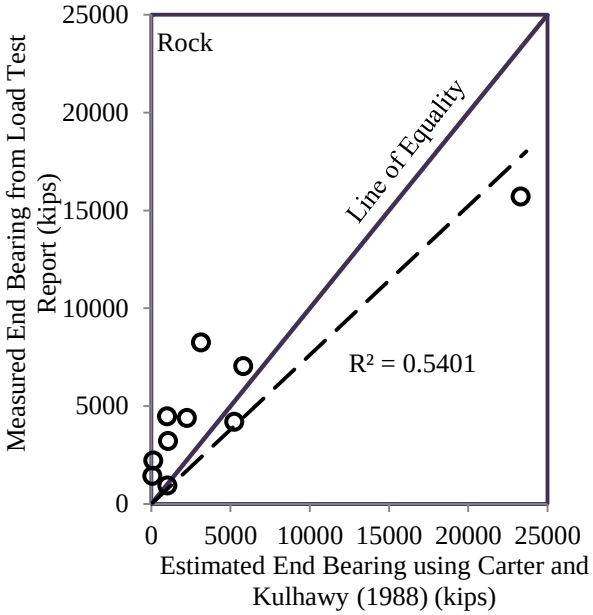

(d) Carter and Kulhawy (1988)

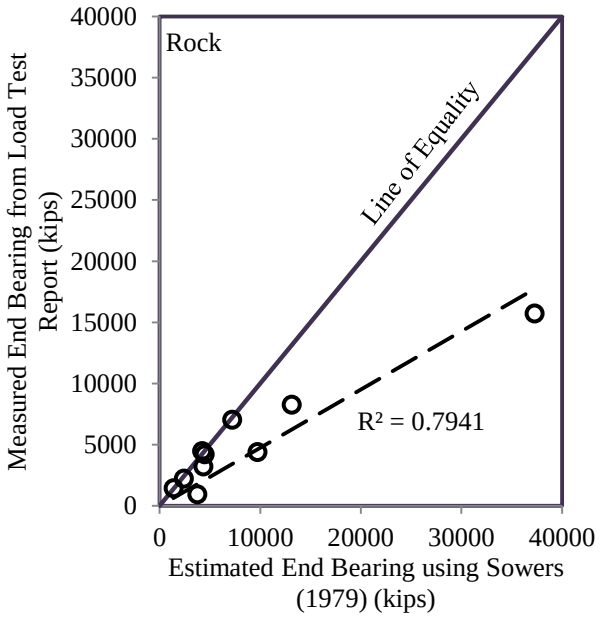

(e) Sowers (1979)

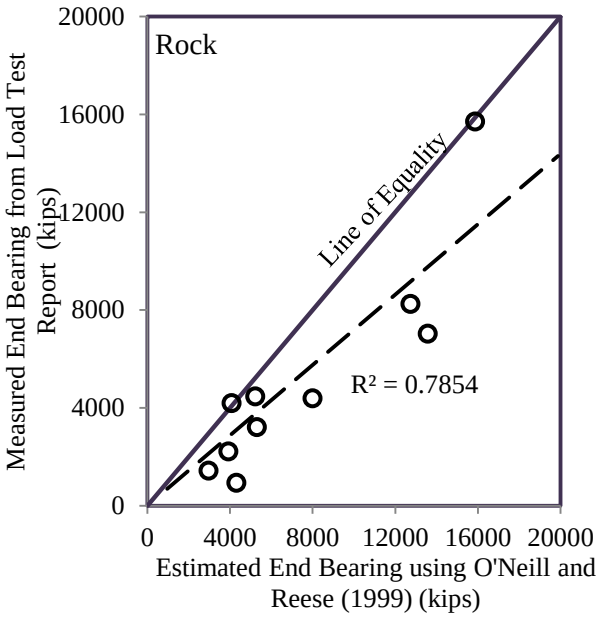

(f) O'Neill and Reese (1999)

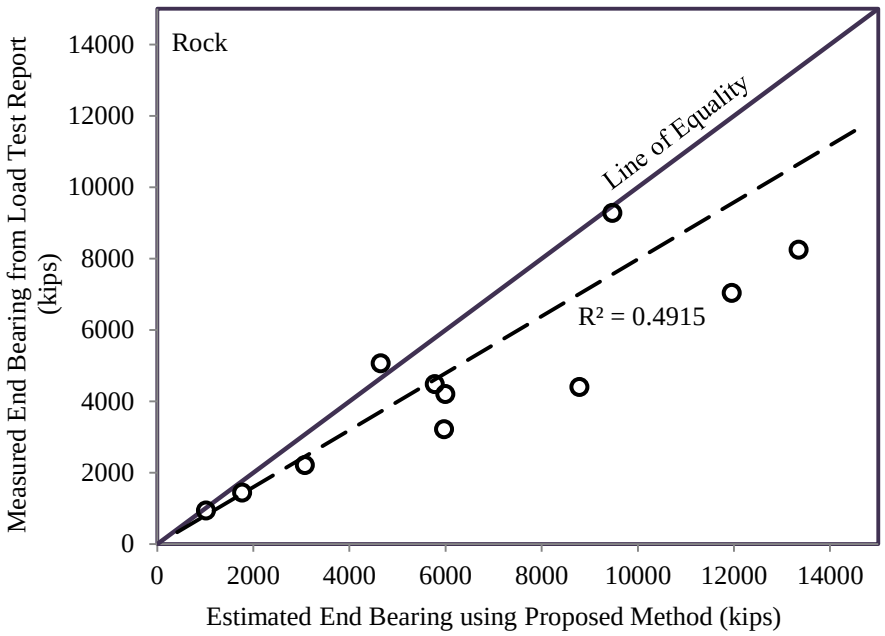

(g) Proposed Method

Figure 4.54. Comparison of measured end bearing obtained directly from load test reports and estimated end bearing in rock for various analytical methods

Analytical methods by Rowe and Armitage (1987), O'Neill and Reese (1999), and the proposed method are likely to overestimate the end bearing with most data points and the best-fit line below the line of equality. Estimations using analytical methods by Terzaghi (1943) and Sowers (1979) for rocks with steeply dipping joints provide reasonable end bearing estimations while the accuracy reduces with increasing end bearing. Similar observations can be made from Figure 4.55 based on the 1-in. displacement criterion.

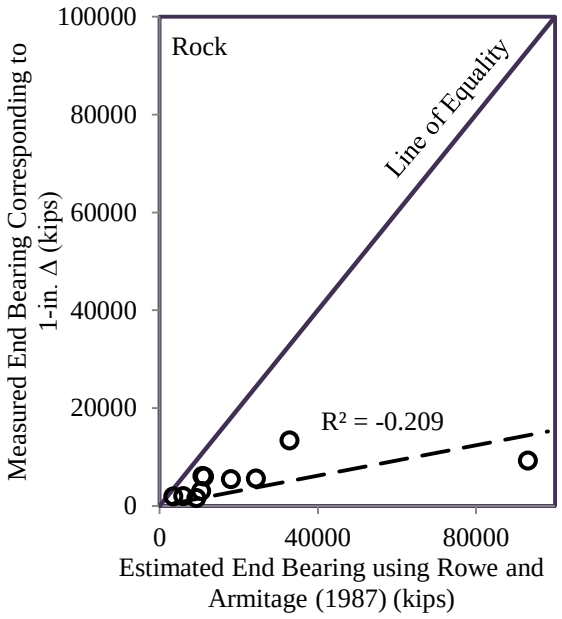

(a) Rowe and Armitage (1987)

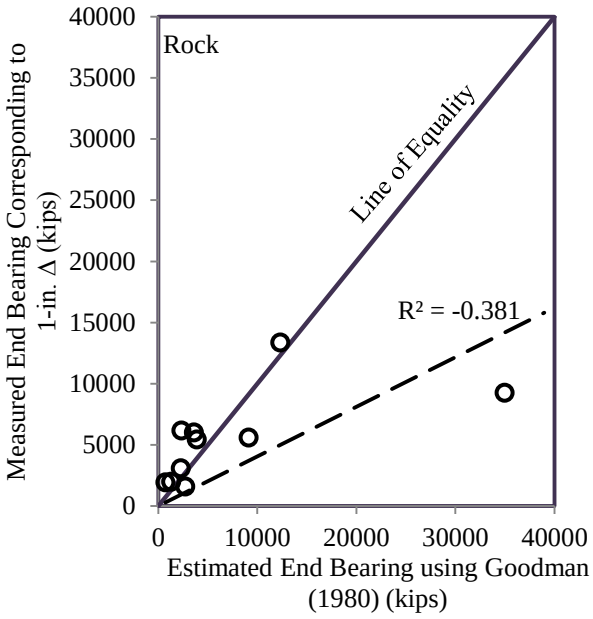

(b) Goodman (1980)

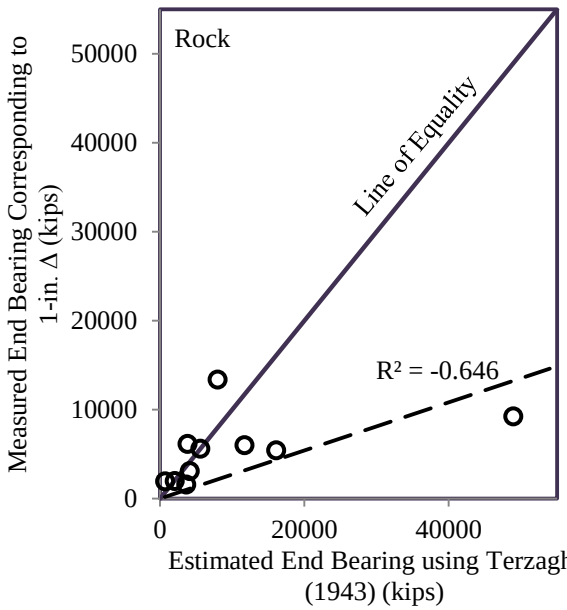

(c) Terzaghi (1943)

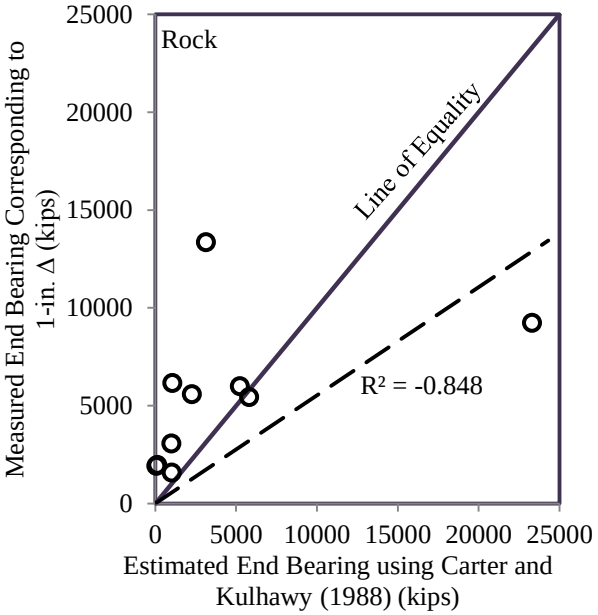

(d) Carter and Kulhawy (1988)

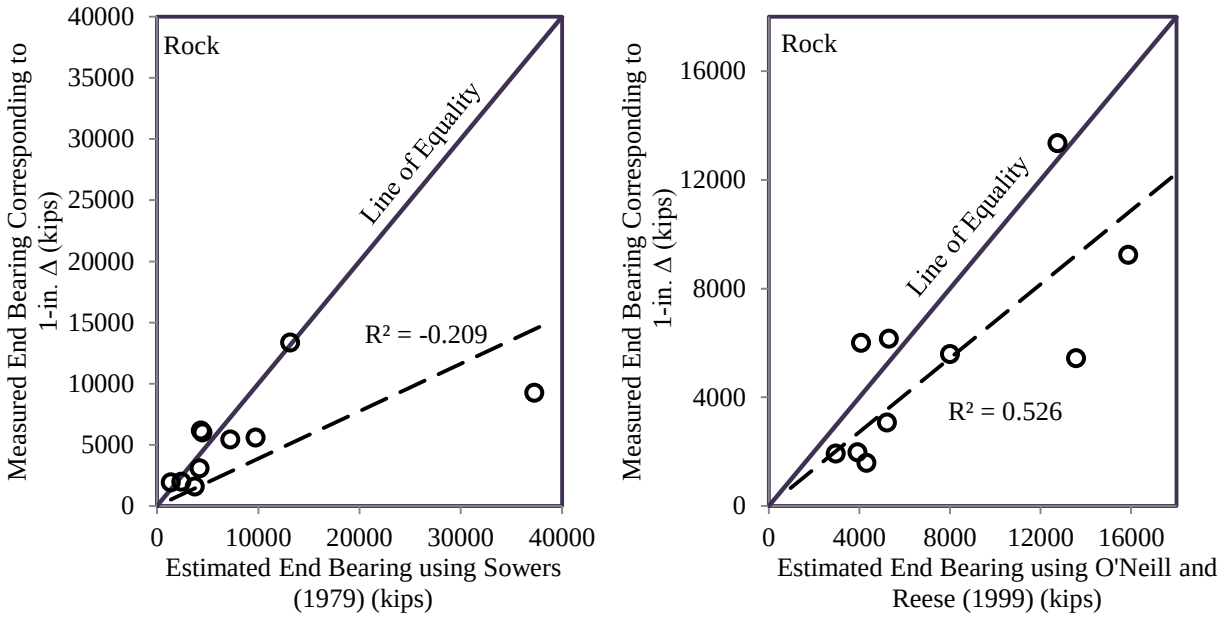

(e) Sowers (1979)

(f) O'Neill and Reese (1999)

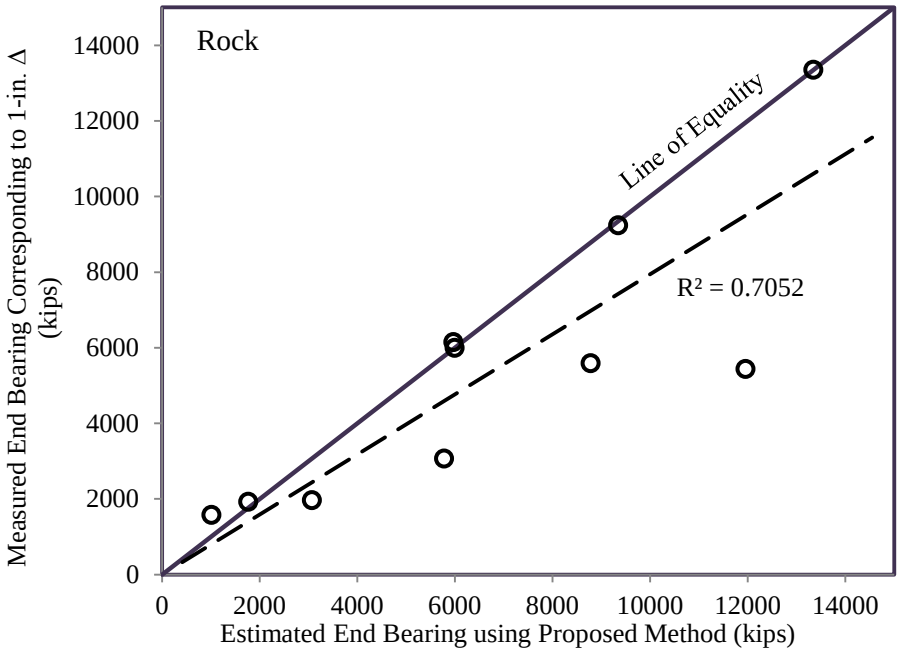

(g) Proposed Method

Figure 4.55. Comparison of measured end bearing corresponding to 1-in. top displacement and estimated end bearing in rock for various analytical methods

Figure 4.56 considering the 5% diameter for displacement criterion shows slightly different observations. All analytical methods except the method by Carter and Kulhawy (1988) provide reasonable end bearing estimations. However, the accuracy of the estimations was influenced by a data point ID No. 29, in which the drilled shaft embedded in limestone with a relatively high

uniaxial compressive strength (q_u) given in Table B.30. Figure 4.56(g) shows that the proposed method provides the best end bearing estimations.

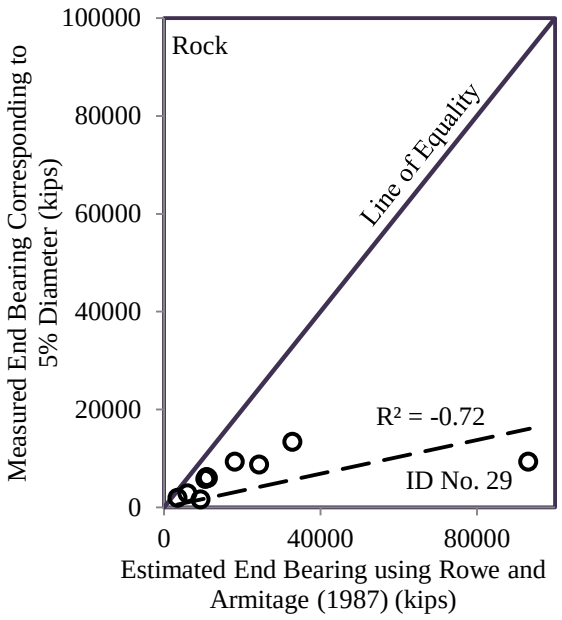

(a) Rowe and Armitage (1987)

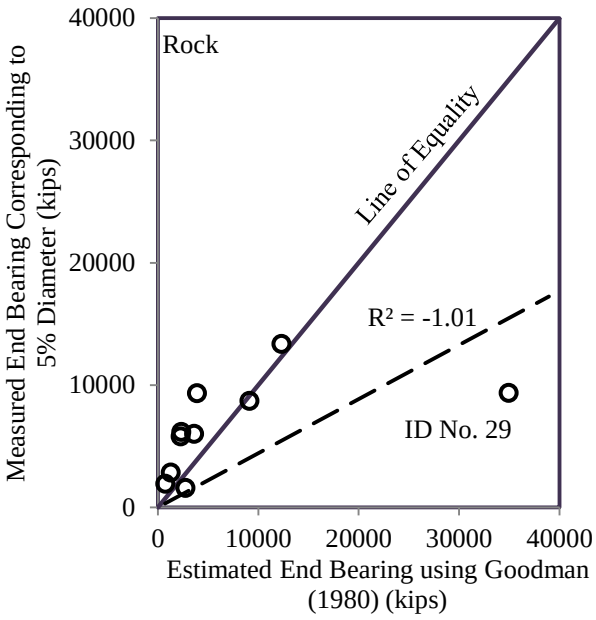

(b) Goodman (1980)

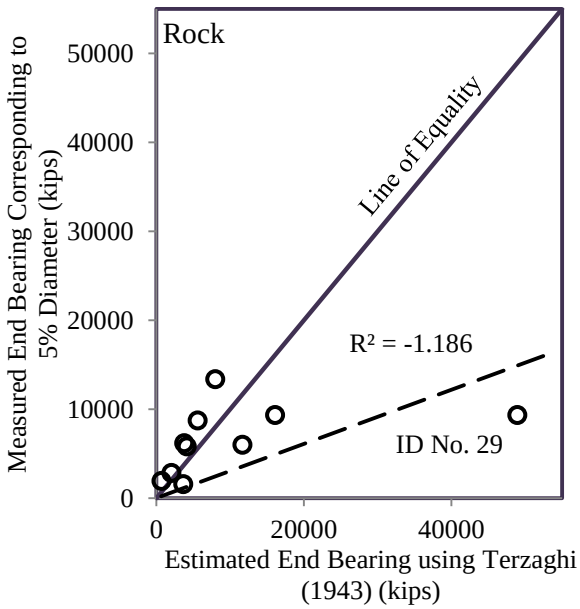

(c) Terzaghi (1943)

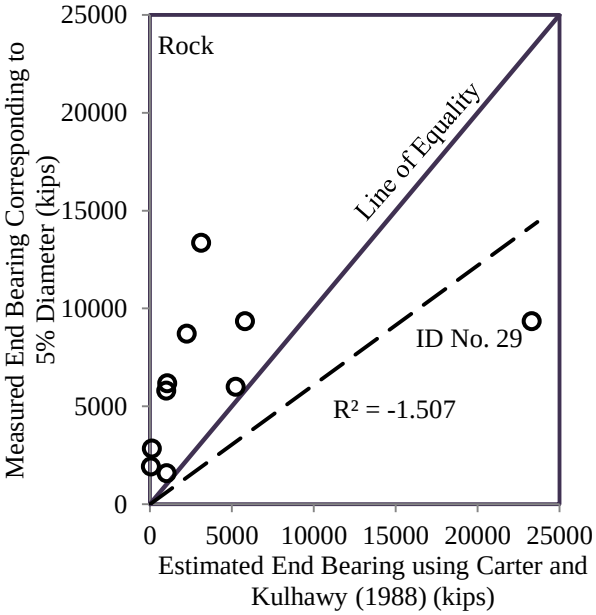

(d) Carter and Kulhawy (1988)

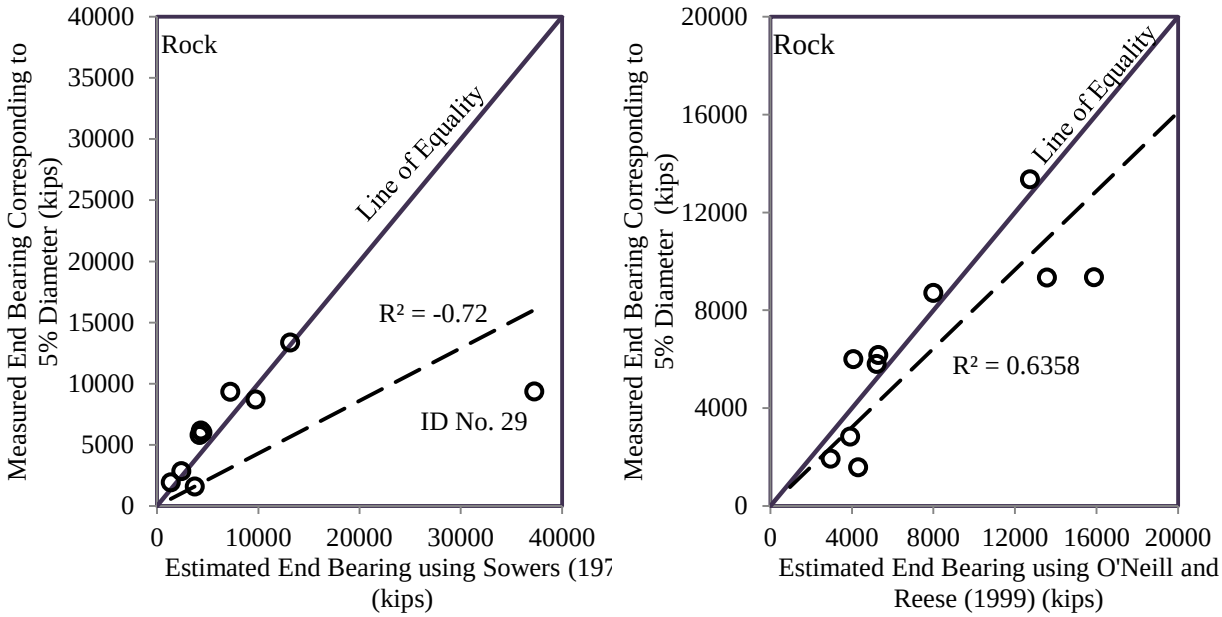

(e) Sowers (1979)

(f) O'Neill and Reese (1999)

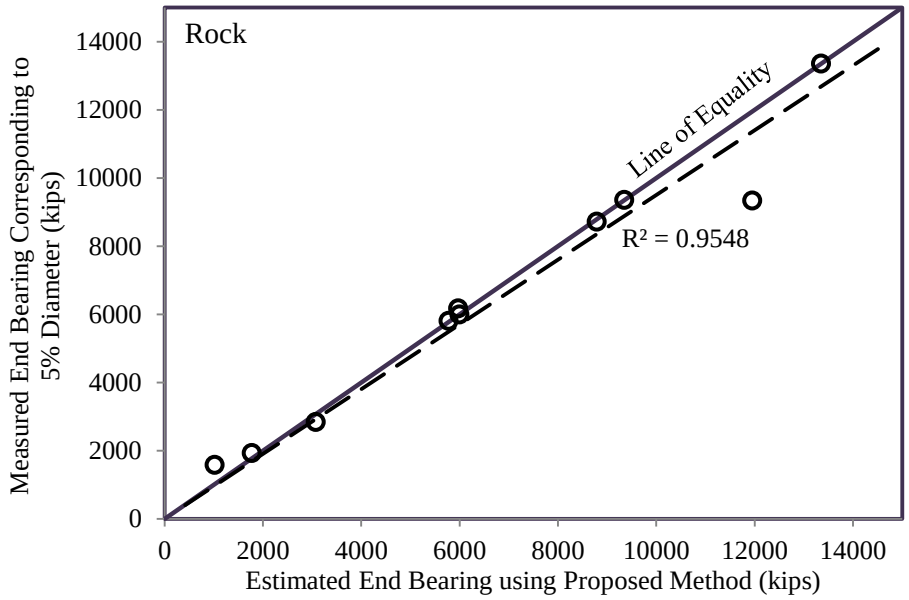

(g) Proposed Method

Figure 4.56. Comparison of measured end bearing corresponding to 5% of shaft diameter for top displacement and estimated end bearing in rock for various analytical methods

Figure 4.57, Figure 4.58, and Figure 4.59 show the Anderson-Darling (AD) (1952) normality tests of the end bearing ratio for three failure criteria.

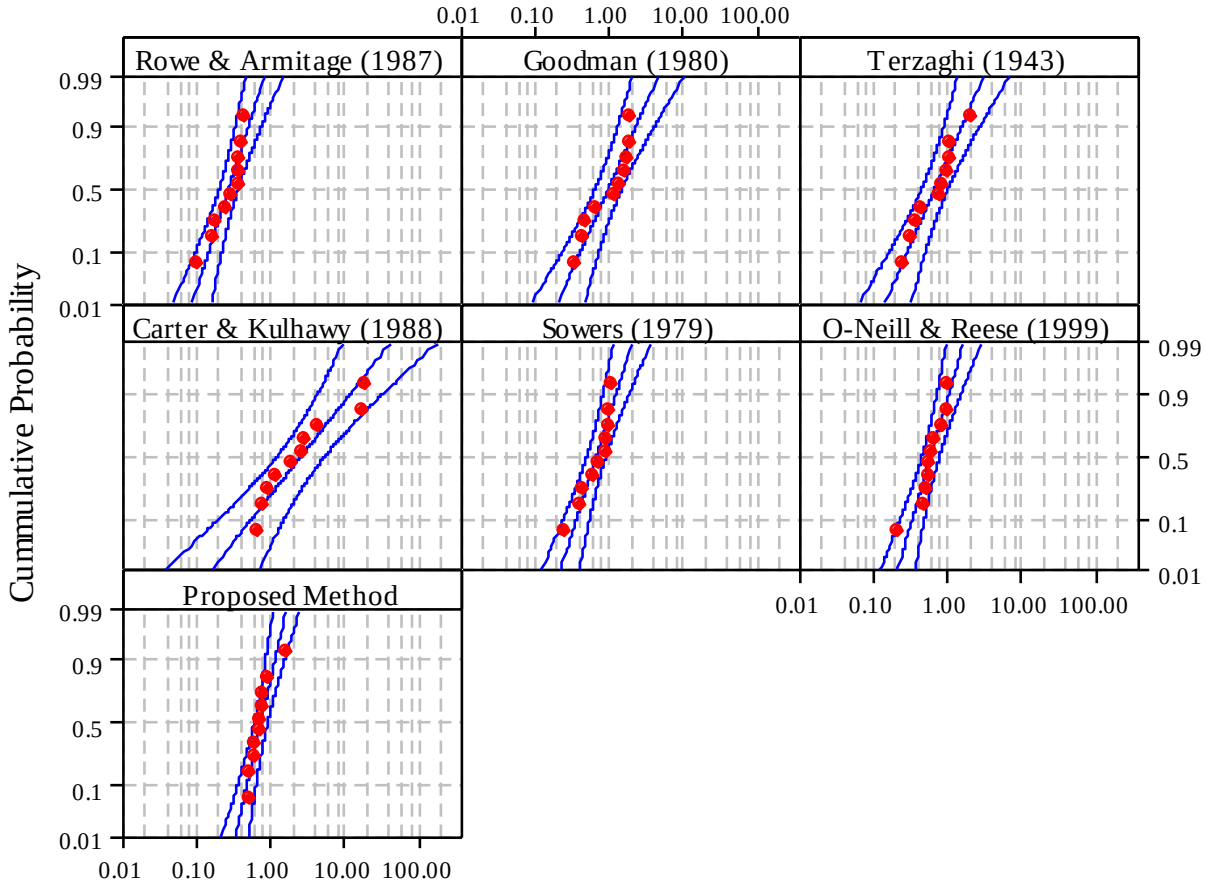

Analytical Method	Loc	Scale	N	AD	CV	Lognormal
Rowe & Armitage (1987)	-1.307	0.483	10	0.584	0.578	No
Goodman (1980)	-0.00992	0.6766	10	0.587	0.578	No
Terzaghi (1943)	-0.3883	0.6644	10	0.362	0.578	Yes
Carter & Kulhawy (1988)	0.9571	1.204	10	0.412	0.578	Yes
Sowers (1979)	-0.3909	0.483	10	0.584	0.578	No
O-Neill & Reese (1999)	-0.5159	0.4457	10	0.482	0.578	Yes
Proposed Method	-0.3042	0.3453	10	0.488	0.578	Yes

Figure 4.57. Goodness of fit test for end bearing in rock based on measured end bearing obtained directly from load test reports for various analytical methods

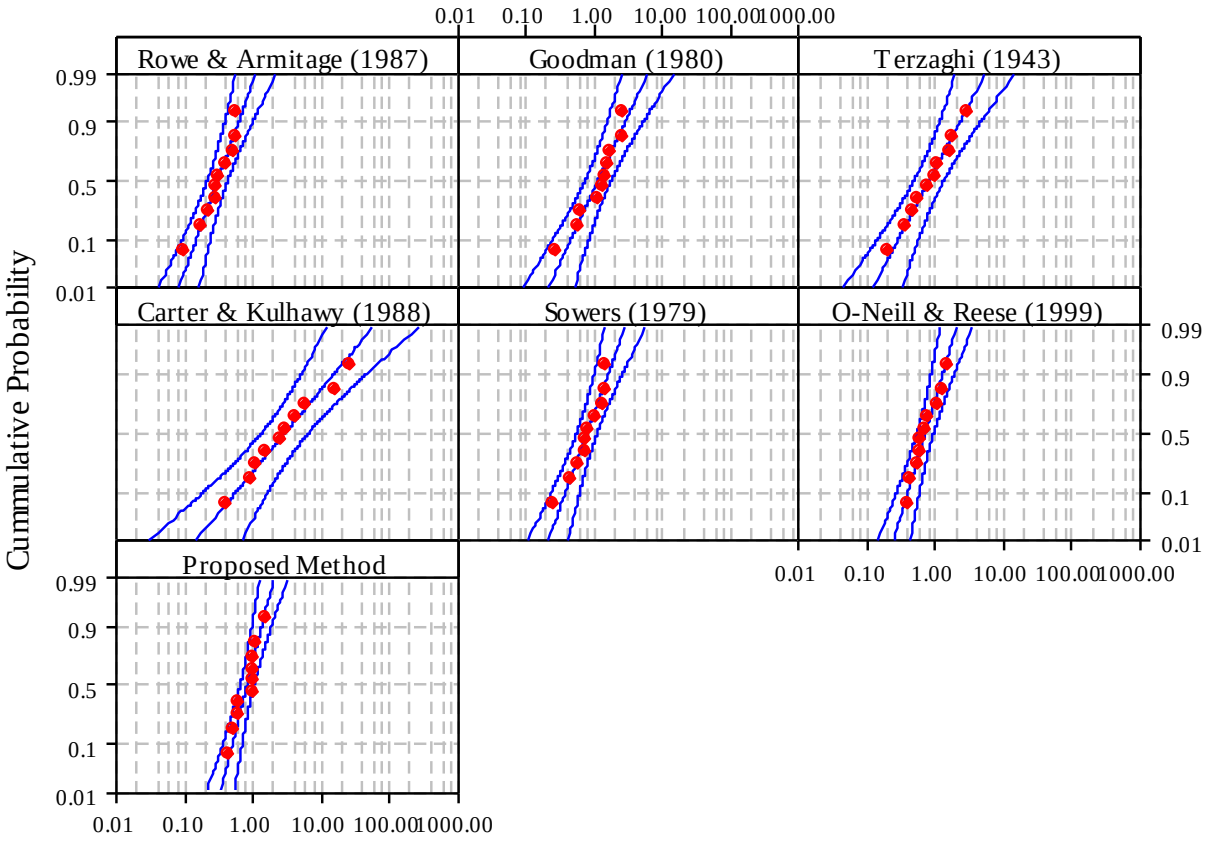

Analytical Method	Loc	Scale	N	AD	CV	Lognormal
Rowe & Armitage (1987)	-1.181	0.5608	10	0.313	0.578	Yes
Goodman (1980)	0.1158	0.7174	10	0.374	0.578	Yes
Terzaghi (1943)	-0.2626	0.8168	10	0.139	0.578	Yes
Carter & Kulhawy (1988)	1.083	1.286	10	0.151	0.578	Yes
Sowers (1979)	-0.2652	0.5608	10	0.313	0.578	Yes
O-Neill & Reese (1999)	-0.3901	0.4561	10	0.273	0.578	Yes
Proposed Method	-0.1784	0.382	10	0.493	0.578	Yes

Figure 4.58. Goodness of fit test for end bearing in rock corresponding to 1-in. top displacement for various analytical methods

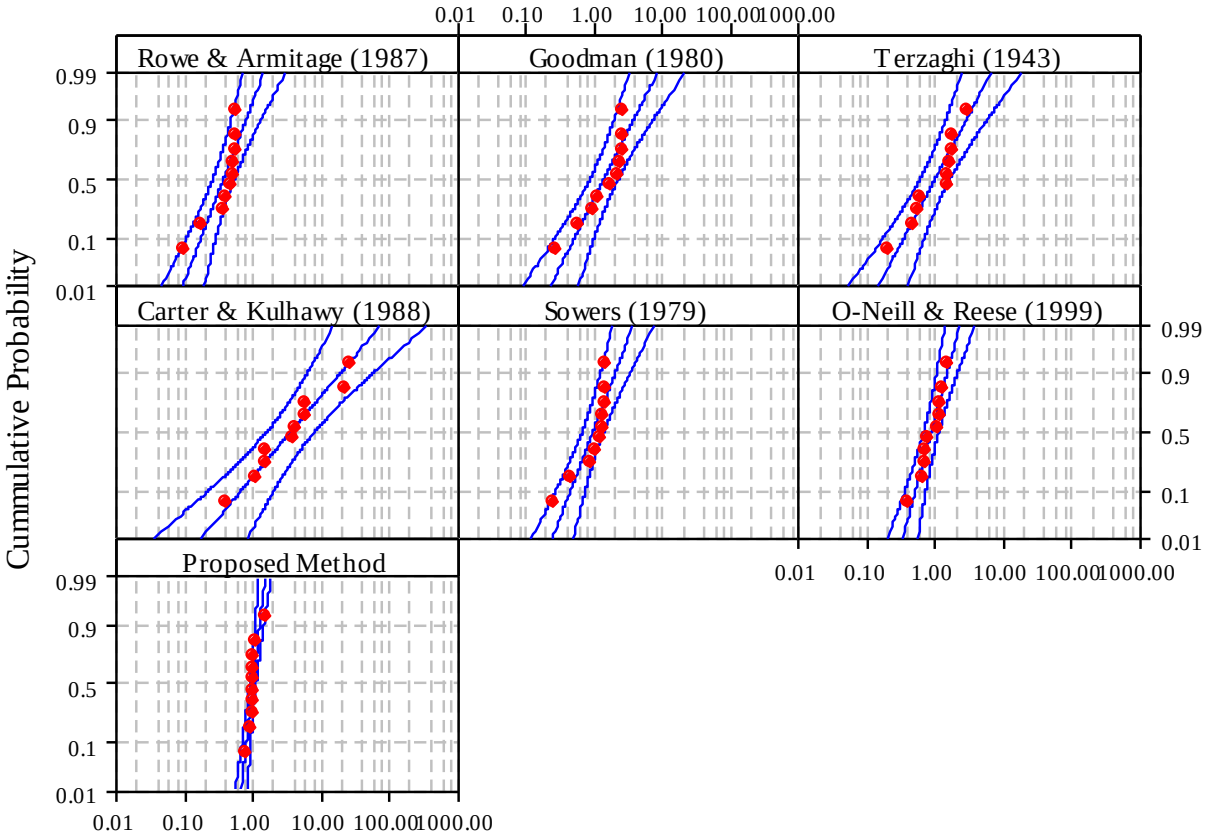

Analytical Method	Loc	Scale	N	AD	CV	Lognormal
Rowe & Armitage (1987)	-0.9804	0.59	10	1.183	0.578	No
Goodman (1980)	0.3169	0.773	10	0.662	0.578	No
Terzaghi (1943)	-0.06153	0.8205	10	0.542	0.578	Yes
Carter & Kulhawy (1988)	1.284	1.305	10	0.252	0.578	Yes
Sowers (1979)	-0.06413	0.59	10	1.183	0.578	No
O-Neill & Reese (1999)	-0.1891	0.4155	10	0.353	0.578	Yes
Proposed Method	0.02265	0.1715	10	1.074	0.578	No

Figure 4.59. Goodness of fit test for end bearing in rock corresponding to 5% of shaft diameter for top displacement for various analytical methods

The end bearing ratio is a ratio of measured to estimated end bearing. The “Loc” and “Scale” represent the mean and standard deviation of the natural logarithm of the datasets. The sample size is represented by “N”. Since the cumulative probability density function was plotted in a logarithmic scale, the assumed logarithmic distribution within the 95% confidence interval (CI) is confirmed when the AD value is smaller than the CV value. Due to the variability of the estimation of end bearing in rock, not all assumed lognormal distributions are confirmed except for the 1-in. displacement criterion. The results of the normality tests are summarized in the figures with “Yes” or “No” indicating whether confirming the lognormal distribution was confirmed.

Figure 4.60, Figure 4.61, and Figure 4.62 show the normal distribution of the end bearing ratio and the statistical characteristics (i.e., mean and standard deviation) necessary for the calibration of resistance factors.

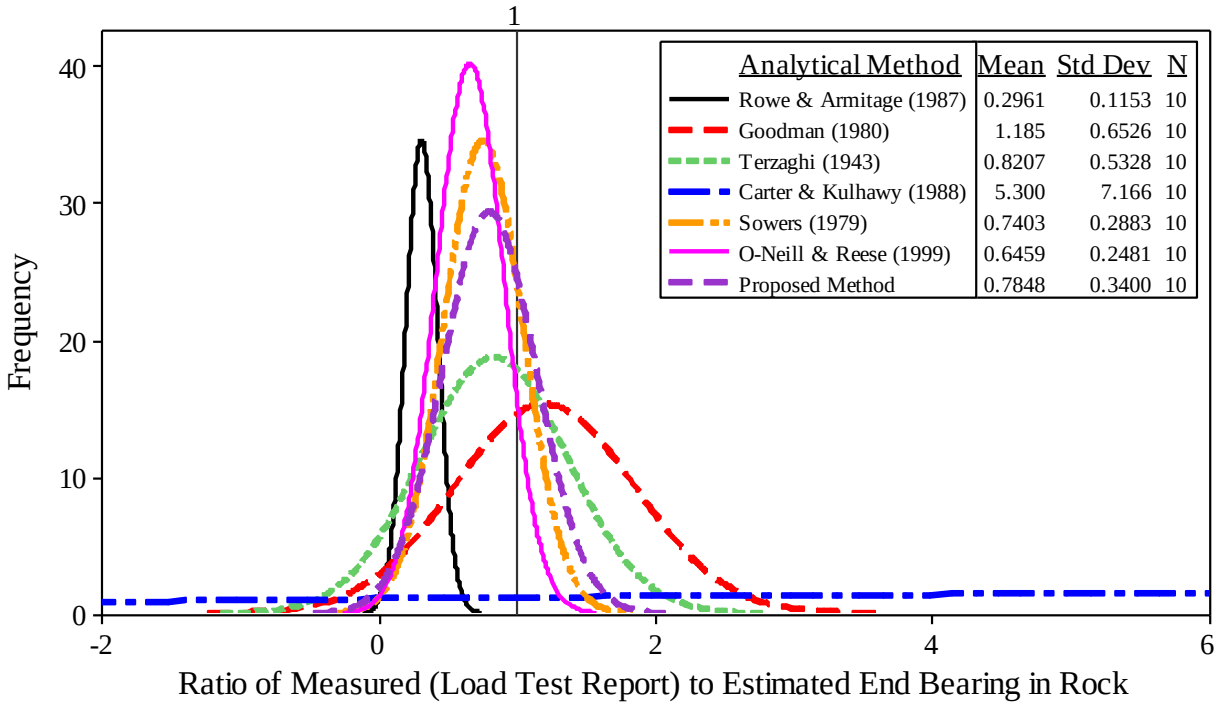

Figure 4.60. Summary of the normal distributed PDFs of the end bearing ratio in rock based on measured end bearing obtained directly from load test reports for various analytical methods

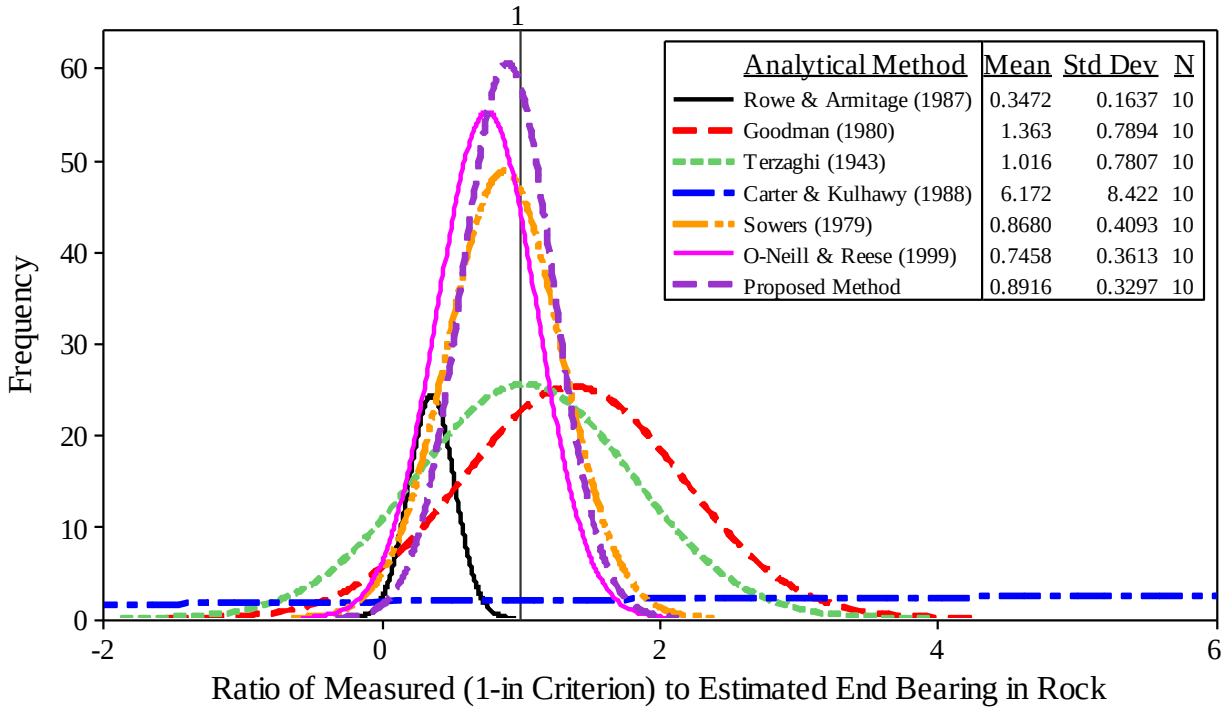

Figure 4.61. Summary of the normal distributed PDFs of the end bearing ratio in rock corresponding to 1-in. top displacement for various analytical methods

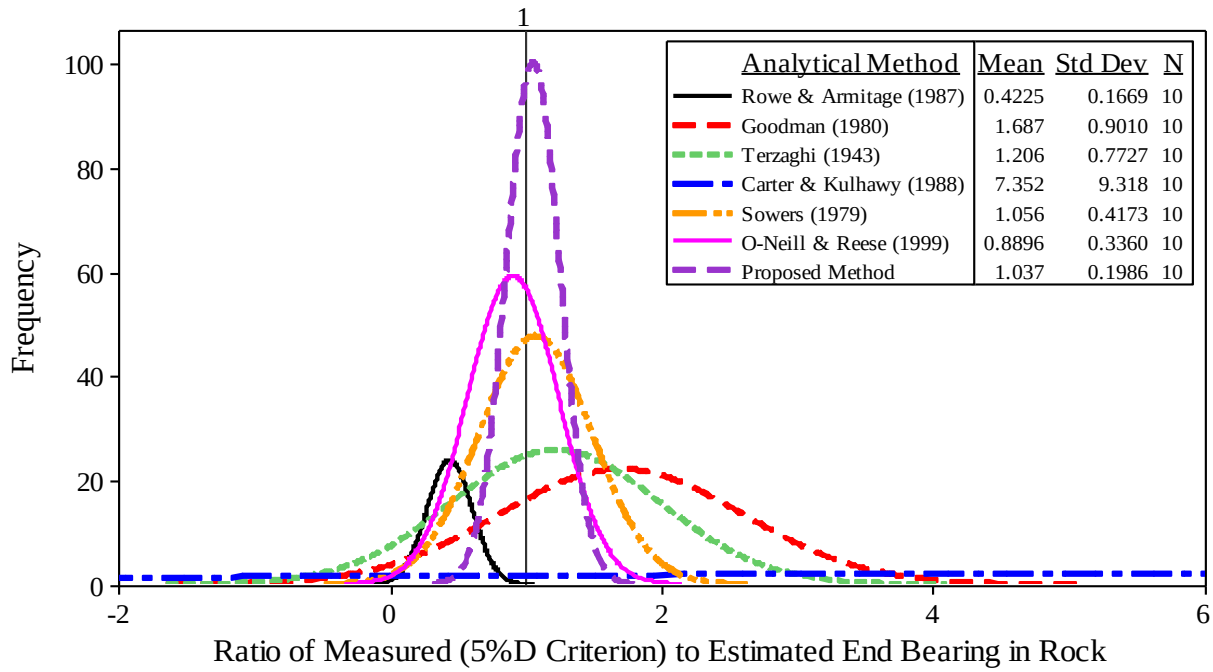

Figure 4.62. Summary of the normal distributed PDFs of the end bearing ratio in rock corresponding to 5% of shaft diameter for top displacement for various analytical methods

The distribution with a mean value larger than one indicates that the estimated end bearing is generally underestimated. Figure 4.60 shows that the analytical method by Terzaghi (1943) has

the mean of 0.821 closest to one while the method by Rowe and Armitage (1987) has the smallest standard deviation of 0.115. Figure 4.61 shows that the analytical method by Terzaghi (1943) has the mean of 1.016 closest to one while the method by Rowe and Armitage (1987) has the smallest standard deviation of 0.164. Figure 4.62 shows that the proposed method has the mean of 1.037 closest to one while the method by Rowe and Armitage (1987) has the smallest standard deviation of 0.167. The statistical characteristics indicate that the end bearing in rock can be reasonably estimated using the analytical methods by Terzaghi (1943), Sowers (1979), O'Neill and Reese (1999), and the proposed method. In contrast, analytical methods by Rowe and Armitage (1987), Goodman (1980), and Carter and Kulhawy (1988) should be cautiously used as they will provide inaccurate estimations of end bearing.

Following the LRFD framework, resistance factors were determined as a function of reliability index as shown in Figure 4.63, Figure 4.64, and Figure 4.65.

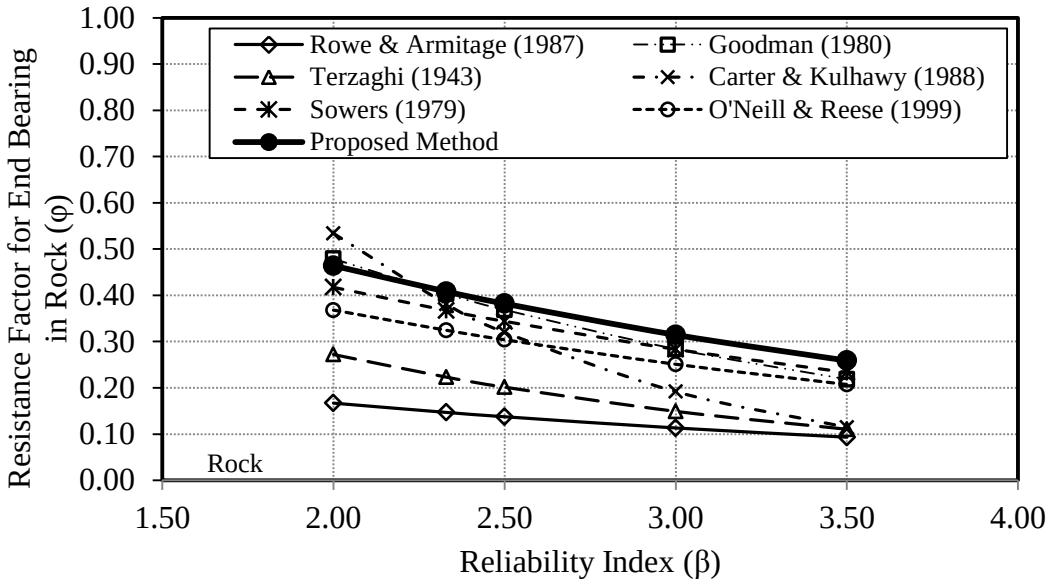

Figure 4.63. LRFD resistance factors for end bearing in rock based on measured end bearing obtained directly from load test reports

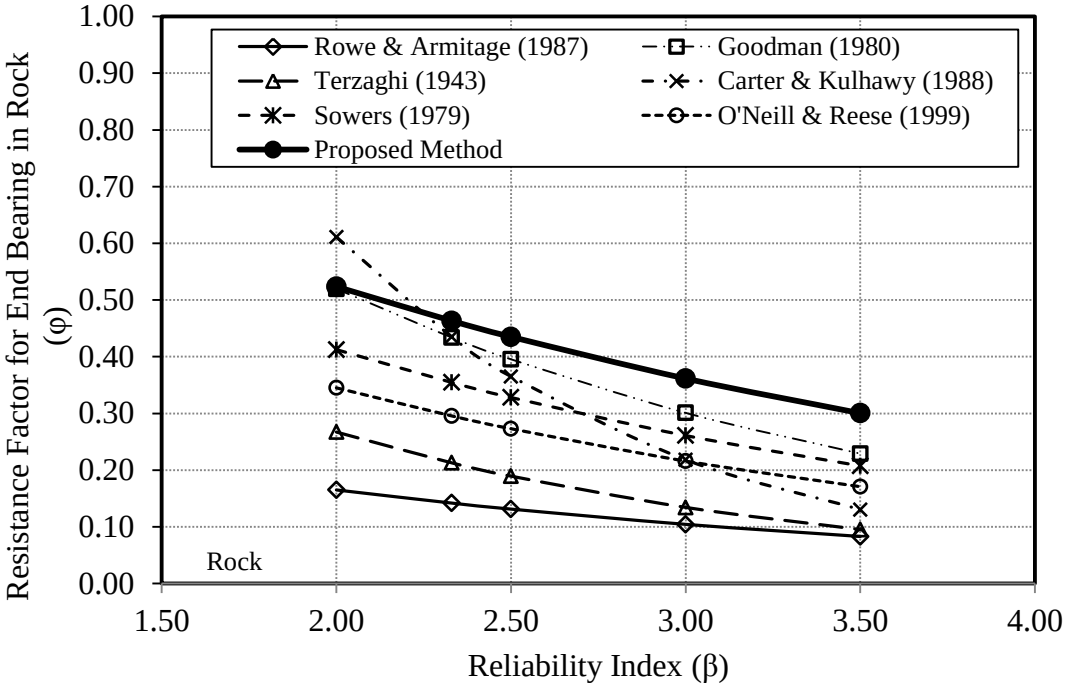

Figure 4.64. LRFD resistance factors for end bearing in rock corresponding to 1-in. top displacement criterion

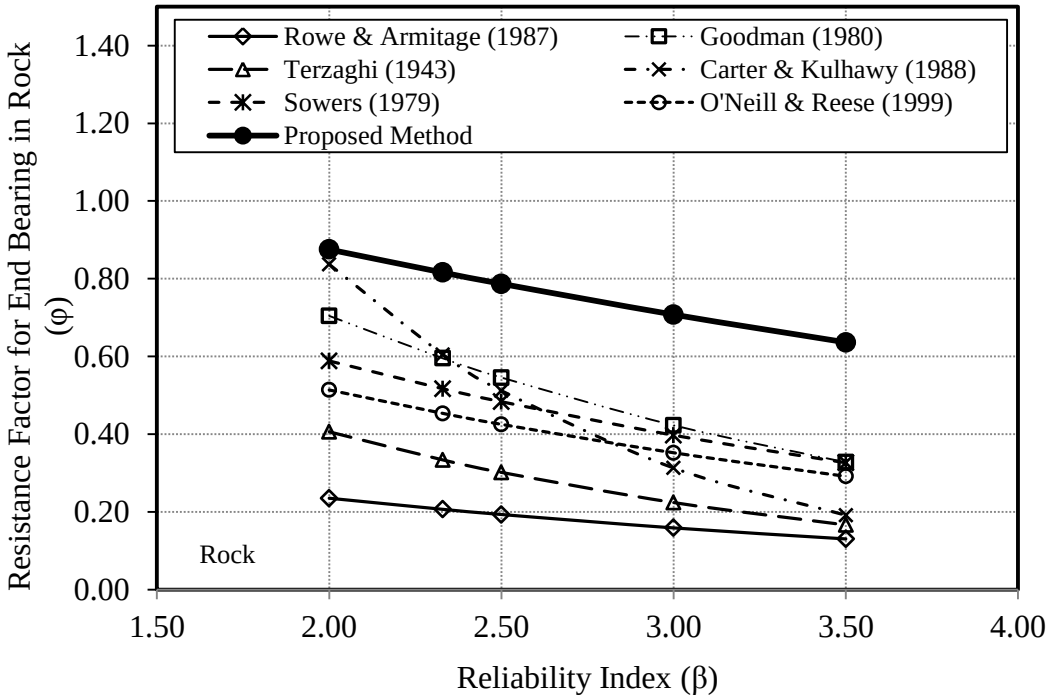

Figure 4.65. LRFD resistance factors for end bearing in rock corresponding to 5% of shaft diameter for top displacement criterion

All resistance factors are below one. The resistance factor decreases when a higher reliability level of the drilled shaft foundation system is desired. Figure 4.66, Figure 4.67, and Figure 4.68 show that the efficiency of the estimation decreases with increasing reliability index. Among the seven analytical methods, the proposed method with the highest efficiency factor provides the most efficient estimation of end bearing in rock.

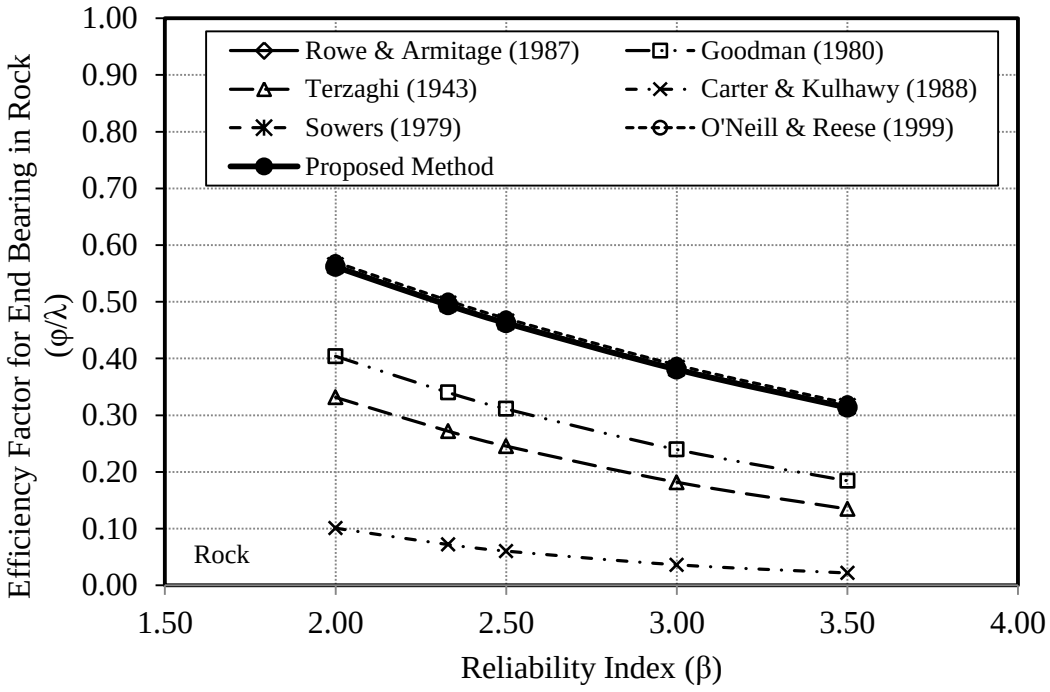

Figure 4.66. Efficiency factors for end bearing in rock based on measured end bearing obtained directly from load test reports

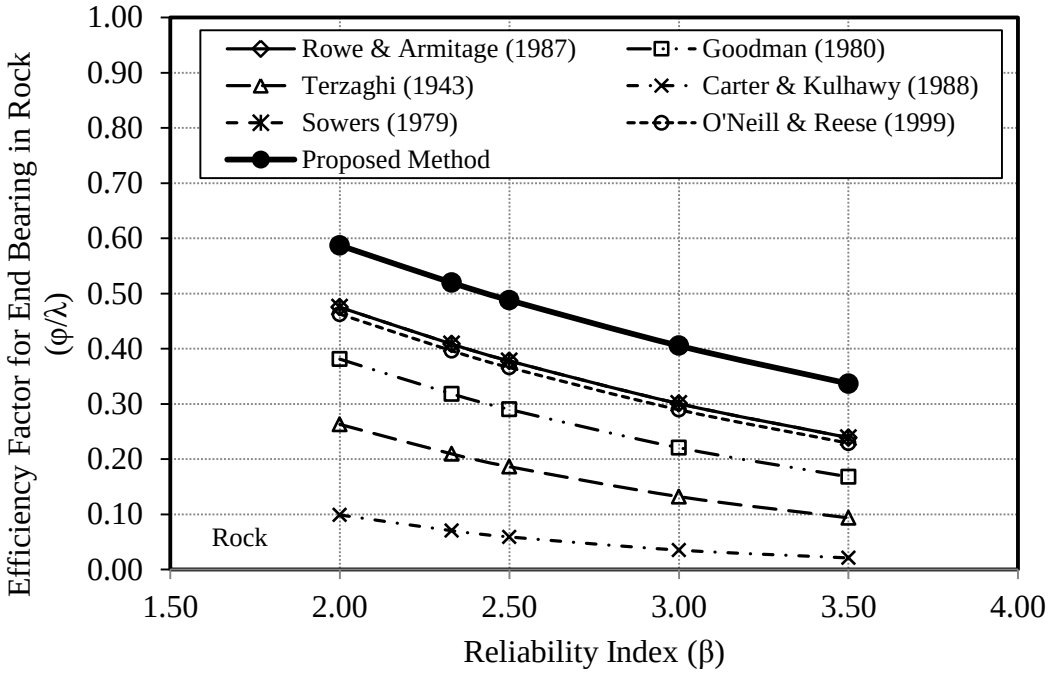

Figure 4.67. Efficiency factors for end bearing in rock corresponding to 1-in. top displacement criterion

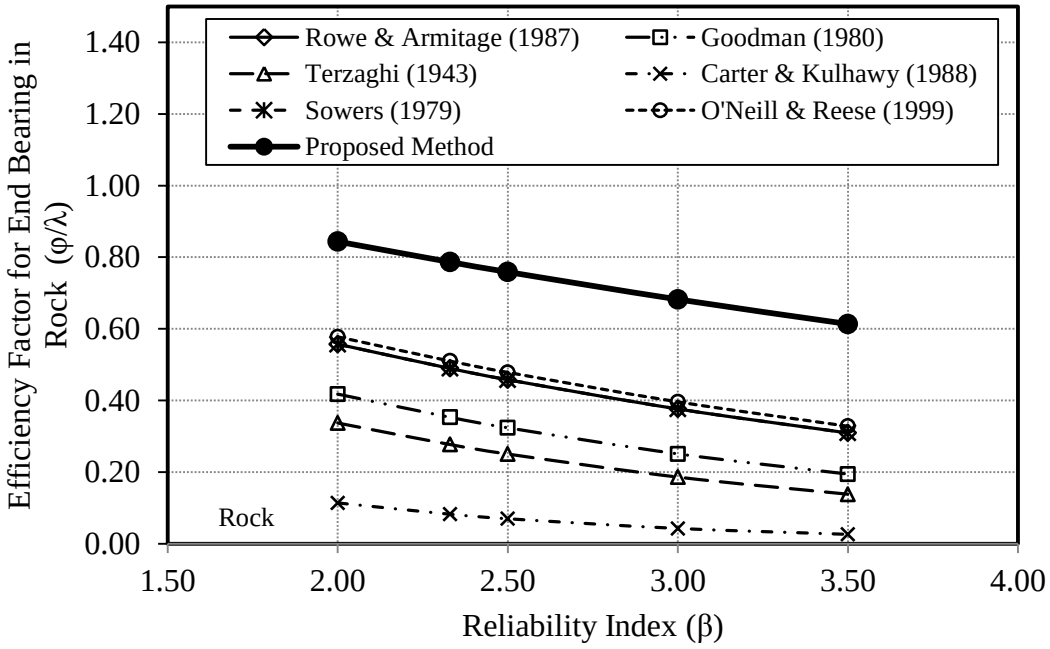

Figure 4.68. Efficiency factors for end bearing in rock corresponding to 5% of shaft diameter for top displacement criterion

4.4. Total Resistance

Total resistance is the summation of all side resistances along a drilled shaft and end bearing. The estimated total nominal resistances are summarized in Appendix C. The measured resistances are summarized in Table 3.7 with respect to the different failure defining criteria. ID No. 7 was neglected because a gap between the shaft base and the bearing rock was identified from the load test results. Hence, a total of 27 data points were used in this analysis. The comparisons of estimated and measured total resistances are shown in 1) Figure 4.69 for the measured resistance obtained directly from the load test report, 2) Figure 4.70 for the measured resistance defined based on the 1-in. top displacement criterion, and 3) Figure 4.71 for the measured resistance defined based on the 5% of shaft diameter for top displacement criterion. The comparisons show that the total resistances were slightly underestimated.

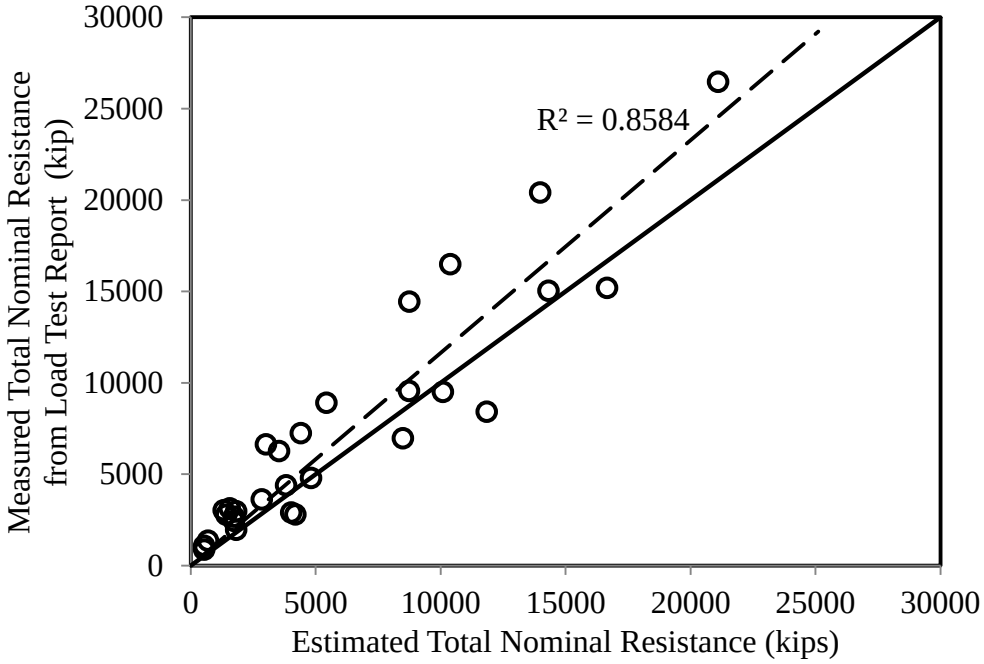

Figure 4.69. Comparison of measured total nominal resistance obtained directly from load test reports and estimated total nominal resistance

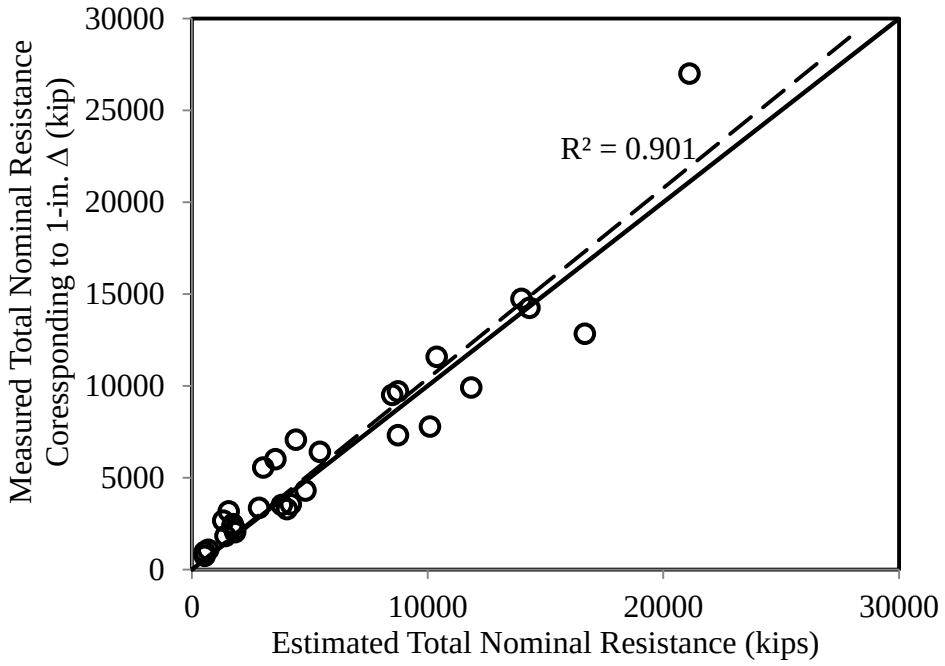

Figure 4.70. Comparison of measured total nominal resistance corresponding to 1-in. top displacement and estimated total nominal resistance

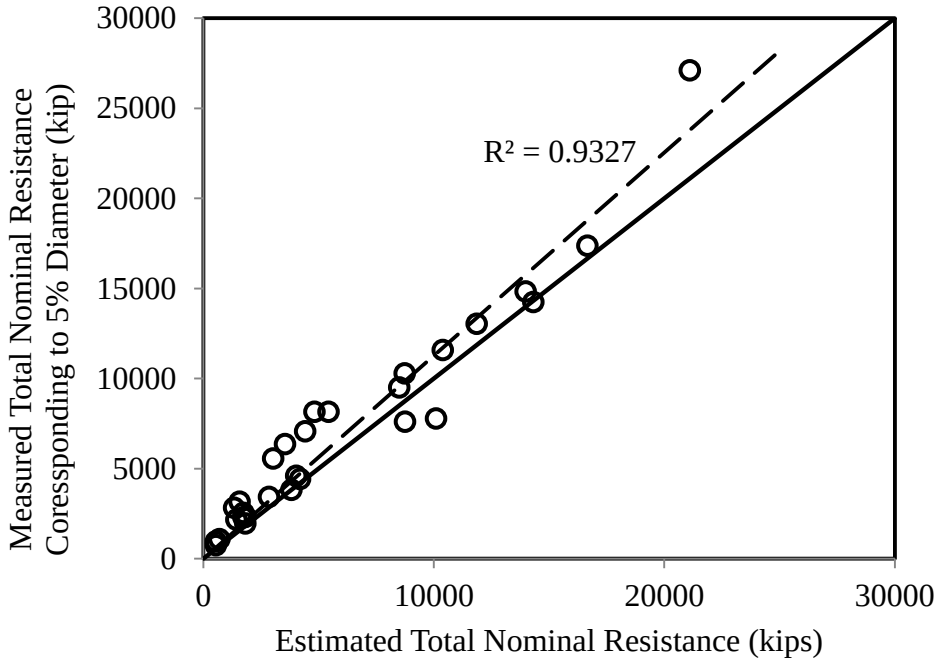

Figure 4.71. Comparison of measured total nominal resistance corresponding to 5% of shaft diameter for top displacement and estimated total nominal resistance

Figure 4.72 shows three Anderson-Darling (AD) (1952) normality tests of the total resistance ratio for three criteria.

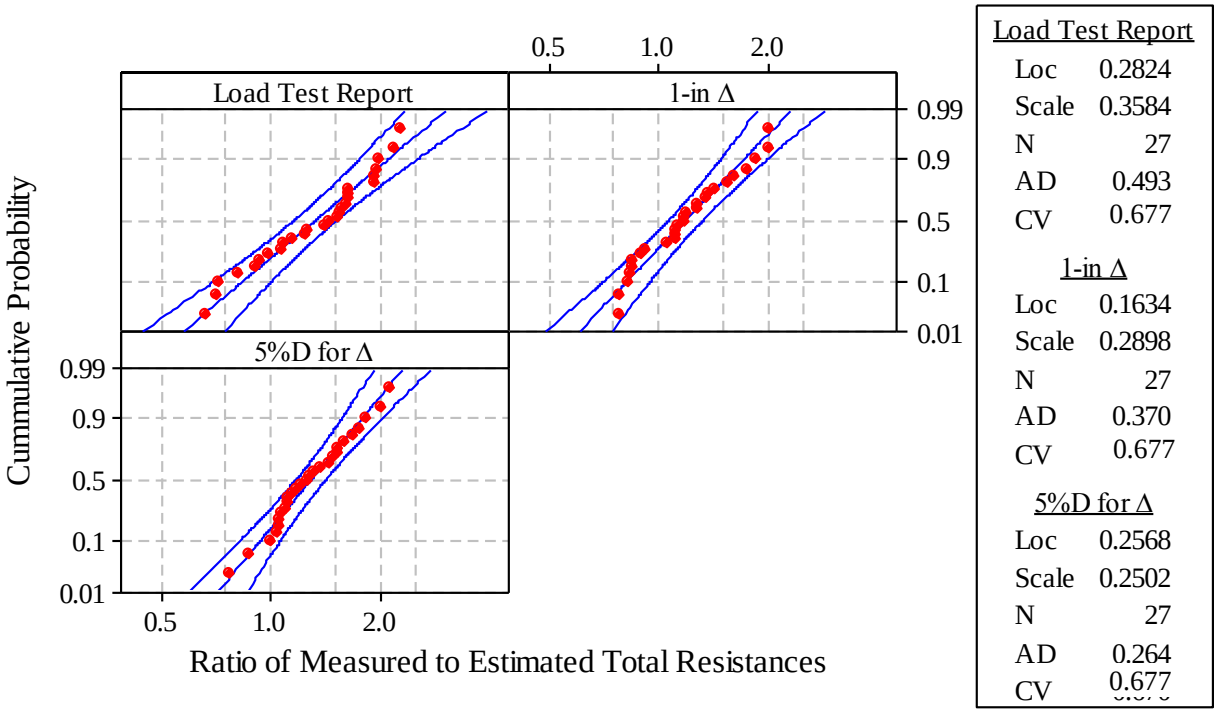

Figure 4.72. Goodness of fit test for total nominal resistance

The total resistance ratio is a ratio of measured to estimated total resistance. The "Loc" and "Scale" represent the mean and standard deviation of the natural logarithm of the datasets. The sample size is represented by "N", which is 27 datasets for all three criteria. Since the cumulative probability density function was plotted in a logarithmic scale, the assumed logarithmic distribution within the 95% confidence interval (CI) is confirmed when the AD value is smaller than the CV value.

Figure 4.73 shows the normal distribution of the resistance ratio and the statistical characteristics (i.e., mean and standard deviation) necessary for the calibration of resistance factors.

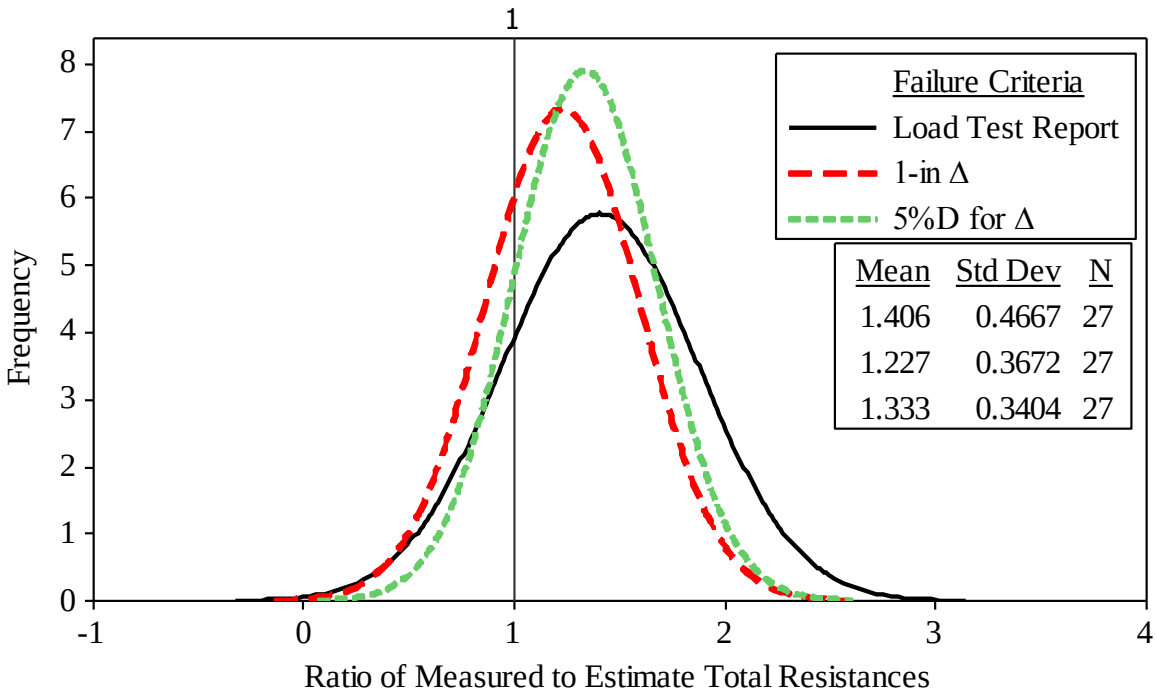

Figure 4.73. Summary of the normal distributed PDFs of total resistance ratio

The three distributions having the mean values larger than one indicate that the estimated total resistances are generally underestimated. Among the three criteria, the distribution for the measured resistance obtained from the load test report has the largest mean and standard deviation. The analysis shows that the estimated total resistance has a relatively better comparison with the measured values based on the 1-in. displacement and the 5% shaft diameter for displacement criteria. Following the LRFD framework, resistance factors were determined as a function of reliability index as shown in Figure 4.74. The resistance factor decreases when a higher reliability level of the drilled shaft foundation system is desired.

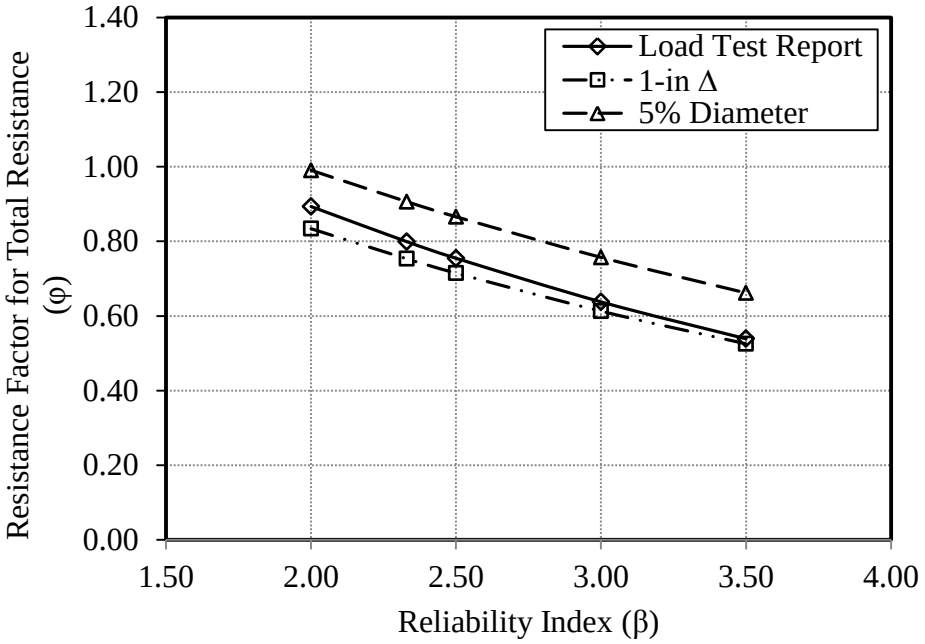

Figure 4.74. LRFD resistance factors for total resistance corresponding to a range of reliability indices

Similarly, Figure 4.75 shows that the efficiency of the estimation decreases with increasing reliability index. Among the three criteria, estimation of total resistance will have the highest efficiency when compared with the measured value based on the 5% of shaft diameter for displacement criterion.

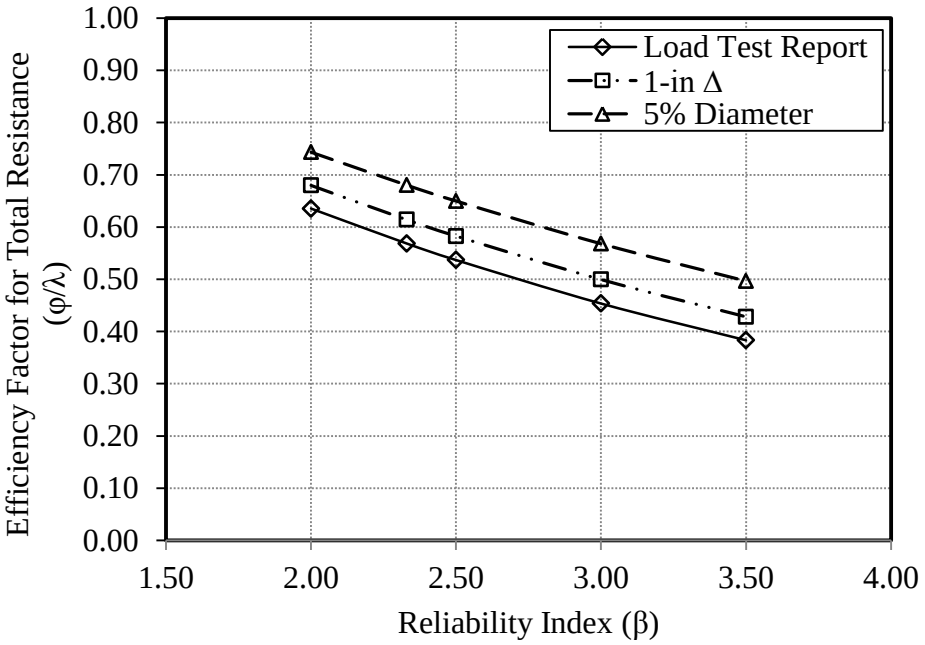

Figure 4.75. Efficiency factors for total resistance corresponding to a range of reliability indices

4.5. Summary and Recommendations

The calibrated resistance factors and the corresponding efficiency factors based on a target reliability index (β_T) of 3.00 are summarized in Table 4.1 for the total resistance component described in Section 4.4. The target reliability index (β_T) of 3.00 was chosen, because a typical drilled shaft cap has four or fewer shafts, which is considered as a nonredundant drilled shaft foundation. Three sets of calibrated values are provided for the three failure-defining criteria. The calibrated resistance factors are compared with the resistance factors recommended in the NCHRP Report 343 by Barker et al. (1991), NCHRP Report 507 by Paikowsky et al. (2004), FHWA-NHI Report 05-052 by Allen (2005), and the AASHTO LRFD Bridge Design Specifications (2010). Table 4.1 shows that the calibrated values are higher than those recommended in NCHRP 343, NHI 05-052, and AASHTO, and are within the range recommended in NCHRP 507.

Table 4.1. Comparison of resistance factors of total resistance

Failure Criteria	Resistance Factors for β_T = 3.00, φ						φ/λ
	NCHRP 343[(a)]	NCHRP 507[(b)]	NHI 05-052[(a)]	NHI 05-052[(c)]	AASHTO (2010)[(d)]	DSHAFT	DSHAFT
LTR	n/a	n/a	n/a	n/a	n/a	0.64	0.45
1-in. Δ	n/a	n/a	n/a	n/a	n/a	0.61	0.50
5% D for Δ[(e)]	0.58	0.30 to 0.75 (φ/λ: 0.36 to 0.63)	0.54	0.53	n/a	0.76	0.57

(a) – calibration by fitting to ASD; (b) – calibration performed using reliability theory (FORM); (c) – calibration performed using reliability theory (Monte Carlo Method); (d) – selected value among NCHRP 343, NCHRP 507 and Allen (2005); (e) – taking average of all resistance factors; LTR – load test report criterion; n/a – not available; Δ – shaft top displacement; D – shaft diameter.

Comparing the efficiency factors of the three criteria, total resistance based on the 5% of shaft diameter for top displacement criterion has the highest efficiency. The results demonstrate that regional LRFD calibration using DSHAFT increases the factored total resistance (φR).

Similarly, resistance and efficiency factors presented in Table 4.2 for side resistances were calibrated based on the target reliability index (β_T) of 3.00.

Table 4.2. Comparison of resistance factors of side resistance

Geo material	Failure Criteria	Resistance Factors for β_T = 3.00, φ					φ/λ	
		NCHRP 343[e]	NCHRP 507[b]	NHI 05-052[a]	NHI 05-052[c]	AASHTO (2010)[d]	DSHAFT	DSHAFT
Clay	LTR	n/a	n/a	n/a	n/a	n/a	0.31	0.15
	1-in. Δ	n/a	n/a	n/a	n/a	n/a	0.20	0.11
	5% D for Δ	0.65	0.36 (φ/λ: 0.41)	0.55	0.60	0.45	0.22	0.12
Sand	LTR	n/a	n/a	n/a	n/a	n/a	0.47	0.34
	1-in. Δ	n/a	n/a	n/a	n/a	n/a	0.48	0.54
	5% D for Δ	n/a	0.31 (φ/λ: 0.28)	0.55	n/a	0.55	0.47	0.53
IGM	LTR	n/a	n/a	n/a	n/a	n/a	0.66	0.26
	1-in. Δ	n/a	n/a	n/a	n/a	n/a	0.63	0.30
	5% D for Δ	n/a	0.51 (φ/λ: 0.41)	0.55	n/a	0.60	0.69	0.32
Rock	LTR	n/a	n/a	n/a	n/a	n/a	0.57	0.39
	1-in. Δ	n/a	n/a	n/a	n/a	n/a	0.55	0.49
	5% D for Δ	0.65	0.38[f] (φ/λ: 0.32)	0.55	0.55	0.55	0.62	0.53

[a] – calibration by fitting to ASD; [b] – calibration performed using reliability theory (FORM); [c] – calibration performed using reliability theory (Monte Carlo Method); [d] – selected value among NCHRP 343, NCHRP 507 and Allen (2005); [e] – recommended value; [f] – based on Carter and Kulhawy (1988); LTR – load test report criterion; n/a – not available; Δ – shaft top displacement; D – shaft diameter.

For each geomaterial along a shaft, three sets of calibrated values are provided for the three failure defining criteria. The calibrated resistance factors are compared with the resistance factors recommended in NCHRP Report 343 by Barker et al. (1991), NCHRP Report 507 by Paikowsky et al. (2004), FHWA-NHI Report 05-052 by Allen (2005), and the AASHTO LRFD Bridge Design Specifications (2010). Table 4.2 shows that the calibrated values for clay are lower than that recommended in NCHRP 343, NCHRP 507, NHI 05-052 and AASHTO. For the case in sand, the calibrated values are higher than that recommended in NCHRP 507 and lower than those recommended in the NCHRP 343, NHI 05-052 and AASHTO. For the case in IGM, the calibrated resistance factors are higher than those recommended in the NCHRP 343, NCHRP 507, NHI 05-052, and AASHTO, while the efficiency factors are lower than the 0.41 determined in tNCHRP 507. For the case in rock, the calibrated values are higher than the recommendations. Among the three different criteria, the criterion with the highest efficiency factor will provide the most design efficiency. The results demonstrate that regional LRFD calibration using DSHAFT increases the factored side resistances (φR_s) in IGM and rock.

Table 4.3 shows the calibrated resistance and efficiency factors for end bearing in sand while no values were calibrated for clay since only one data point was available.

Table 4.3. Comparison of resistance factors of end bearing in clay and sand

Geo material	Failure Criteria	Resistance Factors for β_T = 3.00, φ					φ/λ	
		NCHRP 343[e]	NCHRP 507[b]	NHI 05-052[a]	NHI 05-052[c]	AASHTO (2010)[d]	DSHAFT	DSHAFT
Clay	LTR	n/a	n/a	n/a	n/a	n/a	n/a	n/a
	1-in. Δ	n/a	n/a	n/a	n/a	n/a	n/a	n/a
	5% D for Δ	0.55	0.24 to 0.28 (φ/λ: 0.29 to 0.31)	0.50	0.60	0.40	n/a	n/a
Sand	LTR	n/a	n/a	n/a	n/a	n/a	0.57	0.42
	1-in. Δ	n/a	n/a	n/a	n/a	n/a	0.76	0.51
	5% D for Δ	n/a	0.25 to 0.73 (φ/λ: 0.15 to 0.32)	0.55	n/a	0.50	0.75	0.44

[a] – calibration by fitting to ASD; [b] – calibration performed using reliability theory (FORM); [c] – calibration performed using reliability theory (Monte Carlo Method); [d] – selected value among NCHRP 343, NCHRP 507 and Allen (2005); [e] – recommended value; LTR – load test report criterion; n/a – not available; Δ – shaft top displacement; D – shaft diameter.

Three sets of calibrated values are provided for the three failure defining criteria. The calibrated resistance factors are compared with the resistance factors recommended in NCHRP Report 343 by Barker et al. (1991), NCHRP Report 507 by Paikowsky et al. (2004), FHWA-NHI Report 05-052 by Allen (2005), and the AASHTO LRFD Bridge Design Specifications (2010). Table 4.3 shows that the calibrated resistance factors for sand are higher than those recommended in NCHRP 507, NHI 05-052, and AASHTO. Additionally, the calibrated efficiency factors are higher than those recommended in the NCHRP 507. The results demonstrate that regional LRFD calibration using DSHAFT increases the factored end bearing (φR_p) in sand.

Table 4.4 shows the calibrated resistance and efficiency factors for end bearing in IGM.

Table 4.4. Comparison of resistance factors of end bearing in IGM

Failure Criteria	Analytical Method	Resistance Factors for β_T = 3.00, φ			φ/λ	
		NCHRP 507[(a)]	NHI 05-052[(b)]	AASHTO (2010)[(c)]	DSHAFT	DSHAFT
LTR	Rowe & Armitage (1987)	n/a	n/a	n/a	0.32	0.29
	Goodman (1980)	n/a	n/a	n/a	1.27	0.28
	Terzaghi (1943)	n/a	n/a	n/a	0.29	0.26
	Carter & Kulhawy (1988)	n/a	n/a	n/a	1.46	0.17
	Sowers (1979)	n/a	n/a	n/a	0.67	0.24
	O'Neill & Reese (1999)	n/a	n/a	n/a	0.15	0.18
	Proposed Method	n/a	n/a	n/a	0.59	0.47
1-in. Δ	Rowe & Armitage (1987)	n/a	n/a	n/a	0.32	0.33
	Goodman (1980)	n/a	n/a	n/a	1.41	0.35
	Terzaghi (1943)	n/a	n/a	n/a	0.24	0.23
	Carter & Kulhawy (1988)	n/a	n/a	n/a	1.71	0.22
	Sowers (1979)	n/a	n/a	n/a	0.64	0.27
	O'Neill & Reese (1999)	n/a	n/a	n/a	0.17	0.22
	Proposed Method	n/a	n/a	n/a	0.64	0.58
5% D for Δ	Rowe & Armitage (1987)	n/a	n/a	n/a	0.44	0.36
	Goodman (1980)	n/a	n/a	n/a	1.86	0.36
	Terzaghi (1943)	n/a	n/a	n/a	0.49	0.39
	Carter & Kulhawy (1988)	n/a	n/a	n/a	3.04	0.30
	Sowers (1979)	n/a	n/a	n/a	1.06	0.33
	O'Neill & Reese (1999)	0.57 to 0.65 (φ/λ: 0.44 to 0.48)	0.55	0.55	0.20	0.21
	Proposed Method	n/a	n/a	n/a	0.85	0.62

[(a)] – calibration performed using reliability theory (FORM); [(b)] – calibration by fitting to ASD; [(c)] – selected value among NCHRP 343, NCHRP 507 and Allen (2005); LTR – load test report criterion; n/a – not available; Δ - shaft top displacement; D – shaft diameter.

Three sets of calibrated values are provided for the three failure defining criteria. For each criterion, calibrated values were determined for seven analytical methods. The calibrated resistance factors are compared with the resistance factors recommended in NCHRP Report 507 by Paikowsky et al. (2004), FHWA-NHI Report 05-052 by Allen (2005), and the AASHTO LRFD Bridge Design Specifications (2010). As described in Section 4.3.3, analytical methods by Goodman (1980), Carter and Kulhawy (1988), and Sowers (1979) are not recommended. In addition, Table 4.4 shows that unrealistically high resistance factors were calibrated for these methods.

Among the recommended methods (i.e., Rowe and Armitage (1987), Terzaghi (1943), O'Neill and Reese (1999), and the proposed method), the proposed method has the highest efficiency factor in all three criteria. Table 4.4 shows that the calibrated values based on the proposed method are higher than those recommended in NCHRP 507, NHI 05-052, and AASHTO. Using

the proposed method, the results demonstrated that regional LRFD calibration using DSHAFT increases the factored end bearing (φR_p) in IGM.

Table 4.5 shows the calibrated resistance and efficiency factors for end bearing in rock.

Table 4.5. Comparison of resistance factors of end bearing in rock

Failure Criteria	Analytical Method	Resistance Factors for β_T = 3.00, φ				φ/λ
		NCHRP 507[(a)]	NHI 05-052[(b)]	AASHTO (2010)[(c)]	DSHAFT	DSHAFT
LTR	Rowe & Armitage (1987)	n/a	n/a	n/a	0.11	0.38
	Goodman (1980)	n/a	n/a	n/a	0.28	0.24
	Terzaghi (1943)	n/a	n/a	n/a	0.15	0.18
	Carter & Kulhawy (1988)	n/a	n/a	n/a	0.19	0.04
	Sowers (1979)	n/a	n/a	n/a	0.28	0.38
	O'Neill & Reese (1999)	n/a	n/a	n/a	0.25	0.39
	Proposed Method	n/a	n/a	n/a	0.11	0.18
1-in. Δ	Rowe & Armitage (1987)	n/a	n/a	n/a	0.10	0.30
	Goodman (1980)	n/a	n/a	n/a	0.30	0.22
	Terzaghi (1943)	n/a	n/a	n/a	0.13	0.13
	Carter & Kulhawy (1988)	n/a	n/a	n/a	0.22	0.04
	Sowers (1979)	n/a	n/a	n/a	0.26	0.30
	O'Neill & Reese (1999)	n/a	n/a	n/a	0.22	0.29
	Proposed Method	n/a	n/a	n/a	0.36	0.41
5% D for Δ	Rowe & Armitage (1987)	n/a			0.16	0.38
	Goodman (1980)	n/a			0.42	0.25
	Terzaghi (1943)	n/a			0.22	0.19
	Carter & Kulhawy (1988)	0.45 to 0.49 (φ/λ: 0.37 to 0.38)	0.55[(d)]	0.50[(d)]	0.31	0.04
	Sowers (1979)	n/a			0.40	0.38
	O'Neill & Reese (1999)	n/a			0.35	0.40
	Proposed Method	n/a			0.71	0.68

[(a)] – calibration performed using reliability theory (FORM); [(b)] – calibration by fitting to ASD; [(c)] – selected value among NCHRP 343, NCHRP 507 and Allen (2005); [(d)] – based on Canadian Geotechnical Society (1985); LTR – load test report criterion; n/a – not available; Δ - shaft top displacement; D – shaft diameter.

Three sets of calibrated values are provided for the three failure defining criteria. For each criterion, calibrated values were determined for seven analytical methods. The calibrated resistance factors are compared with the resistance factors recommended in NCHRP Report 507 by Paikowsky et al. (2004), FHWA-NHI Report 05-052 by Allen (2005), and the AASHTO LRFD Bridge Design Specifications (2010). As described in Section 4.3.4, analytical methods by Rowe and Armitage (1987), Goodman (1980) and Carter, and Kulhawy (1988) are not recommended. Among the recommended methods (i.e., Terzaghi (1943), Sowers (1979), O'Neill and Reese (1999), and the proposed method), the method by O'Neill and Reese (1999) has the highest efficiency factor in the load test report criterion while the proposed method has the

highest efficiency factor in the 1-in. and the 5% diameter criteria. Table 4.4 shows that the calibrated values based on the proposed method are higher than those recommended in NCHRP 507, NHI 05-052, and AASHTO. Using the proposed method and the 5% diameter criterion, the results demonstrate that regional LRFD calibration using DSHAFT increases the factored end bearing (φR_p) in rock.

Table 4.6 summarizes the statistical parameters and calibrated values based on drilled shafts constructed in Iowa only (i.e., 11 data points with IDs 2 to 6, 8 to 11, 26, and 27).

Table 4.6. Summary of statistical parameters and calibrated values based on 1-in. top displacement criterion considering only drilled shafts constructed in Iowa

Resistance Component	Geo Material	DSHAFT			Resistance Factors for β_T = 3.00, φ		φ/λ
		N	Mean	COV	AASHTO	DSHAFT	DSHAFT
Total Resistance	All	11	1.181	0.157	n/a	0.89	0.75
Side Resistance	Clay	9	1.706	0.948	0.45	0.14	0.09
	Sand	8	0.903	0.278	0.55	0.48	0.53
	IGM	2	1.486	0.400	0.60	0.55	0.37
	Rock	5	1.126	0.415	0.50	0.40	0.36
End Bearing	Clay	1	n/a	n/a	0.40	n/a	n/a
	Sand	5	1.641	0.194	0.50	1.11	0.68
	IGM	1	n/a	n/a	0.55	n/a	n/a
	Rock	4	0.931	0.213	0.50[(a)]	0.60	0.64

[(a)] – based on the analytical method proposed in the Canadian Geotechnical Society (1985); n/a – not available; N – sample size; COV – coefficient of variation.

Of the 11 shafts, nine shafts have clay layers, eight shafts have sand layers, two shafts have IGM layers, and five shafts have rock layers along the shafts. One shaft was bearing in clay, five shafts in sand, one shaft in IGM, and four shafts in rock. An unrealistically high resistance factor of 1.11 was determined for end bearing in sand, because the analytical method for sand consistently underestimated the end bearing, substantiated with a mean value of 1.1641 larger than one. A relatively low resistance factor of 0.14 and efficiency factor of 0.09 were determined for side resistance in clay, because the α-method underestimated the side resistance (i.e., mean value of 1.706) and generated high variability in the estimations (i.e., COV of 0.948). Compared with the resistance factors recommended in the AASHTO (2010), the local LRFD calibrations using solely the tests in Iowa generally do not increase the resistance factors and improve the design efficiency of the drilled shaft foundations.

Assessing the calibrated resistance factors summarized in Table 4.1 through Table 4.5 as well as the AASHTO recommendations, resistance factors for various resistance components and geomaterials based on the 1-in. top displacement criterion are recommended in Table 4.7.

Table 4.7. Recommended Resistance Factors based on 1-in. top displacement criterion

Resistance Component	Geo Material	Analytical Method	Resistance Factors for β_T = 3.00, φ[(f)]
Total Resistance	All	A combination of methods depending on the subsurface profile	0.60
Side Resistance	Clay	α-method by O'Neill and Reese (1999): Section 2.3.2	0.45[(a)]
	Sand	β-method by Burland (1973) and O'Neill and Reese (1999): Section 2.3.3	0.55[(a)]
	IGM	Eq. (2-11) for cohesive IGM and Eq. (2-14) for cohesionless IGM by O'Neill and Reese (1999): Section 2.3.4	0.60
	Rock	Eq. (2-16) by Horvath and Kenney (1979): Section 2.3.5	0.55
End Bearing	Clay	Total Stress method by O'Neill and Reese (1999): Section 2.4.2	0.40[(a)]
	Sand	Effective stress method by Reese and O'Neill (1989): Section 2.4.3	0.50[(b)]
	IGM	Proposed method described in Section 2.4.5 and Table 3.4 for cohesive IGM and Eq. (2-22) for cohesionless IGM by O'Neill and Reese (1999): Section 2.4.4	0.55[(d)]
	Rock	Proposed method described in Section 2.4.5 and Table 3.4	0.35[(c)]
All	All	Static Load Test	0.70[(e)]

[(a)] – adopted from AASHTO (2010) corresponding to 5% of diameter for top displacement criterion; [(b)] – reduce from 0.76 to 0.50 so that the resistance factor of the end bearing component is smaller than that of the side resistance component; [(c)] – resistance factor of 0.50 can be used if pressuremeter method following the Canadian Geotechnical Society (1985) is used as the analytical method; [(d)] - reduce from 0.64 to 0.50 so that the resistance factor of the end bearing component is smaller than that of the side resistance component; [(e)] – maximum resistance factor recommended in AASHTO was adopted; [(f)] – if a single drilled shaft is used to support a bridge pier, the resistance factors should be reduced by 20%.

The 1-in. criterion is chosen to account for the contribution of end bearing in the strength limit state design as described in Section 2.7.1 and the Iowa DOT LRFD Bridge Design Manual (2011). The recommended resistance factors were rounded to the nearest 0.05. Some of the resistance factors were adjusted to maintain consistency and resolve any anomalies observed among the factors. The rational decision of each adjustment is briefly noted under Table 4.7 while they are explicitly described below with respect to the superscripted notes:

1) Note 'a': The calibrated resistance factor of side resistance in clay is 0.20 (see Table 4.2), which is smaller than 0.45 recommended in AASHTO. To maintain efficiency of drilled shaft foundations in clay, AASHTO's resistance factor of 0.45 is recommended. Similar adjustment was applied to the resistance factor of side resistance in sand, in which AASHTO's recommended resistance factor of 0.55 was selected over the calibrated value of 0.48 given in Table 4.2. The resistance factor 0.40 for end bearing in clay

recommended in AASHTO was adopted since data in DSHAFT are not sufficient for the regional calibration.

2) Note 'b': The resistance factor of end bearing in sand was reduced from the calibrated value of 0.76 to 0.50, so that a slightly lower resistance factor for end bearing than side resistance (i.e., 0.55) is applied to be consistent with the philosophy of having more uncertainties in end bearing than in side resistance estimation (Allen 2005).
3) Note 'c': The calibrated resistance factor of 0.35 is recommended for end bearing in rock. However, the AASHTO recommended value of 0.50 can be used if the pressuremeter method following the Canadian Geotechnical Society (1985) is used as the analytical method. A higher resistance factor could possibly be used since a higher resistance factor of 0.60 was determined based solely on the drilled shafts constructed in Iowa (see Table 4.6).
4) Note 'd': Similar to note 'b', the calibrated resistance factor of end bearing in IGM was reduced from 0.64 to 0.50, so that the resistance factor of the end bearing component is smaller than that of the side resistance component.
5) Note 'e': The maximum resistance factor of 0.70 suggested in AASHTO was adopted for drilled shaft designs when static load tests are conducted.
6) Note 'f': Adopting the rationale suggested in AASHTO, if a single drilled shaft is used to support a bridge pier, the resistance factors should be reduced by 20%.

It is important to recognize that the recommended resistance factors should be applied in accordance with the resistance components, geomaterials, analytical methods, and the redundancy of the drilled shaft foundation.

CHAPTER 5. DESIGN COMPARISON

5.1. Introduction

Using the LRFD recommendations developed in Chapter 4, design comparisons between drilled shafts and driven steel H-piles are evaluated to illustrate the potential and successful use of drilled shafts in Iowa. Through two case studies, the design procedures of drilled shaft foundations are demonstrated and the advantages of drilled shafts are addressed. The design comparisons focus on axial compressive resistance while the lateral resistance and group effects are not considered.

5.2. Case Study No. 1

Case study No.1 is to design a foundation system supporting a frame pier of a 208 ft, three-span, prestressed concrete beam superstructure with zero skew. The bottom of the pier elevation is at 435 ft and no scour is considered. The soil boring with the SPT blow counts at the pier location is given in Figure 5.1. Below the bottom of footing elevation, subsurface conditions generally consist of about 8 ft of fine sand, underlain by about 10 ft of coarse sand, 22 ft of gravelly sand, and deeper granular material. The test boring was terminated at a depth of 70 ft below the existing ground surface, and no ground water was reported to have been encountered at the test boring. The total factored axial compressive load of a bridge pier exerting on the foundation is 2,200 kips. Based upon the design information, the design procedures of driven steel H-pile foundations following the recently established LRFD design guide (Green et al. 2012) and drilled shaft foundations following the aforementioned LRFD recommendations are demonstrated and the design outcomes are compared.

Driven steel H-piles

Assuming that HP 10×57 steel piles are selected, the factored structural resistance (P_u) per pile is 146 kips recommended in the Iowa DOT LRFD BDM to limit pile settlement. The required number of piles is

$$n = \frac{2200}{146} = 15.1 \text{ piles} \cong 16 \text{ piles}$$

Hence, the factored axial load supported by each pile is 137.5 kips. Since only cohesionless soils are present, the soil is expected to fit the sand classification, and the resistance factor for sand using the Iowa Blue Book method as the design approach is 0.55. The required nominal resistance (R_n) per pile is

$$R_n = \frac{137.5}{0.55} = 250 \text{ kips/pile}$$

Based on the unit nominal side resistance and unit end bearing obtained from the Iowa Blue Book as shown in Figure 5.1, the required embedded pile length and the cumulative resistance (R) are

D1 = 8 ft, $R_1 = 2.8 \times 8 = 22.4$ kips
D2 = 10 ft, $R_{1\text{-}2} = 4.0 \times 10 + 22.4 = 62.4$ kips
D3 = 22 ft, $R_{1\text{-}3} = 4.0 \times 22 + 62.4 = 150.4$ kips
D4 = 8.1 ft, $R_{1\text{-}4} = 4.0 \times 8.1 + 4 \times 16.8 + 150.4 = 250$ kips

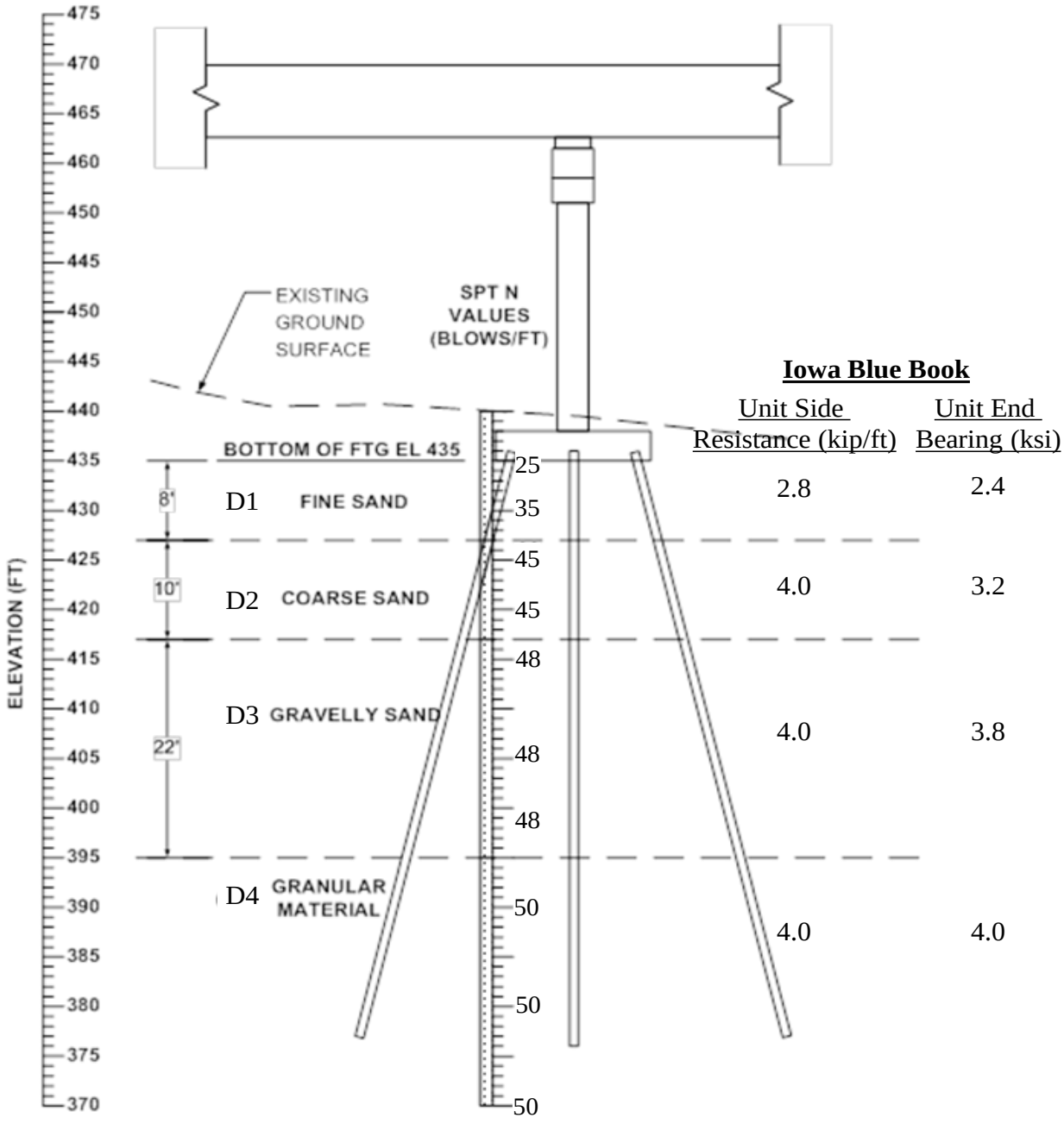

Figure 5.1. Soil profile of case study No. 1

Hence, the total required embedded pile length is 48.1 ft. Allowing 1 ft for cutoff and 1 ft for cap embedment, the required contract length is 50 ft. In summary, sixteen HP 10 × 57 steel piles with 50 ft length each are required. Driveability analysis performed based on a Delmag D19-42 diesel

hammer using WEAP shown in Figure 5.2 indicates that the 50-ft steel H-piles will not exceed the allowable stress limit of 90% of the yield strength (F_y) (i.e., 45 ksi for Grade 50 steel) and early refusal (i.e., 160 blows per foot of pile penetration) will not be encountered.

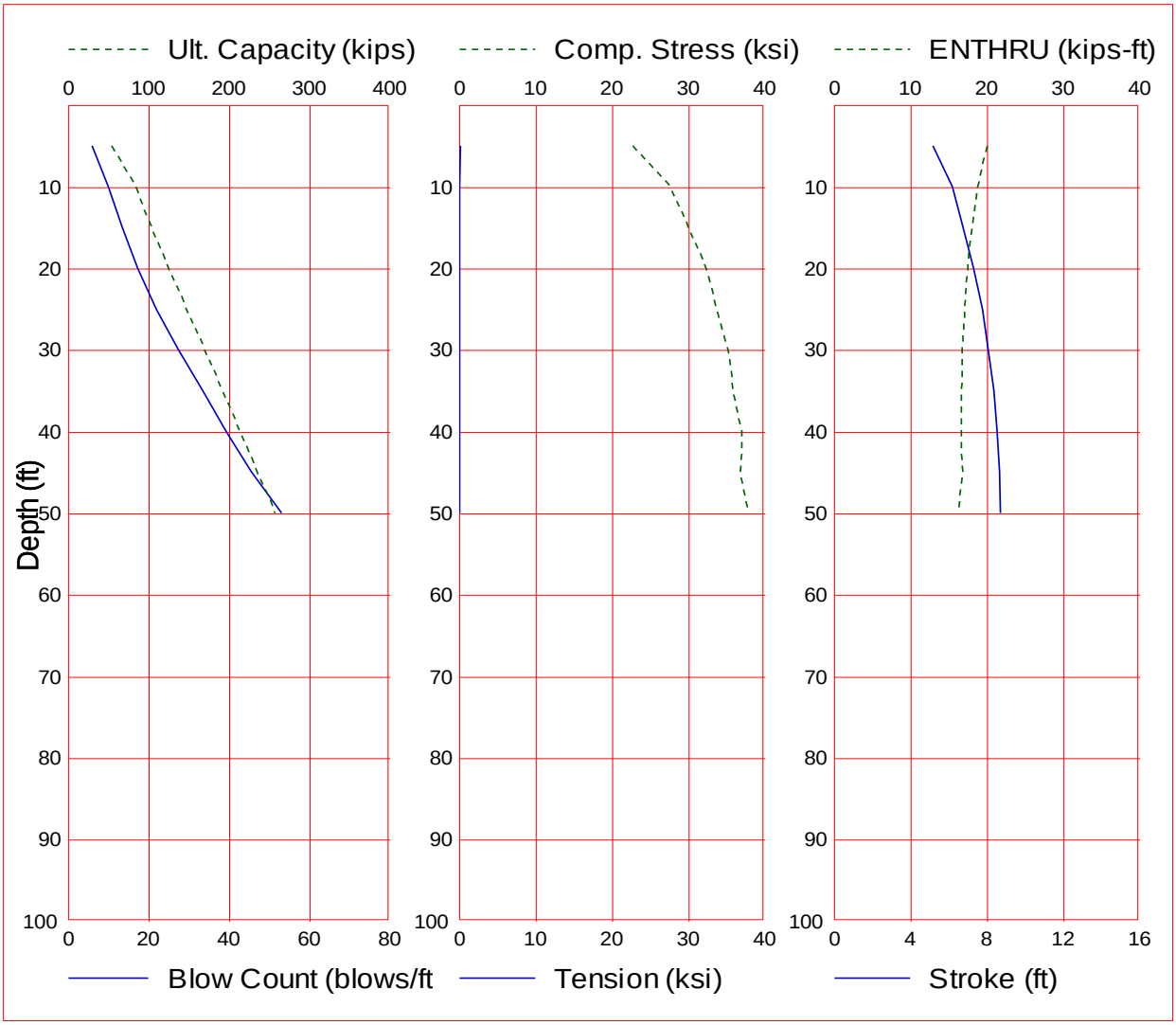

Figure 5.2. Results of driveability analysis of the 50-ft HP 10×57 steel piles

The final layout of the 16 HP 10 × 57 steel H-piles is shown in Figure 5.3.

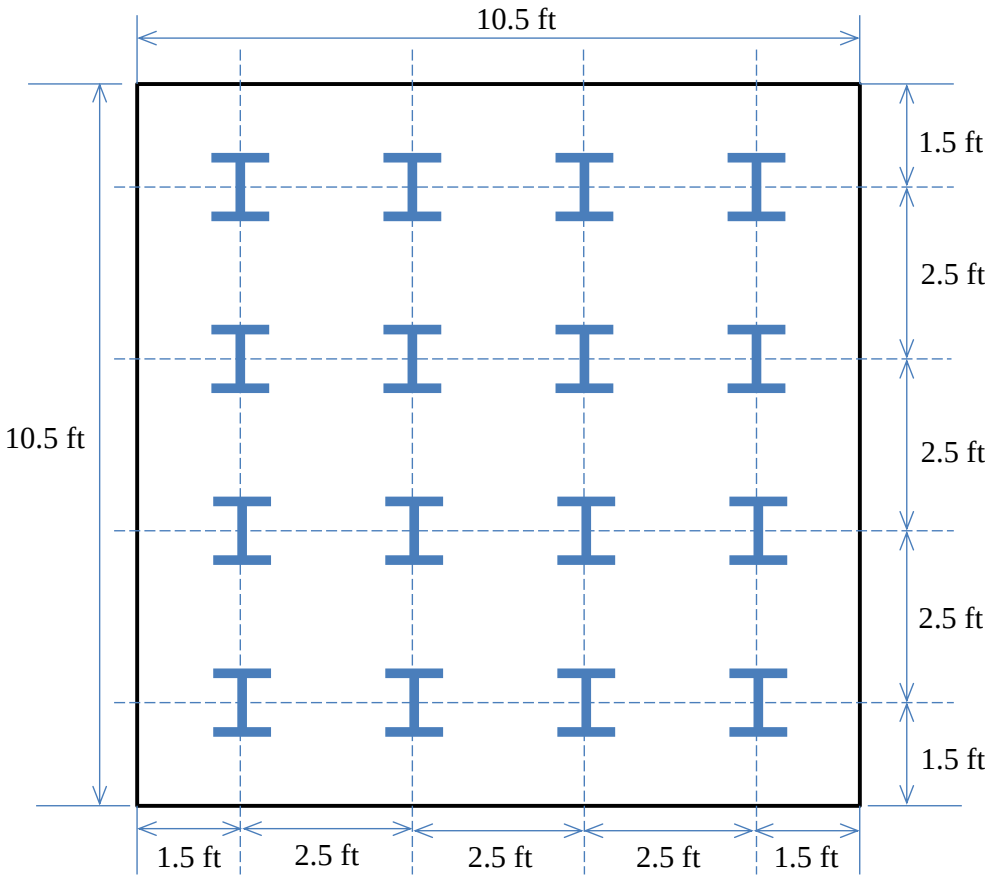

Figure 5.3. Final layout of 16 50-ft long HP 10 × 57 steel H-piles per cap

Drilled Shaft

Drilled shafts are designed to support the applied factored axial load of 2200 kips and satisfy the required axial settlement criteria. For the cohesionless soil profile, the β-method described in Section 2.3.3 was used to estimate the side resistance and effective stress method described in Section 2.4.3 was used to estimate the end bearing. The design procedure of a drilled shaft is an iterative process, in which a trial geometry is chosen for a preliminary analysis. Following the minimum requirements specified in the Iowa DOT BDM for drilled shafts, 3-ft diameter drilled shafts, Grade 60 steel reinforcement and a concrete compressive strength of 3.5 ksi were used. One percent steel reinforcement of the shaft cross-sectional area was assumed over the full depth of the shaft. The estimation of geotechnical resistances for the 3-ft diameter drilled shafts is summarized in Table 5.1.

Table 5.1. Geotechnical resistances of 3-ft diameter drilled shafts

Soil Layer	Thickness Δh (ft)	SPT N-value	Unit Weight, γ (kcf)	z (ft)	β (Limit to 1.20)	σ_v' (ksf)	q_s (ksf)	R_s (kips)	R_p (kips)
1	8	30	0.110	4	1.20	0.44	0.53	39.85	-
2	10	45	0.133	13	1.20	1.54	1.85	174.56	-
3	22	48	0.137	29	1.20	3.71	4.46	923.89	-
4	55	50	0.150	75	0.47	10.48	4.93	3254.69	424.12

Assuming a total embedded length of 110 ft, the side resistance (R_{s1}) in layer 1, the end bearing (R_p) and the total nominal resistance (R_T) per shaft are

$R_{s1} = q_s \times A_s = \beta\, \sigma_v' A_s = \beta \times \gamma z \times \pi \times B \times \Delta h$
$= 1.20 \times 0.11$ kcf $\times 4$ ft $\times \pi \times 3/ \times 8$
$= 39.85$ kips

$R_p = 1.2 \times N \times A_g = 1.2 \times 50 \times \pi\,(B/2)^2 = 424.12$ kips

$R_T = \sum R_{si} + R_p = 39.85 + 174.56 + 923.89 + 3254.69 + 424.12 = 4817.09$ kips

where
q_s = unit side resistance (ksf),
β = the reduction factor described in Section 2.3.3,
σ_v' = vertical geostatic effective stress at soil layer mid-depth (ksf),
z = depth below ground at soil layer mid depth (ft),
A_s = circumferential area (ft^2),
γ = unit weight of soil (kcf) estimated based on correlations provide by Bowles (1996),
B = drilled shaft diameter (ft),
Δh = thickness of a soil layer (ft),
N = SPT N-value, and
A_g = gross cross-sectional area of a drilled shaft.

For a cohesionless soil profile, the required nominal resistance per cap shall be:

$$R = \frac{\gamma Q}{\varphi} = \frac{2200}{0.55} = 4000 \text{ kips}$$

where
γQ = factored axial load (kips), and
φ = resistance factor obtained from Table 4.7.

Since the estimated resistance per shaft is larger the required resistance, one 3-ft diameter 110-ft length drilled shaft may be sufficient. The next step is to estimate the shaft settlement and check against the 1-in. top displacement criterion adopted by Iowa DOT or the settlement requirements proposed by O'Neill and Reese (1999) as shown in Figure 2.22 for side resistance and Figure 2.23 for end bearing in cohesionless soils. The total shaft top settlement (w_T) is estimated using a simple yet method proposed by Vesic (1977) as follows:

$$w_T = w_c + w_{bb} + w_{bs}$$
$$w_c = (Q_h - 0.5Q_{ms})\frac{L}{(AE)_{shaft}}$$
$$w_{bb} = C_p\left(\frac{Q_{mb}}{Bq_{max}}\right)$$

$$w_{bs} = \left(0.93 + 0.16\sqrt{\frac{L}{B}}\right) C_p \left(\frac{Q_{ms}}{L q_{max}}\right)$$

where

w_c = elastic compression of the drilled shaft (in),
w_{bb} = settlement of the base due to load transferred to the shaft base (in),
w_{bs} = settlement of the base due to load transferred along the sides (in),
Q_h = working load applied to the top of the shaft (kips),
Q_{ms} = mobilized side resistance (kips),
L = length of the drilled shaft (ft),
A = cross-sectional area of the shaft (ft^2),
E = composite elastic modulus of the reinforced concrete shaft (ksf)
= $E_c (A_c + n A_s)$,
E_c = modulus of the concrete (ksi),
A_c = cross-sectional area of concrete (ft^2),
A_s = cross-sectional area of longitudinal steel reinforcement (ft^2),
n = modulus ratio = E_s/E_c,
E_s = elastic modulus of steel reinforcement (ksf)
C_p = a factor that depends on soil characteristics (see Table 5.2),
Q_{mb} = load transferred to the shaft base (kips),
B = shaft diameter (ft), and
q_{max} = nominal unit base resistance (ksf).

Table 5.2. Values of C_p based on general description of soil (Vesic 1977)

Soil Description	C_p
Sand (dense to loose)	0.09 to 0.18
Clay (stiff to soft)	0.03 to 0.06
Silt (dense to loose)	0.09 to 0.12

The settlement calculations and verifications are summarized in Table 5.3.

Table 5.3. Settlement calculations and verifications of 3-ft diameter shafts

Description	Number of 3-ft Diameter Shafts Per Cap			
	1	**2**	**3**	**4**
Q_h (kips)	4,000	2,000	1,333	1,000
Q_{ms} (kips)	3,647.82	1,823.91	1,215.94	911.96
L (ft)	110	110	110	110
A (ft^2)	7.07	7.07	7.07	7.07
f_c' (psi)	3,500	3,500	3,500	3,500
E_c (psi)	3,372,165	3,372,165	3,372,165	3,372,165
A_s (ft^2) = 1% A	0.071	0.071	0.071	0.071
Ac (ft^2)	7.00	7.00	7.00	7.00
E_s (psi)	29,000,000	29,000,000	29,000,000	29,000,000
$(AE)_{shaft}$ (kips)	3,693,306	3,693,306	3,693,306	3,693,306
w_c (in)	0.78	0.39	0.26	0.19
C_p for dense sand	0.09	0.09	0.09	0.09
q_{max} (ksi)	0.42	0.42	0.42	0.42
Q_{mb} (kips)	352.18	176.09	117.39	88.04
w_{bb} (in)	2.11	1.06	0.70	0.53
w_{bs} (in)	1.13	0.57	0.38	0.28
w_T (in)	4.02	2.01	1.34	1.00
w_T satisfies 1-in. Criterion	No	No	No	Yes
w_{bs} satisfies 0.8%B = 0.29 in	No	No	No	Yes
w_{bb} satisfies 5%B = 1.8 in	Yes	Yes	Yes	Yes

Although a 3-ft diameter shaft has sufficient supporting capacity, the settlement results show that four 3-ft diameter 110-ft long drilled shafts are required per cap to satisfy the 1-in. top displacement specified in the Iowa DOT BDM, or the 0.8% diameter for accumulated settlement alongside and 5% diameter for base settlement suggested by O'Neill and Reese (1999). It is important to recognize that the settlement analyses were performed based on an approximated method by Vesic (1977) and a more accurate settlement analysis or field load test may reduce the required number of drilled shafts. Alternatively, larger diameter drilled shafts could be designed based on the aforementioned procedure. The design summary of drilled shafts with diameters ranging from 3 ft to 8 ft that satisfy the Iowa DOT 1-in. top displacement criterion is presented in Table 5.4.

Table 5.4. Design summary of drilled shafts that satisfy the Iowa DOT 1-in. top displacement criterion

Description	Shaft Diameter (ft)					
	3	**4**	**5**	**6**	**7**	**8**
Length (ft)	110	90	80	115	105	95
No. of Shafts	4	4	4	3	3	3
w_{bs} (in)	0.53	0.58	0.63	0.64	0.64	0.66
W_{ss} (in)	0.28	0.29	0.29	0.29	0.29	0.29
w_c (in)	0.19	0.09	0.05	0.07	0.05	0.04
w_T (in)	1.00	0.96	0.97	1.00	0.98	0.99
Concrete Volume (ft^3)	3,110	4,524	6,283	9,755	12,123	14,326

Similarly, the design summary of shafts that satisfy the settlement criteria suggested by O'Neill and Reese (1999) is presented in Table 5.5.

Table 5.5. Design summary of drilled shafts that satisfy the 0.8% diameter for w_{ss} and 5% diameter for w_{bs} suggested by O'Neill and Reese (1999)

Description	Shaft Diameter (ft)					
	3	**4**	**5**	**6**	**7**	**8**
Length (ft)	110	95	110	75	145	115
No. of Shafts	4	3	2	2	1	1
w_{bs} (in)	0.53	0.75	0.99	1.3	2.1	1.82
W_{ss} (in)	0.28	0.38	0.46	0.56	0.66	0.77
w_c (in)	0.19	0.13	0.15	0.07	0.21	0.13
w_T (in)	1.00	1.26	1.60	1.93	2.97	2.72
Concrete Volume (ft^3)	3,110	3,581	4,320	4,241	5,580	5,781

The concrete volume for each design is included to possibly compare their costs and help in selecting the most economical design. For both criteria, four 3-ft diameter 110-ft long drilled shafts per cap are chosen. The final layout of the four 3-ft diameter drilled shafts is shown in Figure 5.4.

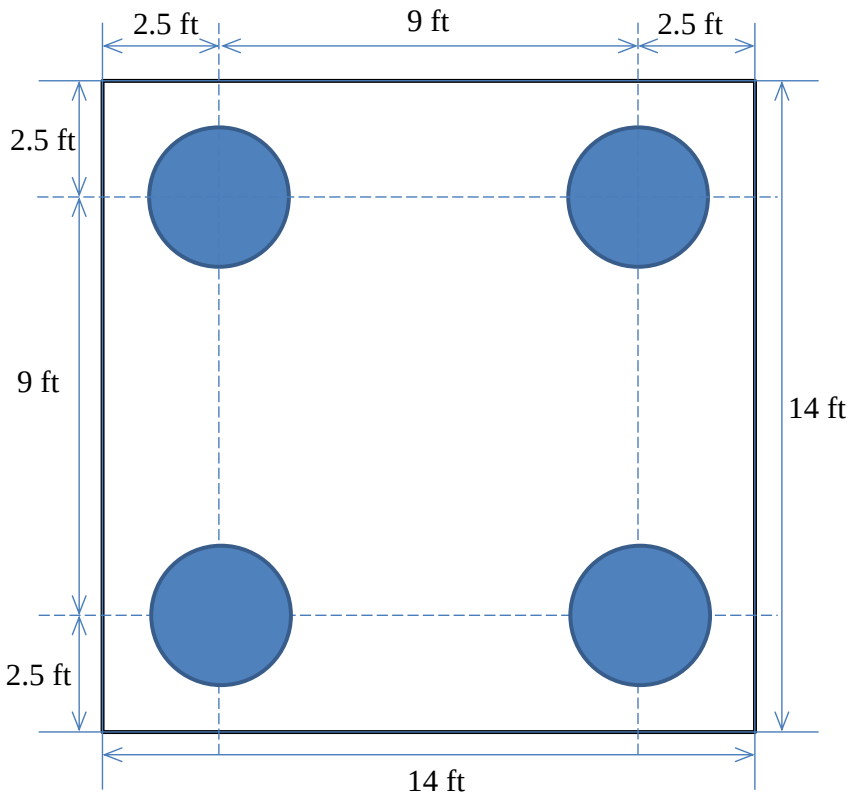

Figure 5.4. Final layout of four 110-ft long 3-ft diameter drilled shafts per cap

5.3. Case Study No. 2

Case study No.2 is to design a foundation system supporting a pier of a 272 ft by 30 ft pretensioned, prestressed concrete beam bridge with 6 ft sidewalk for the Interstate I-235/28th street overpass in Polk county, IA. The soil boring with the SPT blow counts at the pier location is given in Table 5.6.

Table 5.6. Soil profile and parameters of Case Study No. 2

Soil Layer	Material Description	Thickness (ft)	Material Type	Measured Parameters
1	Stiff to firm silty glacial clay	39	Clay	N_{60} = 12; c = 1.572 ksf
2	Firm silty clay	5	Clay	N_{60} = 22; c = 2.934 ksf
3	Clay shale bedrock	22+	Rock	q_u (shaft) = 196.56 ksf; q_u (toe) = 24.37 ksf; RQD = 33%

Below the bottom of footing elevation, subsurface conditions generally consist of about 39 ft of glacial clay, underlain by about 5 ft of silty clay, and 22 ft or more of clay shale bedrock. The test boring was terminated at a depth of 66 ft below the existing ground surface, and no ground water was reported in the test boring. The total factored axial compressive load of a bridge pier acting on the foundation is 3000 kips. Based upon the design information, the design procedures

of driven steel H-pile foundations following the recently established LRFD design guide (Green et al. 2012) and drilled shaft foundation following the aforementioned LRFD recommendations are demonstrated below and the design outcomes are compared.

Driven Steel H-Pile

Assuming that HP 10×57 steel piles are selected, the factored structural resistance (P_u) per pile for Structural Resistance Level 2 is 219 kips as recommended in the Iowa DOT LRFD BDM to limit pile settlement. The required number of piles is

$$n = \frac{3000}{219} = 13.7 \text{ piles or selected } 14 \text{ piles}$$

Hence, the factored axial load supported by each pile is 214.2 kips. Since only cohesive soils are present above the bedrock, the soil is expected to fit the clay classification. The resistance factor for clay using the Iowa Blue Book method as the design approach is 0.65. The resistance factor used for end bearing in rock is 0.70. Based on the unit nominal side resistance and unit end bearing obtained from the Iowa Blue Book as shown in Table 5.7, the required embedded pile length is 44 ft plus 8 ft of shale penetration, and the accumulated nominal resistance including end bearing and ignoring side resistance in rock (R) is 334.4 kips.

Table 5.7. Iowa Blue Book design parameters

Soil Layer	Material Description	Thickness (ft)	Unit Side Resistance (ksf)	Unit End Bearing (ksi)
1	Stiff to firm silty glacial clay	30	2.8	-
		9	3.2	-
2	Firm silty clay	5	4.0	1.0
3	Clay shale bedrock	8	-	12

D1 = 39 ft, R_1 = 2.8×30 + 3.2×9 = 112.8 kips
D2 = 5 ft, $R_{1\text{-}2}$ = 4.0×5 + 112.8 = 132.8 kips
D3 = 8 ft, $R_{1\text{-}3}$ = 12×16.8 + 132.8 = 334.4 kips

The required nominal resistance (R_n) per pile is

$$R_n = 0.65 \times (132.8) + 0.70 \times 201.6 = 227.44 \text{ kips}$$

Since the estimated factored resistance per pile of 227.44 is greater than the factored load of 214.2 kips (i.e., 3000/14), the strength limit state is satisfied and fourteen steel H- piles are confirmed. Allowing 1 ft for cutoff and 1 ft for cap embedment, the required contract length is 55 ft. In summary, 14 HP 10 × 57 steel piles with 55 ft length each are required. Driveability analysis performed based on a Delmag D19-42 diesel hammer using WEAP is shown in Figure 5.5 indicates that the 55-ft steel H-piles will experience early refusal (i.e., 160 blows per foot of pile penetration) at 51 ft while the pile will not exceed the allowable stress limit of 90% of the yield strength (F_y) (i.e., 45 ksi for Grade 50 steel).

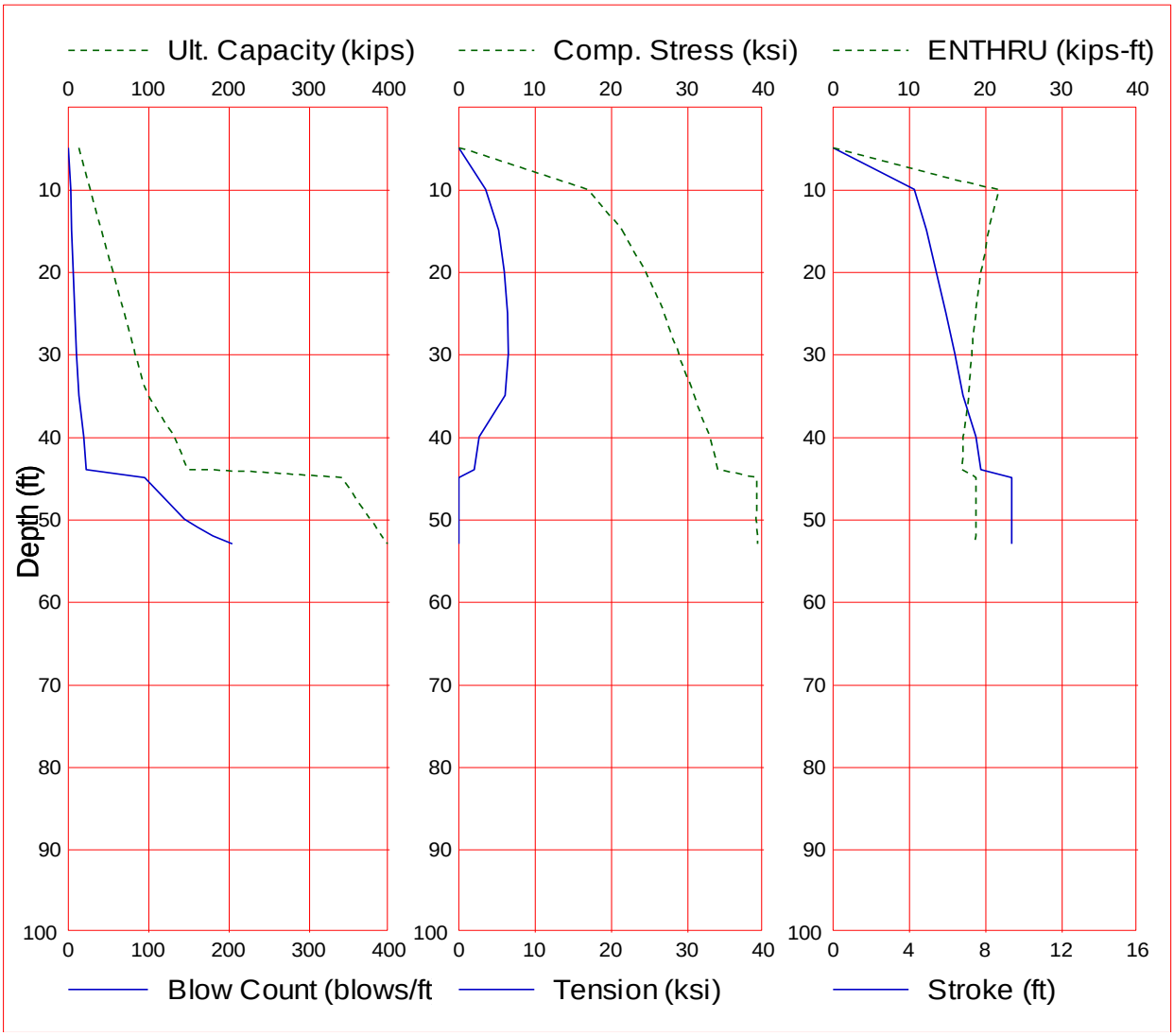

Figure 5.5. Results of driveability analysis of 55-ft HP 10×57 steel piles

The driveability analysis reveals that driving of the steel H-pile 8 ft into the rock layer is either impossible or would require sigificnat effort. The final layout of the 14 HP 10 × 57 steel H-piles is shown in Figure 5.6.

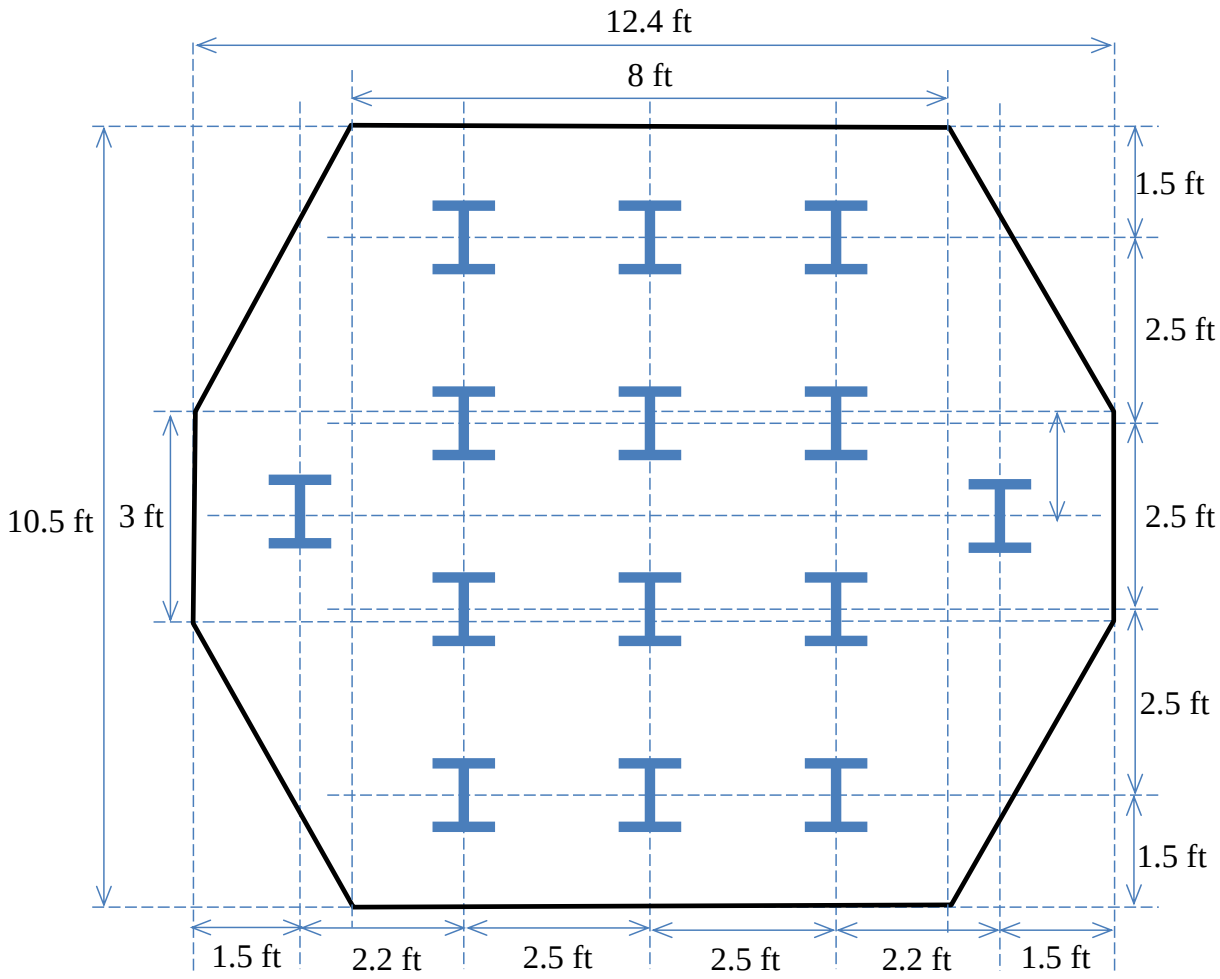

Figure 5.6. Final layout of 14 55-ft long HP 10 ×57 steel H-piles per cap

Drilled Shafts

Drilled shafts are designed to support the applied factored axial load of 3000 kips and satisfy the required axial settlement. For the cohesive soil profile, the α-method described in Section 2.3.2 was used to estimate the side resistance, and the total stress method described in Section 2.4.2 was used to estimate the end bearing. The design procedure of a drilled shaft is an iterative process, in which a trial geometry is chosen for a preliminary analysis. Following the minimum requirements specified in the Iowa DOT BDM for drilled shafts, 3-ftdiameter drilled shafts, Grade 60 steel reinforcement, and a concrete compressive strength of 3.5 ksi were used. One percent steel reinforcement of the shaft cross-sectional area was assumed over the full depth of a drilled shaft. The estimation of geotechnical resistances for the 3-ft diameter drilled shafts is summarized in Table 5.8.

Table 5.8. Geotechnical resistances of 3-ft diameter drilled shafts

Soil Layer	Thickness Δh (ft)	SPT N-value	Undrained Shear Strength, S_u (ksf)	q_u (ksf)	$\alpha;\alpha_E$	q_s (ksf)	R_s (kips)	R_p (kips)
1	39	12	1.572	-	0.55	0.86	277.05	-
2	5	22	2.934	-	0.55	1.61	76.04	-
3	7	-	-	196.56 (shaft); 110.50 (toe)	0.54	7.11	469.21	996.46

Assuming a total embedded length of 51 ft including 7 ft rock-socket length, the side resistance (R_{s1}) in layer 1, the end bearing (R_p) and the total nominal resistance (R_T) per shaft are

$R_{s1} = q_s \times A_s = \alpha\, S_u\, A_s = \alpha \times S_u \times 2\pi \times B/2 \times \Delta h$
$= 0.55 \times 1.572$ ksf $\times$ 4 ft $\times 2\pi \times 3/2 \times (39\text{-}5)$ft
$= 277.05$ kips

$R_p = q_b \times A_g = 140.97 \times \pi\,(B/2)^2 = 996.46$ kips

$R_T = \sum R_{si} + R_p = 277.05 + 76.04 + 469.21 + 996.46 = 1818.76$ kips

where
q_s = unit side resistance (ksf),
q_b = unit end bearing (ksf),
α = reduction factor described in Section 2.3.2,
S_u = undrained shear strength (ksf),
A_s = circumferential area (ft^2),
B = drilled shaft diameter (ft),
Δh = thickness of a soil layer (ft),
A_g = gross cross-sectional area of a drilled shaft.

Based on the resistance factors recommended in Table 4.7, the factored resistance (φR) per shaft is
$\varphi R = \varphi_1 R_{S1} + \varphi 2 R_{S2} + \varphi_3 R_{S3} + \varphi R_p$
$= 0.45 \times 277.05 + 0.45 \times 76.04 + 0.55 \times 469.21 + 0.35 \times 996.46 = 765.72$ kips

The number of shafts per cap required to support the factored axial load of 3,000 kips is

Number of shafts per cap = $\frac{3000}{765.72} = 3.92$; use 4 shafts per cap

The next step is to estimate the shaft settlement and check against the 1-in. top displacement criterion adopted by Iowa DOT. The total shaft top settlement (w_T) is estimated using a closed-form solution proposed by Kulhawy and Carter (1992). Table 5.9 summarizes the final design of drilled shafts with diameters ranging from 3 ft to 8 ft that satisfy the 1-in. top displacement criterion.

Table 5.9. Design summary of drilled shafts that satisfy the Iowa DOT 1-in. top displacement criterion

Description	Shaft Diameter (ft)					
	3	**4**	**5**	**6**	**7**	**8**
Length (ft)	51	52.5	51.5	55.5	54.5	56
No of Shafts	4	3	3	2	2	2
w_T (in)	0.99	1.00	0.82	1.00	0.87	0.75
Concrete Volume (ft^3)	1,442	1,979	3,034	3,138	4,195	5,630

Four 3-ft diameter and 51-ft long drilled shafts per cap, which require the least amount of concrete, are selected. The final layout of the four 3-ft diameter drilled shafts is shown in Figure 5.7.

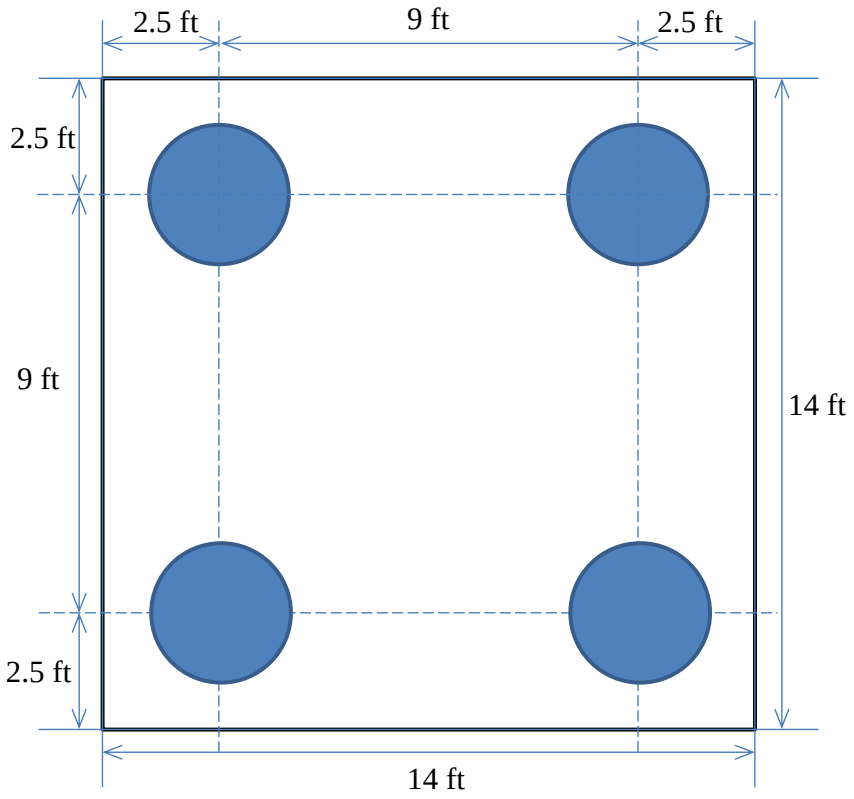

Figure 5.7. Final layout of four 51-ft by 3-ft diameter drilled shafts per cap

5.4. Design Comparisons

Case study No. 1 shows the design comparison of steel H-piles and drilled shafts in a cohesionless profile for supporting a frame pier of a 208 ft, three-span, prestressed concrete beam superstructure with zero skew. The analysis concludes that only 4 No. and 110 ft length of 3-ft diameter drilled shafts per cap are required to support the applied load and satisfy the 1-in. top displacement criterion as opposed to sixteen 50-ft steel HP 10 × 57 piles per cap. The case

study No. 2 shows the comparison of foundation design for supporting a pier of a 272 ft by 30 ft pretensioned, prestressed concrete beam bridge in 44 ft of clay, underlain by a clay shale bedrock. The analysis concludes that only four 51-ft long 3-ft diameter drilled shafts per cap are required to support the applied load and satisfy the 1-in. top displacement criterion as opposed to 14 of the 55-ft long steel HP 10 × 57 piles per cap.

CHAPTER 6. SUMMARY AND FUTURE RESEARCH

6.1. Summary

Despite drilled shafts having many advantages over other foundation types, drilled shafts are used infrequently in the State of Iowa although the soil conditions in several regions of Iowa are ideal for using this foundation option. One of the reasons for the limited use of drilled shafts is primarily attributed to the absence of regional LRFD design guidelines for drilled shafts in the Iowa Bridge Design Manual. As part of the effort in complying with the Federal Highway Administration (FHWA) mandate to utilize the Load and Resistance Factor Design (LRFD) approach for all new bridges initiated in the United States after October 1, 2007, a database for Drilled SHAft Foundation Testing (DSHAFT) was developed and reported by Garder et al. (2012). DSHAFT is aimed at assimilating high quality drilled shaft test data from Iowa and the surrounding regions, which can be efficiently used for the development of regional LRFD guidelines for drilled shafts. DSHAFT is currently housed on a project website (http://srg.cce.iastate.edu/dshaft) and contains data from 41 drilled shaft tests.

The objective of this research is to utilize the DSHAFT database to develop a regional LRFD procedure for drilled shafts in Iowa using probability-based reliability theory. This was done by examining current design and construction practices used by the Iowa DOT, as well as recommendations given in AASHTO LRFD Bridge Design Specifications (2010), the FHWA drilled shaft guidelines prepared by O'Neill and Reese (1999), and Brown et al. (2010). Extensive literature reviews with regard to drilled shaft design philosophy, design methods, construction methods, load testing methods and current practices are presented in Chapter 2. The drilled shaft test data compiled in DSHAFT were examined and the results of analysis are presented in Chapter 3 and appendices. Various analytical methods were used to estimate the side resistance and end bearing of drilled shafts in clay, sand, Intermediate Geo Materials (IGM), and rock. Most of the load test results obtained from O-cell do not acieve the 1-in. top displacement criterion recommended by the Iowa DOT nor the 5% of shaft diameter for top displacement criterion recommended in AASHTO (2010). Hence, measured resistances corresponding to the performance-based criteria cannot be determined for later use in the calibration of resistance factors. To overcome this limitation, three improved procedures are proposed for three different shaft responses to generate and extrapolate equivalent top load-displacement curves. Based on the O-cell test results summarized in DSHAFT, these three different shaft responses are categorized as Cases A, B and C. Case A corresponds to O-cell test results in which side resistance reaches its ultimate value with an excessive upward displacement before end bearing. Case B is the opposite of Case A, in which the end bearing and/or the lower side resistance below the O-cell reach ultimate values with the excessive downward displacement before upper side resistance. When neither the measured side resistance nor end bearing reach their respective ultimate values, the shaft response is categorized as Case C. Using the estimated and measured resistances, regional resistance factors were calibrated following the AASHTO LRFD framework. Resistance factors for each resistance component (i.e., side resistance, end bearing and total resistance) and geomaterial were determined based on the following criteria: 1) maximum measured load reported in the load test reports; 2) 1-in. top displacement; and 3) 5% of shaft diameter for top displacement. Compared with the resistance factors recommended in the NCHRP reports and AASHTO (2010), regional calibration produces

higher resistance factors and efficiency factors except for the side resistance components in clay and sand. The calibrated resistance factors were adjusted to resolve any anomalies observed among the factors. Incorporating the LRFD resistance factors recommended in AASHTO (2010), a set of regional LRFD resistance factors were recommended. To illustrate the potential and successful use of drilled shafts in Iowa, the design procedures of drilled shaft foundations were demonstrated and the advantages of drilled shafts over driven piles are addressed in two case studies. The analyses conclude that fewer drilled shafts per cap are needed to support the applied loads and satisfy the displacement criteria.

6.2. Recommendations for Future Research

Although significant progress was made in the development of LRFD procedure for drilled shafts in Iowa with this project, further advancements can be made for continuous improvements of drilled shaft foundations, including the following:

- Continuously increase the regional drilled shaft test data in DSHAFT
- Conduct detailed soil and rock investigations
- Verify the resistance factors of drilled shafts by performing controlled O-cell load tests in Iowa and make appropriate revisions
- Increase the number of O-cell load tests of drilled shafts in clay and rock materials
- Verify the proposed procedures for generating the equivalent top load-displacement curves

REFERENCES

AbdelSalam, S.S., Ng, K.W., Sritharan, S., Suleiman, M.T., and Roling, M. 2012. *Development of LRFD Design Procedures for Bridge Piles in Iowa – Recommended Resistance Factors with Consideration to Construction Control and Setup.* Final Report Vol. III. IHRB Project No. TR-573. Institute for Transportation, Iowa State Univeristy, Ames, IA. (http://www.intrans.iastate.edu/research/ reports.cfm)

Abu-Hejleh, N., M. W. O'Neill, D. Hanneman, and W. J. Atwooll. 2003. *Improvement of the Geotechnical Axial Design Methodology for Colorado's Drilled Shafts Scoketed in Weak Rocks*. Report No. CDOT-DTD-R-2003-6, Colorado Department of Transportation, 199 p.

Abu-Hejleh, N., and W. J. Atwooll. 2005. *Colorado's Axial Load Tests on Drilled Shafts Socketed in Weak Rocks: Synthesis and Future Needs*. Report No. CDOT-DTD-R-2005-4, Colorado Department of Transportation, 178 p.

Allen, T. M. 2005. *Development of Geotechnical Resistance Factors and Downdrag Load Factors for LRFD Foundation Strength Limit State Design*. FHWA-NHI-05-052, Federal Highway Administration, U.S. Department of Transportation, Washington, D.C.

American Association of State Highway and Transportation Officials (AASHTO). 2009. *AASHTO LRFD Bridge Design Specification: Customary U.S. Units*, Fourth Edition with 2008 and 2009 Interim Revisions, Washington, D.C.

American Association of State Highway and Transportation Officials (AASHTO). 2010. *AASHTO LRFD Bridge Design Specifications*. Interim Revision. Fifth Edition, Washington, D.C.

American Society for Testing and Materials (ASTM)-D1142. 2007. Standard Test Methods for Deep Foundations Under Static Axial Compressive Load. PA.

American Society for Testing and Materials (ASTM)-D4945. 2008. Standard Test Methods for High-Strain Dynamic Testing of Deep Foundations. PA.

American Society for Testing and Materials (ASTM)-D7383. 2008. Standard Test Methods for Axial compressive Force Pulse (Rapid) Testing of Deep Foundations. PA.

Anderson, T. W., and D. A. Darling. 1952. Asymptotic Theory of Certain "Goodness-Of-Fit" Criteria based on Stochastic Processes. *Annals of Mathematical Statistics*, 23: pp. 193-212.

Baecher, G. 2001. *LRFD Deep Foundations Design*. Contribution to a progress research report as part of Project NCHRP 24-17, (unpublished document).

Barker, R., Duncan, J., Rojiani, K., Ooi, P., Tan, C., and Kim, S. (1991). NCHRP Report 343: Manuals for the Design of Bridge Foundations, Transportation Research Board, National Research Council, Washington, D.C.

Bjerrum, L. 1972. Embankments on Soft Ground. *Proceedings, Performance of Earth and Earth-Supported Structures*, Vol. II, ASCE, Reston, VA, pp. 1−54.

Bloomquist, D., M. McVay, and Z. Hu. 2007. *Updating Florida Department of Transportation's (FDOT) Pile/Shaft Design Procedures Based on CPT & DTP Data*. Department of Civil and Coastal Engineering, University of Florida, Gainesville, FL.

Bowles, E. J. 1996. *Foundation Analysis and Design*. The McGraw-Hill Companies, Inc.

Brown, D. A. and Associates. 2008. Load Testing of Drilled Shaft foundations in Limestone, Nashville, TN. Dan A. Brown and Associates Consulting Geotechnical Engineer. http://danbrownandassociates.com/wp-content/uploads/2009/02/load-testing-of-drilled-shaft-foundations-in-limestone-nashville-tn_brown_adsc-se-chapter-2008_feb09.pdf

Brown, D. A., J. P. Turner, and R. J. Castelli. 2010. *Drilled Shafts: Construction Procedures and LRFD Design Methods.* NHI Course No. 132014, Geotechnical Engineering Circular No. 10, National Highway Institute, U.S. Department of Transportation, Federal Highway Administration, Washington, D.C.

Burland, J. B. 1973. *Shaft Friction of Piles in Clay*. Ground Engineering, London, Vol. 6, No. 3, pp. 3042.

Canadian Geotechnical Society. 1985. *Canadian Foundation Manual*. Second Edition. Bitech Publishers, Ltd., Vancouver, British Columbia, Canada, 460 p.

Carter, J.P. and Kulhawy, F.H. 1988. *Analysis and Design of Drilled Shaft Foundations Socketed into Rock*. Report EL-5918, Electric Power Research Institute, Palo Alto, CA, 188 p.

Chang, N. Y. 2006. *CDOT Foundation Design Practice and LRFD Strategic Plan*. Report No. CDOT-DTD-R-2006-7, Colorado Department of Transportation, 209 p.

Deere, D.U., and D.W. Deere. 1989. *Rock Quality Designation (RQD) After Twenty Years*. Contract Report GL-89-1, U. S. Army Engineer Waterways Experiment Station, Vicksburg, MS.

Federal Highway Administrations (FHWA). 2009. *Geotechnical Program Review-Iowa Department of Transportation*. Federal Highway Administration, U.S. Department of Transportation, Washington, D.C.

Garder, J., K.W Ng, S. Sritharan, and M. Roling. 2012. *An Electronic Database for Drilled Shaft Foundation Testing (DSHAFT).* Final Report to Iowa Department of Transportation. Institute for Transportation, Iowa State University, Ames, IA

Goble, G. G., Likins, G. E., and Rausche, F. 1975. *Bearing Capacity of Piles from Dynamic Measurements*. Final Report, Department of Civil Engineering, Case Western Reserve University, Cleveland, OH.

Goodman, R. E. 1980. *Introduction to Rock Mechanics*. Wiley, New York.

Green, D., Ng, K.W., Dunker, K., Sritharan, S., and Michael Nop. 2012. *Development of LRFD Design Procedures for Bridge Piles in Iowa –Design Guide and Track Examples*. Final Report Vol. IV. Institute for Transportation, Iowa State Univeristy, Ames, IA.

Hassan, K.M, O'Neill, M.W., Sheikh, S.A., and Ealy, C.D. 1997. Design method for drilled shafts in soft argillaceous rock. *Journal of Geotechnical and Geoenvironmental Engineering*, ASCE, Vol. 123, No.3, pp. 272−280.

Hoek, E. and E.T. Brown. 1988. *The Hoek–Brown Failure Criterion—A 1988 Update*. Rock Engineering for Underground Excavations, Proceedings 15th Canadian Rock Mechanics Symposium, Toronto, ON, Canada, pp. 31–38.

Hoek, E., C. Carranza-Torres, and B. Corkum. 2002. *Hoek–Brown Failure Criterion−2002 Edition*. Proceedings, North American Rock Mechanics Society Meeting, July 8–10, Toronto, ON, Canada.

Horvath, R.G. and Kenney, T.C. 1979. *Shaft Resistance of Rock Socketed Drilled Piers*. Proceedings, Symposium on Deep Foundations, ASCE, New York, pp. 182-214.

Horvath, R.G., Kenney, T.C., and Kozicki, P. (1983). Methods of Improvding the Performance of Drilled Piers in Weak Rock. *Canadian Geotechnical Journal*, Vol. 20, pp. 758-772.

Illinois Department of Transportation (IDOT). 2012. *Bridge Manual*. Bureau of Bridges and Structures, January. http://www.dot.il.gov/bridges/pdf/bridge manual 2012.exe

Iowa Department of Transportation (Iowa DOT). 2011. *LRFD Bridge Design Manual* – Section 6.3: Drilled Shafts. February 22. http://www.iowadot.gov/bridge/manuallrfd.htm

Kentucky Department of Transportation (KDOT). 2005. *Geotechnical Guidance Manual*. Commonwealth of Kentucky Transportation Cabinet. June. http://transportation.ky.gov/organizational-resources/policy manuals library/geotechnical.pdf

Kulhawy, F.H. and J.P. Carter. 1992. Settlement and Bearing Capacity of Foundations on Rock Masses. In *Engineering in Rock Masses*, F.G. Bell, Ed., Butterworth–Heinemann, Oxford, England, pp. 231–245.

Kulhawy, F.H. and R.E. Goodman. 1980. *Design of Foundations on Discontinuous Rock.* Proceedings, International Conference on Structural Foundations on Rock, Vol. 1, Sydney, Australia, pp. 209–220.

Kulhawy, F. H., and K. K. Phoon. 2006. Some critical issues in Geo-RBD calibrations for foundations. *Proceedings, GeoCongress: Geotechnical Engineering in the Information Technology Age*, ASCE, Reston, VA.

Loadtest, Inc. 2006. *Report On Drilled Shaft Load Testing (Osterberg Method): I-215 Airport Connector-Las Vegas, NV-TS-1*. Report No. LT-9289, October.

Loehr, J.E., B.L. Rosenblad, and T.T. Vu. 2011a. *MoDOT Transportation Geotechnics Research Program: Drilled Shaft Axial Load Test Program Interpretation Report,* Missouri Department of Transportation (in preparation).

Loehr, J.E., S.A. Grant, and B.L. Rosenblad. 2011b. *Calibration of Resistance Factors for Design of Drilled Shafts at Strength Limit States Using Laboratory Test Measurements*, Missouri Department of Transportation (in preparation).

Mayne, P.W., and Harris, D.E. 1993. *Axial Load-Displacement Behavior of Drilled Shaft Foundations in Piedmont Residuum.* FHWA Reference No. 41-30-2175, Georgia Tech Research Corporation, Geotechnical Engineering Division, Georgia Institute of Technology, School of Civil Engineering, Atlanta, February.

McCarthy, F. D. 2007. *Essentials of Soil Mechanics and Foundations*. Seventh Edition, Pearson Prentice Hall, Pearson Education, Inc., NJ.

Minnesota Department of Transportation (MnDOT). 2012. *LRFD Bridge Design Manual*. Bridge Office. http://www.dot.state.mn.us/bridge/manuals/lrfd/pdf/lrfdmanual20120412.pdf

Missouri Department of Transportation (MoDOT). 2003. *Section 701-Drilled Shafts*. http://www.modot.mo.gov/business/standards_and_specs/Sec0701.pdf

Missouri Department of Transportation (MoDOT). 2011. *Engineering Policy Guidelines for Design of Drilled Shafts*. Report cmr12003. http://ftandc.com/specs/1292195767-drilledshafts.pdf

Mullins, G., D. Winter, and S. Dapp. 2006. Predicting End Bearing Capacity of Post-Grouted Drilled Shaft in Cohesionless Soils. *Journal of Geotechnical and Geoenvironmental Engineering*, ASCE, Vol. 132, No. 4, pp. 478−487.

Nevada Department of Transportation (NDOT). 2008. *Structural Manual*. Structures Division. http://www.nevadadot.com/uploadedfiles/ndot/about_ndot/ndot_divisions/engineering/structures_manual.pdf

Nebraska Department of Roads (NDOR). 2012. *Bridge Office Policies and Procedures*. Bridge Division. http://www/nebraskatransportation.org/design/bridge/bopp/bopp-manual.pdf

Nowak, A. 1999. *Calibration of LRFD Bridge Design Code*. NCHRP Report 368, Transportation Research Board, Washington, D.C.

O'Neill, M.W. and L.C. Reese. 1999. *Drilled Shafts: Construction Procedures and Design Methods.* Publication No. FHWA-IF-99-025. Federal Highway Administration, Washington, D.C.

O'Neill, M.W., F.C. Townsend, K.H. Hassan, A. Buller, and P.S. Chan. 1996. *Load Transfer for Drilled Shafts in Intermediate Geomaterials*. Publication No. FHWA-RD-95-171, Federal Highway Administration, McClean, VA, 1996, 184 p.

Osterberg, J. O. 1992. *The Osterberg Load Cell for Testing Drilled Shafts and Driven Piles*. Report to the Federal Highway Administration, Washington, D.C.

Osterberg, J. O. 1994. *Recent Advances in Load Testing Driven Piles and Drilled Shafts Using the Osterberg Load Cell Method*. Geotechnical Division, Illinois Section, ASCE, 79 pp.

Paikowsky, S.G. with Contributions from B. Birgisson, M. McVay, T. Nguyen, C. Kuo, G. Baecher, B. Ayyab, K. Stenersen, K. O′Malley, L. Chernauskas, and M. O'Neill. 2004. *Load and Resistance Factor Design (LRFD) for Deep Foundations*. NCHRP Report 507, Transportation Research Board, Washington, D.C.

Pierce, M.D., J.E. Loehr, and B.L. Rosenblad. 2011. *Calibration of LRFD Resistance Factors for Design of Drilled Shafts at Strength Limit States Using In situ Test Measurements*, Missouri Department of Transportation (in preparation).

Potyondy, J. G. 1961. Skin Friction between Various Soils and Construction Materials. *Geotechnique*, Vol. 11, No. 4, pp. 339–353.

Reese, L.C. and M.W. O'Neill. 1988.Field Load Tests of Drilled Shafts. *Deep Foundations on Bored Auger Piles*, Proceedings, 1st International Geotechnical Seminar on Deep Foundations on Bored and Auger Piles, W. F. Vanimpe, Editor, pp. 145–191.

Reese, L.C. and M.W. O'Neill. 1989. New Design Method for Drilled Shafts from Common Soil and Rock Tests. *Foundation Engineering: Current Principles and Practices*, Vol. 2, F.H. Kulhawy, Editor, ASCE, New York, pp. 1026–1039.

Roling, M, S. Sritharan, and M. Suleiman. 2010. *Development of LRFD Procedures for Bridge Pile Foundations in Iowa Volume I: An Electronic Database for PIle LOad Tests in Iowa (PILOT)*. IHRB Project No. TR-573. Institute for Transportation, Iowa State University, Ames, IA.

Romeu, J. L. 2010. *Anderson-Darling: A Goodness of Fit Test for Small Samples Assumptions*. START 2003-5, Vol. 10, Number 5, Reliability Analysis Center, Rome. http://www.theriac.org/riacapps/startsheets/?category=Reliability

Rowe, R.K. and H.H. Armitage. 1987. A Design Method for Drilled Piers in Soft Rock. *Canadian Geotechnical Journal*, Vol. 24, pp. 126–142.

Sowers, G.F. 1976. Foundation Bearing in Weathered Rock. *Rock Engineering for Foundations and Slopes*, ASCE, New York, NY, pp. 32-42.

Terzaghi, K. 1943. *Theoretical Soil Mechanics.* New York: John Wiley and Sons, Inc.

Tomlinson, M. J. 1971. Some Effects of Pile Driving on Skin Friction. Proceeding Conference on Behavior of Piles, Institute of Civil Engineers, London, pp. 107−114.

Turner, J.P. 2006. *Rock-Socketed Shafts for Highway Structure Foundations*. NCHRP Synthesis 360, Transportation Research Board, Washington, D.C., 148 p.

U.S. Army Corps of Engineers. 1994. *Rock Foundations*. Engineering Manual EM 1110-1-2908, Washington, D.C.

Vesic, A.S. 1977. *NCHRP Synthesis 42: Design of Pile Foundations*. Transportation Research Board, National Research Council, Washington, D.C., 68 p.
Wyllie, D.C. 1999. *Foundations on Rock,* E & FN Spon, Second Edition, 401 p.

APPENDIX A: CONSTRUCTION OF THE EQUIVALENT TOP-LOADED LOAD-SETTLEMENT CURVE FROM THE RESULTS OF AN O-CELL TEST (ADAPTED FROM LOADTEST, INC. 2006)

Procedure Part I: Figure A.1 shows O-cell test results and Figure A.2 shows the constructed equivalent top loaded settlement curve. Note that each of the curves shown has pairs of points numbered from 1 to 12 such that the same point number on each curve has the same magnitude of movement. For example, point 4 has an upward and downward movement of 0.40 inches in Figure A.1 and the same 0.40 inches downward in Figure A.2. For conservative reconstruction of the top-loaded settlement curve, we first convert both of the O-cell components at a given movement to net load. Using the assumptions described in Section 2.5.3, construct the equivalent curve as follows: Select an arbitrary movement such as 0.40 inches to give point 4 on the shaft-side shear load movement curve in Figure A.1 and record the 2,090 kips load in shear at that movement. Because we have initially assumed a rigid pile, the top of pile moves downward the same as the bottom. Therefore, find point 4 with 0.40 inches of downward movement on the end bearing load movement curve and record the corresponding load of 1,060 kips. Adding these two loads will give the total load of 3,150 kips due to side shear plus end bearing at the same movement and thus gives point 4 on Figure A.2 load settlement curve for an equivalent top-loaded test. One can use the above procedure to obtain all the points in Figure A.2 up to the component that moved the least at the end of the test, in this case point 5 in side shear. To take advantage of the fact that the test produced end bearing movement data up to point 12, we need to make an extrapolation of the side shear curve. We usually use a convenient and suitable hyperbolic curve fitting technique for this extrapolation. Deciding on the maximum number of data points to provide a good fit (a high R^2 correlation coefficient) requires some judgment. In this case we omitted point 1 to give an $R^2 = 0.999$ (including point 1 gave an $R^2 = 0.966$) with the result shown as points 6 to 12 on the dotted extension of the measured side shear curve. Using the same movement matching procedure described earlier we can then extend the equivalent curve to points 6 to 12. The results, shown in Figure A.2 as a dashed line, signify that this part of the equivalent curve depends partly on extrapolated data. Sometimes, if the data warrants, we will use extrapolations of both side shear and end bearing to extend the equivalent curve to a greater movement than the maximum measured (point 12).

Procedure Part II: The elastic compression in the equivalent top load test always exceeds that in the O-cell test. It not only produces more top movement, but also additional side shear movement, which then generates more side shear, which produces more compression. Figure A.4 gives the equations for the elastic compressions that occur in the O-cell load test (OLT) with one or two levels of O-cells. Figure A.5 gives the equations for the elastic compressions that occur in the equivalent top load test (TLT). Both sets of equations do not include the elastic compression below the O-cell because the same compression takes place in both the OLT and the TLT. Subtracting the OLT from the TLT compression gives the desired additional elastic compression at the top of the TLT. We then add the additional elastic compression to the ‘rigid’ equivalent curve obtained from Part I to obtain the final, corrected equivalent load-settlement curve for the TLT on the same pile as the actual OLT. Note that Figure A.4 and Figure A.5 give equations for each of three assumed patterns of developed side shear stress along the pile. The pattern shown in the center of the three applies to any approximately determined side shear distribution. Figure A.3 compares the corrected with the rigid curve of Figure A.2.

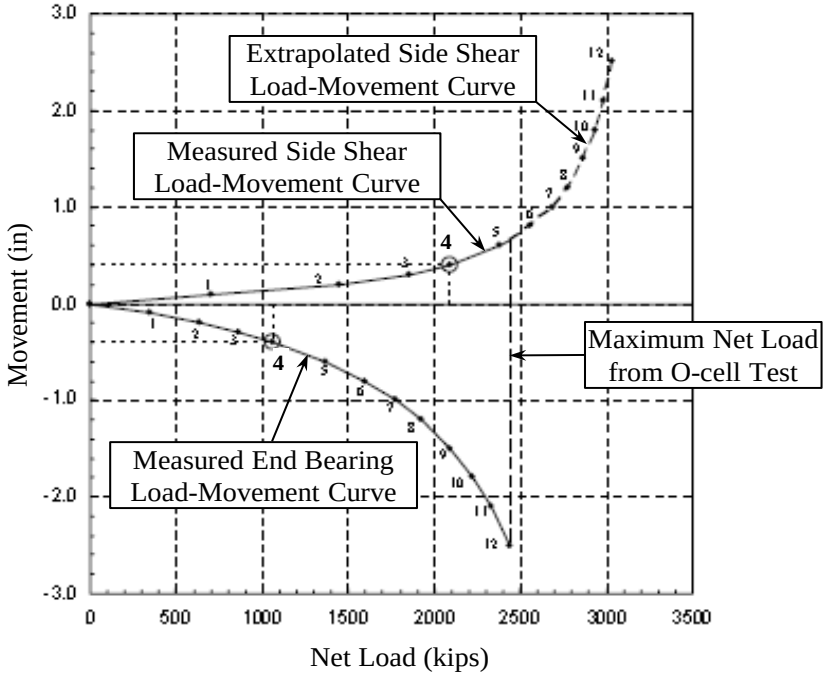

Figure A.1. Measured and extrapolated O-cell load-displacement curves

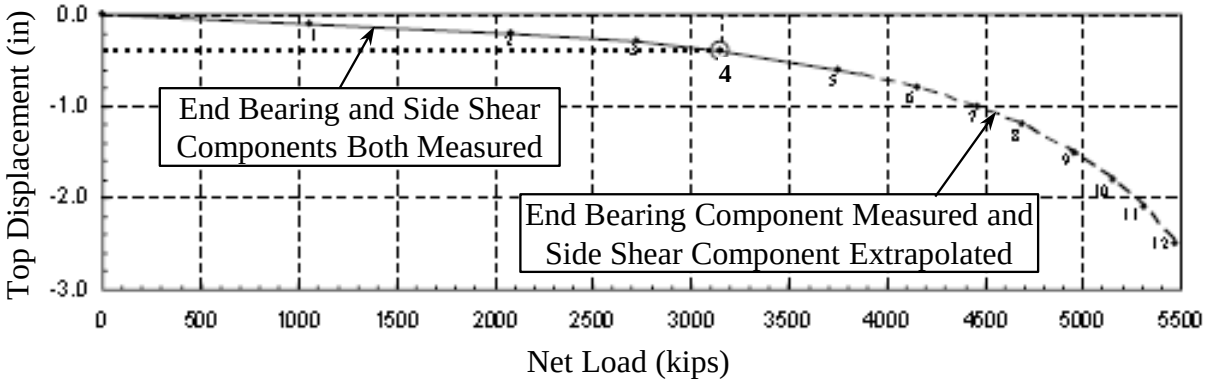

Figure A.2. Equivalent top-loaded displacement curve

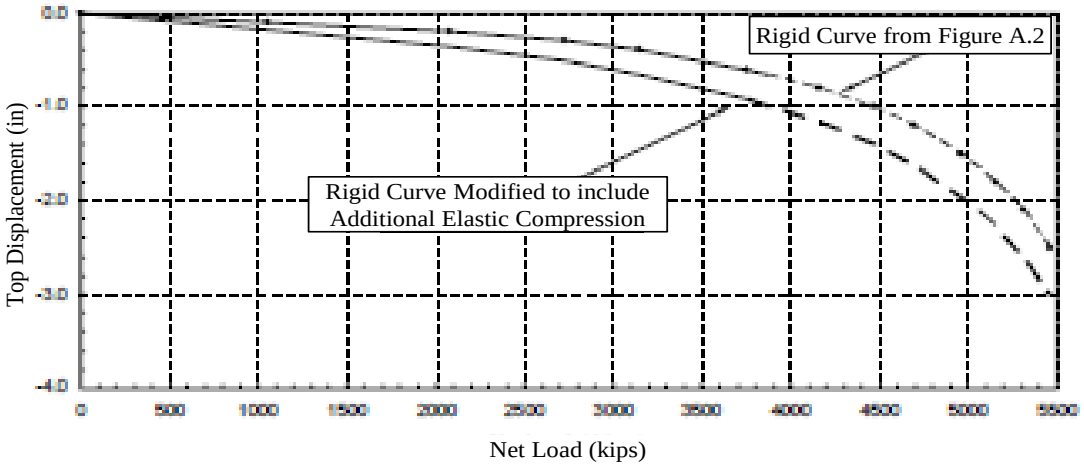

Figure A.3. Equivalent top-loaded displacement curve including elastic compression

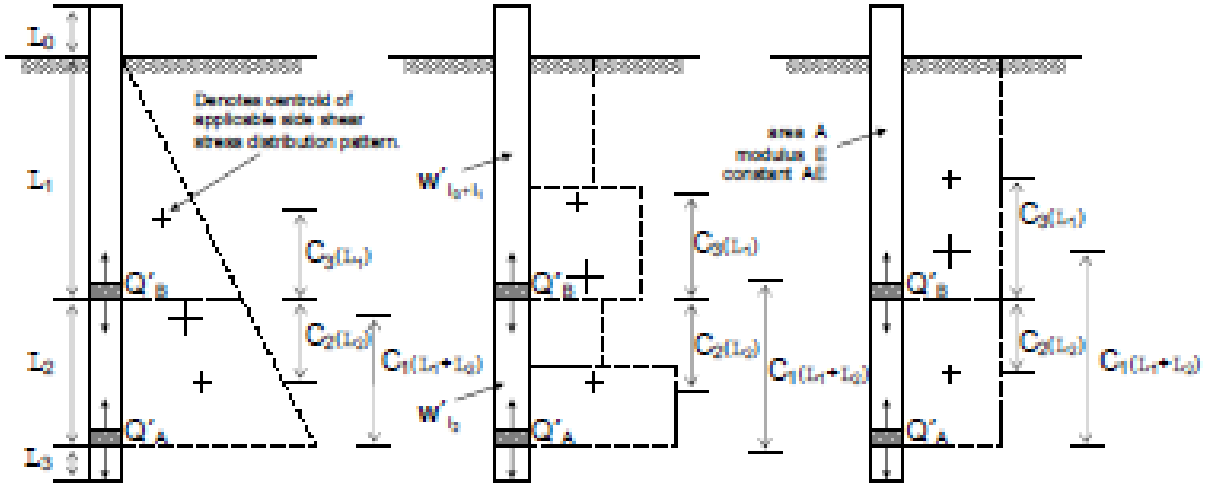

1-Stage Single Level Test (Q'_A only):

$$\delta_{QLT} = \delta_{T(l_1+l_2)}$$

$C_1 = \frac{1}{3}$	Centroid Factor = C_1	$C_1 = \frac{1}{2}$
$\delta_{T(l_1+l_2)} = \frac{1}{3}\frac{Q'_{TA}(l_1+l_2)}{AE}$	$\delta_{T(l_1+l_2)} = C_1\frac{Q'_{TA}(l_1+l_2)}{AE}$	$\delta_{T(l_1+l_2)} = \frac{1}{2}\frac{Q'_{TA}(l_1+l_2)}{AE}$

3-Stage Multi Level Test (Q'_A and Q'_B): $\delta_{QLT} = \delta_{T1_1} + \delta_{L1_2}$

$C_3 = \frac{1}{3}$	Centroid Factor = C_3	$C_3 = \frac{1}{2}$
$\delta_{T1_1} = \frac{1}{3}\frac{Q'_{TB}l_1}{AE}$	$\delta_{T1_1} = C_3\frac{Q'_{TB}l_1}{AE}$	$\delta_{T1_1} = \frac{1}{3}\frac{Q'_{TB}l_1}{AE}$
$C_2 = \frac{1}{3}\left(\frac{3l_1+2l_2}{2l_1+l_2}\right)$	Centroid Factor = C_2	$C_2 = \frac{1}{2}$
$\delta_{L1_2} = \frac{1}{3}\left(\frac{3l_1+2l_2}{2l_1+l_2}\right)\frac{Q'_{LB}l_2}{AE}$	$\delta_{L1_2} = C_2\frac{Q'_{LB}l_2}{AE}$	$\delta_{L1_2} = \frac{1}{2}\frac{Q'_{LB}l_2}{AE}$

Net Loads:

$$Q'_{TA} = Q_{TA} - w'_{l_2+l_1+l_2} \qquad Q'_{TB} = Q_{TB} - w'_{l_2+l_1} \qquad Q'_{LB} = Q'_{LB} + w'_{l_2}$$

w' = pile weight, buoyant where below water table

Figure A.4. Theoretical elastic compression in O-cell test

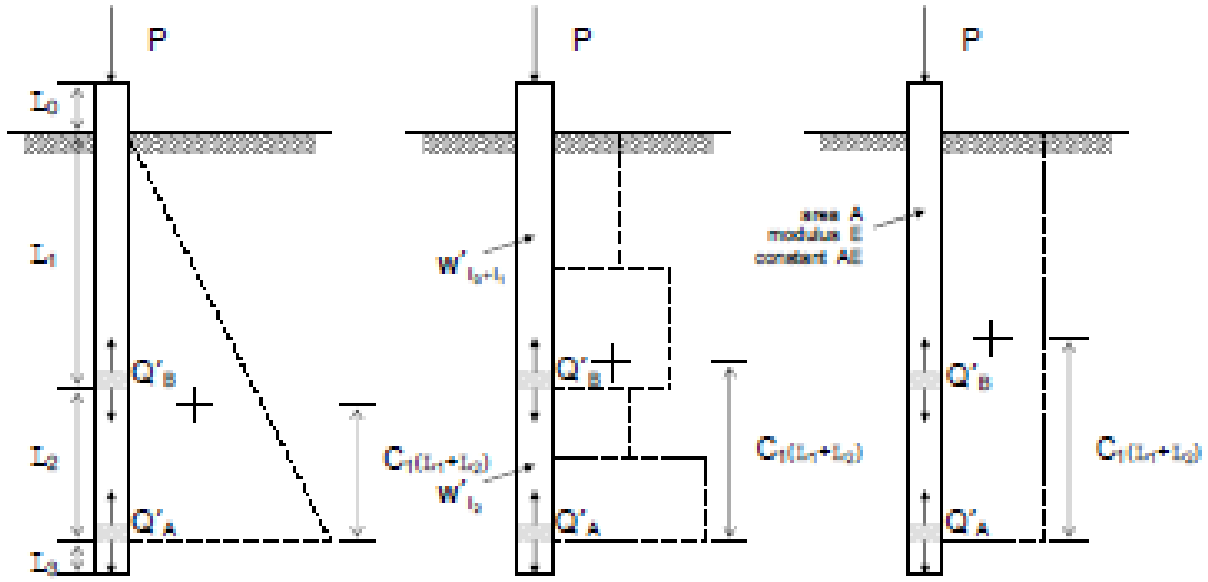

Top Loaded Test: $\delta_{TLT} = \delta_{L_0} + \delta_{L_1+L_2}$

$\delta_{L_0} = \frac{PL_0}{AE}$	$\delta_{L_0} = \frac{PL_0}{AE}$	$\delta_{L_0} = \frac{PL_0}{AE}$
$C_1 = \frac{1}{3}$	Centroid Factor = C_1	$C_1 = \frac{1}{2}$
$\delta_{L_1+L_2} = \frac{(Q'_{LA}+2P)}{3}\frac{(L_1+L_2)}{AE}$	$\delta_{L_1+L_2} = [(C_1)Q'_{LA}+(1-C_1)P]\frac{(L_1+L_2)}{AE}$	$\delta_{L_1+L_2} = \frac{(Q'_{LA}+P)}{2}\frac{(L_1+L_2)}{AE}$

Net and Equivalent Loads:

$Q'_{LA} = Q_{LA} - W'_{L_2+L_3}$ $\quad P_{single} = Q'_{LA}+Q'_{TA}$ $\quad P_{multi} = Q'_{LA}+Q'_{TB}+Q'_{LB}$

Component loads Q selected at the same ($\pm$) Δ_{QLT}.

Figure A.5. Theoretical elastic compression in top-loaded test

APPENDIX B: DSHAFT DATA

Table B.1. A summary of DSHAFT data

ID	State	Shaft Diameter (ft)	Embedded Length (ft)	Concrete f_c' (ksi)	Geomaterials		Rock/IGM Socket	Construction Method	Testing Method	Usable Data
					Shaft	Base				
1	IA	4	67.9	4.47	Clay	IGM[(a)]	Yes	Wet	Osterberg	No
2	IA	3	12.7	5.86	Rock	Rock	Yes	Wet	Osterberg	Yes
3	IA	4	65.8	3.8	Clay+Rock	Rock	Yes	Wet	Osterberg	Yes
4	IA	3.5	72.7	3.44	Mixed+IGM	IGM	Yes	Casing	Osterberg	Yes
5	IA	4	79.3	3.9	Clay+IGM+Rock	Rock	Yes	Wet	Osterberg	Yes
6	IA	2.5	64	3.48	Clay	Clay	No	Casing	Osterberg	Yes
7	IA	3	34	4.1	Clay+Rock	Rock	Yes	Wet	Osterberg	Yes
8	IA	5.5	105.2	3.8	Mixed+Rock	Rock	Yes	Casing	Osterberg	Yes
9	IA	5	66.25	5.78	Sand	Sand	No	Wet	Statnamic	Yes
10	IA	5	55.42	5.58	Mixed	Sand	No	Wet	Statnamic	Yes
11	IA	5	54.78	5.77	Mixed	Sand	No	Wet	Statnamic	Yes
12	MN	6.5	93.9	4.819	Sand+Rock[(a)]	Rock[(a)]	Yes	Wet	Osterberg	No
13	KS	6	49	6.011	IGM	IGM	Yes	Dry	Osterberg	Yes
14	MO	6	40.6	6	IGM+Rock	IGM	Yes	Dry	Osterberg	Yes
15	KS	3.5	19	4.55	IGM	IGM	Yes	Wet	Osterberg	Yes
16	KS	6	34	5.62	IGM	IGM	Yes	Dry	Osterberg	Yes
17	KY	8	105.2	n/a	IGM+Rock	Rock	Yes	Wet	Osterberg	Yes
18	MO	6.5	69.5	7.52	Sand+IGM[(a)]	IGM[(a)]	Yes	Wet	Osterberg	No
19	KS	6	26.24	5.419	IGM	IGM	Yes	Dry	Osterberg	Yes
20	MN	6	55.3	5.9	Sand	Sand	No	Casing	Osterberg	Yes
21	KS	5	93.99	6.47	Sand+IGM[(a)]	IGM[(a)]	Yes	Dry	Osterberg	No
22	MO	3.83	32	4.07	Mixed+Rock[(a)]	Rock[(a)]	Yes	Wet	Osterberg	No
23	MN	4	28	n/a	Sand+Rock[(a)]	Rock[(a)]	Yes	Casing	Osterberg	No
24	IL	5.17	75.112	5.28	IGM+Rock	Rock[(a)]	Yes	Dry	Osterberg	No
25	IL	3.5	37.5	4.1	Clay+IGM	Rock	Yes	Dry	Osterberg	Yes
26	IA	5	75.17	6.01	Sand	Sand	No	Wet	Osterberg	Yes
27	IA	5	75	5.63	Sand	Sand	No	Wet	Osterberg	Yes
28	TN	4	16	5.771	Rock	Rock	Yes	Dry	Osterberg	Yes
29	TN	4	23	5.9	Rock	Rock	Yes	Dry	Osterberg	Yes
30	NV	4	103	n/a	Mixed	Clay	No	Wet	Osterberg	No
31	NE	4	69.09	4.67	Mixed+IGM	IGM	Yes	Wet	Osterberg	No
32	SD	8	107.3	3.256	Sand+IGM[(a)]	IGM[(a)]	Yes	Wet	Osterberg	No

Table B.1. A summary of DSHAFT data (continued)

ID	State	Shaft Diameter (ft)	Embedded Length (ft)	Concrete f_c' (ksi)	Geomaterials		Rock/IGM Socket	Construction Method	Testing Method	Usable Data
					Shaft	Base				
33	CO	3.5	22.6	3.423	IGM	IGM	Yes	Dry	Osterberg	Yes
34	CO	3.5	16	3.193	Clay	IGM	Yes	Dry	Osterberg	Yes
35	CO	4	25.3	3.41	IGM	IGM	Yes	Casing	Osterberg	Yes
36	CO	3.5	40.6	3.936	Rock	Rock	Yes	Casing	Osterberg	Yes
37	CO	4.5	39.7	n/a	Sand+Rock[(a)]	Rock[(a)]	Yes	Dry	Osterberg	No
38	CO	3	11.25	4.88	Rock	Rock	Yes	Dry	Osterberg	Yes
39	CO	4	20	3.54	Rock	Rock	Yes	Casing	Osterberg	Yes
40	IA	4	59.5	3	Clay+IGM[(a)]	IGM[(a)]	Yes	Casing	Osterberg	No
41	MO	4.5	28.4	4.075	Rock[(a)]	Rock[(a)]	Yes	Casing	Osterberg	No

ID – identification number; n/a – not available; IGM – intermediate geomaterial; f_c' – concrete compressive strength; [(a)] – assumed geomaterials.

Table B.2. Subsurface profile and material parameters for test ID No. 1

Soil Layer	Material Description	Embedded Length (ft)	Material Type	Measured Parameters	Estimated Parameters
1	Firm glacial clay	8.2	Clay	n/a	n/a
2	Firm silty glacial clay	7.9	Clay	n/a	n/a
3	Stiff silty clay	20	Clay	n/a	n/a
4	Firm glacial clay	12.1	Clay	n/a	n/a
5	Soft shale	16.4	Cohesive IGM or rock	n/a	n/a
6	Firm shale	3.3	Cohesive IGM or rock	n/a	n/a

Table B.3. Subsurface profile and material parameters for test ID No. 2

Soil Layer	Material Description	Embedded Length (ft)	Material Type	Measured Parameters	Estimated Parameters
1	Slightly weathered dolomite	12.7	Rock	q_u (shaft/toe) = 637.2 ksf; RQD = 93%	$E_m/E_i = 0.90^{(a)}$; $\alpha_E = 0.96^{(d)}$; RMR = $84^{(b)}$; m = $2.4^{(c)}$; s = $0.082^{(c)}$

[(a)] –estimated from Table 2.5; [(b)] –determined from Table 2.12; [(c)] –determined from Table 2.11; [(d)] –estimated from Table 2.4.

Table B.4. Subsurface profile and material parameters for data point ID No. 3

Soil Layer	Material Description	Embedded Length (ft)	Material Type	Measured Parameters	Estimated Parameters
1	Stiff to firm silty glacial clay	39	Clay	N_{60} = 12; c = 1.572 ksf	S_u = 1.572 ksf[(d)]
2	Firm silty clay	4.92	Clay	N_{60} = 22; c = 2.934 ksf	S_u = 2.934 ksf[(d)]
3	Clay shale bedrock	21.88	Rock	q_u (shaft) = 196.56 ksf; q_u (toe) = 110.46 ksf; RQD = 70%	$E_m/E_i = 0.093^{(a)}$; $\alpha_E = 0.536^{(e)}$; RMR = $49^{(b)}$; m = $0.183^{(c)}$; s = $0.00009^{(c)}$

[(a)] –estimated from Table 2.5; [(b)] –determined from Table 2.12; [(c)] –determined from Table 2.11; [(d)] –assumed similar to cohesion; [(e)] –estimated from Table 2.4.

Table B.5. Subsurface profile and material parameters for test ID No. 4

Soil Layer	Material Description	Embedded Length (ft)	Material Type	Measured Parameters	Estimated Parameters
1	Stiff sandy glacial clay	10.496	Clay	N_{60} = 23; c = 3.067 ksf	S_u = 3.067 ksf[(d)]; γ = 0.128 kcf[(a)]
2	Fine to medium sand	32.5	Sand	N_{60} = 14; c = 1.857 ksf	γ = 0.114 kcf[(a)]
3	Clay shale	29.7	Cohesive IGM	q_u (shaft) = 91.584 ksf; q_u (toe) = 93.67 ksf; RQD = 93%	$\sigma_n = 3.9^{(b)}$; RMR = $83^{(c)}$; m = $3.43^{(e)}$; s = $0.082^{(e)}$

[(a)] –estimated using N_{60} based on recommendation provided by Bowles (1996); [(b)] –estimated using Eq. (2-13); [(c)] –determined from Table 2.12; [(d)] –assumed similar to cohesion; [(e)] –determined from Table 2.11.

Table B.6. Subsurface profile and material parameters for data point ID No. 5

Soil Layer	Material Description	Embedded Length (ft)	Material Type	Measured Parameters	Estimated Parameters
1	Silty sandy lean clay	7.9	Clay	N_{60} = 5; c = 0.625 ksf	S_u = 0.625 ksf[(g)]; γ = 0.115 kcf[(a)]
2	Silty lean clay	4.9	Clay	N_{60} = 11; c = 1.429 ksf	S_u = 1.429 ksf[(g)]; γ = 0.127 kcf[(a)]
3	Silty sandy lean clay	27.6	Clay	N_{60} = 15; c = 2 ksf	S_u = 2 ksf[(g)]; γ = 0.138 kcf[(a)]
4	Gravel with sand	1.6	Sand	N_{60} = 100; c = 4 ksf;	γ = 0.15 kcf[(a)]
5	Clay shale	23.3	Cohesive IGM	γ = 0.126 kcf; q_u = 14.4 ksf; RQD = 58%	σ_n = 3.9
6	Coal	3	Cohesive IGM	n/a	q_u = 5.76 ksf[(b)]; σ_n = 3.9
7	Clay shale	7.5	Cohesive IGM	γ = 0.12 kcf; q_u = 5.76 ksf	σ_n = 3.9
8	Carboniferous clay shale	3.5	Rock	γ = 0.131 kcf; q_u (shaft) = 138.63 ksf; q_u (toe) = 191.81 ksf	RQD = 37%[(c)]; E_m/E_i = 0.106[(d)]; RMR = 38[(e)]; m = 0.183[(f)]; s = 0.00009[(f)]

[(a)] –estimated using N_{60} based on recommendation provided by Bowles (1996); [(b)] –assumed similar value of clay shale; [(c)] –estimated based on q_u value; [(d)] –estimated from Table 2.5; [(e)] –determined from Table 2.12; [(f)] –determined from Table 2.11; [(g)] –assumed similar to cohesion.

Table B.7. Subsurface profile and material parameters for data point ID No. 6

Soil Layer	Material Description	Embedded Length (ft)	Material Type	Measured Parameters	Estimated Parameters
1	Firm clay fill	5.9	Clay	N_{60} = 10; c = 1.286 ksf	S_u = 1.286 ksf[(a)]
2	Stiff silty clay	21	Clay	N_{60} = 5; c = 0.625 ksf	S_u = 0.625 ksf[(a)]
3	Firm glacial clay	18.7	Clay	N_{60} = 13; c = 1.715 ksf	S_u = 1.715 ksf[(a)]
4	Very Firm sandy glacial clay	18.4	Clay	N_{60} = 23; c = 3.067 ksf	S_u = 3.067 ksf[(a)]

[(a)] –assumed similar to cohesion.

Table B.8. Subsurface profile and material parameters for data point ID No. 7

Soil Layer	Material Description	Embedded Length (ft)	Material Type	Measured Parameters	Estimated Parameters
1	Lean clay	4	Clay	N_{60} = 20; c = 1.286 ksf	S_u = 1.286 ksf[(a)]; γ = 0.125 kcf[(b)]
2	Lean clay with sand	9	Clay	N_{60} = 10; c = 2.667 ksf	S_u = 2.667 ksf[(a)]; γ = 0.125 kcf[(b)]
3	Mod weathered limestone	1.1	Rock	q_u = 555.84 ksf;	RQD = 70%[(c)]; E_m/E_i = 0.7[(d)]; α_E = 0.88[(e)]
4	Fresh limestone	2.3	Rock	q_u = 1388.16 ksf; RQD = 79%	E_m/E_i = 0.79[(d)]; E_m/E_i = 0.79[(d)]; α_E = 0.916[(e)]
5	Calcareous sandstone	4.3	Rock	q_u = 862.56 ksf; RQD = 83%	E_m/E_i = 0.83[(d)]; α_E = 0.932[(e)]
6	Fractured Limestone with weathered shale	1.3	Rock	q_u = 1175.04 ksf	RQD = 50%[(c)]; E_m/E_i = 0.15[(d)]; α_E = 0.55[(e)]
7	Fresh limestone	12	Rock	q_u (shaft) = 817.2 ksf; q_u (toe) = 760.32 ksf; RQD = 96%	E_m/E_i = 0.96[(d)]; α_E = 0.984[(e)]

[(a)] –assumed similar to cohesion; [(b)] –estimated using N_{60} based on recommendation provided by Bowles (1996); [(c)] –estimated based on q_u value; [(d)] –estimated from Table 2.5; [(e)] –estimated from Table 2.4.

Table B.9. Subsurface profile and material parameters for data point ID No. 8

Soil Layer	Material Description	Embedded Length (ft)	Material Type	Measured Parameters	Estimated Parameters
1	Silty clay	10	Clay	N_{60} = 12; c = 1.572 ksf	S_u = 1.572 ksf[(a)]; γ = 0.13 kcf[(b)]
2	Silt with minor sand	17	Clay	N_{60} = 2; c = 0.25 ksf	S_u = 0.25 ksf[(a)]; γ = 0.121 kcf[(b)]
3	Fine to medium sand with fine gravel	42	Sand	N_{60} = 30; c = 4 ksf	γ = 0.13 kcf[(b)]
4	Medium to coarse sand with gravel	21.5	Sand	N_{60} = 21; c = 2.8 ksf	γ = 0.121 kcf[(b)]
5	Fresh limestone	14.7	Rock	q_u (shaft) = 510.34 ksf; q_u (toe) = 553.40 ksf; RQD = 77%	E_m/E_i = 0.96[(c)]; α_E = 0.984[(d)]; RMR = 60[(e)]; m = 0.58[(f)]; s = 0.0029[(f)]

[(a)] –assumed similar to cohesion; [(b)] –estimated using N_{60} based on recommendation provided by Bowles (1996); [(c)] –estimated from Table 2.5; [(d)] –estimated from Table 2.4; [(e)] –determined from Table 2.12; [(f)] –determined from Table 2.11.

Table B.10. Subsurface profile and material parameters for data point ID No. 9

Soil Layer	Material Description	Embedded Length (ft)	Material Type	Measured Parameters	Estimated Parameters
1	Stiff silty clay	10	Clay	N_{60} = 7; c = 0.875 ksf	S_u = 0.875 ksf[(a)]; γ = 0.125 kcf[(b)]
2	Soft to stiff silty clay	10	Clay	N_{60} = 4; c = 0.5 ksf	S_u = 0.5 ksf[(a)]; γ = 0.110 kcf[(b)]
3	Silty fine sand	10	Sand	N_{60} = 13; c = 1.715 ksf	γ = 0.113 kcf[(b)]
4	Fine sand	25	Sand	N_{60} = 20; c = 2.667 ksf	γ = 0.120 kcf[(b)]
5	Soft silty sand	5	Sand	N_{60} = 2; c = 0.25 ksf	γ = 0.085 kcf[(b)]
6	Coarse sand	6.25	Sand	N_{60} = 16; c = 2.134 ksf	γ = 0.116 kcf[(b)]

[(a)] –assumed similar to cohesion; [(b)] –estimated using N_{60} based on recommendation provided by Bowles (1996).

Table B.11. Subsurface profile and material parameters for data point ID No. 10

Soil Layer	Material Description	Embedded Length (ft)	Material Type	Measured Parameters	Estimated Parameters
1	Stiff silty clay	5	Clay	N_{60} = 12; c = 1.572 ksf	S_u = 1.572 ksf[(a)]; γ = 0.130 kcf[(b)]
2	Soft to stiff silty clay	10	Clay	N_{60} = 7; c = 0.875 ksf	S_u = 0.875 ksf[(a)]; γ = 0.127 kcf[(b)]
3	Soft silty clay	5	Clay	N_{60} = 5; c = 0.625 ksf	S_u = 0.625 ksf[(a)]; γ = 0.122 kcf[(b)]
4	Fine sand	35	Sand	N_{60} = 15; c = 2 ksf	γ = 0.115 kcf[(b)]
5	Coarse sand with trace gravel	0.42	Sand	N_{60} = 18; c = 2.4 ksf	γ = 0.118 kcf[(b)]

[(a)] –assumed similar to cohesion; [(b)] –estimated using N_{60} based on recommendation provided by Bowles (1996).

Table B.12. Subsurface profile and material parameters for data point ID No. 11

Soil Layer	Material Description	Embedded Length (ft)	Material Type	Measured Parameters	Estimated Parameters
1	Stiff silty clay	5	Clay	N_{60} = 14; c = 0.625 ksf	S_u = 0.625 ksf[(a)]; γ = 0.135 kcf[(b)]
2	Soft to stiff silty clay	15	Clay	N_{60} = 5; c = 1.857 ksf	S_u = 1.857 ksf[(a)]; γ = 0.115 kcf[(b)]
3	Fine sand	34.78	Sand	N_{60} = 17; c = 2.267 ksf	γ = 0.117 kcf[(b)]

[(a)] –assumed similar to cohesion; [(b)] –estimated using N_{60} based on recommendation provided by Bowles (1996).

Table B.13. Subsurface profile and material parameters for data point ID No. 12

Soil Layer	Material Description	Embedded Length (ft)	Material Type	Measured Parameters	Estimated Parameters
1	Fill/Sand	10	Sand	N_{60} = 14	γ = 0.114 kcf[(a)]
2	Sand with gravel dense/saturated	24	Sand	N_{60} = 57	γ = 0.15 kcf[(a)]
3	Fine sand w/ gravel	18	Sand	N_{60} = 32	γ = 0.112 kcf[(a)]
4	Sandstone	41.9	n/a	n/a	n/a

[(a)] –estimated using N_{60} based on recommendation provided by Bowles (1996).

Table B.14. Subsurface profile and material parameters for data point ID No. 13

Soil Layer	Material Description	Embedded Length (ft)	Material Type	Measured Parameters	Estimated Parameters
1	Fine grained silty sand	7	Sand	n/a	n/a
2	Medium to coarse grained silty sand	15	Sand	n/a	n/a
3	Shale	22	Cohesive IGM	q_u = 15.42 ksf; RQD = 47.5%	$\alpha = 0.21^{(a)}$
4	Sandstone	2	Cohesive IGM	q_u = 41.54 ksf; RQD = 52%	$\alpha = 0.15^{(a)}$
5	Shale	3	Cohesive IGM	q_u (shaft) = 76.21 ksf; q_u (toe) = 76.21 ksf; RQD = 52%	$\alpha = 0.10^{(a)}$; m = $0.365^{(b)}$; s = $0.0009^{(b)}$

(a) – determined from Figure 2.1; (b) –determined from Table 2.11.

Table B.15. Subsurface profile and material parameters for data point ID No. 14

Soil Layer	Material Description	Embedded Length (ft)	Material Type	Measured Parameters	Estimated Parameters
1	Weathered chanute shale	7	Cohesive IGM	q_u = 14.2 ksf	RQD = 0%; $\alpha = 0.0^{(a)}$; $\phi = 0.45^{(b)}$
2	Unweathered chanute shale	11	Cohesive IGM	q_u = 19.6 ksf; RQD = 14%	$\alpha = 0.16^{(a)}$; $\phi = 0.45^{(b)}$
3	Cement city limestone	5	Rock	q_u = 1334 ksf; RQD = 28%	$\alpha = 0.07^{(a)}$; $\phi = 0.49^{(b)}$
4	Quivira shale	6	Cohesive IGM	q_u = 57.2 ksf; RQD = 14%	$\alpha = 0.12^{(a)}$; $\phi = 0.45^{(b)}$
5	Westerville limestone	7	Rock	q_u = 1850 ksf; RQD = 58%	$\alpha = 0.08^{(a)}$; $\phi = 0.7^{(b)}$
6	Weathered shale	4.6	Cohesive IGM	q_u (shaft) = 102.4 ksf; q_u (toe) = 99.5 ksf; RQD = 30%	$\alpha = 0.1^{(a)}$; $\phi = 0.50^{(b)}$

(a) – determined from Figure 2.1; (b) –determined from Table 2.3Table 2.11.

Table B.16. Subsurface profile and material parameters for data point ID No. 15

Soil Layer	Material Description	Embedded Length (ft)	Material Type	Measured Parameters	Estimated Parameters
1	Sandstone	0	n/a	n/a	n/a
2	Competent Shale	12.5	Cohesive IGM	q_u = 30.3 ksf; RQD = 20%	$\alpha = 0.12^{(a)}$; $\phi = 0.45^{(c)}$
3	Shaley sandstone	6.5	Cohesive IGM	q_u (shaft) = 34.16 ksf; q_u (toe) = 34.16 ksf; RQD = 85%	$\alpha = 0.115^{(a)}$; $\phi = 0.925^{(b)}$

(a) – determined from Figure 2.1; (b) –determined from Table 2.3Table 2.11.

Table B.17. Subsurface profile and material parameters for data point ID No. 16

Soil Layer	Material Description	Embedded Length (ft)	Material Type	Measured Parameters	Estimated Parameters
1	Silty Clay (with casing)	4.8	n/a	n/a	n/a
2	Shale (with casing)	6.42	n/a	n/a	n/a
3	Shale	22.78	Cohesive IGM	q_u (shaft) = 36.74 ksf; q_u (toe) = 50.4 ksf	RQD = 100%; $\alpha = 0.12^{(a)}$; $\phi = 0.45^{(b)}$

(a) – determined from Figure 2.1; (b) –determined from Table 2.3

Table B.18. Subsurface profile and material parameters for data point ID No. 17

Soil Layer	Material Description	Embedded Length (ft)	Material Type	Measured Parameters	Estimated Parameters
1	Overburnden soil	70.8	n/a	n/a	n/a
2	Shale soft to very soft	16	Cohesive IGM	q_u = 43.2 ksf; RQD = 53%	$\alpha = 0.16^{(a)}$; $\phi = 0.64^{(b)}$
3	Coal	2	Cohesive IGM	q_u = 28.8 ksf; RQD = 60%	$\alpha = 0.22^{(a)}$; $\phi = 0.725^{(b)}$
4	Gray Shale-soft	7.9	Cohesive IGM	q_u = 43.2 ksf; RQD = 60%	$\alpha = 0.16^{(a)}$; $\phi = 0.725^{(b)}$
5	Gray Shale-medium hard to hard	1.6	Rock	q_u = 187.5 ksf; RQD = 60%	$\alpha_E = 0.763^{(c)}$
6	Gray Shale-soft	2.3	Rock	q_u = 144 ksf; RQD = 60%	$\alpha_E = 0.763^{(c)}$
7	Gray sandy Shale-soft	4.6	Cohesive IGM	q_u = 72 ksf; RQD = 58%	$\alpha = 0.14^{(a)}$; $\phi = 0.70^{(b)}$
8	Gray Shale-medium hard to hard	0	Rock	q_u (toe) = 144 ksf; RQD = 94%	RMR = $73^{(d)}$; m = $1.865^{(e)}$; s = $0.0346^{(e)}$

(a) – determined from Figure 2.1; (b) –determined from Table 2.3Table 2.11; (c) –estimated from Table 2.4; (d) – determined from Table 2.12; (e) –determined from Table 2.11.

Table B.19. Subsurface profile and material parameters for data point ID No. 18

Soil Layer	Material Description	Embedded Length (ft)	Material Type	Measured Parameters	Estimated Parameters
1	Medium and coarse dense sand	18.5	Sand	n/a	n/a
2	Clay shale	51	n/a	n/a	n/a

Table B.20. Subsurface profile and material parameters for data point ID No. 19

Soil Layer	Material Description	Embedded Length (ft)	Material Type	Measured Parameters	Estimated Parameters
1	Overburden alluvium soil	0	n/a	n/a	n/a
2	Shale	10.7	Cohesive IGM	q_u = 25.8 ksf; RQD = 39.33%	$\alpha = 0.13^{(a)}$; $\phi = 0.547^{(b)}$
3	Shale	9.5	Cohesive IGM	N_{60} = 86; q_u = 17.11 ksf; RQD = 74%	$\alpha = 0.15^{(a)}$; $\phi = 0.87^{(b)}$
4	Sandstone	6.04	Cohesionless IGM	q_u = 4.24 ksf; RQD = 47%	$N_{60} = 86^{(c)}$; $K_o = 0.927^{(d)}$; $\phi' = 61.8^{o}$ (d)

(a) – determined from Figure 2.1; (b) – determined from Table 2.3Table 2.11; (c) – assumed the same SPT N-value of overlaying shale; (d) – refer to Eq. (2-14).

Table B.21. Subsurface profile and material parameters for data point ID No. 20

Soil Layer	Material Description	Embedded Length (ft)	Material Type	Measured Parameters	Estimated Parameters
1	Loamy sand	6	Sand	$N_{60} = 8$	$\gamma = 0.105$ kcf[(a)]
2	Sand with organic matter	3	Sand	$N_{60} = 10$	$\gamma = 0.115$ kcf[(a)]
3	Sandy loam	2	Sand	$N_{60} = 8$	$\gamma = 0.107$ kcf[(a)]
4	Sand	5	Sand	$N_{60} = 19$	$\gamma = 0.119$ kcf[(a)]
5	Sand	9	Sand	$N_{60} = 32$	$\gamma = 0.112$ kcf[(a)]
6	Sand with gravel	4	Sand	$N_{60} = 30$	$\gamma = 0.130$ kcf[(a)]
7	sand and gravel	6	Sand	$N_{60} = 25$	$\gamma = 0.125$ kcf[(a)]
8	Loamy fine sand	5	Sand	$N_{60} = 37$	$\gamma = 0.121$ kcf[(a)]
9	Sand with gravel	5	Sand	$N_{60} = 60$	$\gamma = 0.150$ kcf[(a)]
10	Loamy sand	5	Sand	$N_{60} = 39$	$\gamma = 0.124$ kcf[(a)]
11	Loamy sand	5.3	Sand	$N_{60} = 46$	$\gamma = 0.134$ kcf[(a)]

[(a)] – estimated using N_{60} based on recommendation provided by Bowles (1996).

Table B.22. Subsurface profile and material parameters for data point ID No. 21

Soil Layer	Material Description	Embedded Length (ft)	Material Type	Measured Parameters	Estimated Parameters
1	Silty shale	93.99	n/a	n/a	n/a

Table B.23. Subsurface profile and material parameters for data point ID No. 22

Soil Layer	Material Description	Embedded Length (ft)	Material Type	Measured Parameters	Estimated Parameters
1	Weathered shaley limestone	4.9	n/a	n/a	n/a
2	Fine grained sandstone	14.8	n/a	n/a	n/a
3	Moderately hard shale	12.3	n/a	n/a	n/a

Table B.24. Subsurface profile and material parameters for data point ID No. 23

Soil Layer	Material Description	Embedded Length (ft)	Material Type	Measured Parameters	Estimated Parameters
1	Friable sandstone	28	n/a	n/a	n/a

Table B.25. Subsurface profile and material parameters for data point ID No. 24

Soil Layer	Material Description	Embedded Length (ft)	Material Type	Measured Parameters	Estimated Parameters
1	Sandstone	0.72	n/a	n/a	n/a
2	GR Laminated Shale	17.32	Cohesive IGM	q_u = 16.71 ksf; RQD = 50%	$\alpha = 0.16^{(a)}$; $\phi = 0.6^{(b)}$
3	GR to GRN GR Massive shale	2	Cohesive IGM	q_u = 8.35 ksf; RQD = 63%	$\alpha = 0.2^{(a)}$; $\phi = 0.7625^{(b)}$
4	LT GR to GRN GR Laminated shale	3	Cohesive IGM	q_u = 16.71 ksf; RQD = 71%	$\alpha = 0.16^{(a)}$; $\phi = 0.85^{(b)}$
5	Massive silty shale	17	Rock	q_u = 223.47 ksf; RQD = 75%	$\alpha_E = 0.613^{(c)}$
6	Francis creek shale	35.136	Rock	q_u (shaft) = 223.4 ksf; RQD (shaft) = 75%; (No geomaterial information beneath the shaft base)	$\alpha_E = 0.613^{(c)}$

(a) – determined from Figure 2.1; (b) –determined from Table 2.3Table 2.11; (c) –estimated from Table 2.4.

Table B.26. Subsurface profile and material parameters for data point ID No. 25

Soil Layer	Material Description	Embedded Length (ft)	Material Type	Measured Parameters	Estimated Parameters
1	Sandy loam and shaley clay	9.84	Clay	N_{60} = 9	$S_u = 0.989$ ksf$^{(f)}$; $\gamma = 0.127$ kcf$^{(g)}$
2	Very dense shale	2.73	Cohesive IGM	q_u = 9 ksf; RQD = 0%	$\alpha = 0.2^{(a)}$; $\phi = 0.45^{(b)}$
3	Shale	18.27	Cohesive IGM	q_u = 9 ksf; RQD = 0%	$\alpha = 0.2^{(a)}$; $\phi = 0.45^{(b)}$
4	Sandstone	6.65	Cohesive IGM	q_u = 62 ksf; RQD = 35%	$\alpha = 0.14^{(a)}$; $\phi = 0.525^{(b)}$
5	Sandstone (toe)	0	Rock	q_u (toe) = 389 ksf; RQD (toe) = 67%	RMR = 65$^{(d)}$; m = 0.821$^{(e)}$; s = 0.0029$^{(e)}$

(a) – determined from Figure 2.1; (b) –determined from Table 2.3Table 2.11; (c) –estimated from Table 2.4; (d) – determined from Table 2.12; (e) –determined from Table 2.11; (f) – estimated from Eq. (2-9); (g) – estimated using N_{60} based on recommendation provided by Bowles (1996).

Table B.27. Subsurface profile and material parameters for data point ID No. 26

Soil Layer	Material Description	Embedded Length (ft)	Material Type	Measured Parameters	Estimated Parameters
1	Lean clay	10	Clay	N_{60} = 4	$S_u = 0.424$ ksf$^{(a)}$; $\gamma = 0.120$ kcf$^{(b)}$
2	Fine sand	8.5	Sand	N_{60} = 4	$\gamma = 0.090$ kcf$^{(b)}$
3	Silty clay	5	Clay	N_{60} = 3	$S_u = 0.350$ ksf$^{(a)}$; $\gamma = 0.110$ kcf$^{(b)}$
4	Fine sand	51.67	Sand	N_{60} = 11	$\gamma = 0.110$ kcf$^{(b)}$

(a) – estimated using Eq. (2-9); (b) – estimated using N_{60} based on recommendation provided by Bowles (1996).

Table B.28. Subsurface profile and material parameters for data point ID No. 27

Soil Layer	Material Description	Embedded Length (ft)	Material Type	Measured Parameters	Estimated Parameters
1	Lean clay	10	Clay	$N_{60} = 7$	$S_u = 0.742$ ksf[(a)]; $\gamma = 0.125$ kcf[(b)]
2	Fine sand	8.5	Sand	$N_{60} = 5$	$\gamma = 0.094$ kcf[(b)]
3	Silty clay	5	Clay	$N_{60} = 5$	$S_u = 0.53$ ksf[(a)]; $\gamma = 0.115$ kcf[(b)]
4	Fine sand	51.5	Sand	$N_{60} = 13$	$\gamma = 0.113$ kcf[(b)]

[(a)] – estimated using Eq. (2-9); [(b)] – estimated using N_{60} based on recommendation provided by Bowles (1996).

Table B.29. Subsurface profile and material parameters for data point ID No. 28

Soil Layer	Material Description	Embedded Length (ft)	Material Type	Measured Parameters	Estimated Parameters
1	Limestone	2.5	Rock	$q_u = 1744.63$ ksf; RQD = 26%	$\alpha_E = 0.47$[(a)]
2	Limestone	5	Rock	$q_u = 904.56$ ksf; RQD = 26%	$\alpha_E = 0.47$[(a)]
3	Limestone	5	Rock	$q_u = 1218.43$ ksf; RQD = 38%	$\alpha_E = 0.51$[(a)]
4	Limestone	3.5	Rock	q_u (shaft) = 775.44 ksf; RQD (shaft) = 37%; q_u (toe) = 775.44 ksf; RQD (toe) = 75%	$\alpha_E = 0.507$[(a)]; RMR = 64[(b)]; m = 0.554[(c)]; s = 0.0028[(c)]

[(a)] –estimated from Table 2.4; [(b)] –determined from Table 2.12; [(c)] –determined from Table 2.11.

Table B.30. Subsurface profile and material parameters for data point ID No. 29

Soil Layer	Material Description	Embedded Length (ft)	Material Type	Measured Parameters	Estimated Parameters
1	Limestone	6	Rock	n/a	$\alpha_E = 0.45$[(a)]
2	Limestone	5	Rock	$q_u = 1080$ ksf; RQD = 19%	$\alpha_E = 0.523$[(a)]
3	Limestone	5	Rock	$q_u = 2934$ ksf; RQD = 42%	$\alpha_E = 0.55$[(a)]
4	Limestone	5	Rock	$q_u = 1720.8$ ksf; RQD = 52%	$\alpha_E = 0.55$[(a)]
5	Limestone	2	Rock	q_u (shaft) = 3024 ksf; RQD (shaft) = 54%; q_u (toe) = 2966.4 ksf; RQD (toe) = 60%	$\alpha_E = 0.55$[(a)]; RMR = 72[(b)]; m = 1.13[(c)]; s = 0.027[(c)]

[(a)] – determined from Table 2.4; [(b)] –determined from Table 2.12; [(c)] –determined from Table 2.11.

Table B.31. Subsurface profile and material parameters for data point ID No. 30

Soil Layer	Material Description	Embedded Length (ft)	Material Type	Measured Parameters	Estimated Parameters
1	Caliche	3	Sand	N_{60} = 50	γ = 0.15 kcf[(a)]
2	Clayey sand	8	Sand	N_{60} = 29	γ = 0.129 kcf[(a)]
3	Caliche	6.5	Sand	N_{60} = 200	γ = 0.15 kcf[(a)]
4	Clay w/ sand	5.5	Clay	N_{60} = 6	γ = 0.12 kcf[(a)]; S_u = 0.636 ksf[(b)]
5	Silty, clayey sand	5	Sand	N_{60} = 16	γ = 0.116 kcf[(a)]
6	Clayey sand	10	Sand	N_{60} = 15	γ = 0.115 kcf[(a)]
7	Sandy clay	3	Clay	N_{60} = 60	γ = 0.14 kcf[(a)]; S_u = 6.36 ksf[(b)]
8	Caliche	2	Sand	N_{60} = 50	γ = 0.15 kcf[(a)]
9	Clayey sand	6	Sand	N_{60} = 24	γ = 0.124 kcf[(a)]
10	Caliche	1.5	Sand	N_{60} = 150	γ = 0.15 kcf[(a)]
11	Sandy clay	5	Clay	N_{60} = 19	γ = 0.124 kcf[(a)]; S_u = 2.014 ksf[(b)]
12	Silty clay	5	Clay	N_{60} = 18	γ = 0.124 kcf[(a)]; S_u = 1.908 ksf[(b)]
13	Sandy clay	6.5	Clay	N_{60} = 40	γ = 0.14 kcf[(a)]; S_u = 4.24 ksf[(b)]
14	Silty sand	4	Sand	N_{60} = 11	γ = 0.111 kcf[(a)]
15	Sandy clay	7	Clay	N_{60} = 25	γ = 0.131 kcf[(a)]; S_u = 2.65 ksf[(b)]
16	Silty sand	3	Sand	N_{60} = 8	γ = 0.107 kcf[(a)]
17	Sandy clay	22	Clay	n/a	n/a)

[(a)] – estimated using N_{60} based on recommendation provided by Bowles (1996); [(b)] – estimated using Eq. (2-9)

Table B.32. Subsurface profile and material parameters for data point ID No. 31

Soil Layer	Material Description	Embedded Length (ft)	Material Type	Measured Parameters	Estimated Parameters
1	Fine to medium sand	35	Sand	N_{60} = 17	n/a
2	Fat clay	6	Clay	N_{60} = 12; q_u = 1 ksf	n/a
3	Sandy lean clay	9	Clay	N_{60} = 13	n/a
4	Fine to medium sand-weathered sandstone	11	Sand	N_{60} = 47	n/a
5	Lean clay-weathered shale	8.9	Cohesive IGM	q_u = 7.5 ksf	n/a

Table B.33. Subsurface profile and material parameters for data point ID No. 32

Soil Layer	Material Description	Embedded Length (ft)	Material Type	Measured Parameters	Estimated Parameters
1	Loose to medium dense sand	21	Sand	N_{60} = 11	n/a
2	Medium dense fine grained sand	11.5	Sand	N_{60} = 20	n/a
3	Hard shale	74.8	n/a	N_{60} = 48	n/a

Table B.34. Subsurface profile and material parameters for data point ID No. 33

Soil Layer	Material Description	Embedded Length (ft)	Material Type	Measured Parameters	Estimated Parameters
1	Firm to medium claystone bedrock	10	Cohesive IGM	N_{60} = 32; q_u = 8.3 ksf; RQD = 50%	$\alpha = 0.2^{(a)}$; $\phi = 0.6^{(b)}$
2	Medium hard to hard brown claystone with sandstone	6.1	Cohesive IGM	N_{60} = 55; q_u = 12.3 ksf; RQD = 50%	$\alpha = 0.22^{(a)}$; $\phi = 0.6^{(b)}$
3	Medium hard to hard brown claystone with sandstone	0	Cohesionless IGM	N_{60} = 58; q_u = 13.1 ksf; RQD = 50%	n/a

(a) – determined from Figure 2.1; (b) –determined from Table 2.3Table 2.11.

Table B.35. Subsurface profile and material parameters for data point ID No. 34

Soil Layer	Material Description	Embedded Length (ft)	Material Type	Measured Parameters	Estimated Parameters
1	Medium hard brown silty and very weak sandstone bedrock	2	Sand	N_{60} = 30	$\gamma = 0.12$ kcf$^{(a)}$
2	Medium hard claystone bedrock layer (olive to light gray)	14	Clay	N_{60} = 37; q_u = 6.05 ksf; RQD = 50%	$\gamma = 0.106$ kcf$^{(a)}$; S_u = 3.024 ksf$^{(b)}$
3	Hard claystone bedrock (toe)	0	Cohesive IGM	N_{60} (toe) = 61; q_u (toe) = 16.85 ksf; RQD (toe) = 50%	$\gamma = 0.111$ kcf$^{(a)}$

(a) – estimated using N_{60} based on recommendation provided by Bowles (1996); (b) – estimated using Eq. (2-9).

Table B.36. Subsurface profile and material parameters for data point ID No. 35

Soil Layer	Material Description	Embedded Length (ft)	Material Type	Measured Parameters	Estimated Parameters
1	Sandy and clayey sand soils	4.5	Sand	n/a	n/a
2	Very hard sandy to very sandy claystone with very clayey sandstone interbeds	20.8	Cohesive IGM	N_{60} = 150; q_u = 63.94 ksf; RQD = 80%	$\alpha = 0.1^{(a)}$; $\phi = 0.9^{(b)}$
3	Very hard dark gray and very sandy claystone	0	Cohesive IGM	N_{60} = 120; q_u = 71 ksf; RQD = 80%	n/a

(a) – determined from Figure 2.1; (b) –determined from Table 2.3Table 2.11; (c) –determined from Table 2.12; (d) – determined from Table 2.11.

Table B.37. Subsurface profile and material parameters for data point ID No. 36

Soil Layer	Material Description	Embedded Length (ft)	Material Type	Measured Parameters	Estimated Parameters
1	Light brown claystone	3	Rock	N_{60} = 200; q_u = 97.056 ksf; RQD = 75%	$\alpha_E = 0.90^{(a)}$
2	Very clayey, fine to medium grained, well cemented sandstone	15	Rock	N_{60} = 218; q_u = 293.04 ksf; RQD = 85%	$\alpha_E = 0.94^{(a)}$
3	Blue clayey to very clayey sandstone bedrock	12.1	Rock	N_{60} = 166; q_u (shaft) = 219.024 ksf; q_u (toe) = 219.024 ksf; RQD = 75%	$\alpha_E = 0.90^{(a)}$; RMR = $58^{(b)}$; m = $0.396^{(c)}$; s = $0.001577^{(c)}$

(a) – determined from Table 2.4; (b) –determined from Table 2.12; (c) –determined from Table 2.11.

Table B.38. Subsurface profile and material parameters for data point ID No. 37

Soil Layer	Material Description	Embedded Length (ft)	Material Type	Measured Parameters	Estimated Parameters
1	Silty sandy gravel-overburden	5.9	n/a	n/a	n/a
2	Weathered shale bedrock	3.60	n/a	n/a	n/a
3	Shale bedrock	41.50	n/a	RQD = 89%	n/a

Table B.39. Subsurface profile and material parameters for data point ID No. 38

Soil Layer	Material Description	Embedded Length (ft)	Material Type	Measured Parameters	Estimated Parameters
1	Pierre Shale Bedrock	11.25	Rock	q_u (shaft) = 373.104 ksf; q_u (toe) = 346.34 ksf; RQD = 94%	$\alpha_E = 0.976^{(a)}$; RMR = $48^{(b)}$; m = $0.699^{(c)}$; s = $0.002543^{(c)}$

(a) – determined from Table 2.4; (b) –determined from Table 2.12; (c) –determined from Table 2.11.

Table B.40. Subsurface profile and material parameters for data point ID No. 39

Soil Layer	Material Description	Embedded Length (ft)	Material Type	Measured Parameters	Estimated Parameters
1	Pierre Shale Bedrock	20	Rock	q_u (shaft) = 406.46 ksf; RQD (shaft) = 75.5%; q_u (toe) = 335.98 ksf; RQD (toe) = 88%	$\alpha_E = 0.902^{(a)}$; RMR = $48^{(b)}$; m = $0.699^{(c)}$; s = $0.002447^{(c)}$

(a) – determined from Table 2.4; (b) –determined from Table 2.12; (c) –determined from Table 2.11.

Table B.41. Subsurface profile and material parameters for data point ID No. 40

Soil Layer	Material Description	Embedded Length (ft)	Material Type	Measured Parameters	Estimated Parameters
1	Hard shale	32.5	Rock	$N_{60} > 100$	n/a

Table B.42. Subsurface profile and material parameters for data point ID No. 41

Soil Layer	Material Description	Embedded Length (ft)	Material Type	Measured Parameters	Estimated Parameters
1	Clay Shale, Moderately Hard	0.77	Clay	q_u = 7.056 ksf; RQD = 100%	n/a
2	Fine Grained Limestone, Hard	1.18	n/a	RQD = 100%	n/a
3	Clay Shale, Moderately Hard	0.2	n/a	RQD = 100%	n/a
4	Clay Shale and Coal	2.39	n/a	n/a	n/a
5	Clay Shale, Soft	0.36	n/a	n/a	n/a
6	Clay Shale, Hard and Brittle	0.59	n/a	n/a	n/a
7	Fine Grained Limestone, Very Hard	0.33	n/a	n/a	n/a
8	Clay Shale, Soft	8.86	Cohesive IGM	q_u = 35.42 ksf	n/a
9	Shaly Limestone, Very Hard	1.12	n/a	n/a	n/a
10	Clay Shale, Moderately Hard but Brittle	7.68	Cohesive IGM	q_u = 16.416 ksf	n/a
11	Silt Shale, Hard	2.79	n/a	n/a	n/a
12	Clay Shale, Moderately Hard	0.66	n/a	n/a	n/a
13	Shale to Coal, Moderately Hard	0.13	n/a	n/a	n/a
14	Soft clay shale	1.34	Cohesive IGM	q_u = 19 ksf	n/a

APPENDIX C: SUMMARY OF ESTIMATED SHAFT RESISTANCES

Table C.1. Estimated shaft resistances for test ID No. 1

Soil Layer	Geomaterial	Unit Side Resistance (ksf)	Side Resistance (kips)	Unit End Bearing (ksf)	End Bearing (kip)	Total Resistance (kip)
1	Clay	n/a	n/a	n/a	n/a	n/a
2	Clay	n/a	n/a	n/a	n/a	n/a
3	Clay	n/a	n/a	n/a	n/a	n/a
4	Clay	n/a	n/a	n/a	n/a	n/a
5	Cohesive IGM or rock	n/a	n/a	n/a	n/a	n/a
6	Cohesive IGM or rock	n/a	n/a	n/a	n/a	n/a

Table C.2. Estimated shaft resistances for data point ID No. 2

Soil Layer	Geomaterial	Unit Side Resistance (ksf)	Side Resistance (kips)	Unit End Bearing (ksf)	End Bearing (kip)	Total Resistance (kip)
1	Rock	22.93	2745	954.25[(a)]	5996[(b)]	8741

[(a)] – average value of intact and fracture rock mass; [(b)] – structural capacity governs.

Table C.3. Estimated shaft resistances for data point ID No. 3

Soil Layer	Geomaterial	Unit Side Resistance (ksf)	Side Resistance (kips)	Unit End Bearing (ksf)	End Bearing (kip)	Total Resistance (kip)
1	Clay	0.87	369[(b)]	n/a	n/a	4196
2	Clay	1.61	100	n/a	n/a	
3	Rock	7.11	1956	140.97[(a)]	1770	

[(a)] – average value of intact and fracture rock mass; [(b)] –side resistance at top five feet ofclay layer neglected.

Table C.4. Estimated shaft resistances for data point ID No. 4

Soil Layer	Geomaterial	Unit Side Resistance (ksf)	Side Resistance (kips)	Unit End Bearing (ksf)	End Bearing (kip)	Total Resistance (kip)
1	Clay	Neglected due to casing		n/a	n/a	5436
2	Sand	Neglected due to casing		n/a	n/a	
3	Cohesive IGM	10.07	3183	234.18	2253	

Table C.5. Estimated shaft resistances for data point ID No. 5

Soil Layer	Geomaterial	Unit Side Resistance (ksf)	Side Resistance (kips)	Unit End Bearing (ksf)	End Bearing (kip)	Total Resistance (kip)
1	Clay	0.34	13[(a)]	n/a	n/a	4828
2	Clay	0.79	48	n/a	n/a	
3	Clay	1.10	382	n/a	n/a	
4	Sand	4.00	80	n/a	n/a	
5	Cohesive IGM	2.59	759	n/a	n/a	
6	Cohesive IGM	1.49	56	n/a	n/a	
7	Cohesive IGM	1.49	141	n/a	n/a	
8	Rock	6.18	272	244.77	3076	

[(a)] – the side resistance at the upper five feet clay layer was neglected.

Table C.6. Estimated shaft resistances for data point ID No. 6

Soil Layer	Geomaterial	Unit Side Resistance (ksf)	Side Resistance (kips)	Unit End Bearing (ksf)	End Bearing (kip)	Total Resistance (kip)
1	Clay	0.71	5[(a)]	n/a	n/a	546
2	Clay	0.34	57	n/a	n/a	
3	Clay	0.94	139	n/a	n/a	
4	Clay	1.69	211	27.60	134	

[(a)] – the side resistance at the upper five feet clay layer was neglected.

Table C.7. Estimated shaft resistances for data point ID No. 7

Soil Layer	Geomaterial	Unit Side Resistance (ksf)	Side Resistance (kips)	Unit End Bearing (ksf)	End Bearing (kip)	Total Resistance (kip)
1	Clay	0.71	0.00[(a)]	n/a	n/a	14767
2	Clay	1.47	111	n/a	n/a	
3	Rock	19.64	204	n/a	n/a	
4	Rock	32.30	700	n/a	n/a	
5	Rock	25.91	1050	n/a	n/a	
6	Rock	17.84	219	n/a	n/a	
7	Rock	26.62	3011	1340.14[(b)]	9473	

[(a)] – the side resistance at the upper five feet clay layer was neglected; [(b)] – average value of intact and fracture rock mass.

Table C.8. Estimated shaft resistances for data point ID No. 8

Soil Layer	Geomaterial	Unit Side Resistance (ksf)	Side Resistance (kips)	Unit End Bearing (ksf)	End Bearing (kip)	Total Resistance (kip)
1	Clay	0.86	75[(a)]	n/a	n/a	21111
2	Clay	0.14	40	n/a	n/a	
3	Sand	2.44	1772	n/a	n/a	
4	Sand	2.54	944	n/a	n/a	
5	Rock	19.41	4931	757.78[(b)]	13350	

[(a)] – the side resistance at the upper five feet clay layer was neglected; [(b)] – average value of intact and fracture rock mass.

Table C.9. Estimated shaft resistances for data point ID No. 9

Soil Layer	Geomaterial	Unit Side Resistance (ksf)	Side Resistance (kips)	Unit End Bearing (ksf)	End Bearing (kip)	Total Resistance (kip)
1	Clay	0.481	38[(a)]	n/a	n/a	1735
2	Clay	0.275	43	n/a	n/a	
3	Sand	1.683	264	n/a	n/a	
4	Sand	2.063	810	n/a	n/a	
5	Sand	0.261	21	n/a	n/a	
6	Sand	1.850	182	19.2	377	

[(a)] – the side resistance at the upper five feet clay layer was neglected.

Table C.10. Estimated shaft resistances for data point ID No. 10

Soil Layer	Geomaterial	Unit Side Resistance (ksf)	Side Resistance (kips)	Unit End Bearing (ksf)	End Bearing (kip)	Total Resistance (kip)
1	Clay	0.87	0[(a)]	n/a	n/a	1732
2	Clay	0.48	76	n/a	n/a	
3	Clay	0.34	27	n/a	n/a	
4	Sand	2.16	1187	n/a	n/a	
5	Sand	2.79	18	21.60	424	

[(a)] – the side resistance at the upper five feet clay layer was neglected.

Table C.11. Estimated shaft resistances for data point ID No. 11

Soil Layer	Geomaterial	Unit Side Resistance (ksf)	Side Resistance (kips)	Unit End Bearing (ksf)	End Bearing (kip)	Total Resistance (kip)
1	Clay	0.34	0[(a)]	n/a	n/a	1829
2	Clay	1.02	241	n/a	n/a	
3	Sand	2.26	1235	18	353	

[(a)] – the side resistance at the upper five feet clay layer was neglected.

Table C.12. Estimated shaft resistances for data point ID No. 12

Soil Layer	Geomaterial	Unit Side Resistance (ksf)	Side Resistance (kips)	Unit End Bearing (ksf)	End Bearing (kip)	Total Resistance (kip)
1	Sand	1.03	211	n/a	n/a	n/a
2	Sand	10.96	5371	n/a	n/a	
3	Sand	6.55	2409	n/a	n/a	
4	n/a	n/a	n/a	n/a	n/a	

Table C.13. Estimated shaft resistances for data point ID No. 13

Soil Layer	Geomaterial	Unit Side Resistance (ksf)	Side Resistance (kips)	Unit End Bearing (ksf)	End Bearing (kip)	Total Resistance (kip)
1	Sand	Neglected due to casing		n/a	n/a	4028
2	Sand	Neglected due to casing		n/a	n/a	
3	Cohesive IGM	1.90	799	n/a	n/a	
4	Cohesive IGM	3.89	169	n/a	n/a	
5	Cohesive IGM	4.76	218	100.56[(a)]	2843	

[(a)] – average value of intact and fracture rock mass.

Table C.14. Estimated shaft resistances for data point ID No. 14

Soil Layer	Geomaterial	Unit Side Resistance (ksf)	Side Resistance (kips)	Unit End Bearing (ksf)	End Bearing (kip)	Total Resistance (kip)
1	Cohesive IGM	0.00	0	n/a	n/a	8748
2	Cohesive IGM	1.41	293	n/a	n/a	
3	Rock	25.30	2385	n/a	n/a	
4	Cohesive IGM	3.09	349	n/a	n/a	
5	Rock	40.00	5278	n/a	n/a	
6	Cohesive IGM	5.12	444	Neglected end bearing		

Table C.15. Estimated shaft resistances for data point ID No. 15

Soil Layer	Geomaterial	Unit Side Resistance (ksf)	Side Resistance (kips)	Unit End Bearing (ksf)	End Bearing (kip)	Total Resistance (kip)
1	n/a	Neglected due to casing		n/a	n/a	1333
2	Cohesive IGM	1.64	225	n/a	n/a	
3	Cohesive IGM	4.01	285	85.41	823	

Table C.16. Estimated shaft resistances for data point ID No. 16

Soil Layer	Geomaterial	Unit Side Resistance (ksf)	Side Resistance (kips)	Unit End Bearing (ksf)	End Bearing (kip)	Total Resistance (kip)
1	Clay	Neglected due to casing		n/a	n/a	4414
2	IGM[(a)]	Neglected due to casing		n/a	n/a	
3	Cohesive IGM	1.98	851	126.00	3563	

[(a)] – assumed geomaterial.

Table C.17. Estimated shaft resistances for data point ID No. 17

Soil Layer	Geomaterial	Unit Side Resistance (ksf)	Side Resistance (kips)	Unit End Bearing (ksf)	End Bearing (kip)	Total Resistance (kip)
1	n/a	Neglected due to casing		n/a	n/a	16674
2	Cohesive IGM	4.42	1779	n/a	n/a	
3	Cohesive IGM	4.59	231	n/a	n/a	
4	Cohesive IGM	5.01	995	n/a	n/a	
5	Rock	9.88	397	n/a	n/a	
6	Rock	8.67	501	n/a	n/a	
7	Cohesive IGM (shaft) and Rock (toe)	7.06	816	237.84[(a)]	11955	

[(a)] – average value of intact and fracture rock mass.

Table C.18. Estimated shaft resistances for data point ID No. 18

Soil Layer	Geomaterial	Unit Side Resistance (ksf)	Side Resistance (kips)	Unit End Bearing (ksf)	End Bearing (kip)	Total Resistance (kip)
1	Sand	n/a	n/a	n/a	n/a	n/a
2	n/a	n/a	n/a	n/a	n/a	

Table C.19. Estimated shaft resistances for data point ID No. 19

Soil Layer	Geomaterial	Unit Side Resistance (ksf)	Side Resistance (kips)	Unit End Bearing (ksf)	End Bearing (kip)	Total Resistance (kip)
1	n/a	0.00	0[(a)]	n/a	n/a	2848
2	Cohesive IGM	1.83	370	n/a	n/a	
3	Cohesive IGM	2.23	400	n/a	n/a	
4	Cohesionless IGM	6.12	696	48.88	1382	

[(a)] – the side resistance at the upper five feet clay layer was neglected.

Table C.20. Estimated shaft resistances for data point ID No. 20

Soil Layer	Geomaterial	Unit Side Resistance (ksf)	Side Resistance (kips)	Unit End Bearing (ksf)	End Bearing (kip)	Total Resistance (kip)
1	Sand	Neglected due to casing		n/a	n/a	3819
2	Sand	Neglected due to casing		n/a	n/a	
3	Sand	Neglected due to casing		n/a	n/a	
4	Sand	Neglected due to casing		n/a	n/a	
5	Sand	2.38	403	n/a	n/a	
6	Sand	4.00	302	n/a	n/a	
7	Sand	4.00	452	n/a	n/a	
8	Sand	2.57	242	n/a	n/a	
9	Sand	4.00	377	n/a	n/a	
10	Sand	2.52	238	n/a	n/a	
11	Sand	2.45	244	55.2	1561	

Table C.21. Estimated shaft resistances for data point ID No. 21

Soil Layer	Geomaterial	Unit Side Resistance (ksf)	Side Resistance (kips)	Unit End Bearing (ksf)	End Bearing (kip)	Total Resistance (kip)
1	n/a	n/a	n/a	n/a	n/a	n/a

Table C.22. Estimated shaft resistances for data point ID No. 22

Soil Layer	Geomaterial	Unit Side Resistance (ksf)	Side Resistance (kips)	Unit End Bearing (ksf)	End Bearing (kip)	Total Resistance (kip)
1	n/a	n/a	n/a	n/a	n/a	n/a
2	n/a	n/a	n/a	n/a	n/a	
3	n/a	n/a	n/a	n/a	n/a	

Table C.23. Estimated shaft resistances for data point ID No. 23

Soil Layer	Geomaterial	Unit Side Resistance (ksf)	Side Resistance (kips)	Unit End Bearing (ksf)	End Bearing (kip)	Total Resistance (kip)
1	n/a	n/a	n/a	n/a	n/a	n/a

Table C.24. Estimated shaft resistances for data point ID No. 24

Soil Layer	Geomaterial	Unit Side Resistance (ksf)	Side Resistance (kips)	Unit End Bearing (ksf)	End Bearing (kip)	Total Resistance (kip)
1	n/a	n/a	n/a	n/a	n/a	14325
2	Cohesive IGM	1.60	451	n/a	n/a	
3	Cohesive IGM	1.27	42	n/a	n/a	
4	Cohesive IGM	2.27	110	n/a	n/a	
5	Rock	8.67	2392	n/a	n/a	
6	Rock	8.67	4950	304.36[(a)]	6381	

[(a)] – average value of intact and fracture rock mass.

Table C.25. Estimated shaft resistances for data point ID No. 25

Soil Layer	Geomaterial	Unit Side Resistance (ksf)	Side Resistance (kips)	Unit End Bearing (ksf)	End Bearing (kip)	Total Resistance (kip)
1	Clay	0.54	29[(a)]	n/a	n/a	1566
2	Cohesive IGM	0.81	24	n/a	n/a	
3	Cohesive IGM	0.81	163	n/a	n/a	
4	Cohesive IGM (shaft) and Rock (toe)	4.56	333	105.72	1017	

[(a)] – the side resistance at the upper five feet clay layer was neglected.

Table C.26. Estimated shaft resistances for data point ID No. 26

Soil Layer	Geomaterial	Unit Side Resistance (ksf)	Side Resistance (kips)	Unit End Bearing (ksf)	End Bearing (kip)	Total Resistance (kip)
1	Clay	0.23	18[(a)]	n/a	n/a	1427
2	Sand	0.37	50	n/a	n/a	
3	Clay	0.19	15	n/a	n/a	
4	Sand	1.16	943	20.40	401	

[(a)] – the side resistance at the upper five feet clay layer was neglected.

Table C.27. Estimated shaft resistances for data point ID No. 27

Soil Layer	Geomaterial	Unit Side Resistance (ksf)	Side Resistance (kips)	Unit End Bearing (ksf)	End Bearing (kip)	Total Resistance (kip)
1	Clay	0.41	32[(a)]	n/a	n/a	1830
2	Sand	0.49	65	n/a	n/a	
3	Clay	0.29	23	n/a	n/a	
4	Sand	1.46	1177	27.13[(b)]	533	

[(a)] – the side resistance at the upper five feet clay layer was neglected; (b) – included effect of grouting.

Table C.28. Estimated shaft resistances for data point ID No. 28

Soil Layer	Geomaterial	Unit Side Resistance (ksf)	Side Resistance (kips)	Unit End Bearing (ksf)	End Bearing (kip)	Total Resistance (kip)
1	Rock	18.58	584	n/a	n/a	11858
2	Rock	13.38	841	n/a	n/a	
3	Rock	16.85	1059	n/a	n/a	
4	Rock	13.36	588	1059.25[(a)]	8787	

[(a)] – average value of intact and fracture rock mass.

Table C.29. Estimated shaft resistances for data point ID No. 29

Soil Layer	Geomaterial	Unit Side Resistance (ksf)	Side Resistance (kips)	Unit End Bearing (ksf)	End Bearing (kip)	Total Resistance (kip)
1	Rock	Neglected due to casing		n/a	n/a	13990
2	Rock	14.00	879	n/a	n/a	
3	Rock	26.81	1685	n/a	n/a	
4	Rock	21.59	1357	n/a	n/a	
5	Rock	28.62	719	1855.33	9350[(b)]	

[(a)] – the side resistance at the upper five feet clay layer was neglected; [(b)] – structural capacity governs.

Table C.30. Estimated shaft resistances for data point ID No. 30

Soil Layer	Geomaterial	Unit Side Resistance (ksf)	Side Resistance (kips)	Unit End Bearing (ksf)	End Bearing (kip)	Total Resistance (kip)
1	Sand	3.77	142	n/a	n/a	
2	Sand	4.00	402	n/a	n/a	
3	Sand	4.00	327	n/a	n/a	
4	Clay	0.35	24	n/a	n/a	
5	Sand	3.55	223	n/a	n/a	
6	Sand	3.58	450	n/a	n/a	
7	Clay	2.54	96	n/a	n/a	
8	Sand	5.48	138	n/a	n/a	
9	Sand	3.48	263	n/a	n/a	3546
10	Sand	5.08	96	n/a	n/a	
11	Clay	1.11	70	n/a	n/a	
12	Clay	1.05	66	n/a	n/a	
13	Clay	2.12	173	n/a	n/a	
14	Sand	2.64	133	n/a	n/a	
15	Clay	1.46	128	n/a	n/a	
16	Sand	1.98	75	n/a	n/a	
17	Clay	1.46	403	26.93	338	

Table C.31. Estimated shaft resistances for data point ID No. 31

Soil Layer	Geomaterial	Unit Side Resistance (ksf)	Side Resistance (kips)	Unit End Bearing (ksf)	End Bearing (kip)	Total Resistance (kip)
1	Sand	n/a	n/a	n/a	n/a	
2	Clay	n/a	n/a	n/a	n/a	
3	Clay	n/a	n/a	n/a	n/a	n/a
4	Sand	n/a	n/a	n/a	n/a	
5	Cohesive IGM	n/a	n/a	n/a	n/a	

Table C.32. Estimated shaft resistances for data point ID No. 32

Soil Layer	Geomaterial	Unit Side Resistance (ksf)	Side Resistance (kips)	Unit End Bearing (ksf)	End Bearing (kip)	Total Resistance (kip)
1	Sand	n/a	n/a	n/a	n/a	
2	Sand	n/a	n/a	n/a	n/a	n/a
3	n/a	n/a	n/a	n/a	n/a	

Table C.33. Estimated shaft resistances for data point ID No. 33

Soil Layer	Geomaterial	Unit Side Resistance (ksf)	Side Resistance (kips)	Unit End Bearing (ksf)	End Bearing (kip)	Total Resistance (kip)
1	Cohesive IGM	1.00	110	n/a	n/a	542
2	Cohesive IGM	1.62	109	33.66	324	

Table C.34. Estimated shaft resistances for data point ID No. 34

Soil Layer	Geomaterial	Unit Side Resistance (ksf)	Side Resistance (kips)	Unit End Bearing (ksf)	End Bearing (kip)	Total Resistance (kip)
1	Sand	0.14	3	n/a	n/a	700
2	Clay (shaft) and Cohesive IGM (toe)	1.66	293	32.17	404	

Table C.35. Estimated shaft resistances for data point ID No. 35

Soil Layer	Geomaterial	Unit Side Resistance (ksf)	Side Resistance (kips)	Unit End Bearing (ksf)	End Bearing (kip)	Total Resistance (kip)
1	Cohesive IGM	5.75	1316	177.50	1708	3024

Table C.36. Estimated shaft resistances for data point ID No. 36

Soil Layer	Geomaterial	Unit Side Resistance (ksf)	Side Resistance (kips)	Unit End Bearing (ksf)	End Bearing (kip)	Total Resistance (kip)
1	Rock	8.39	356	n/a	n/a	10394
2	Rock	15.23	3229	n/a	n/a	
3	Rock	12.61	2156	292.53[(a)]	4653	

[(a)] – average value of intact and fracture rock mass.

Table C.37. Estimated shaft resistances for data point ID No. 37

Soil Layer	Geomaterial	Unit Side Resistance (ksf)	Side Resistance (kips)	Unit End Bearing (ksf)	End Bearing (kip)	Total Resistance (kip)
1	n/a	n/a	n/a	n/a	n/a	n/a
2	n/a	n/a	n/a	n/a	n/a	
3	n/a	n/a	n/a	n/a	n/a	

Table C.38. Estimated shaft resistances for data point ID No. 38

Soil Layer	Geomaterial	Unit Side Resistance (ksf)	Side Resistance (kips)	Unit End Bearing (ksf)	End Bearing (kip)	Total Resistance (kip)
1	Rock	17.84	2522	475.33[(a)]	5973	8495

[(a)] – average value of intact and fracture rock mass.

Table C.39. Estimated shaft resistances for data point ID No. 39

Soil Layer	Geomaterial	Unit Side Resistance (ksf)	Side Resistance (kips)	Unit End Bearing (ksf)	End Bearing (kip)	Total Resistance (kip)
1	Rock	17.21	4325.50	459.96[(a)]	5780	10105

[(a)] – average value of intact and fracture rock mass.

Table C.40. Estimated shaft resistances for data point ID No. 40

Soil Layer	Geomaterial	Unit Side Resistance (ksf)	Side Resistance (kips)	Unit End Bearing (ksf)	End Bearing (kip)	Total Resistance (kip)
1	Rock	n/a	n/a	n/a	n/a	n/a

Table C.41. Estimated shaft resistances for data point ID No. 41

Soil Layer	Geomaterial	Unit Side Resistance (ksf)	Side Resistance (kips)	Unit End Bearing (ksf)	End Bearing (kip)	Total Resistance (kip)
1	Clay	n/a	n/a	n/a	n/a	n/a
2	n/a	n/a	n/a	n/a	n/a	
3	n/a	n/a	n/a	n/a	n/a	
4	n/a	n/a	n/a	n/a	n/a	
5	n/a	n/a	n/a	n/a	n/a	
6	n/a	n/a	n/a	n/a	n/a	
7	n/a	n/a	n/a	n/a	n/a	
8	Cohesive IGM	n/a	n/a	n/a	n/a	
9	n/a	n/a	n/a	n/a	n/a	
10	Cohesive IGM	n/a	n/a	n/a	n/a	
11	n/a	n/a	n/a	n/a	n/a	
12	n/a	n/a	n/a	n/a	n/a	
13	n/a	n/a	n/a	n/a	n/a	
14	Cohesive IGM	n/a	n/a	n/a	n/a	

s